

**ANALYTICAL SOLUTIONS FOR THE
THERMO-ELASTIC ANALYSIS OF FGM PLATES
USING HIGHER ORDER REFINED THEORIES**

Thesis

Submitted in partial fulfillment of the requirements for the degree of

DOCTOR OF PHILOSOPHY

by

SANGEETHA D. M.



**DEPARTMENT OF CIVIL ENGINEERING
NATIONAL INSTITUTE OF TECHNOLOGY KARNATAKA,
SURATHKAL, MANGALORE – 575 025**

JULY, 2017

D E C L A R A T I O N

By the Ph.D. Research Scholar

I hereby *declare* that the Research Thesis entitled **Analytical Solutions for the Thermo-Elastic Analysis of FGM Plates Using Higher Order Refined Theories**, which is being submitted to the **National Institute of Technology Karnataka, Surathkal** in partial fulfilment of the requirements for the award of the Degree of **Doctor of Philosophy in Civil Engineering**, is a *bonafide report of the research work* carried out by me. The material contained in this Research Thesis has not been submitted to any University or Institution for the award of any degree.

102007CV10F04, SANGEETHA D. M.

(Register Number, Name & Signature of the Research Scholar)

Department of Civil Engineering

Place: NITK-Surathkal

Date:

C E R T I F I C A T E

This is to *certify* that the Research Thesis entitled **Analytical Solutions for the Thermo-Elastic Analysis of FGM Plates Using Higher Order Refined Theories** submitted by SANGEETHA D. M. (Register Number: 102007CV10F04) as the record of the research work carried out by her, is *accepted as the Research Thesis submission* in partial fulfilment of the requirements for the award of degree of Doctor of Philosophy.

Prof. K. Swaminathan

Research Guide

Prof. Varghese George

Chairman - DRPC

ACKNOWLEDGEMENT

I sincerely wish to express my deep sense of gratitude and indebtedness to my research supervisor Dr. K. Swaminathan, Professor, Department of Civil Engineering, National Institute of Technology Karnataka, Surathkal for his inspiring guidance, constant encouragement and painstaking assistance which enabled me to undertake the studies reported in this thesis. The timely guidance, and scientific support received from my supervisor is sincerely acknowledged.

I would like to express my sincere thanks to Head of the Department Prof. Varghese George, former Head of the Department Prof. D. Venkat Reddy and all the members of the DRPC, Department of Civil Engineering, NITK, Surathkal for extending all facilities during the period of my research work.

I am thankful to the members of RPAC members, Prof. Subba Rao, Department of Applied mechanics and Hydraulics and Prof. A. Chitharanjan Hegde, Department of Chemistry, NITK, Surathkal for their critical evaluation and very useful suggestions during the progress of the work.

I am very much thankful to all the teaching faculty and supporting staff of the Civil Engineering Department, for their encouragement, help and support provided during the research work.

I would like to thank all the research scholars in and outside the department of civil engineering for their constant encouragement and support throughout my research work. Special mention goes to my colleagues Dr. Reginald Fernandis and Dr. NaveenKumar for their consistent support and encouragement.

Most importantly, I would like to thank my family members, especially my husband Dr. Vinay Kumar V. and my sweet little daughter Sanvi, who always supported and encouraged me in this endeavor. Finally, I am grateful to everyone who helped and encouraged me during this research work.

Place: NITK, Surathkal

Date:

(*Sangeetha D.M.*)

ABSTRACT

Analytical formulations and solutions are presented for the thermo-elastic analysis of Functionally Graded Material (FGM) plates based on a set of higher order refined shear deformation theories. The displacement components in these computational models are based on Taylor's series expansions, which incorporates parabolic variation of transverse strains across the plate thickness. The displacement model with twelve degrees of freedom considers the effects of both transverse shear and normal strain/stress while the other model with nine degrees of freedom includes only the effect of transverse shear deformation. Besides these, a higher order model and a first order model with five degrees of freedom that are developed by other investigators and are reported in the literature are also used in the present investigation for evaluation purposes. A simply supported FGM plate subjected to thermal load is considered throughout as a test problem. The material properties are mathematically modeled based on power law function. The temperature is assumed to vary nonlinearly and obey one-dimensional steady state heat conduction equation throughout the plate thickness while in-plane is sinusoidal. Along with this constant and linearly varying temperatures are also considered in the study. The equations of equilibrium are derived using the Principle of Minimum Potential Energy (PMPE) and closed form solutions are obtained using Navier's solution technique. Firstly, numerical results obtained using various displacement models are compared with the three-dimensional elasticity solutions available in the literature in order to establish the accuracy of higher order models considered in the study. After establishing the accuracy of the solution method benchmark results and comparison of solutions are presented for Monel/Zirconia, Titanium-Alloy/Zirconia and Aluminium/Alumina FGM plate by varying edge ratio, slenderness ratio and power law parameter. Numerical and graphical results are presented for in-plane, transverse displacements and stresses for all the models by considering different temperature profiles.

Keywords: FGM Plate; Analytical solution; Navier's technique; Higher Order Theory; Shear Deformation; Thermal Load; Stress Analysis.

CONTENTS

	Page No.
LIST OF TABLES	v
LIST OF FIGURES	xi
NOMENCLATURE	xv
1. INTRODUCTION	1
1.1 Preliminary Remarks	1
1.2 Aim and Scope	3
1.3 Layout of the Thesis	5
2. LITERATURE REVIEW	7
2.1 Preliminary Remarks	7
2.2 Thermal Stress Analysis	11
2.2.1 Three dimensional temperature variation	11
2.2.2 one-dimensional nonlinear temperature variation	13
2.2.2.1 Analytical methods	13
2.2.2.2 Numerical methods	17
2.2.3 One-dimensional constant and linear temperature variation	19
2.2.3.1 Analytical methods	20
2.2.3.2 Numerical methods	21
2.3 Final Remarks	22
3. THEORETICAL FORMULATIONS	25
3.1 Preliminary Remarks	25
3.2 Definition of Displacement Field	25
3.2.1 Displacement models	27
3.3 Stress Strain Relations for an FGM Plate	29
3.4 Strain Displacement Relations	32

3.4.1 Strain Expressions Corresponding to HSDT-12 Model	33
3.5 Stress-Resultant and Middle-Plane-Strain Relations	35
3.5.1 Constitutive relations for FGM plate based on HSDT-12 model.	36
3.6 Equations of Equilibrium and Natural Boundary Conditions	39
3.6.1 Thermal stress analysis	39
3.7 Closure	45
4. ANALYTICAL SOLUTION METHOD	49
4.1 Preliminary Remarks	49
4.2 Navier Solution Technique	49
4.2.1 In-Plane Stresses	50
4.2.1.1 Transverse Stress ($\tau_{xz}, \tau_{yz}, \sigma_z$)	57
4.3 Closure	60
5. NUMERICAL RESULTS AND DISCUSSION	61
5.1 Preliminary Remarks	61
5.2 Thermal Stress Analysis	62
5.2.1 Description of examples and discussions	63
5.3 Closure	77
6. CONCLUSION	143
6.1 General	143
6.2 Suggestions for Future Work	146
REFERENCE	147
APPENDIX – I	Equilibrium equations obtained using various displacement models for stress analysis of FGM plates 157

APPENDIX – II	Elements of plate stiffness matrices $[A]$, $[A']$, $[C_T]$, $[B]$, $[B']$, $[D]$, $[D']$, $[E]$, $[E']$ for various displacement models used in the thermo-elastic analysis of FGM plates	159
APPENDIX – III	Elements of the coefficient matrix $[X]$ using various displacement models for thermo-elastic analysis of FGM plates	171
APPENDIX – IV	Elements of Thermal Force Matrix $\{ F_T \}$ for various displacement models used in the thermo-elastic analysis of FGM plates	177

LIST OF TABLES

Table No.	Description	Page No.
5.1	Nondimensionalized in-plane displacement (\bar{u}) at the bottom ($z = -h/2$), middle ($z=0$) and top ($z= h/2$) surface of a simply supported square FGM (Monel-Zirconia, M1) plate subjected to transverse sinusoidal mechanical load (with various a/h ratios, $m=n=1$ and $p=2$)	78
5.2	Nondimensionalized transverse displacement (\bar{w}) at the bottom ($z= -h/2$), middle ($z=0$) and top ($z= h/2$) surface of a simply supported square FGM (Monel-Zirconia, M1) plate subjected to transverse sinusoidal mechanical load (with various a/h ratios, $m=n=1$ and $p=2$)	79
5.3	Nondimensionalized in-plane normal stress ($\bar{\sigma}_x$) at the bottom ($z= -h/2$), middle ($z=0$) and top ($z= h/2$) surface of a simply supported square FGM (Monel-Zirconia, M1) plate subjected to transverse sinusoidal mechanical load (with various a/h ratios, $m=n=1$ and $p=2$)	80
5.4	Nondimensionalized transverse shear stress ($\bar{\tau}_{xz}$) and transverse normal stress ($\bar{\sigma}_z$) at the middle ($z=0$) surface of a simply supported square FGM (Monel-Zirconia, M1) plate subjected to transverse sinusoidal mechanical load (with various a/h ratios, $m=n=1$ and $p=2$)	81
5.5	Nondimensionalized in-plane displacements (\bar{u} , \bar{v}) and transverse displacement (\bar{w}) at the top ($z = h/2$) surface of a rectangular FGM (Monel-Zirconia, M1) plate subjected to nonlinear (T_{NL}) thermal load (with various a/b ratios, $a/h=4$ and $p=3$)	82
5.6	Nondimensionalized in-plane normal stresses ($\bar{\sigma}_x$, $\bar{\sigma}_y$), in-plane shear stress ($\bar{\tau}_{xy}$) and transverse shear stresses ($\bar{\tau}_{xz}$, $\bar{\tau}_{yz}$) at the middle ($z=0$) surface of a rectangular FGM (Monel-Zirconia, M1) plate subjected to nonlinear (T_{NL}) thermal load (with various a/b ratios, $a/h=4$ and $p=3$)	83
5.7	Nondimensionalized in-plane displacement (\bar{u}) at the bottom ($z= -h/2$), middle ($z=0$) and top ($z= h/2$) surface of a FGM (Monel-Zirconia, M1) plate subjected to nonlinear (T_{NL}) thermal load (with various a/h ratios, p values and $a/b=1.5$)	84
5.8	Nondimensionalized in-plane normal stress ($\bar{\sigma}_x$) at the bottom ($z= -h/2$), middle ($z=0$) and top ($z= h/2$) surface of a FGM (Monel-Zirconia, M1) plate subjected to nonlinear (T_{NL}) thermal load (with various a/h ratios, p values and $a/b=1.5$)	85

5.9	Nondimensionalized in-plane displacement (\bar{u}) at the top ($z = h/2$) surface of a square FGM (Monel-Zirconia, M1) plate subjected to nonlinear (T_{NL}) thermal load (with various a/h ratios and p values)	86
5.10	Nondimensionalized transverse displacement (\bar{w}) at the top ($z = h/2$) surface of a square FGM (Monel-Zirconia, M1) plate subjected to nonlinear (T_{NL}) thermal load (with various a/h ratios and p values)	87
5.11	Nondimensionalized in-plane normal stress ($\bar{\sigma}_x$) at the top ($z = h/2$) surface of a square FGM (Monel-Zirconia, M1) plate subjected to nonlinear (T_{NL}) thermal load (with various a/h ratios and p values)	88
5.12	Nondimensionalized in-plane shear stress ($\bar{\tau}_{xy}$) at the top ($z = h/2$) surface of a square FGM (Monel-Zirconia, M1) plate subjected to nonlinear (T_{NL}) thermal load (with various a/h ratios and p values)	89
5.13	Nondimensionalized transverse shear stress ($\bar{\tau}_{xz}$) at the middle ($z = 0$) surface of a square FGM (Monel-Zirconia, M1) plate subjected to nonlinear (T_{NL}) thermal load (with various a/h ratios and p values)	90
5.14	Nondimensionalized in-plane displacements (\bar{u} , \bar{v}) and transverse displacement (\bar{w}) at the top ($z = h/2$) surface of a rectangular FGM (Aluminium-Alumina, M2) plate subjected to nonlinear (T_{NL}) thermal load (with various a/h ratios, $a/b=2$ and $p=2$)	91
5.15	Nondimensionalized in-plane normal stresses ($\bar{\sigma}_x$, $\bar{\sigma}_y$), in-plane shear stress ($\bar{\tau}_{xy}$) and transverse shear stresses ($\bar{\tau}_{xz}$, $\bar{\tau}_{yz}$) at the middle ($z=0$) surface of a rectangular FGM (Aluminium-Alumina, M2) plate subjected to nonlinear (T_{NL}) thermal load (with various a/h ratios, $a/b=2$ and $p=2$)	92
5.16	Nondimensionalized in-plane displacement (\bar{v}) at the bottom ($z = -h/2$), middle ($z=0$) and top ($z = h/2$) surface of a FGM (Aluminium-Alumina, M2) plate subjected to nonlinear (T_{NL}) thermal load (with various a/b ratios, p values and $a/h=20$)	93
5.17	Nondimensionalized in-plane shear stress ($\bar{\tau}_{xy}$) at the bottom ($z = -h/2$), middle ($z=0$) and top ($z = h/2$) surface of a FGM (Aluminium-Alumina, M2) plate subjected to nonlinear (T_{NL}) thermal load (with various a/b ratios, p values and $a/h=20$)	94
5.18	Nondimensionalized in-plane displacement (\bar{u}) at the top ($z = h/2$) surface of a FGM (Aluminium-Alumina, M2) plate subjected to nonlinear (T_{NL}) thermal load (with various a/b ratios, p values and $a/h=10$)	95

5.19	Nondimensionalized transverse displacement (\bar{w}) at the top ($z = h/2$) surface of a FGM (Aluminium-Alumina, M2) plate subjected to nonlinear (T_{NL}) thermal load (with various a/b ratio, p values and $a/h=10$)	96
5.20	Nondimensionalized in-plane normal stress ($\bar{\sigma}_x$) at the top ($z = h/2$) surface of a FGM (Aluminium-Alumina, M2) plate subjected to nonlinear (T_{NL}) thermal load (with various a/b ratios, p values and $a/h=10$)	97
5.21	Nondimensionalized in-plane shear stress ($\bar{\tau}_{xy}$) at the top ($z = h/2$) surface of a FGM (Aluminium-Alumina, M2) plate subjected to nonlinear (T_{NL}) thermal load (with various a/b ratio, p values and $a/h=10$)	98
5.22	Nondimensionalized transverse shear stress ($\bar{\tau}_{xz}$) at the middle ($z = 0$) surface of a FGM (Aluminium-Alumina, M2) plate subjected to nonlinear (T_{NL}) thermal load (with various a/b ratio, p and $a/h=10$)	99
5.23	Nondimensionalized in-plane displacements (\bar{u} , \bar{v}) and transverse displacement (\bar{w}) at the top ($z = h/2$) surface of a rectangular FGM (Titanium Alloy-Zirconia, M3) plate subjected to nonlinear (T_{NL}) thermal load (with various values of p , $a/h=10$ and $a/b=2$)	100
5.24	Nondimensionalized in-plane normal stresses ($\bar{\sigma}_x$, $\bar{\sigma}_y$), in-plane shear stress ($\bar{\tau}_{xy}$) and transverse shear stresses ($\bar{\tau}_{xz}$, $\bar{\tau}_{yz}$) at the middle ($z=0$) surface of a rectangular FGM (Titanium Alloy-Zirconia, M3) plate subjected to nonlinear (T_{NL}) thermal load (with various values of p , $a/h=10$ and $a/b=2$)	101
5.25	Nondimensionalized transverse displacement (\bar{w}) at the bottom ($z = -h/2$), middle ($z=0$) and top ($z = h/2$) surface of a FGM (Titanium Alloy-Zirconia, M3) plate subjected to nonlinear (T_{NL}) thermal load (with various a/b ratios, a/h ratios and $p=1$)	102
5.26	Nondimensionalized in-plane normal stress ($\bar{\sigma}_y$) at the bottom ($z = -h/2$), middle ($z=0$) and top ($z = h/2$) surface of a FGM (Titanium Alloy-Zirconia, M3) plate subjected to nonlinear (T_{NL}) thermal load (with various a/b ratios, a/h ratios and $p=1$)	103
5.27	Nondimensionalized in-plane displacements (\bar{u} , \bar{v}) and transverse displacement (\bar{w}) at the top ($z = h/2$) surface of a rectangular FGM plate subjected to nonlinear (T_{NL}) thermal load (with various E_c/E_m ratios, a/h ratios, $a/b=2$ and $p=2$)	104

5.28	Nondimensionalized in-plane normal stresses ($\bar{\sigma}_x, \bar{\sigma}_y$), in-plane shear stress ($\bar{\tau}_{xy}$) and transverse shear stresses ($\bar{\tau}_{xz}, \bar{\tau}_{yz}$) at the middle ($z=0$) surface of a rectangular FGM plate subjected to nonlinear (T_{NL}) thermal load (with various E_c/E_m ratios, a/h , $a/b=2$ and $p=2$)	105
5.29	Nondimensionalized in-plane displacement (\bar{u}) at the top ($z = h/2$) surface of a square FGM plate subjected to nonlinear (T_{NL}) thermal load (with various E_c/E_m ratios, p values, $a/b=1.5$ and $a/h=10$)	106
5.30	Nondimensionalized in-plane normal stress ($\bar{\sigma}_x$) at the top ($z = h/2$) surface of a FGM plate subjected to nonlinear (T_{NL}) thermal load (with various E_c/E_m ratios, p values, $a/b=1.5$ and $a/h=10$)	107
5.31	Nondimensionalized in-plane displacements (\bar{u}, \bar{v}) and transverse displacement (\bar{w}) at the top ($z = h/2$) surface of a FGM plate subjected to nonlinear (T_{NL}) thermal load (with various k_c/k_m ratios, a/b ratios, $a/h=10$ and $p=2$)	108
5.32	Nondimensionalized in-plane normal stresses ($\bar{\sigma}_x, \bar{\sigma}_y$), in-plane shear stress ($\bar{\tau}_{xy}$) and transverse shear stresses ($\bar{\tau}_{xz}, \bar{\tau}_{yz}$) at the middle ($z=0$) surface of a FGM plate subjected to nonlinear (T_{NL}) thermal load (with various k_c/k_m ratios, a/b ratios, $a/h=10$ and $p=2$)	109
5.33	Nondimensionalized transverse displacement (\bar{w}) at the top ($z = h/2$) surface of a square FGM plate subjected to nonlinear (T_{NL}) thermal load (with various k_c/k_m ratios, p values and $a/h=20$)	110
5.34	Nondimensionalized in-plane normal stress ($\bar{\sigma}_y$) at the top ($z = h/2$) surface of a square FGM plate subjected to nonlinear (T_{NL}) thermal load (with various k_c/k_m ratios, p values and $a/h=20$)	111
5.35	Nondimensionalized in-plane displacement (\bar{u}) and transverse displacement (\bar{w}) at the top ($z = h/2$) surface of a FGM plate subjected to nonlinear (T_{NL}), linear (T_L) and constant (T_C) thermal loads (with various E_c/E_m ratios, a/b ratios, $a/h=4$ and $p=2$)	112
5.36	Nondimensionalized in-plane normal stresses ($\bar{\sigma}_x, \bar{\sigma}_y$), at the middle ($z = 0$) surface of a FGM plate subjected to nonlinear (T_{NL}), linear (T_L) and constant (T_C) thermal loads (with various E_c/E_m ratios, a/b ratios, $a/h=4$ and $p=2$)	113
5.37	Nondimensionalized in-plane shear stress ($\bar{\tau}_{xy}$) at the top ($z = h/2$) surface of a FGM plate subjected to nonlinear (T_{NL}), linear (T_L) and constant (T_C) thermal loads (with various E_c/E_m ratios, a/b ratios, $a/h=4$ and $p=2$)	114

5.38	Nondimensionalized transverse shear stresses ($\bar{\tau}_{xz}, \bar{\tau}_{yz}$) at a distance 0.1h from the bottom surface of a FGM plate subjected to nonlinear (T_{NL}), linear (T_L) and constant (T_C) thermal loads (with various E_c/E_m ratios, a/b ratios, a/h=4 and p=2)	115
5.39	Nondimensionalized in-plane displacement (\bar{u}) and transverse displacement (\bar{w}) at the top ($z = h/2$) surface of a FGM plate subjected to nonlinear (T_{NL}), linear (T_L) and constant (T_C) thermal loads (with various k_c/k_m ratios, a/h ratios, a/b=2 and p=2)	116
5.40	Nondimensionalized in-plane normal stresses ($\bar{\sigma}_x, \bar{\sigma}_y$) at the middle ($z = 0$) surface of a FGM plate subjected to nonlinear (T_{NL}), linear (T_L) and constant (T_C) thermal loads (with various k_c/k_m ratios, a/h ratios, a/b=2 and p=2)	117
5.41	Nondimensionalized in-plane shear stress ($\bar{\tau}_{xy}$) at the top ($z = h/2$) surface of a FGM plate subjected to nonlinear (T_{NL}), linear (T_L) and constant (T_C) thermal loads (with various k_c/k_m ratios, a/h ratios, a/b=2 and p=2)	118
5.42	Nondimensionalized transverse shear stresses ($\bar{\tau}_{xz}, \bar{\tau}_{yz}$) at a distance 0.1h from the bottom surface of a FGM plate subjected to nonlinear (T_{NL}), linear (T_L) and constant (T_C) thermal loads (with various k_c/k_m ratios, a/h ratios, a/b=2 and p=2)	119

LIST OF FIGURES

Fig. No.	Description	Page No.
2.1	Deformation patterns of transverse normal according to the CLPT, FSDT and TSDT	9
3.1	FGM plate geometry with positive set of reference axes and displacement components	47
3.2	Variation of the generalized displacement components across the thickness of an FGM plate using (a) HSDT-12, (b) HSDT-9, (c) HSDT-5 and (d) FSDT displacement models.	48
5.1	Variation of (a) Volume fraction distribution (V_f) of ceramic-metal constituent phase and (b) Nondimensionalized Temperature field through the thickness (z/h) of an FGM plate for various power law parameters.	120
5.2	Variation of effective material properties through the thickness (z/h) of Monel-Zirconia (M1) FGM plate (a) Young's modulus of elasticity, (b) Thermal coefficient of expansion and (c) Thermal conductivity.	121
5.3	Variation of effective material properties through the thickness (z/h) of Aluminium-Alumina (M2) FGM plate (a) Young's modulus of elasticity, (b) Thermal coefficient of expansion and (c) Thermal conductivity.	122
5.4	Variation of effective material properties through the thickness (z/h) of Titanium Alloy-Zirconia (M3) FGM plate (a) Young's modulus of elasticity, (b) Thermal coefficient of expansion and (c) Thermal conductivity.	123
5.5	Variation of nondimensionalized transverse displacement (\bar{w}) through the thickness (z/h) of a simply supported square Monel-Zirconia (M1) FGM plate subjected to nonlinear thermal load for (a) $a/h = 5$, (b) $a/h=10$ and (c) $a/h=20$.	124
5.6	Variation of nondimensionalized transverse shear stress ($\bar{\tau}_{xz}$) through the thickness (z/h) of a simply supported square Monel-Zirconia (M1) FGM plate subjected to nonlinear thermal load for (a) $a/h = 5$, (b) $a/h=10$ and (c) $a/h=20$.	125

5.7	Variation of nondimensionalized transverse normal stress ($\bar{\sigma}_z$) through the thickness (z/h) of a simply supported square Monel-Zirconia (M1) FGM plate subjected to nonlinear thermal load for (a) $a/h = 5$, (b) $a/h=10$ and (c) $a/h=20$.	126
5.8	Variation of nondimensionalized in-plane displacement (\bar{u}) through the thickness (z/h) of a simply supported rectangular Monel-Zirconia (M1) FGM plate subjected to nonlinear (T_{NL}) thermal load.	127
5.9	Variation of nondimensionalized in-plane displacement (\bar{v}) through the thickness (z/h) of a simply supported rectangular Monel-Zirconia (M1) FGM plate subjected to nonlinear (T_{NL}) thermal load	127
5.10	Variation of nondimensionalized transverse displacement (\bar{w}) through the thickness (z/h) of a simply supported rectangular Monel-Zirconia (M1) FGM plate subjected to nonlinear (T_{NL}) thermal load	128
5.11	Variation of nondimensionalized in-plane shear stress ($\bar{\tau}_{xy}$) through the thickness (z/h) of a simply supported rectangular Monel-Zirconia (M1) FGM plate subjected to nonlinear (T_{NL}) thermal load	128
5.12	Variation of nondimensionalized in-plane normal stress ($\bar{\sigma}_x$) through the thickness (z/h) of a simply supported rectangular Monel-Zirconia (M1) FGM plate subjected to nonlinear (T_{NL}) thermal load	129
5.13	Variation of nondimensionalized in-plane normal stress ($\bar{\sigma}_y$) through the thickness (z/h) of a simply supported rectangular Monel-Zirconia (M1) FGM plate subjected to nonlinear (T_{NL}) thermal load	129
5.14	Variation of nondimensionalized transverse shear stress ($\bar{\tau}_{xz}$) through the thickness (z/h) of a simply supported rectangular Monel-Zirconia (M1) FGM plate subjected to nonlinear (T_{NL}) thermal load	130
5.15	Variation of nondimensionalized transverse shear stress ($\bar{\tau}_{yz}$) through the thickness (z/h) of a simply supported rectangular Monel-Zirconia (M1) FGM plate subjected to nonlinear (T_{NL}) thermal load	130

5.16	Variation of nondimensionalized in-plane displacement (\bar{u}) through the thickness (z/h) of a simply supported square Aluminium-Alumina (M2) FGM plate subjected to nonlinear (T_{NL}) thermal load.	131
5.17	Variation of nondimensionalized transverse displacement (\bar{w}) through the thickness (z/h) of a simply supported square Aluminium-Alumina (M2) FGM plate subjected to nonlinear (T_{NL}) thermal load.	131
5.18	Variation of nondimensionalized in-plane normal stress ($\bar{\sigma}_x$) through the thickness (z/h) of a simply supported square Aluminium-Alumina (M2) FGM plate subjected to nonlinear (T_{NL}) thermal load.	132
5.19	Variation of nondimensionalized in-plane shear stress ($\bar{\tau}_{xy}$) through the thickness (z/h) of a simply supported square Aluminium-Alumina (M2) FGM plate subjected to nonlinear (T_{NL}) thermal load.	132
5.20	Variation of nondimensionalized transverse shear stress ($\bar{\tau}_{xz}$) through the thickness (z/h) of a simply supported square Aluminium-Alumina (M2) FGM plate subjected to nonlinear (T_{NL}) thermal load.	133
5.21	Variation of nondimensionalized in-plane displacement (\bar{u}) through the thickness (z/h) of a simply supported rectangular Titanium Alloy-Zirconia (M3) FGM plate subjected to nonlinear (T_{NL}), linear (T_L) and constant (T_C) thermal loads based on (a) HSDT-12, (b) HSDT-9, (c) HSDT-5 and (d) FSDT displacement models.	134
5.22	Variation of nondimensionalized in-plane displacement (\bar{v}) through the thickness (z/h) of a simply supported rectangular Titanium Alloy-Zirconia (M3) FGM plate subjected to nonlinear (T_{NL}), linear (T_L) and constant (T_C) thermal loads based on (a) HSDT-12, (b) HSDT-9, (c) HSDT-5 and (d) FSDT displacement models.	135
5.23	Variation of nondimensionalized transverse displacement (\bar{w}) through the thickness (z/h) of a simply supported rectangular Titanium Alloy-Zirconia (M3) FGM plate subjected to nonlinear (T_{NL}), linear (T_L) and constant (T_C) thermal loads based on (a) HSDT-12, (b) HSDT-9, (c) HSDT-5 and (d) FSDT displacement models.	136

- 5.24 Variation of nondimensionalized in-plane normal stress ($\bar{\sigma}_x$) through the thickness (z/h) of a simply supported rectangular Titanium Alloy-Zirconia (M3) FGM plate subjected to nonlinear (T_{NL}), linear (T_L) and constant (T_C) thermal loads based on (a) HSDT-12, (b) HSDT-9, (c) HSDT-5 and (d) FSDT displacement models. 137
- 5.25 Variation of nondimensionalized in-plane normal stress ($\bar{\sigma}_y$) through the thickness (z/h) of a simply supported rectangular Titanium Alloy-Zirconia (M3) FGM plate subjected to nonlinear (T_{NL}), linear (T_L) and constant (T_C) thermal loads based on (a) HSDT-12, (b) HSDT-9, (c) HSDT-5 and (d) FSDT displacement models. 138
- 5.26 Variation of nondimensionalized in-plane shear stress ($\bar{\tau}_{xy}$) through the thickness (z/h) of a simply supported rectangular Titanium Alloy-Zirconia (M3) FGM plate subjected to nonlinear (T_{NL}), linear (T_L) and constant (T_C) thermal loads based on (a) HSDT-12, (b) HSDT-9, (c) HSDT-5 and (d) FSDT displacement models. 139
- 5.27 Variation of nondimensionalized transverse shear stress ($\bar{\tau}_{xz}$) through the thickness (z/h) of a simply supported rectangular Titanium Alloy-Zirconia (M3) FGM plate subjected to nonlinear (T_{NL}), linear (T_L) and constant (T_C) thermal loads based on (a) HSDT-12, (b) HSDT-9, (c) HSDT-5 and (d) FSDT displacement models. 140
- 5.28 Variation of nondimensionalized transverse shear stress ($\bar{\tau}_{yz}$) through the thickness (z/h) of a simply supported rectangular Titanium Alloy-Zirconia (M3) FGM plate subjected to nonlinear (T_{NL}), linear (T_L) and constant (T_C) thermal loads based on (a) HSDT-12, (b) HSDT-9, (c) HSDT-5 and (d) FSDT displacement models. 141

NOMENCLATURE

x, y, z	Cartesian co-ordinate system for an FGM plate and is named as FGM plate axes
u, v, w	Displacement components along x, y and z directions respectively at any point (x, y, z) in the FGM plate space.
$\bar{u}, \bar{v}, \bar{w}$	Nondimensionalized quantities of u, v and w
u_0, v_0, w_0	Displacement components along x, y and z directions respectively at any point $(x, y, 0)$ in the FGM plate space.
θ_x, θ_y	Rotation of transverse normal at the plate mid-surface about y and x axes respectively
$u_0^*, v_0^*, \theta_z^*, \theta_z$	Higher-order membrane displacement components in the Taylor's series expansion corresponding to x, y and z directions respectively at any point $(x, y, 0)$ in the FGM plate space.
$\theta_x^*, \theta_y^*, \theta_z^*$	Higher-order flexure displacement components in the y, x and z directions respectively at any point $(x, y, 0)$ in the FGM plate space.
w^+	Transverse displacement at any point on the top surface of the FGM plate
$\sigma_x, \sigma_y, \sigma_z$	Normal stresses at any point in the plate with reference to the FGM plate axes.
$\bar{\sigma}_x, \bar{\sigma}_y, \bar{\sigma}_z$	Nondimensionalized quantities of σ_x, σ_y and σ_z
$\tau_{xy}, \tau_{yz}, \tau_{xz}$	Shear stresses at any point in the plate with reference to the FGM plate axes.
$\bar{\tau}_{xy}, \bar{\tau}_{yz}, \bar{\tau}_{xz}$	Nondimensionalized quantities of $\tau_{xy}, \tau_{yz},$ and τ_{xz}
$\epsilon_x, \epsilon_y, \epsilon_z$	Normal strains at any point in the plate with reference to the plate axes.
$\gamma_{xy}, \gamma_{yz}, \gamma_{xz}$	Shear strains at any point in the plate with reference to the FGM plate axes.
$\epsilon_{x_0}, \epsilon_{y_0}, \epsilon_{xy_0}, \epsilon_z$	Membrane strains at any point $(x, y, 0)$ in the plate with reference to the plate axes

$\varepsilon_{x_0}^*, \varepsilon_{y_0}^*, \varepsilon_{xy_0}^*, \varepsilon_{z_0}^*$	Higher-order membrane strains at any point (x, y, 0) with reference to the FGM plate axes.
$\kappa_x, \kappa_y, \kappa_{xy}$	Flexure strains at any point (x, y, 0) in the plate with reference to the plate axes.
ϕ_x, ϕ_y	Transverse shear strains at any point (x, y, 0) in the plate with reference to the plate axes
$\kappa_x^*, \kappa_y^*, \kappa_{xy}^*, \kappa_z, \kappa_{xz}^*, \kappa_{yz}^*$	Higher order flexure strains at any point (x, y, 0) in the plate with reference to the plate axes
$\kappa_{xz}, \kappa_{yz}^*, \phi_x^*, \phi_y^*$	Higher-order transverse shear strains at any point (x, y, 0) in the plate with reference to the plate axes
ΔT	Temperature gradient or Change in Temperature at any point (x, y, z) in the FGM plate space.
$T(x,y)$	Temperature distribution in the plane of the plate (x, y)
T_z	Temperature variation in an FGM plate across the thickness direction
T_{NL}, T_C, T_L	Nonlinear, constant and linear variations in temperatures across the thickness direction.
T_0, T_1	Temperature at bottom and top surface in an FGM plate.
E_z, k_z, α_z	Variation of young's modulus of elasticity, thermal conductivity and thermal coefficient of expansion in an FGM plate across the plate thickness direction
E_c, E_m	Young's modulus of ceramic and metal in an FGM plate respectively
k_c, k_m	Thermal conductivity coefficient of metal and ceramic in an FGM plate respectively
α_m, α_c	Thermal coefficient of expansion of metal and ceramic in an FGM plate respectively
ν	Poisson's ratio.
V_f	Volume fraction
p	Power law parameter.
Q_{ij}	Material stiffness matrix with reference to the plate axes.
D_M, D_B, D_S	Membrane, flexure and shear rigidity matrix respectively
D_C	Membrane – flexure coupling rigidity matrix

A, dA	Area and differential area of the FGM plate element respectively
V, dV	Volume and differential volume of the FGM plate element respectively
N, M, Q	Membrane, flexure and transverse shear stress resultant vector respectively.
N_T, M_T	Membrane and flexure stress resultant vector due to thermal effects respectively.
N_x, N_y, N_{xy}	Membrane stress-resultants at any point in the plate mid-surface with reference to the FGM plate axes.
$N_{x_T}, N_{y_T}, N_{xy_T}$	Membrane stress-resultants at any point in the plate mid-surface due to thermal effects with reference to FGM plate axes.
$N_x^*, N_y^*, N_{xy}^*, N_z, N_z^*$	Higher-order membrane stress-resultants at any point in the plate mid-surface with reference to the FGM plate axes.
$N_{x_T}^*, N_{y_T}^*, N_{xy_T}^*, N_{z_T}, N_{z_T}^*$	Higher-order membrane stress-resultants at any point in the plate mid-surface due to thermal effects
M_x, M_y, M_{xy}	Flexure stress-resultants at any point in the plate mid-surface with reference to the FGM plate axes.
$M_{x_T}, M_{y_T}, M_{xy_T}$	Flexure stress-resultants at any point in the plate mid-surface due to thermal effect with reference to the FGM plate axes.
$M_x^*, M_y^*, M_{xy}^*, M_z, M_z^*$	Higher-order flexure stress-resultants at any point in the plate mid-surface with reference to the FGM plate axes
$M_{x_T}^*, M_{y_T}^*, M_{xy_T}^*, M_{z_T}, M_{z_T}^*$	Higher-order flexure stress-resultants at any point in the plate mid-surface due to thermal effects with reference to the FGM plate axes
Q_x, Q_y	Transverse shear stress-resultants at any point in the plate mid-surface with reference to the FGM plate axes.
$S_x, S_y, S_x^*, S_y^*, Q_x^*, Q_y^*$	Higher-order transverse shear stress-resultants at any point in the plate mid-surface with reference to the FGM plate axes.
U	Internal strain energy of the FGM plate

Π	Total potential energy of the FGM plate.
W	Work done by external forces.
p_0	Amplitude of sinusoidal varying transverse mechanical load at the plate centre.
p_z^+	Transverse mechanical load applied on the top surface of the plate.
t	Superscript denoting transpose of a matrix/vector.
a, b	Plate dimensions.
h	Total thickness of the plate.
δ	Variational symbol

CHAPTER 1

INTRODUCTION

1.1 PRELIMINARY REMARKS

Laminated composite plates have established their potential applications in various sectors like aerospace, marine, medical, nuclear and automotive industries as well as in other fields involving advanced high performance materials. Developments in the field of materials have revolutionized the application of multilayered composites with a new innovative material called Functionally Graded Material (FGM). The smooth variation of thermo-mechanical properties in FGM was found to be most efficient in handling high temperature gradients than that of composite laminates. The rapid change in material properties at the laminate interface promotes the development of interlaminar stresses resulting in de-bonding of fibers and matrix, cracking and delamination effects at elevated temperatures. These problems can be mitigated in FGMs due to the smooth and continuous gradation of material properties through the thickness and hence finding major use in high temperature applications viz., rocket nozzles, heat exchange panels, space craft truss structures, bullet proof jackets, armor plates, combustion chamber components in aircrafts and automobiles.

FGM are the advanced composite materials formed by continuous change in composition of two or more constituent phases over a specified volume. FGMs can also be defined as a material which possesses gradual variations in thermo-mechanical properties due to material heterogeneity. The smooth gradation of physical properties can be either unidirectional or multidirectional and also it can be continuously or discontinuously varied between any two points or surfaces. Most commonly FGMs are used as a thermal coating or a heat shielding material to resist high temperature exposures and hence manufactured using ceramics and metals. A heat resisting ceramic material is used on high temperature side and the material composition is gradually graded to a tough metal with high thermal conductivity on the other side. Such bi-material graded composites can incorporate most of the advantageous

physical and chemical properties of both the materials, thereby increasing the bond strength, fracture toughness, thermal properties and also by reducing the interfacial stresses, thermal stresses, stress intensity factors and crack driving forces. Some of the commonly used FGMs are Monel-Zirconia, Aluminium-Silicon Carbide, Titanium Alloy-Zirconia, Aluminium-Alumina, Silicon Carbide-Carbon, Nickel-Zirconia, etc.

Structural analysis of FGM plates plays a vital role in predicting the static, dynamic and stability behavior of plates subjected to mechanical / thermal loads. The governing factors include thermo-physical properties, boundary conditions and applied mechanical/thermal loads. In the present investigation, a continuously graded, simply supported, ceramic-metal FGM plate subjected to thermal load is considered for the analysis. The static responses are examined for different temperature profiles, plate geometries and material compositions.

Most of the FGMs are found in high temperature resisting structural elements like thermal shielding materials, combustion chamber parts and space shuttle components involving very high surface temperatures of 2100K with a temperature gradient of 1600K across a section with less than 10mm thickness (Koizumi, 1997). Hence mathematical modeling and analysis of these structural elements under thermal environments have attracted substantial attention of researchers and consequently aiming in developing a precise, accurate and efficient theoretical model for thermo-elastic analysis of FGM plates.

Most of the modeling and analysis techniques used for FGM plates are the extensions of composite laminate / isotropic plates. Classical Plate Theory (CPT) based analysis was found to be inaccurate for FGM plate analysis, as it neglects the transverse deformation effects. Hence refined theories were developed by incorporating the effects of transverse shear stress/strain. The First Order Shear Deformation Theory (FSDT) commonly known as *Reissner-Mindlin's* plate theory assumes linear variations of transverse displacements/stresses and hence a shear correction coefficient has to be introduced to rectify the variation of shear stress/strain across the thickness of the FGM plate. These limitations of FSDT forced the development of higher-order refined theories. The second and third order theories involve additional

terms in the expression for the in-plane displacements which are parabolic and cubic respectively in thickness direction coordinate. These higher order theories consider the realistic parabolic variation of transverse shear stress through the plate thickness.

1.2 AIM AND SCOPE

Analytical modeling plays a vital role in the design and development of FGM plates because experimental studies are not feasible to evaluate the stresses and displacements, as the plate thickness is very small compared to the lateral dimensions. Also, investigations related to ultimate stress, critical buckling load, failure analysis, crack propagation, etc. can only be examined analytically but not experimentally. Therefore, in recent decades many publications have been reported on the analytical evaluation of thermo-elastic responses of FGM plates using various three-dimensional (3-D) and two-dimensional (2-D) theories. Though 3-D methods of analysis are found to be the most accurate, it is very difficult to obtain solutions for various plate geometries, loading and boundary conditions. Hence a 3-D plate problem has to be reduced to a 2-D plate problem using suitable assumptions and the accuracy of the assumed 2-D plate theory has to be established by comparing the results obtained using the theory with the 3-D exact elasticity solutions that are already reported in the literature. Then the most accurate 2-D theory can be formulated using Finite Element Methods (FEM) and can be further used for the development of commercial FEM packages.

It has been found from the literature that in all the earlier investigations the through the thickness temperature profiles assumed were either constant or linear. Moreover, most of the studies using various two-dimensional theories for the thermo-elastic analysis of FGM plates were confined towards establishing the accuracy of results obtained using a particular model developed based on any two-dimensional theory by comparing the results with that of three-dimensional exact solutions already available in the literature. Analytical evaluation of various two-dimensional higher order refined theories especially with higher order polynomial terms in the displacement fields (viz., HSDT12, HSDT9) using more realistic non-linear variation of temperature across the thickness (using heat conduction equation) in predicting the

different responses of FGM plates and also the evaluation with regard to their relative accuracy in predicting the displacements and stresses have not been reported yet. Owing to the above limitations, there is a need to evaluate analytically the various higher order refined theories for the thermo-elastic analysis of FGM plates subjected to different temperature profiles and to present the numerical results hitherto not reported in the literature. Keeping this in view the aims and objectives set for the present work are as follows:

1. To develop analytical formulations and solutions using a set of higher order refined theories with twelve and nine degrees of freedom for the thermo-elastic analysis of FGM plates.

2. To determine the various responses (Displacements, Stresses) of thermally loaded FGM plates subjected to different temperature profiles namely non-linear, linear and constant temperature.

3. To calculate the accuracy of the solutions obtained by comparing them with the three-dimensional elasticity solutions wherever available in the literature, for validating the accuracy of the displacement models considered in the study.

4. To evaluate the accuracy of the solution obtained in (1) in comparison to the accuracy of solutions obtained by independently developing the analytical formulations and solutions using other higher-order theory with five degrees of freedom and the first-order theory already available in the literature and by comparing the solutions of all the theories with exact 3-D elasticity solutions. The physical interpretation of the calculated results are discussed through various example problems.

5. To establish benchmark analytical solutions for the thermo-elastic analysis of FGM plates using various theories, material properties and temperature profiles considered in the present study.

For mathematical modelling purposes, the material properties are assumed to vary across the thickness direction of the plate based on power law function, while the in-plane variation is assumed to be isotropic. The temperature is assumed to vary sinusoidally along the plane of the plate, while its variation across the thickness can either be constant/linear or non-linear. One-dimensional steady state heat conduction

equation is used to obtain the nonlinear variation of temperature across the plate thickness.

The theories are applied to study the thermo-elastic response of FGM plates subjected to different temperature profiles explained above. For all the problems a simply supported plate is considered for the analysis. The equations of equilibrium using different displacement models are obtained using the Principle of Minimum Potential Energy (PMPE) and solutions in closed-form are obtained using *Navier's* solution technique by solving the Boundary Value Problem (BVP).

The scope of this study is restricted to small deformation thermo-elasto-static analysis of simply supported FGM plate using Power-Law variation of material properties and is subjected to constant, linear and nonlinear distribution of temperature profiles across the plate thickness.

1.3 LAYOUT OF THE THESIS

The extensive work carried out in this investigation to achieve the above mentioned aims and objectives is presented systematically in different chapters as follows:

Chapter 2 contains a detailed literature review of the research works concerning the different methods of analysis to evaluate the thermal stresses in FGM plates using various three-dimensional and two-dimensional plate theories. Based on the type of temperature distribution adopted in the analysis, this has been presented under three broad headings, viz., 1) Three dimensional temperature variation, 2) One dimensional nonlinear temperature variation, 3) One dimensional constant and linear temperature variation. Available literatures under both analytical and numerical methods are reviewed to give a clear picture of research work carried out on the thermo-elastic analysis of FGM plates.

Chapter 3 contains a list of various displacement models (theories) used in the present investigation. Detailed theoretical formulation is presented for HSDT-12 displacement model only for brevity sake. Following the similar procedure adopted for the model HSDT-12, the equilibrium equations obtained for the thermo-elastic analysis using all other displacement models are given in Appendix - I.

In Chapter 4 analytical solution method using *Navier's* solution technique is presented in detail for the thermo-elastic analysis of simply supported FGM plates using HSDT-12 displacement model only. The same procedure is used to obtain solutions using all other displacement models. The elements of the plate stiffness matrices $[A]$, $[A']$, $[C_T]$, $[B]$, $[B']$, $[D]$, $[D']$, $[E]$, $[E']$, the coefficient matrix $[X]$, and the elements of thermal force matrix $\{F_T\}$ using different displacement models are given in Appendices II, III and IV respectively.

In Chapter 5 numerical results and discussion are presented for the thermo-elastic analysis of FGM plates. The results obtained using various displacement models are first compared with the available three dimensional elasticity solutions. After establishing the accuracy of the model, parametric studies are performed for Monel-Zirconia, Titanium Alloy-Zirconia and Aluminium-Alumina FGM plates. Benchmark results are presented for nonlinearly, linearly and constantly varying temperature profiles across the plate thickness.

Chapter 6 contains the general conclusions that are drawn from the present investigation using the four computational models and also the suggestions for future work.

CHAPTER 2

LITERATURE REVIEW

2.1 PRELIMINARY REMARKS

Generally, FGMs are the nonhomogeneous particulate composites formed by continuous gradation of constituents with variable composition profile, which can be tailored to achieve desired strength and stiffness. The concept of FGM was first introduced at National Aerospace Laboratories of Japan in 1984 to create a thermal barrier material for a space shuttle, which can withstand high surface temperature of 2100K with a temperature gradient of 1600K across a 10mm thick section. Often FGMs are used in structures where extreme temperatures gradients are involved, due to which structure confronts to sudden stretching and bending forces. Therefore it is very important to understand the deformation characteristics and stress distribution pattern for a wide range of temperatures. A remarkable effort has been devoted in the recent decades for the development of computational models for studying the responses of FGM structural elements/plates subjected to thermal loads. Many mathematical modelling techniques with various degrees of freedom have been evolved. Most of these theories are extensions of the models used in the analysis of composite laminates/ isotropic plates. Thus various approaches used for the modelling and analysis of FGM plates can be grouped into the following categories:

- (1) Three-dimensional (3-D) elasticity theory
- (2) Two-dimensional (2-D) plate theories
 - a) Classical Plate Theory (CPT)
 - b) First-Order Shear Deformation Theories (FSDTs)
 - c) Higher-Order Shear Deformation Theories (HSDTs)

The exact solutions to boundary value problem using three-dimensional elasticity theories are very difficult and tedious to solve. Analytical solutions to 3-D elasticity

equations would not be feasible for plates with complex geometries and boundary conditions. Further, solutions to functionally graded plates will still get complicated with the use of power law function and three dimensional variations in temperature. Therefore 3-D elasticity theories are simplified by making suitable assumptions based on kinematics of deformation and constitutive behaviour, called as 2-D plate theories. Most of these theories are reported in the literature and are based on displacement fields and stress functions. The Classical Plate Theory (Reissner and Stavsky 1961) which is an extension of Classical Plate Theory (Timoshenko and Woinowsky-Krieger 1959, Szilard 1974) neglects the effect of out-of-plane strains. It was observed that the CPT fails to predict accurately the static and dynamic response in the case of FGM plates which are rather thick and/or exhibit high anisotropy ratios. Thus the CPT is not suitable for modelling of FGM plates. Theories which include the effects of transverse shear deformation effect and at times the transverse normal strain effect become necessary. First-order shear deformation theory based on Reissner (1945) and Mindlin (1951) assume linear displacement and/or stress variation across the plate thickness direction. Since FSDT account for constant transverse shear stress, shear correction coefficients are needed to rectify the unrealistic variation of the shear strain/ stress through the thickness. Whitney and Pagano (1970) was the first to use FSDT for the static analysis of laminated composite plates. The limitations encountered in FSDT have been resolved in HSDTs by using higher-order terms in the Taylor's expansions of displacements in the thickness coordinate. The second and third-order theories involve additional terms in the expression for in-plane displacements which are parabolic and cubic respectively in thickness direction. Kant (1982) was the first to derive the complete set of variationally consistent governing equations for the flexure of a symmetrically laminated plate incorporating both distortion of transverse normal and effects of transverse normal stress/strain by utilizing the complete three-dimensional generalized Hooke's law. Reddy (1984b) derived a set of variationally consistent equilibrium equations for the kinematic models originally proposed by Levinson (1980) and Murthy (1981). Rohwer et al. (2001) were the first investigators to report the significance of using higher order polynomials for the displacement fields for the thermo-elastic analysis of laminated composite plates. Later, Kant and Swaminathan (2002), Swaminathan and

Ragounadin (2004), Swaminathan et al. (2006), Swaminathan and Patil (2007) presented analytical formulations and solutions using higher order refined computational models for the stress analysis of composite and sandwich plates. The deformation patterns of transverse normal according to various theories are represented in Fig. 2.1.

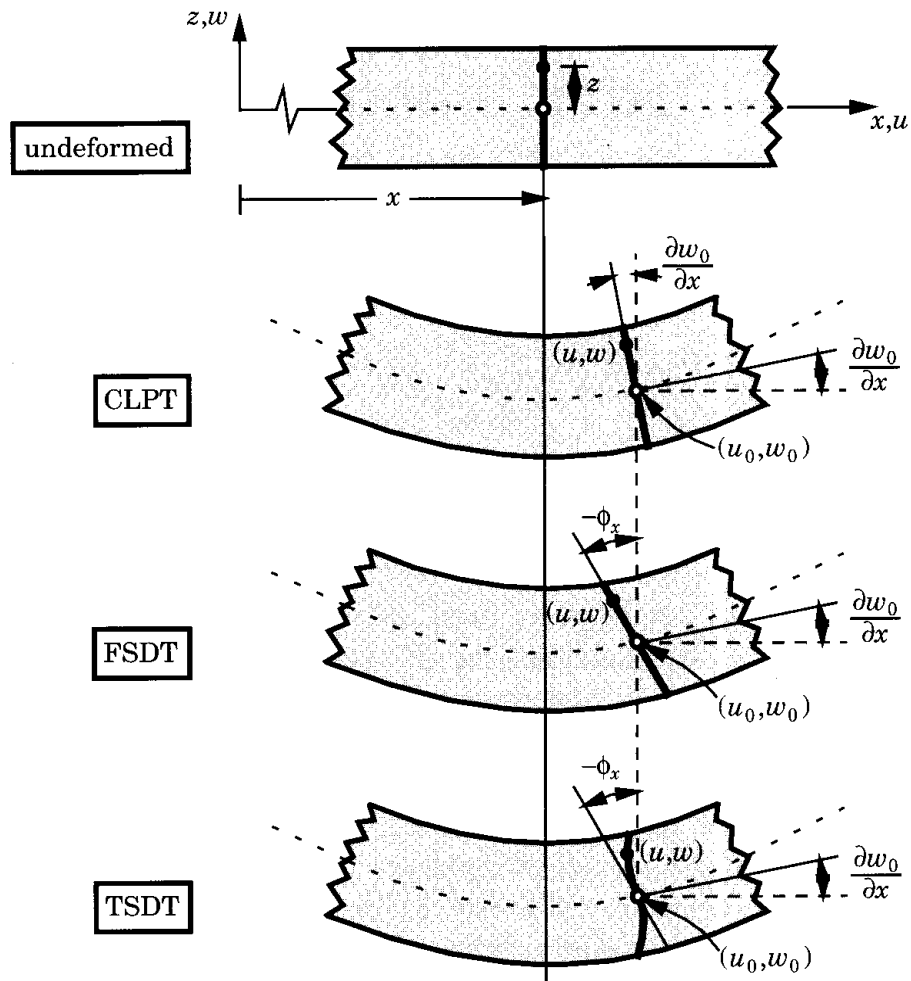


Fig. 2.1. Deformation patterns of transverse normal according to the CLPT, FSDT and TSDT. (Reddy, 1996)

The above theories that are discussed for laminated plates are extended for modelling and analysis of FGM plates. Extensive investigations are reported in the literature on the evaluation of various responses of FGM plates subjected to high temperature gradients. Tanigawa (1995) reviewed the developments related to thermo-elastic

analysis of FGMs till the year 1995. It was found that the behaviour of FGMs can be predicted more accurately through precise modeling of material nonhomogeneity and thermal field. Markworth et al. (1995) discussed the various techniques that are involved in modeling the microstructure dependent thermophysical properties of FGMs. Based on review, some modeling methods were recommended for additional studies and hence few approaches for the improvement were also suggested. The behaviour of crack-tip fields in an FGM were dealt by Jin and Batra (1996) and its fracture related problems were summarized based on crack-bridging concept and rule of mixture. Jha et al. (2013) presented a review on aero thermo elastic and vibration analyses on FGMs since 1998, in which historical development and its application were also discussed. Swaminathan et al. (2014) presented a critical review of various three dimensional and two dimensional theories based on analytical and numerical methods; and its solution techniques that are employed for the stress, vibration and buckling analyses of FGM plate subjected to mechanical and thermomechanical loads. Thai and Kim (2015) reviewed various theories like CPT, First Order Shear Deformation Theory (FSDT), Third Order Shear Deformation Theory (TSDT), Higher Order Shear Deformation Theory (HSDT), Simplified Theories, Mixed theories, three dimensional elasticity theories and CUF based models that are used for modeling and analysis of FGM plates and shells. Wu and Liu (2016) presented an overview of various semi-analytical numerical methods like Finite Layer Method, State Space Method (SSM), Asymptotic Method, Sampling Surface method (SAS), that are adopted for the analysis of laminated composite and sandwich functionally graded elastic/piezoelectric materials plates and shells for various combination of boundary conditions and micro mechanical schemes. In recent years, significant research works have been published in analysis of FGM plates exposed to thermal environments. In the following sections, an attempt has been made to include all the important contributions related to thermal stress analysis of FGM plates and the classification of all the available literature is done based on the different type of temperature distribution as given below. The various analytical and numerical methods are dealt in subsections.

1. Three dimensional temperature variation

2. One dimensional nonlinear temperature variation
 - a. Analytical methods
 - b. Numerical methods
3. One dimensional constant and linear temperature variation
 - a. Analytical methods
 - b. Numerical methods

2.2 THERMAL STRESS ANALYSIS

The developments related thermal stress analysis of FGM plates are discussed based on the type of temperature profile used for obtaining the solution. Generally, 3-D exact methods adopt three dimensional distribution of temperature field which can be obtained by solving heat equation. But 2-D plate theories adopt one dimensional distribution of temperature field which varies only across the plate thickness direction and can be assumed as constant, linear or nonlinearly varying. Thus various research works related to the current study are presented in the following sequence: three dimensional variation of temperature, one dimensional nonlinear variation of temperature and one-dimensional constant and linear variation of temperature which includes three-dimensional (3-D) elasticity theory, two-dimensional (2-D) plate theory, finite element methods and meshless methods.

2.2.1 Three Dimensional Temperature Variation

Three dimensional elasticity solutions formulated based on 3-D temperature profiles were found to be the most accurate methods for thermal analysis of FGM plates. Mian and Spencer (1998) developed 3-D elasticity solutions for an inhomogeneous plate across the thickness direction based on the two dimensional solutions of classical thin plate theory for the equivalent plate. Theoretical formulations and solution methods were presented for rectangular, cylindrical polar coordinates systems and radially symmetric systems. Reddy and Cheng (2001a, 2001b) adopted asymptotic technique for square and smart FGM plates with piezoelectric actuators subjected to thermal and mechanical loads. It was found that the assumption of constant transverse displacement across the plate thickness is not valid for plates subjected to thermal loads and the maximum longitudinal compressive stress appears at the top surface of

the plate. Wang et al. (2016) obtained asymptotic solutions for thin FGM plates subjected to sudden change in temperature at the boundary based on Lord and Shulman theory (L–S theory) with power law distribution of material properties. Vel and Batra (2002) used power series method to study the thermomechanical deformations of a simply supported rectangular plate, in which the material properties were evaluated using either self consistent method or Mori-Tanaka method or the combination of both. Parametric studies were performed and a comparative study with CLPT, FSDT and HSDT models was presented. Significant difference was observed in displacements and stresses obtained using exact solutions and 2-D plate theories. It was observed that the results obtained using different material schemes agree qualitatively but differ quantitatively. Later this work was extended to study transient thermal stresses by Vel and Batra (2003), in which the transient longitudinal stress was found to be nearly eight times greater than the steady state value for rapid time dependent surface temperature condition. Ootao and Tanigawa (1999) adopted exponential variation of material properties to study the transient thermal stresses in a simply supported rectangular FGM plate subjected to partial heat supply. The work was extended to study the plate behaviour under non-uniform heat supply by Ootao and Tanigawa (2005, 2007). Analytical formulations were developed using heat conduction, Laplace and Finite cosine transformations and the solutions were obtained using series expansion of Bessel functions. It was found that the most precise evaluation of transverse stresses is possible in transient state. Further, Ootao and Ishihara (2013) adopted piece wise exponential law to study the response of two and three layered rectangular plate models. It was concluded that the maximum value of thermal stresses can be reduced by using multi layered FGM plates instead of single layered FGM plates in transient analysis. Xu et al. (2010) presented exact thermo-elastic solutions for a simply supported exponentially graded rectangular plate with variable thickness using double fourier sinusoidal series expansions. Thermo elastic solutions for circular FGM plates subjected to axisymmetric loads were studied by Jabbari et al. (2014).

Ying et al. (2009) developed semi-analytical solutions for a FGM plate with one pair of opposite edges simply supported using State Space Method (SSM). Solutions for

Mori-Tanaka FGM plates were obtained using Levy's method and Differential Quadrature Method (DQM), which makes it feasible to treat non-simply supported edges. Alibeigloo (2010) obtained 3-D elasticity solutions for an exponentially graded rectangular plates with simply supported edges using Fourier series and SSM technique. Further, it was extended for solid and annular circular FGM plates by Alibeigloo (2012) and for sandwich circular plate with a layer of FGM core by Alibeigloo (2016). Analytical solutions for various support conditions were obtained using DQM technique. It was observed that, the neutral surface and middle surface will not coincide with each other and it depends on the variation of young's modulus of elasticity across the plate thickness. Liu and Zhong (2011) presented Peano-Baker series solution for an orthotropic simply supported and isothermal functionally graded rectangular plate based on SSM method. It was observed that the material gradient distribution significantly effects the total stiffness, deflection and temperature field distribution of the plate. Jiang et al. (2017) developed analytical solution for three-dimensional steady thermodynamic analysis of a piezoelectric laminated plate using refined plate theory and Galerkin method. It was concluded that considering geometrical nonlinearity would enlarge the stiffness of the piezoelectric laminated plate and thus decreasing the magnitude of deflection and stresses.

2.2.2 One-Dimensional Nonlinear Temperature Variation

Most of the two-dimensional theories adopt nonlinear or parabolic variation of temperatures across the plate thickness which are either based on heat conduction equation or polynomial functions. The related studies are discussed under two categories namely, analytical and numerical methods. The various analytical methods using either two or three dimensional theories are presented under analytical methods whereas the finite element and the meshless methods are dealt under numerical methods.

2.2.2.1 Analytical Methods

Tanigawa (1993) used transient heat conduction problem to study the associated thermal stress problems for a nonhomogeneous FGM plate. Thereafter optimization problems were discussed in order to obtain optimum material composition for the

purpose of reducing the thermal stress distribution. Noda and Jin (1993) discussed stress intensity factors relating to crack development in an exponentially graded FGM plates subjected to prescribed surface temperature and its responses due to thermal shock were dealt by Jin and Noda (1994). It was found that, the crack close to heating side of the strip will be more likely to be unstable than that of the cooling side. Noda (1999) discussed crack propagation path, thermal stresses and thermal stress intensity factors in FGM plates subjected to steady state temperature fields and thermal shocks. Significant decrease in stresses was observed by adopting a precise and appropriate gradation of material properties. Ravichandran (1995) studied the effect of residual thermal stresses that arises during the fabrication of FGM system. Both temperature dependent and independent gradation forms were evaluated for continuous and discrete change in composition across the thickness direction. It was found that, the residual stresses can be decreased by adopting multiple layers of FGM (greater than 11) plates with constant composition and thickness. Bouchafa et al. (2010) employed exponential gradation of material properties to evaluate residual thermal stresses in $\text{Al}_2\text{O}_3\text{-Ni}$ FGM system. It was concluded that, the magnitude of stresses increases by adding a fully ceramic or metal surface in the middle of graded regions and hence should be kept minimum to avoid cracking at interfaces.

A new higher order micromechanical theory for FGM plates “HOTFGM” which includes both local and global effects have been developed by Aboudi et al. (1994a,1994b). The accuracy of the method has been established and proved to be efficient tool for the analysis of FGM plates. Theoretical formulations were developed in cartesian-coordinate system with temperature gradient across the thickness direction. The theory was extended by Aboudi et al. (1995a, 1995b) to incorporate partial homogenization scheme normal to the functionally graded direction and temperature dependent response of the constituent phases respectively. Further it was extended to develop a two dimensional frame work for modeling FGM plates by enabling nonuniform spacing of fibers in two directions by Aboudi et al. (1996).

Reddy (2000) developed analytical formulations and Navier’s solutions for a simply supported rectangular FGM plates which accounts the effects of thermomechanical coupling, time dependency and geometric nonlinearity. The response of plates has

been studied using HSDT and FSDT models for various loading and boundary conditions. Woo and Meguid (2001) studied large deflection in FGM plates subjected to steady state temperature field under different types of thermomechanical loads. The nonlinear bending responses were investigated by Shen (2007), for simply supported FGM plates with or without piezoelectric actuators and subjected to both thermal and electrical loads. Also, Yang and Huang (2007) obtained asymptotic solutions for nonlinear transient response of FGM plates with initial geometric imperfections using improved perturbation technique. It was found that, the effect of heat conduction and temperature dependency could not be neglected while evaluating the response of FGM plates. Brischetto et al. (2008) presented Unified Formulations (UF) for simply supported rectangular plates subjected to steady state thermal loads. The accuracy with the exact solutions was achieved by using higher order expansion terms across the thickness coordinate. Asymptotic solutions were formulated by Zhao et al. (2008) for an infinite sandwich plate with double sided FGM coatings under convective boundary conditions to investigate transient heat conduction and thermal stresses. Some design rules were suggested for FGM cutting tools to resist high thermal shocks. Based on layerwise theory and perturbation technique, Tahani and Mirzababae (2009) derived solutions for cylindrical bending of FGM plates subjected to mechanical, thermal and thermomechanical loads. Significant increase in the magnitude of transverse deflection was observed due to the effect of geometric nonlinearity. Zenkour (2010, 2012) used Sinusoidal Shear Deformation Theory (SSDT) to formulate solutions using power law function and exponentially function for FGM plates subjected to hygro-thermo-mechanical loads respectively. Polynomial form of temperature profile was assumed to evaluate static bending response of the plate and hence the effects of temperature and moisture concentrations were discussed. Further, the studies were extended for FGM sandwich plates by Zenkour and Alghamdi (2010) and the results obtained from SSDT were compared with HSDT, FSDT and CPT. Fahsi et al. (2012), Boudierba et al. (2013) and Zidi et al. (2014) adopted a new four variable refined theory to study the bending behaviour of FGM plates subjected to thermomechanical loads with or without resting on elastic foundations. Further, the work was extended by Houari et al. (2013) and Tounsi et al. (2013) for FGM sandwich plates. The accuracy of theory was established by

comparing the results with various other theories that were reported in the literature. Mantari and Granados (2015) obtained analytical solutions using quasi-3D hybrid type HSDT with six unknowns for FGM sandwich plates subjected to generalized nonlinear temperature field. The deflections and stresses were found to be highly sensitive to polynomial forms adopted to define the temperature field. Ramos et al. (2016) investigated thermoelastic response of a simply supported rectangular FGM sandwich plates using Unified Formulations, which includes several shear strain shape functions related to non-polynomial displacement fields like sinusoidal, hybrid and hyperbolic deformation theories. Later, the author proposed a new set of plate theories and by performing comparative studies it was revealed that, these theories are effective in predicting similar results as that of classical polynomial based functions. Dong and Li (2017) developed unified nonlinear analytical solutions for simply-supported FG rectangular plates subjected to thermal load using temperature dependent material properties. Effects of material heterogeneity and thermal load are discussed using various higher order shear deformation theories and mathematical models based on P-FGM, S-FGM and E-FGMs. Li et al.(2017) adopted four variable refined theory to study the responses in FGM sandwich plates with face sheets and core. It was observed that the power index p and inhomogeneity parameter k play an important role in eliminating interface problems of sandwich plates and thus the stresses distributions remain continuous throughout the plate thickness.

Cheng and Batra (2000) presented 3-D solutions using Mori-Tanaka estimation and asymptotic scheme to study the thermomechanical deformations of a rigidly clamped FGM elliptical plate. Behravan and Shariyat (2016) and Behravan (2015) used semi-analytical methods for the thermo-elastic analysis of exponentially graded plates circular/ annular plates subjected to asymmetric loads and plates resting on gradient hybrid foundation respectively. The influence of thermal gradient index on displacement and stresses were found to be more than the elastic grading indices. Nosier and Fallah (2008) reformulated the bending and extension equations of Mindlin–Reissner plate theory by relating to interior and edge zone problems of FGM circular plates. The nonlinear behaviour of FGM circular plates subjected to asymmetric thermo-mechanical loads were studied by Fallah and Nosier (2012) for

various combinations of clamped and simply supported boundary conditions. Zhang and Zhou (2015) used HSDT with multi-term Ritz method to evaluate the nonlinear bending response of FGM circular plates. Temperature dependent material properties are assumed according to power law function and solutions obtained for three different cases of temperature fields. Kiani (2016) analyzed steady state thermo-elastic response of rotating functionally graded nanoplates using surface elasticity approach. Static bending problems in a thermally stressed annular and circular micro plates were discussed by Eshraghi et al. (2016) using DQM. The effect of influencing factors like applied loads, plate geometry ratios and material inhomogeneity were discussed. Yang et al. (2017) carried out thermo-mechanical bending analysis of functionally graded polymer nanocomposite circular and annular plates reinforced with the graphene nanoplatelets (GPLs) by employing three-dimensional elasticity theory and the generalized Mian and Spencer method. It was observed that, among the three GPL distribution patterns adopted the parabolic distribution provides the best reinforcing effect with smallest deflection, followed by uniform then linear distribution patterns

2.2.2.2 Numerical Methods

Tanaka et al. (1993a) presented a new thermoelastic material design called Mori-Tanaka's theory to reduce thermal stresses in FGM plates. Incremental finite element methods with direct sensitivity analysis and optimization techniques were used to arrive at the optimal volume fraction of phases in FGM. Further, Tanaka et al. (1993b) discussed improved solutions, which considered multiple design parameters and accounted volume fraction dependence of material properties to estimate the micro structural behaviour. The differences in optimized stresses predicted using Mori-Tanaka's theory was found to be small, because it predicts a lesser value of ceramic rich FGM phase. Reddy and Chin (1998) performed parametric studies on FGM cylinders and plates subjected to abrupt thermal loads using power law function. Thermomechanical coupling effects were discussed by comparing the results of coupled and uncoupled formulations. The static and dynamic thermo-elastic responses for FGM plates including geometric nonlinear effects were discussed by Praveen and Reddy (1998) and for FGM cylinders exposed to rapid heating conditions by Praveen

et al. (1999). FEM models based on HSDT were developed by Reddy (2000), which accounted the time dependency effect along with thermomechanical coupling and geometric nonlinearity. Cho and Oden (2000) presented parametric studies for thermally stressed FGM plates using Crank-Nicolson-Galerkin scheme. Significant difference was observed in the thermal characteristics of transient and steady-state responses. Apalak and Gunes (2005) adopted eight noded isoparametric multilayered finite element to study the effect of thermal residual stresses and discussed the method to determine optimum material composition to reduce the effect of stresses. Muliana (2009) introduced a new micromechanical modeling method by idealizing the spatial distribution of spherical particles in a homogeneous matrix for predicting the thermo-visco-elastic response of FGM plates. Static and dynamic characteristics of Reissner–Mindlin plates were studied using Non-Uniform Rational B-spline (NURBS) based iso-geometric FEM by Valizadeh et al. (2013) and cell-based smoothed FEM with discrete shear gap technique by Natarajan et al. (2014) for Mori-Tanaka FGM plates. Gulshan-Taj et al. (2013) used HSDT with C^0 continuous isoparametric Lagrangian finite element with seven degrees of freedom at each node to study the static response of FGM skew plates. Kulikov and Plotnikova (2015) dealt with the implementation of sampling surfaces method and state space method to study the response of laminated FGM plates. In three dimensional stress problems, convergence of results was observed by introducing sampling surfaces inside each layer at Chebyshev polynomial nodes. Thai et al. (2016) presented shear and normal deformation theory with four unknown variables to predict the static and dynamic response of FGM isotropic and sandwich plates using both Mori-Tanka and power law homogenization schemes. FEM formulations were developed using NURBS based isogeometric analysis and are discretized using C^1 continuity of displacement field. The accuracy of the model has been established by comparing with various other models. Pandeya and Pradyumna (2017) developed FEM formulations for FGM sandwich beams subjected to thermal shock using layerwise higher order theory to study the transient stresses under various geometric and thermal boundary conditions.

In recent decades, many investigations have been reported based on meshless or meshfree based interpolation methods. Dai et al. (2005) presented dynamic response

of FGM plates with piezoelectric sensors and actuators based on FSDT, and by using element free Galerkin method and Moving Least Square method with C^1 continuity. Golmakani and Kadkhodayan (2011) studied nonlinear large deflections of circular and annular plates using power law function for temperature dependent and temperature independent variation of material properties across the plate thickness. The solutions for FSDT model were obtained using dynamic relaxation method (DRM) and finite difference discretization technique. It was concluded that, the value of deflections and stresses predicted for plates with simply supported edges are greater than for plates with clamped edges. Wu et al. (2012) used meshless collocation method based on the differential reproducing kernel (DRK) interpolation technique for the analysis of multilayered FGM electro-thermo-elastic plates. Edge cracking of FGM plates subjected to thermal shock has been discussed by Burlayenko et al (2016). A meshless local Petrov–Galerkin (MLPG) approach have been adopted by Sladek et al. (2013) for the bending analysis of circular piezoelectric FGM plates under static and transient dynamic mechanical and thermal loads. The physical quantities were approximated using Moving Least Square method and Local integral equations. It was concluded that, the mechanical deflection and electric potential are highly influenced by gradation of thermal expansion coefficient rather than other parameters. Jafarinezhad and Eslami (2017) performed parametric studies on an annular FGM annular plate subjected to lateral thermal shock load using FSDT and Galerkin finite element method. The differences in the solutions obtained using coupled and uncoupled theories are found to be very much different from each other and the effect of large coupling coefficient has a major impact on the dynamic behavior of the plate. Burlayenko et al. (2017) presented formulations and theoretical framework to develop a graded finite element which can be applied for a coupled thermo-mechanical analysis of FGM plates.

2.2.3 One-Dimensional Constant and Linear Temperature Variation

Few researchers carried out thermal stress analysis of FGM plates subjected to either constant or linearly varying temperatures across the plate thickness. Some of the articles dealing with the evaluation of both linear and nonlinear temperature profiles are already discussed in the previous sections and hence for brevity they are not dealt

here again. Based on the method of analysis, the reported research studies are grouped under two sections namely analytical and numerical methods.

2.2.3.1 Analytical Methods

Fukui et al. (1993) studied thermal stresses for a thick walled FGM tubes subjected to uniform thermal loads. It was found that the, distribution of stresses and strains mainly depends upon the gradation of components in the radial direction. Tsukamoto (2003) presented combined micro- and macro-mechanical approaches, for the analyses of an FGM plate subjected to transient thermal stresses. In-plane and out-of-plane micro stresses were derived using Eshelby's equivalent inclusion method and Mori-Tanaka's mean-field approximation, and the macro-mechanical analysis is carried out based on the CPT. The significance of considering inelastic deformations for elastic, elastic-plastic and elastic-plastic-creep analysis has been discussed. Chung and Chang (2008) obtained Fourier series solutions for a simply supported rectangular plates using CPT by considering power-law function, exponential function and sigmoidal function for material property variations. It was observed that FGMs based on sigmoidal functions are most sensitive to the variations in the ratio of thermal coefficient of expansions than that of power-law and exponential based functions.

Shen (2002) considered temperature dependence of material properties to study the nonlinear bending response of a simply supported rectangular FGM plate. Governing equations were derived for HSDT and the solutions were obtained using mixed Galerkin-perturbation technique. This work was extended by Yang and Shen (2003) for combined mechanical and thermal loads with different boundary conditions. It was found that the material gradation, volume fraction, temperature variation, plate geometry, boundary conditions, transverse shear deformations have significant effect in determining the nonlinear bending behaviour of FGM plates, while the effect of in-plane constraints were negligible. Matsunaga (2009) adopted higher order shear deformation theory for the thermal stress analysis of a simply supported FGM plate subjected to constant and linear variation of thermal loads. The effect of geometric nonlinearity in FGM plates were examined by Kumar et al (2011). It was observed that nonlinear deflections were more in plates subjected to thermal loads. Analytical

and numerical models were developed by Sadowski et al. (2015) to study the response of structural elements under thermal and mechanical loads. Accuracy of solutions obtained by analytical formulations and finite element methods were found to be in good correlation with each other. Trinh et al. (2017) adopted general quasi-3D and higher-order shear deformation models to study the mechanical and thermal behaviours of FG sandwich microplates. It was observed that, the thickness stretching thermal strain induces out- of-plane thermal load in the thermal analysis which leads to the higher deflections and stresses.

2.2.3.2 Numerical Methods

Apalak and Gunes (2005) discussed the effect of residual stresses in FGM plates using 3D eight noded isoparametric multilayered finite element with three degrees of freedom at each node and with 2500 layers through the plate thickness. Bhandari and Purohit (2015) adopted eight-node quadratic Lagrange element and performed comparative studies on FGM plates subjected to thermomechanical loads for different material gradient laws (power-law function, exponential function and sigmoidal function) and boundary conditions (simply supported, clamped, free and combined) using FSDT. The deflections and stresses were found to remain closer to each other with increase in power law parameter in FGM plates with sigmoidal function than that of other material gradation laws. Natarajan and Ganapathi (2012) considered QUAD-8 shear flexible element to study the bending behaviour of sandwich plates using zig-zag functions. The accuracy of HSDT with 13 degrees-of-freedom at each node was established by comparing the results with other lower order models with 11, 9 and 5 degrees of freedom at each node. Sadowski et al. (2015) investigated mechanical and thermal responses of structural elements using finite element method for an airplane made of FGM. Comparative studies were performed with simplified analytical models and a good conformability between the two methods was established. Bui et al. (2016) developed FEM formulations to study the static bending behaviour of heated FGM plates using HSDT and power law function. Parametric studies were performed using ZrO_2/SUS_3O_4 , Al_2O_3/SUS_3O_4 and Si_3N_4/SUS_3O_4 FGM plates with different shape configurations. Due to the nonlinear behaviour of

constituent phases and thermal expansion coefficients, the response predicted by ZrO_2/SUS_3O_4 was found to be quite different from other materials.

2.3 FINAL REMARKS

A literature review of various approaches used for the thermal stress analysis of FGM plates has been presented in the preceding section. The general remarks from the current literature survey are as follows:

1. The majority of the methodologies used for the investigation of FGM plates are the extensions of the similar methodologies used either for laminated composite plates / isotropic plates.

2. As a result of the coupling between bending and stretching, analytical evaluation of static responses in FGM plates is exceptionally difficult, unless plate is simply supported.

3. Three-dimensional theories can predict the three-dimensional stress state at the boundaries more accurately than the 2-D plate theories, but their solution methods involve mathematical complexities and are very difficult and tedious to solve.

4. Based on suitable assumptions, several 2-D plate theories were developed and are used to investigate the thermal response of FGM plates. However, CPT, FSDT and most of the higher order theories considers only transverse shear deformation effects. But to obtain accurate results in thermal analysis of FGM plates, the effect of both transverse shear and transverse normal deformation are very important.

5. Several investigations are reported on analytical evaluation of FGM plates subjected to thermal loads using CPT and FSDT. It was observed that CPT fails to predict accurate responses, whereas FSDT can provide reasonable accurate results by using shear correction factor to rectify the nonlinear variation of shear stress/ strain through the plate thickness.

6. It has been concluded that, accurate prediction of thermal plate responses using 2-D plate theories is only possible by using higher order polynomials in the in-plane and transverse displacement expressions.

7. Exact solutions for the thermo-elastic analysis of FGM plates are still not yet reported for simply supported FGM plates with power law variation of material properties and steady state heat conduction type variation of temperature.

8. Micromechanical modelling methods adopted for the estimation of material property gradation plays a vital role in predicting the structural behaviour of FGM plates. The volume fraction index and anisotropy of the constituent phases are the important factors which governs the material nonhomogeneity of FGM plates, which further complicates the solution.

9. The distribution of temperature field has a direct impact in predicting thermal response of FGM plates. Therefore during thermal analysis, three dimensional evaluation of temperature field is found to be the most appropriate method for obtaining accurate results. But obtaining solutions using 3-D heat conduction equation is very complex in nature and hence in most of the 2-D plate analysis it is reduced to one dimensional heat conduction equation, by assuming temperature variation only across the plate thickness direction and in-plane being either constant / sinusoidal. Several other forms of one dimensional temperature distributions are also reported namely; constant distribution, linearly varying, polynomial form of variation, etc.

10. In most of the two-dimensional theories developed till date, the accuracy of the solutions obtained using a particular theory was established by comparing them with the results of three-dimensional elasticity theory, and a very few studies are reported on the analytical evaluation of various higher order theories in predicting the thermo-elastic responses of FGM plates subjected to different temperature profiles through the thickness.

11. Because of complexities, analytical solutions for FGM plates exist for plates with simple geometry, loading and boundary conditions. Therefore more

emphasis has been placed on the use of numerical methods especially when the FGM plate problem involves complex geometry, loading and boundary conditions.

12. 3-D thermal analysis of FGM plates using numerical methods (FEM/Meshless) requires large computer core memory, computational effort and time as compared to 2-D thermal analysis. Thus reducing a 3-D plate problem to a 2-D plate problem can drastically reduce the cost incurred in the analysis with little compromising in the accuracy of results.

13. Meshless methods have been proved by various researchers as one of the best alternative to FEM methods for thermal analysis of FGM plates. But few difficulties in computational methods, handling the boundary conditions and the temperature effects still have to be resolved in meshless methods.

Most of the analytical 2-D higher order theories discussed till date consider only transverse shear deformation effect and neglects normal deformation effects. But in thermal analysis of FGM plates, the higher order polynomials in the transverse displacement field plays a crucial role in predicting accurate results closer to that of 3-D exact solutions. Therefore in the present investigation, analytical formulations are developed for higher order displacement model with twelve degrees (HS-DT-12) of freedom which includes the effect of transverse shear and normal stress/ strain. Material modelling based on power law function and temperature profile based on steady state heat conduction equation is not reported for simply supported flat panels and hence adopted in the present study. Comparative studies using various displacement models, material sets and temperature profiles that are already reported in the literature are also included in the present investigation to emphasize the accuracy of HS-DT-12 displacement model in predicting thermal responses in an FGM plate.

CHAPTER 3

THEORETICAL FORMULATIONS

3.1 PRELIMINARY REMARKS

In this chapter a set of higher-order refined theories and their theoretical formulations are presented for thermal stress analysis of geometrically thin and thick FGM plates. The displacement model with 12 degrees-of-freedom (dof) includes the effect of both transverse shear and normal strain/stress and the other model with 9 degrees of freedom considers the effect of transverse shear deformation only. In addition to above, another higher-order theory and the first-order theory both having five degrees of freedom developed by other investigators and reported in the literature are also considered. The theoretical formulation using the displacement model with 12 dof is presented in detail. The governing equations of equilibrium using various theories for the thermo-elastic analysis are derived using the Principle of Minimum Potential Energy (PMPE). Rule of mixtures based on Power-Law estimation is used to obtain the effective material properties across the thickness of the FGM plate. Through the thickness variation of temperature is assumed to be nonlinear and obeys one dimensional steady state heat conduction equation. Along with this constant and linearly varying temperatures across the plate thickness are also considered during the study. The complete theoretical formulations for the thermo-elastic analysis of FGM plates based on the Higher Order Shear Deformation Theory with twelve degrees of freedom (HSDT-12) only are presented in detail in the following sections.

3.2 DEFINITION OF DISPLACEMENT FIELD

The Taylor's series expansion method is used to deduce a two-dimensional formulation of a three-dimensional elasticity problem (Hildebrand et al. (1949)) and the following set of equations are obtained by expanding the displacement components $u(x, y, z)$, $v(x, y, z)$ and $w(x, y, z)$ of any point in the FGM plate in terms of the thickness coordinate, z , viz.,

$$\begin{aligned}
u(x, y, z) &= u(x, y, 0) + z \left(\frac{\partial u}{\partial z} \right)_0 + \frac{1}{2!} z^2 \left(\frac{\partial^2 u}{\partial z^2} \right)_0 + \frac{1}{3!} z^3 \left(\frac{\partial^3 u}{\partial z^3} \right)_0 + \dots + \infty \\
v(x, y, z) &= v(x, y, 0) + z \left(\frac{\partial v}{\partial z} \right)_0 + \frac{1}{2!} z^2 \left(\frac{\partial^2 v}{\partial z^2} \right)_0 + \frac{1}{3!} z^3 \left(\frac{\partial^3 v}{\partial z^3} \right)_0 + \dots + \infty \\
w(x, y, z) &= w(x, y, 0) + z \left(\frac{\partial w}{\partial z} \right)_0 + \frac{1}{2!} z^2 \left(\frac{\partial^2 w}{\partial z^2} \right)_0 + \frac{1}{3!} z^3 \left(\frac{\partial^3 w}{\partial z^3} \right)_0 + \dots + \infty
\end{aligned}
\tag{3.1}$$

According to Reissner (1975) and Lo et al. (1977a, 1977b) it is sufficient to retain only the first four terms for all displacements. The expansions of the in-plane displacements u and v imply a nonlinear variation of these through the plate thickness. Thus, the warping of the cross section is automatically incorporated. The expansions of transverse displacement, w imply a non-vanishing transverse normal strain. Thus the limitations of the usual Kirchhoff's hypothesis Timoshenko and Woinoswsky-Krieger (1959) as well as the Reissner (1945) /Mindlin (1951) type first-order shear deformation theories are completely eliminated. The expressions given by Equation 3.1 are now written in a concise form by grouping the terms corresponding to membrane behaviour and flexure behaviour as follows:

Membrane	Flexure
$u(x, y, z) = u_0(x, y) + z^2 u_0^*(x, y) + \dots + \theta_x(x, y) + z^3 \theta_x^*(x, y) + \dots$	
$v(x, y, z) = v_0(x, y) + z^2 v_0^*(x, y) + \dots + \theta_y(x, y) + z^3 \theta_y^*(x, y) + \dots$	
$w(x, y, z) = z \theta_z(x, y) + z^3 \theta_z^*(x, y) + \dots + w_0(x, y) + z^2 w_0^*(x, y) + \dots$	

(3.2)

In the above relation, the terms u , v and w are the displacements of a general point (x, y, z) in the plate domain in the x , y and z direction respectively, the parameters u_0 , v_0 , are the in-plane displacements and w_0 is the transverse displacements of a point

(x, y) on the middle plane. The functions θ_x, θ_y are rotations of the normal to the middle plane about y and x axes respectively. The parameters $u_0^*, v_0^*, w_0^*, \theta_x^*, \theta_y^*, \theta_z^*$ and θ_z are the higher-order terms in the Taylor's series expansion and represent the transverse cross sectional deformation modes. The geometry of an FGM plate with positive set of coordinate axes is shown in Fig. 3.1.

3.2.1 Displacement Models

The membrane-flexure coupling phenomenon exhibited by an FGM plate necessitates the use of a displacement field containing both, membrane as well as flexural deformation terms which contribute to the overall response of the plate. Thus, the displacement field derived from the expanded Taylor's series in terms of the thickness coordinates z and defined by Equation 3.2 is considered. This displacement field contains both, membrane as well as flexure terms. Further, if the variation of transverse displacement component $w(x, y, z)$ in Equation 3.2 is assumed to be constant through the plate thickness and thus setting $\varepsilon_z = 0$, then the displacement field may be expressed as

$$\begin{aligned} u(x, y, z) &= u_0(x, y) + z\theta_x(x, y) + z^2u_0^*(x, y) + z^3\theta_x^*(x, y) \\ v(x, y, z) &= v_0(x, y) + z\theta_y(x, y) + z^2v_0^*(x, y) + z^3\theta_y^*(x, y) \\ w(x, y, z) &= w_0(x, y) \end{aligned} \tag{3.3}$$

Finally, the first displacement model assumed for thermal stress analysis of FGM plate is based on the higher order refined theory which includes the effects of both transverse shear and normal strain/stress (i.e., Higher Order Shear Deformation theory with 12 degrees of freedom, HSDT-12). The complete theoretical formulation is given below with the reference literature in which the model was reported earlier.

HSDT-12 (Kant and Manjunatha 1988)

$$u(x, y, z) = u_0(x, y) + z\theta_x(x, y) + z^2u_0^*(x, y) + z^3\theta_x^*(x, y)$$

$$v(x, y, z) = v_0(x, y) + z\theta_y(x, y) + z^2v_0^*(x, y) + z^3\theta_y^*(x, y)$$

$$w(x, y, z) = w_0(x, y) + z\theta_z(x, y) + z^2w_0^*(x, y) + z^3\theta_z^*(x, y)$$

(3.4)

The second displacement model is Higher order Shear Deformation Theory with Nine degrees of freedom (HSDT-9) which neglects the effect of transverse normal strain/stress and is given below along with the reference literature in which the model was reported earlier.

HSDT-9 (Pandya and Kant 1988)

$$u(x, y, z) = u_0(x, y) + z\theta_x(x, y) + z^2u_0^*(x, y) + z^3\theta_x^*(x, y)$$

$$v(x, y, z) = v_0(x, y) + z\theta_y(x, y) + z^2v_0^*(x, y) + z^3\theta_y^*(x, y)$$

$$w(x, y, z) = w_0(x, y)$$

(3.5)

In addition to the above, the Higher order Shear Deformation Theory with Five degrees of freedom (HSDT-5) and the First-order Shear Deformation Theory (FSDT) developed by other investigators that are reported in the literature are also considered during the study.

HSDT-5 (Reddy 1984)

$$u(x, y, z) = u_0(x, y) + z \left[\theta_x(x, y) - \frac{4}{3} \left(\frac{z}{h} \right)^2 \left\{ \theta_x(x, y) + \frac{\partial w_0}{\partial x} \right\} \right]$$

$$v(x, y, z) = v_0(x, y) + z \left[\theta_y(x, y) - \frac{4}{3} \left(\frac{z}{h} \right)^2 \left\{ \theta_y(x, y) + \frac{\partial w_0}{\partial y} \right\} \right]$$

$$w(x, y, z) = w_0(x, y)$$

(3.6)

FSDT (Whitney and Pagano 1970)

$$u(x, y, z) = u_0(x, y) + z\theta_x(x, y)$$

$$v(x, y, z) = v_0(x, y) + z\theta_y(x, y)$$

$$w(x, y, z) = w_0(x, y)$$

(3.7)

In the following sections, the detailed formulations using the displacement model HSDT-12 are presented for the analysis of FGM plates subjected to thermal loads. The same procedure is followed for the formulations using all other displacement models.

3.3 STRESS STRAIN RELATIONS FOR AN FGM PLATE

An FGM plate is assumed to behave as a homogeneous and orthotropic material with three orthogonal planes of material symmetry. Generalized Hooke's law based on linear theory of elasticity relates the thermal stresses and strains in an FGM plate, and can be written in contracted form as

$$\sigma_i = Q_{ij} \varepsilon_j - Q_{ij} \alpha_j \Delta T ; \quad i, j = 1 \text{ to } 6$$

(3.8)

Where, σ_i is the stress vector, ε_j is the engineering strain vector and Q_{ij} is the functionally graded material stiffness matrix. The coefficient of thermal expansion α_j is assumed to vary across the thickness direction z , while in-plane remains constant. Therefore, thermal expansion coefficients $\alpha_1 = \alpha_2 = \alpha_3 = \alpha_z$ and $\alpha_4 = \alpha_5 = \alpha_6 = 0$. Also, ΔT is the change in temperature from a stress free state. In Equation 3.8 the first three components are normal stress and strains and last three components are shearing stress and strains respectively. In an FGM plate there is no interaction between normal stresses $\sigma_1, \sigma_2, \sigma_3$ and shearing strains $\gamma_{12}, \gamma_{23}, \gamma_{31}$, and hence the coefficients of stiffness matrix Q_{ij} for an FGM plate can be written as follows

$$\begin{Bmatrix} \sigma_x \\ \sigma_y \\ \sigma_z \\ \tau_{xy} \\ \tau_{yz} \\ \tau_{xz} \end{Bmatrix} = \begin{bmatrix} Q_{11} & Q_{12} & Q_{13} & 0 & 0 & 0 \\ Q_{12} & Q_{22} & Q_{23} & 0 & 0 & 0 \\ Q_{13} & Q_{23} & Q_{33} & 0 & 0 & 0 \\ 0 & 0 & 0 & Q_{44} & 0 & 0 \\ 0 & 0 & 0 & 0 & Q_{55} & 0 \\ 0 & 0 & 0 & 0 & 0 & Q_{66} \end{bmatrix} \begin{Bmatrix} \varepsilon_x - \alpha_z \Delta T \\ \varepsilon_y - \alpha_z \Delta T \\ \varepsilon_z - \alpha_z \Delta T \\ \gamma_{xy} \\ \gamma_{yz} \\ \gamma_{xz} \end{Bmatrix}$$

(3.9a)

Where,

$$Q_{11} = Q_{22} = Q_{33} = \frac{E_z(1-\nu^2)}{\eta};$$

$$Q_{44} = Q_{55} = Q_{66} = \frac{E_z}{(1-\nu^2)};$$

$$Q_{13} = Q_{23} = Q_{12} = Q_{21} = Q_{31} = Q_{32} = \frac{E_z(\nu+\nu^2)}{\eta};$$

$$\eta = (1-3\nu^2-2\nu^3) \quad (3.9b)$$

In the above equation the material properties are defined using Power-Law function. The volume fraction V_f and power-law parameter p defines the gradation of material from metal at bottom surface to the ceramic at the top surface of the plate. Through the thickness variation of physical properties like young's modulus of elasticity E_z , thermal coefficient of expansion α_z , thermal conductivity k_z and volume fraction V_f are evaluated using the relation given below,

$$E_z = E_m + (E_c - E_m) V_f^p \quad (3.10a)$$

$$\alpha_z = \alpha_m + (\alpha_c - \alpha_m) V_f^p \quad (3.10b)$$

$$k_z = k_m + (k_c - k_m) V_f^p \quad (3.10c)$$

$$V_f = \left(\frac{z}{h} + \frac{1}{2} \right) \quad (3.10d)$$

Temperature change from stress free state ΔT is assumed to vary sinusoidally across the plane $T(x,y)$ and nonlinearly across the thickness direction T_z and is given by

$$\Delta T = T(x, y, z) = T(z) \times T(x, y) = T_z \times T(x, y) \quad (3.11)$$

The nonlinear variation of temperature across the thickness direction T_z , is obtained by solving one dimensional steady state heat conduction equation with boundary conditions at top and bottom surface of the plate as in Equation 3.12a. The solution for heat conduction equation is given by Equation 3.12b.

$$-\frac{d}{dz} \left(k_z \frac{dT}{dz} \right) = 0; \quad T \left(z = \frac{h}{2} \right) = T_1 \quad \text{and} \quad T \left(z = -\frac{h}{2} \right) = T_0 \quad (3.12a)$$

$$T_z = T_{NL} = T_0 + (T_1 - T_0) \frac{\sum_{n=0}^{\infty} \frac{(-1)^n \left(\frac{k_c - k_m}{k_m} \right)^n}{(np+1)} V_f^{(np+1)}}{\sum_{n=0}^{\infty} \frac{(-1)^n \left(\frac{k_c - k_m}{k_m} \right)^n}{(np+1)}} \quad (3.12b)$$

In addition to above, constant and linear variation of temperature across the plate thickness are also considered during the study. Constant temperature is achieved by applying same temperatures at top and bottom surface i.e., $T_0=T_1$ in Equation 3.12b. Linear temperature distribution from bottom to top surface is achieved by neglecting higher order terms and retaining only first term in the series expansion of

Equation 3.12b. Constant and linear variations of temperature across the plate thickness are given by Equation 3.13a and 3.13b respectively.

$$T_z = T_C = T_0 = T_1 \quad (3.13a)$$

$$T_z = T_L = T_0 + (T_1 - T_0)V_f \quad (3.13b)$$

Where;

p = Power law parameter

V_f = Volume fraction.

E_m = Young's modulus of elasticity of metal (at bottom surface)

E_c = Young's modulus of elasticity of ceramic (at top surface).

k_m = Thermal conductivity of metal (at bottom surface)

k_c = Thermal conductivity of ceramic (at top surface).

α_m = Thermal coefficient of expansion of metal (at bottom surface)

α_c = Thermal coefficient of expansion of ceramic (at top surface).

T_0 = Temperature at bottom surface of the plate.

T_1 = Temperature at top surface of the plate.

T_{NL} , T_C , T_L = Nonlinear, constant and linear variation of temperatures across the thickness direction.

3.4 STRAIN DISPLACEMENT RELATIONS

The relationship between the strains at any point within the plate and the corresponding deformations are functions of the assumed displacement fields. With

the definitions of strains from linear theory of elasticity, the general linear strain displacement relations are given as follows (Timoshenko and Goodier 1970)

$$\begin{aligned}\varepsilon_x &= \frac{\partial u}{\partial x}; & \varepsilon_y &= \frac{\partial v}{\partial y}; & \varepsilon_z &= \frac{\partial w}{\partial z} \\ \gamma_{xy} &= \frac{\partial u}{\partial y} + \frac{\partial v}{\partial x}; & \gamma_{xz} &= \frac{\partial u}{\partial z} + \frac{\partial w}{\partial x}; & \gamma_{yz} &= \frac{\partial v}{\partial z} + \frac{\partial w}{\partial y}\end{aligned}\tag{3.14}$$

The six quantities, three-unit elongations in three perpendicular directions ($\varepsilon_x, \varepsilon_y, \varepsilon_z$) and three unit shear strains ($\gamma_{xy}, \gamma_{xz}, \gamma_{yz}$) related to the three orthogonal planes are called components of strain at a point. The component of strain displacement relations for HSDT-12 model is discussed in the following sections.

3.4.1 Strain Expressions Corresponding to HSDT-12 Model

The strains corresponding to the displacement model in Equation 3.4 can be written as

$$\begin{aligned}\varepsilon_x &= \varepsilon_{x_0} + z\kappa_x + z^2\varepsilon_{x_0}^* + z^3\kappa_x^* \\ \varepsilon_y &= \varepsilon_{y_0} + z\kappa_y + z^2\varepsilon_{y_0}^* + z^3\kappa_y^* \\ \varepsilon_z &= \varepsilon_{z_0} + z\kappa_z + z^2\varepsilon_{z_0}^* \\ \gamma_{xy} &= \varepsilon_{xy_0} + z\kappa_{xy} + z^2\varepsilon_{xy_0}^* + z^3\kappa_{xy}^* \\ \gamma_{yz} &= \phi_y + z\kappa_{yz} + z^2\phi_y^* + z^3\kappa_{yz}^* \\ \gamma_{xz} &= \phi_x + z\kappa_{xz} + z^2\phi_x^* + z^3\kappa_{xz}^*\end{aligned}\tag{3.15a}$$

Where,

$$\begin{aligned}\left(\varepsilon_{x_0}^*, \varepsilon_{y_0}^*, \varepsilon_{xy_0}^*\right) &= \left(\frac{\partial u_0^*}{\partial x}, \frac{\partial v_0^*}{\partial y}, \frac{\partial u_0^*}{\partial y} + \frac{\partial v_0^*}{\partial x}\right) \\ \left(\varepsilon_{z_0}^*, \varepsilon_{z_0}^*\right) &= \left(\theta_z, 3\theta_z^*\right)\end{aligned}$$

$$\begin{aligned}
(\kappa_x, \kappa_y, \kappa_z^*, \kappa_{xy}) &= \left(\frac{\partial \theta_x}{\partial x}, \frac{\partial \theta_y}{\partial y}, 2w_0^*, \frac{\partial \theta_x}{\partial y} + \frac{\partial \theta_y}{\partial x} \right) \\
(\kappa_x^*, \kappa_y^*, \kappa_{xy}^*) &= \left(\frac{\partial \theta_x^*}{\partial x}, \frac{\partial \theta_y^*}{\partial y}, \frac{\partial \theta_x^*}{\partial y} + \frac{\partial \theta_y^*}{\partial x} \right) \\
(\phi_x, \phi_x^*, \phi_y, \phi_y^*) &= \left(\theta_x + \frac{\partial w_0}{\partial x}, 3\theta_x^* + \frac{\partial w_0^*}{\partial x}, \theta_y + \frac{\partial w_0}{\partial y}, 3\theta_y^* + \frac{\partial w_0^*}{\partial y} \right) \\
(\kappa_{xz}, \kappa_{yz}, \kappa_{xz}^*, \kappa_{yz}^*) &= \left(2u_0^* + \frac{\partial \theta_z}{\partial x}, 2v_0^* + \frac{\partial \theta_z}{\partial y}, \frac{\partial \theta_z^*}{\partial x}, \frac{\partial \theta_z^*}{\partial y} \right)
\end{aligned} \tag{3.15b}$$

The strains expressions in Equation 3.15a can be represented in matrix form as follows:

$$\begin{aligned}
\varepsilon_{MB} &= \begin{Bmatrix} \varepsilon_x \\ \varepsilon_y \\ \varepsilon_z \\ \gamma_{xy} \end{Bmatrix} = \begin{Bmatrix} \varepsilon_{x_0} \\ \varepsilon_{y_0} \\ \varepsilon_{z_0} \\ \gamma_{xy_0} \end{Bmatrix} + Z \begin{Bmatrix} \kappa_x \\ \kappa_y \\ \kappa_z \\ \kappa_{xy} \end{Bmatrix} + Z^2 \begin{Bmatrix} \varepsilon_{x_0}^* \\ \varepsilon_{y_0}^* \\ \varepsilon_{z_0}^* \\ \varepsilon_{xy_0}^* \end{Bmatrix} + Z^3 \begin{Bmatrix} \kappa_x^* \\ \kappa_y^* \\ 0 \\ \kappa_{xy}^* \end{Bmatrix} \\
\varepsilon_{MB} &= \varepsilon_0 + Z \kappa + Z^2 \varepsilon_0^* + Z^3 \kappa^*
\end{aligned} \tag{3.16a}$$

$$\begin{aligned}
\varepsilon_S &= \begin{Bmatrix} \gamma_{yz} \\ \gamma_{xz} \end{Bmatrix} = \begin{Bmatrix} \phi_y \\ \phi_x \end{Bmatrix} + Z \begin{Bmatrix} \kappa_{yz} \\ \kappa_{xz} \end{Bmatrix} + Z^2 \begin{Bmatrix} \phi_y^* \\ \phi_x^* \end{Bmatrix} + Z^3 \begin{Bmatrix} \kappa_{yz}^* \\ \kappa_{xz}^* \end{Bmatrix} \\
\varepsilon_S &= \phi_0 + Z \kappa_x + Z^2 \phi_0^* + Z^3 \kappa_x^*
\end{aligned} \tag{3.16b}$$

This completes the derivation of strain expressions for FGM plates based on HSDT-12 displacement model. Same procedure is adopted to obtain the strain expressions for other displacement models used for the thermal analysis of FGM plates.

3.5 STRESS-RESULTANT AND MIDDLE-PLANE-STRAIN RELATIONS

In this section, the membrane, the flexure and the shear stress resultants of an FGM plate will be expressed as a function of the middle plane stretching, curvatures and shear rotations strain terms respectively. The resulting equations are referred as plate constitutive relation and are derived for HSDT-12 model as follows:

The total potential energy Π of the plate with volume V middle surface A can be written as, p

$$\Pi = U - W$$

$$\text{or} \quad \Pi = \frac{1}{2} \int_V \boldsymbol{\varepsilon}^t \boldsymbol{\sigma} dV - \int_A \mathbf{u}^t p dA$$

(3.17)

Where U is the strain energy stored in the plate, W represents the work done by externally applied load and p is the vector of surface load intensities corresponding to the generalized displacement vector u defined at the middle plane and these are expressed as,

$$\boldsymbol{\sigma} = (\sigma_x, \sigma_y, \sigma_z, \tau_{xy}, \tau_{yz}, \tau_{xz})^t$$

$$\boldsymbol{\varepsilon} = (\varepsilon_x, \varepsilon_y, \varepsilon_z, \gamma_{xy}, \gamma_{yz}, \gamma_{xz})^t$$

$$\mathbf{u} = (u, v, w)^t$$

$$p = (p_x, p_y, p_z)^t$$

(3.18)

The expressions for the strain components are substituted in Equation 3.17 and the following relation results when an explicit integration is carried out through the plate thickness,

$$\Pi = \frac{1}{2} \int_A \bar{\varepsilon}^t \bar{\sigma} dA - \int_A \bar{u}^t p dA \quad (3.19)$$

in which $\bar{\varepsilon}$, $\bar{\sigma}$, \bar{u} for the HSDT-12 model is written as follows:

3.5.1 Constitutive Relations for FGM Plate based on HSDT-12 Model.

$$\begin{aligned} \bar{\sigma} &= \left(N_x, N_y, N_{xy}, N_x^*, N_y^*, N_{xy}^*, N_z, N_z^*, M_x, M_y, M_{xy}, \right. \\ &\quad \left. M_x^*, M_y^*, M_{xy}^*, M_z^*, Q_x, Q_y, Q_x^*, Q_y^*, S_x, S_y, S_x^*, S_y^* \right)^t \\ \bar{\varepsilon} &= \left(\varepsilon_{x_0}, \varepsilon_{y_0}, \varepsilon_{xy_0}, \varepsilon_{x_0}^*, \varepsilon_{y_0}^*, \varepsilon_{xy_0}^*, \varepsilon_{z_0}, \varepsilon_{z_0}^*, \kappa_x, \kappa_y, \kappa_{xy}, \right. \\ &\quad \left. \kappa_x^*, \kappa_y^*, \kappa_{xy}^*, \kappa_z^*, \phi_x, \phi_y, \phi_x^*, \phi_y^*, \kappa_{xz}, \kappa_{yz}, \kappa_{xz}^*, \kappa_{yz}^* \right)^t \\ \bar{u} &= \left(u_0, v_0, w_0, \theta_x, \theta_y, \theta_z, u_0^*, v_0^*, w_0^*, \theta_x^*, \theta_y^*, \theta_z^* \right)^t \\ N_T &= \left(N_{x_T}, N_{y_T}, N_{xy_T}, N_{x_T}^*, N_{y_T}^*, N_{xy_T}^*, N_{z_T}, N_{z_T}^*, M_{x_T}, M_{y_T}, \right. \\ &\quad \left. M_{xy_T}, M_{x_T}^*, M_{y_T}^*, M_{xy_T}^*, M_{z_T}^*, 0, 0, 0, 0, 0, 0, 0 \right)^t \end{aligned} \quad (3.20)$$

The components of the stress resultant vector $\bar{\sigma}$ for an FGM plate are defined as,

$$\begin{aligned} \begin{bmatrix} N_x & N_x^* \\ N_y & N_y^* \\ N_z & N_z^* \\ N_{xy} & N_{xy}^* \end{bmatrix} &= \int_{-h/2}^{+h/2} \begin{Bmatrix} \sigma_x \\ \sigma_y \\ \sigma_z \\ \tau_{xy} \end{Bmatrix} (1, z^2) dz \\ &= \int_{-h/2}^{+h/2} \begin{bmatrix} Q_{11} & Q_{12} & Q_{13} & 0 \\ Q_{12} & Q_{22} & Q_{23} & 0 \\ Q_{13} & Q_{23} & Q_{33} & 0 \\ 0 & 0 & 0 & Q_{44} \end{bmatrix} \begin{Bmatrix} \varepsilon_x \\ \varepsilon_y \\ \varepsilon_z \\ \gamma_{xy} \end{Bmatrix} (1, z^2) dz - \begin{bmatrix} N_{x_T} & N_{x_T}^* \\ N_{y_T} & N_{y_T}^* \\ N_{z_T} & N_{z_T}^* \\ 0 & 0 \end{bmatrix} \end{aligned} \quad (3.21a)$$

$$\begin{bmatrix} N_{x_T} & N_{x_T}^* \\ N_{y_T} & N_{y_T}^* \\ N_{z_T} & N_{z_T}^* \\ 0 & 0 \end{bmatrix} = \int_{-h/2}^{+h/2} \begin{bmatrix} Q_{11} & Q_{12} & Q_{13} & 0 \\ Q_{12} & Q_{22} & Q_{23} & 0 \\ Q_{13} & Q_{23} & Q_{33} & 0 \\ 0 & 0 & 0 & 0 \end{bmatrix} (1, z^2) \alpha_z \Delta T dz$$

(3.21b)

$$\begin{bmatrix} M_x & M_x^* \\ M_y & M_y^* \\ M_z^* & 0 \\ M_{xy} & M_{xy}^* \end{bmatrix} = \int_{-h/2}^{+h/2} \begin{Bmatrix} \sigma_x \\ \sigma_y \\ \sigma_z \\ \tau_{xy} \end{Bmatrix} (z, z^3) dz$$

$$= \int_{-h/2}^{+h/2} \begin{bmatrix} Q_{11} & Q_{12} & Q_{13} & 0 \\ Q_{12} & Q_{22} & Q_{23} & 0 \\ Q_{13} & Q_{23} & Q_{33} & 0 \\ 0 & 0 & 0 & Q_{44} \end{bmatrix} \begin{Bmatrix} \varepsilon_x \\ \varepsilon_y \\ \varepsilon_z \\ \gamma_{xy} \end{Bmatrix} (z, z^3) dz - \begin{bmatrix} M_{x_T} & M_{x_T}^* \\ M_{y_T} & M_{y_T}^* \\ M_{z_T}^* & 0 \\ 0 & 0 \end{bmatrix}$$

(3.21c)

$$\begin{bmatrix} M_{x_T} & M_{x_T}^* \\ M_{y_T} & M_{y_T}^* \\ M_{z_T}^* & 0 \\ 0 & 0 \end{bmatrix} = \int_{-h/2}^{+h/2} \begin{bmatrix} Q_{11} & Q_{12} & Q_{13} & 0 \\ Q_{12} & Q_{22} & Q_{23} & 0 \\ Q_{13} & Q_{23} & Q_{33} & 0 \\ 0 & 0 & 0 & 0 \end{bmatrix} (z, z^3) \alpha_z \Delta T dz$$

(3.21d)

$$\begin{bmatrix} Q_x & Q_x^* & S_x & S_x^* \\ Q_y & Q_y^* & S_y & S_y^* \end{bmatrix} = \int_{-h/2}^{+h/2} \begin{Bmatrix} \tau_{xz} \\ \tau_{yz} \end{Bmatrix} (1, z^2, z, z^3) dz$$

(3.21e)

Upon integration, these expressions are rewritten in the matrix form as,

$$\begin{Bmatrix} N \\ M \\ Q \end{Bmatrix} = \begin{bmatrix} D_M & D_C & 0 \\ D_C^t & D_B & 0 \\ 0 & 0 & D_S \end{bmatrix} \begin{Bmatrix} \varepsilon \\ \kappa \\ \phi \end{Bmatrix} - \begin{Bmatrix} N_T \\ M_T \\ 0 \end{Bmatrix}$$

(3.22)

$$\text{or} \quad \{\bar{\sigma}\} = [D]\{\bar{\varepsilon}\} - \{N_T\} \quad (3.23a)$$

In which,

$$\begin{aligned} N &= (N_x, N_y, N_{xy}, N_x^*, N_y^*, N_{xy}^*, N_z, N_z^*)^t \\ M &= (M_x, M_y, M_{xy}, M_x^*, M_y^*, M_{xy}^*, M_z^*)^t \\ Q &= (Q_x, Q_y, Q_x^*, Q_y^*, S_x, S_y, S_x^*, S_y^*)^t \\ \varepsilon &= (\varepsilon_{x_0}, \varepsilon_{y_0}, \varepsilon_{xy_0}, \varepsilon_{x_0}^*, \varepsilon_{y_0}^*, \varepsilon_{xy_0}^*, \varepsilon_{z_0}, \varepsilon_{z_0}^*)^t \\ \kappa &= (\kappa_x, \kappa_y, \kappa_{xy}, \kappa_x^*, \kappa_y^*, \kappa_{xy}^*, \kappa_z^*)^t \\ \phi &= (\phi_x, \phi_y, \phi_x^*, \phi_y^*, \kappa_{xz}, \kappa_{yz}, \kappa_{xz}^*, \kappa_{yz}^*)^t \\ N_T &= (N_{x_T}, N_{y_T}, N_{xy_T}, N_{x_T}^*, N_{y_T}^*, N_{xy_T}^*, N_{z_T}, N_{z_T}^*)^t \\ M_T &= (M_{x_T}, M_{y_T}, M_{xy_T}, M_{x_T}^*, M_{y_T}^*, M_{xy_T}^*, M_{z_T}^*)^t \end{aligned} \quad (3.23b)$$

and

$$D_M = \int_{-h/2}^{h/2} \begin{bmatrix} Q_{11} & Q_{12} & 0 & Q_{11}z^2 & Q_{12}z^2 & 0 & Q_{13} & Q_{13}z^2 \\ & Q_{22} & 0 & Q_{12}z^2 & Q_{22}z^2 & 0 & Q_{23} & Q_{23}z^2 \\ & & Q_{44} & 0 & 0 & Q_{44}z^2 & 0 & 0 \\ & & & Q_{11}z^4 & Q_{12}z^4 & 0 & Q_{13}z^2 & Q_{13}z^4 \\ & & & & Q_{22}z^4 & 0 & Q_{23}z^2 & Q_{23}z^4 \\ & & & & & Q_{44}z^3 & 0 & 0 \\ \text{symmetric} & & & & & & Q_{33} & Q_{33}z^2 \\ & & & & & & & Q_{33}z^4 \end{bmatrix} dz \quad (3.23c)$$

$$D_s = \int_{-h/2}^{h/2} \begin{bmatrix} Q_{66} & 0 & Q_{66}z^2 & 0 & Q_{66}z & 0 & Q_{66}z^3 & 0 \\ & Q_{55} & 0 & Q_{55}z^2 & 0 & Q_{55}z & 0 & Q_{55}z^3 \\ & & Q_{66}z^4 & 0 & Q_{66}z^3 & 0 & Q_{66}z^5 & 0 \\ & & & Q_{55}z^4 & 0 & Q_{55}z^3 & 0 & Q_{55}z^5 \\ & \text{symmetric} & & & Q_{66}z^2 & 0 & Q_{66}z^4 & 0 \\ & & & & & Q_{55}z^2 & 0 & Q_{55}z^4 \\ & & & & & & Q_{66}z^6 & 0 \\ & & & & & & & Q_{55}z^6 \end{bmatrix} dz \quad (3.23d)$$

The coefficients of D_C matrix can be obtained by multiplying the terms in matrix D_M with z before integrating. Similarly the coefficients of D_B matrix can be obtained by multiplying the terms in matrix D_M with z^2 before integrating.

3.6 EQUATIONS OF EQUILIBRIUM AND NATURAL BOUNDARY CONDITIONS

The equilibrium equations for thermal stress analysis of FGM plates using various displacement models are derived from Principle of Minimum Potential Energy (PMPE) (Dym and Shames 1973, Reddy 1984a, b). This method is chosen due to its simplicity and also its application gives simultaneously the natural boundary conditions that are to be used with the theory. In the following sections, the equations of equilibrium and the natural boundary conditions for the stress analysis of a simply supported FGM plates subjected to thermal loads are presented using HSDT-12 displacement model. Same procedure is used to derive the equilibrium equations using other displacement models also.

3.6.1 Thermal Stress Analysis

The potential energy Π for the plate element is defined as,

$$\Pi = U - W_s - W_{ex} - W_{ey} \quad (3.24)$$

Where,

U = strain energy of the plate

W_s = work done by surface tractions

W_{ex} = work done by edge stress on edge x =constant

W_{ey} = work done by edge stress on edge y =constant

For equilibrium, the total potential energy Π for the plate must be stationary,

i.e.,

$$\delta\Pi = \delta\left(U - W_s - W_{ex} - W_{ey}\right) = 0 \quad (3.25)$$

The individual terms of the above equations are evaluated as follows

$$\delta U = \iiint_{x y z} \left(\sigma_x \delta \varepsilon_x + \sigma_y \delta \varepsilon_y + \sigma_z \delta \varepsilon_z + \tau_{xy} \delta \gamma_{xy} + \tau_{xz} \delta \gamma_{xz} + \tau_{yz} \delta \gamma_{yz} \right) dx dy dz \quad (3.26)$$

Substituting the appropriate strain expressions using Equations 3.15a and 3.15b and integrating through the thickness to get the stress resultants as defined in Equations 3.21a, 3.21b, 3.21c, 3.21d and 3.21e and then, integrating the resulting expressions by parts transforms the Equation 3.26 into the following form

$$\begin{aligned} \delta U = & \oint_x \left[N_y \delta v_0 + N_{xy} \delta u_0 + Q_y \delta w_0 + M_{xy} \delta \theta_x + M_y \delta \theta_y + S_y \delta \theta_z \right. \\ & \left. + N_{xy}^* \delta u_0 + N_y^* \delta v_0^* + Q_y^* \delta w_0^* + M_{xy}^* \delta \theta_x^* + M_y^* \delta \theta_y^* + S_y^* \delta \theta_z^* \right] dx \\ & + \oint_y \left[N_x \delta u_0 + N_{xy} \delta v_0 + Q_x \delta w_0 + M_{xy} \delta \theta_y + M_x \delta \theta_x + S_x \delta \theta_z \right. \\ & \left. + N_{xy}^* \delta v_0 + N_x^* \delta u_0^* + Q_x^* \delta w_0^* + M_{xy}^* \delta \theta_y^* + M_x^* \delta \theta_x^* + S_x^* \delta \theta_z^* \right] dy \end{aligned}$$

$$\begin{aligned}
& - \iint_{x y} \left[\left(\frac{\partial N_x}{\partial x} + \frac{\partial N_{xy}}{\partial y} \right) \delta u_0 + \left(\frac{\partial N_y}{\partial y} + \frac{\partial N_{xy}}{\partial x} \right) \delta v_0 + \left(\frac{\partial Q_x}{\partial x} + \frac{\partial Q_y}{\partial y} \right) \delta w_0 \right. \\
& + \left(\frac{\partial M_x}{\partial x} + \frac{\partial M_{xy}}{\partial y} - Q_x \right) \delta \theta_x + \left(\frac{\partial M_y}{\partial y} + \frac{\partial M_{xy}}{\partial x} - Q_y \right) \delta \theta_y \\
& + \left(\frac{\partial S_x}{\partial x} + \frac{\partial S_y}{\partial y} - N_z \right) \delta \theta_z + \left(\frac{\partial N_x^*}{\partial x} + \frac{\partial N_{xy}^*}{\partial y} - 2S_x \right) \delta u_0^* \\
& + \left(\frac{\partial N_y^*}{\partial y} + \frac{\partial N_{xy}^*}{\partial x} - 2S_y \right) \delta v_0^* + \left(\frac{\partial Q_x^*}{\partial x} + \frac{\partial Q_y^*}{\partial y} - 2M_z^* \right) \delta w_0^* \\
& + \left(\frac{\partial M_x^*}{\partial x} + \frac{\partial M_{xy}^*}{\partial y} - 3Q_x^* \right) \delta \theta_x^* + \left(\frac{\partial M_y^*}{\partial y} + \frac{\partial M_{xy}^*}{\partial x} - 3Q_y^* \right) \delta \theta_y^* \\
& \left. + \left(\frac{\partial S_x^*}{\partial x} + \frac{\partial S_y^*}{\partial y} - 3N_z^* \right) \delta \theta_z^* \right] dx dy
\end{aligned} \tag{3.27}$$

The work done by surface tractions, W_s may be calculated as follows,

$$W_s = \frac{1}{2} \iint_{x y} (p_z^+ w^+) dx dy \tag{3.28}$$

Where w^+ is the transverse displacement at any point at the top surface of the plate and is given by

$$w^+ = w_0 + h^+ \theta_z + h^{+2} w_0^* + h^{+3} \theta_z^* \tag{3.29}$$

Therefore,

$$W_s = \frac{1}{2} \iint_{x y} \left\{ p_z^+ w_0 + (p_z^+ h^+) \theta_z + (p_z^+ h^{+2}) w_0^* + (p_z^+ h^{+3}) \theta_z^* \right\} dx dy \tag{3.30}$$

And the variation of W_s for $h^+=h/2$,

$$\delta W_s = \iint_{x,y} \left\{ p_z^+ \left(\delta w_0 + \frac{h}{2} \delta \theta_z + \frac{h^2}{4} \delta w_0^* + \frac{h^3}{8} \delta \theta_z^* \right) \right\} dx dy \quad (3.31)$$

The work done by the edge stresses is

$$W_{ex} = \frac{1}{2} \iint_{y,z} \left(\bar{\sigma}_x u + \bar{\tau}_{xy} v + \bar{\tau}_{xz} w \right) dy dz \quad \text{on an edge } x = \text{constant.} \quad (3.32)$$

$$W_{ey} = \frac{1}{2} \iint_{x,z} \left(\bar{\tau}_{xy} u + \bar{\sigma}_y v + \bar{\tau}_{yz} w \right) dx dz \quad \text{on an edge } y = \text{constant.} \quad (3.33)$$

Where, the bars on the quantities refer to edge values. On integration through the thickness the variation of these expressions takes the form

$$\begin{aligned} \delta W_{ex} = \int_y \left(\bar{N}_x \delta u_0 + \bar{N}_{xy} \delta v_0 + \bar{Q}_x \delta w_0 + \bar{M}_x \delta \theta_x + \bar{M}_{xy} \delta \theta_y + \bar{S}_x \delta \theta_z \right. \\ \left. + \bar{N}_x^* \delta u_0^* + \bar{N}_{xy}^* \delta v_0^* + \bar{Q}_x^* \delta w_0^* + \bar{M}_x^* \delta \theta_x^* + \bar{M}_{xy}^* \delta \theta_y^* + \bar{S}_x^* \delta \theta_z^* \right) dy \end{aligned} \quad (3.34)$$

and

$$\begin{aligned} \delta W_{ey} = \int_x \left(\bar{N}_{xy} \delta u_0 + \bar{N}_y \delta v_0 + \bar{Q}_y \delta w_0 + \bar{M}_{xy} \delta \theta_x + \bar{M}_y \delta \theta_y + \bar{S}_y \delta \theta_z \right. \\ \left. + \bar{N}_{xy}^* \delta u_0^* + \bar{N}_y^* \delta v_0^* + \bar{Q}_y^* \delta w_0^* + \bar{M}_{xy}^* \delta \theta_x^* + \bar{M}_y^* \delta \theta_y^* + \bar{S}_y^* \delta \theta_z^* \right) dx \end{aligned} \quad (3.35)$$

The variational Equation 3.25 takes the following form when the relevant foregoing expressions are substituted for its individual terms.

$$\begin{aligned}
& \iint_{x y} \left[\left(\frac{\partial N_x}{\partial x} + \frac{\partial N_{xy}}{\partial y} \right) \delta u_0 + \left(\frac{\partial N_y}{\partial y} + \frac{\partial N_{xy}}{\partial x} \right) \delta v_0 + \left(\frac{\partial Q_x}{\partial x} + \frac{\partial Q_y}{\partial y} + p_z^+ \right) \delta w_0 \right. \\
& + \left(\frac{\partial M_x}{\partial x} + \frac{\partial M_{xy}}{\partial y} - Q_x \right) \delta \theta_x + \left(\frac{\partial M_y}{\partial y} + \frac{\partial M_{xy}}{\partial x} - Q_y \right) \delta \theta_y \\
& + \left(\frac{\partial S_x}{\partial x} + \frac{\partial S_y}{\partial y} - N_z + \frac{h}{2} p_z^+ \right) \delta \theta_z + \left(\frac{\partial N_x^*}{\partial x} + \frac{\partial N_{xy}^*}{\partial y} - 2S_x \right) \delta u_0^* \\
& + \left(\frac{\partial N_y^*}{\partial y} + \frac{\partial N_{xy}^*}{\partial x} - 2S_y \right) \delta v_0^* + \left(\frac{\partial Q_x^*}{\partial x} + \frac{\partial Q_y^*}{\partial y} - 2M_z + \frac{h^2}{4} p_z^+ \right) \delta w_0^* \\
& + \left(\frac{\partial M_x^*}{\partial x} + \frac{\partial M_{xy}^*}{\partial y} - 3Q_x^* \right) \delta \theta_x^* + \left(\frac{\partial M_y^*}{\partial y} + \frac{\partial M_{xy}^*}{\partial x} - 3Q_y^* \right) \delta \theta_y^* \\
& \left. + \left(\frac{\partial S_x^*}{\partial x} + \frac{\partial S_y^*}{\partial y} - 3N_z^* + \frac{h^3}{8} p_z^+ \right) \delta \theta_z^* \right] dx dy \\
& + \oint_x \left[(N_{xy} - \bar{N}_{xy}) \delta u_0 + (N_y - \bar{N}_y) \delta v_0 + (Q_y - \bar{Q}_y) \delta w_0 + (M_{xy} - \bar{M}_{xy}) \delta \theta_x \right. \\
& + (M_y - \bar{M}_y) \delta \theta_y + (S_y - \bar{S}_y) \delta \theta_z + (N_{xy}^* - \bar{N}_{xy}^*) \delta u_0^* + (N_y^* - \bar{N}_y^*) \delta v_0^* \\
& \left. + (Q_y^* - \bar{Q}_y^*) \delta w_0^* + (M_{xy}^* - \bar{M}_{xy}^*) \delta \theta_x^* + (M_y^* - \bar{M}_y^*) \delta \theta_y^* + (S_y^* - \bar{S}_y^*) \delta \theta_z^* \right] dx \\
& + \oint_y \left[(N_x - \bar{N}_x) \delta u_0 + (N_{xy} - \bar{N}_{xy}) \delta v_0 + (Q_x - \bar{Q}_x) \delta w_0 + (M_{xy} - \bar{M}_{xy}) \delta \theta_y \right. \\
& + (M_x - \bar{M}_x) \delta \theta_x + (S_x - \bar{S}_x) \delta \theta_z + (N_x^* - \bar{N}_x^*) \delta u_0^* + (N_{xy}^* - \bar{N}_{xy}^*) \delta v_0^* \\
& \left. + (Q_x^* - \bar{Q}_x^*) \delta w_0^* + (M_x^* - \bar{M}_x^*) \delta \theta_x^* + (M_{xy}^* - \bar{M}_{xy}^*) \delta \theta_y^* + (S_x^* - \bar{S}_x^*) \delta \theta_z^* \right] dy = 0
\end{aligned} \tag{3.36}$$

The above Equation 3.36 will be an identity only if each of the coefficients of the arbitrary variation vanishes. The vanishing of the surface integral defines twelve equilibrium equations, while that of the line integrals defines the consistent natural boundary conditions that are to be used with this theory along the two edges. Setting the individual integral terms in Equation 3.36 to zero, the following equations of equilibrium and the consistent boundary conditions are obtained.

$$\begin{aligned}
\delta u_0 &: \left(\frac{\partial N_x}{\partial x} + \frac{\partial N_{xy}}{\partial y} \right) = 0 \\
\delta v_0 &: \left(\frac{\partial N_y}{\partial y} + \frac{\partial N_{xy}}{\partial x} \right) = 0 \\
\delta w_0 &: \left(\frac{\partial Q_x}{\partial x} + \frac{\partial Q_y}{\partial y} + p_z^+ \right) = 0 \\
\delta \theta_x &: \left(\frac{\partial M_x}{\partial x} + \frac{\partial M_{xy}}{\partial y} - Q_x \right) = 0 \\
\delta \theta_y &: \left(\frac{\partial M_y}{\partial y} + \frac{\partial M_{xy}}{\partial x} - Q_y \right) = 0 \\
\delta \theta_z &: \left(\frac{\partial S_x}{\partial x} + \frac{\partial S_y}{\partial y} - N_z + \frac{h}{2} p_z^+ \right) = 0 \\
\delta u_0^* &: \left(\frac{\partial N_x^*}{\partial x} + \frac{\partial N_{xy}^*}{\partial y} - 2S_x \right) = 0 \\
\delta v_0^* &: \left(\frac{\partial N_y^*}{\partial y} + \frac{\partial N_{xy}^*}{\partial x} - 2S_y \right) = 0 \\
\delta w_0^* &: \left(\frac{\partial Q_x^*}{\partial x} + \frac{\partial Q_y^*}{\partial y} - 2M_z^* + \frac{h^2}{4} p_z^+ \right) = 0 \\
\delta \theta_x^* &: \left(\frac{\partial M_x^*}{\partial x} + \frac{\partial M_{xy}^*}{\partial y} - 3Q_x^* \right) = 0 \\
\delta \theta_y^* &: \left(\frac{\partial M_y^*}{\partial y} + \frac{\partial M_{xy}^*}{\partial x} - 3Q_y^* \right) = 0 \\
\delta \theta_z^* &: \left(\frac{\partial S_x^*}{\partial x} + \frac{\partial S_y^*}{\partial y} - 3N_z^* + \frac{h^3}{8} p_z^+ \right) = 0
\end{aligned}$$

(3.37)

and the boundary conditions on the edge $x = \text{constant}$

$$\begin{aligned}
u_0 = \bar{u}_0 \quad \text{or} \quad N_x = \bar{N}_x & & v_0 = \bar{v}_0 \quad \text{or} \quad N_{xy} = \bar{N}_{xy} \\
w_0 = \bar{w}_0 \quad \text{or} \quad Q_x = \bar{Q}_x & & \theta_x = \bar{\theta}_x \quad \text{or} \quad M_x = \bar{M}_x \\
\theta_y = \bar{\theta}_y \quad \text{or} \quad M_{xy} = \bar{M}_{xy} & & \theta_z = \bar{\theta}_z \quad \text{or} \quad S_x = \bar{S}_x \\
u_0^* = \bar{u}_0^* \quad \text{or} \quad N_x^* = \bar{N}_x^* & & v_0^* = \bar{v}_0^* \quad \text{or} \quad N_{xy}^* = \bar{N}_{xy}^* \\
w_0^* = \bar{w}_0^* \quad \text{or} \quad Q_x^* = \bar{Q}_x^* & & \theta_x^* = \bar{\theta}_x^* \quad \text{or} \quad M_x^* = \bar{M}_x^* \\
\theta_y^* = \bar{\theta}_y^* \quad \text{or} \quad M_{xy}^* = \bar{M}_{xy}^* & & \theta_z^* = \bar{\theta}_z^* \quad \text{or} \quad S_x^* = \bar{S}_x^*
\end{aligned} \tag{3.38a}$$

On the edge $y = \text{constant}$

$$\begin{aligned}
u_0 = \bar{u}_0 \quad \text{or} \quad N_{xy} = \bar{N}_{xy} & & v_0 = \bar{v}_0 \quad \text{or} \quad N_y = \bar{N}_y \\
w_0 = \bar{w}_0 \quad \text{or} \quad Q_y = \bar{Q}_y & & \theta_x = \bar{\theta}_x \quad \text{or} \quad M_{xy} = \bar{M}_{xy} \\
\theta_y = \bar{\theta}_y \quad \text{or} \quad M_y = \bar{M}_y & & \theta_z = \bar{\theta}_z \quad \text{or} \quad S_y = \bar{S}_y \\
u_0^* = \bar{u}_0^* \quad \text{or} \quad N_{xy}^* = \bar{N}_{xy}^* & & v_0^* = \bar{v}_0^* \quad \text{or} \quad N_y^* = \bar{N}_y^* \\
w_0^* = \bar{w}_0^* \quad \text{or} \quad Q_y^* = \bar{Q}_y^* & & \theta_x^* = \bar{\theta}_x^* \quad \text{or} \quad M_{xy}^* = \bar{M}_{xy}^* \\
\theta_y^* = \bar{\theta}_y^* \quad \text{or} \quad M_y^* = \bar{M}_y^* & & \theta_z^* = \bar{\theta}_z^* \quad \text{or} \quad S_y^* = \bar{S}_y^*
\end{aligned} \tag{3.38b}$$

The same procedure is followed to obtain the equilibrium equations for FGM plates using other displacement models and the corresponding equilibrium equations are given in Appendix - I.

3.7 CLOSURE

In this chapter, detailed theoretical formulations for the thermal stress analysis of FGM plates based on higher order refined theories which take into account the effects of both transverse shear strain / stress and normal strain / stress are presented. Three-

dimensional constitutive relations and the Principle of Minimum Potential Energy (PMPE) are used to derive the governing equations of equilibrium. A modified and reduced version of stress-strain constitutive relations is used for models that do not consider the effect of transverse normal deformations. Theoretical formulations for HSDT-12 displacement model are discussed in detail and the equations of equilibrium obtained using other models are given in the appendix. In the following chapter, analytical solution method using Navier's solution technique is presented for the different displacement models considered in the present study.

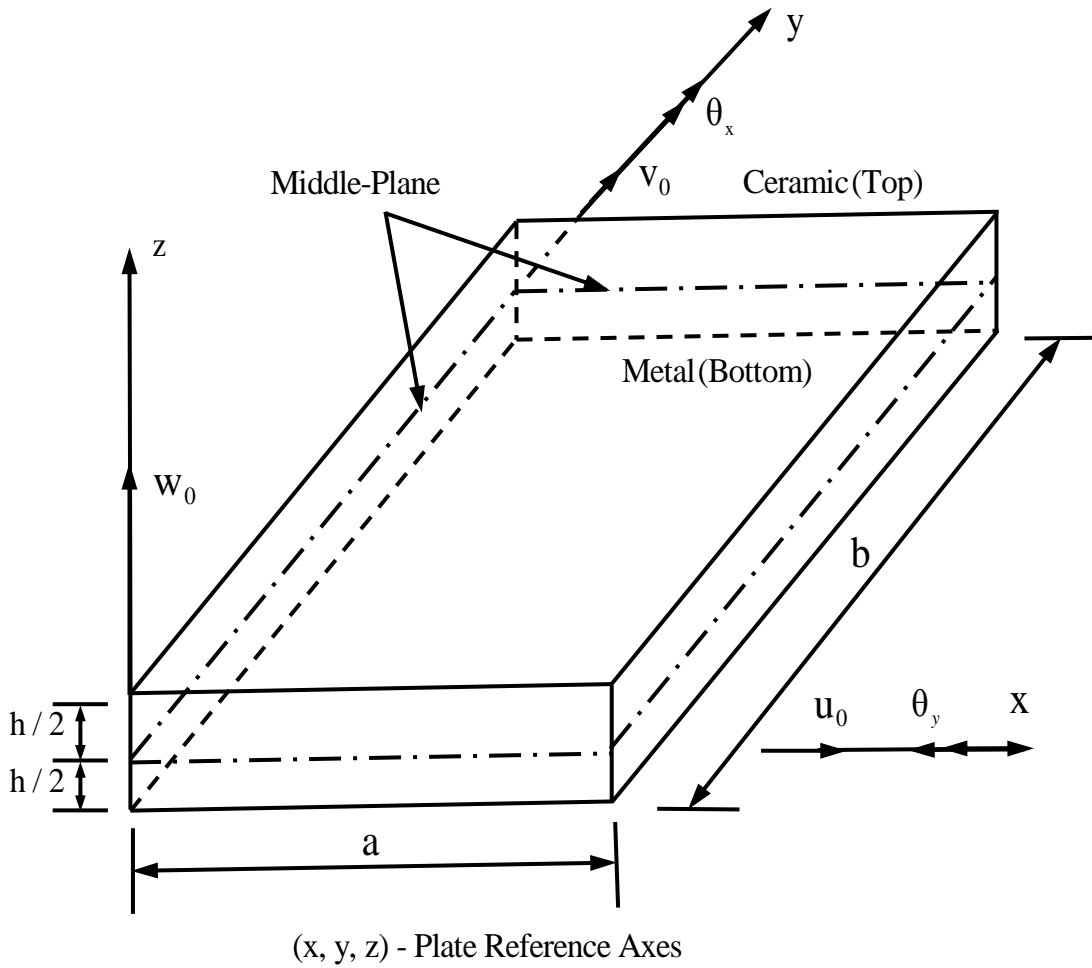


Fig. 3.1: FGM plate geometry with positive set of reference axes and displacement components

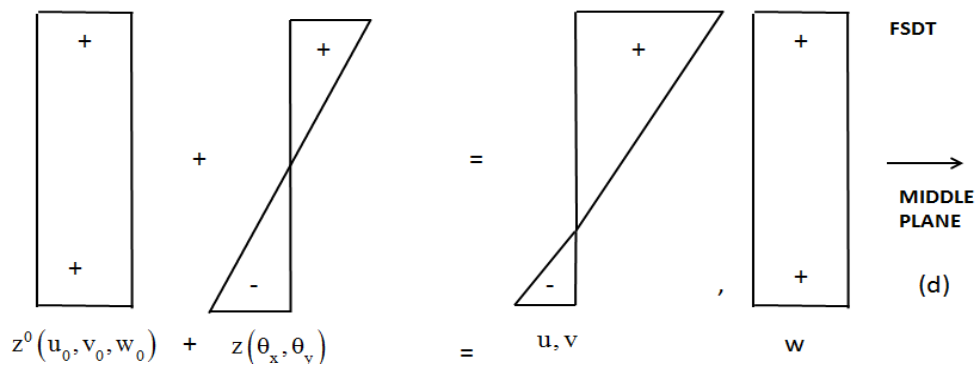
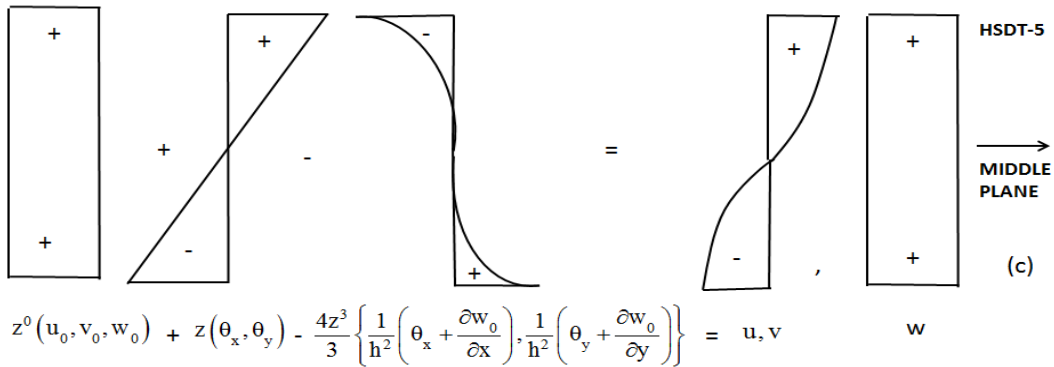
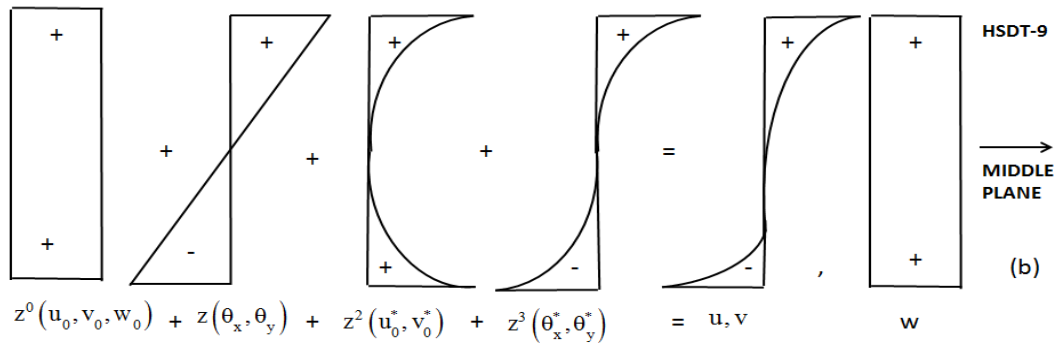
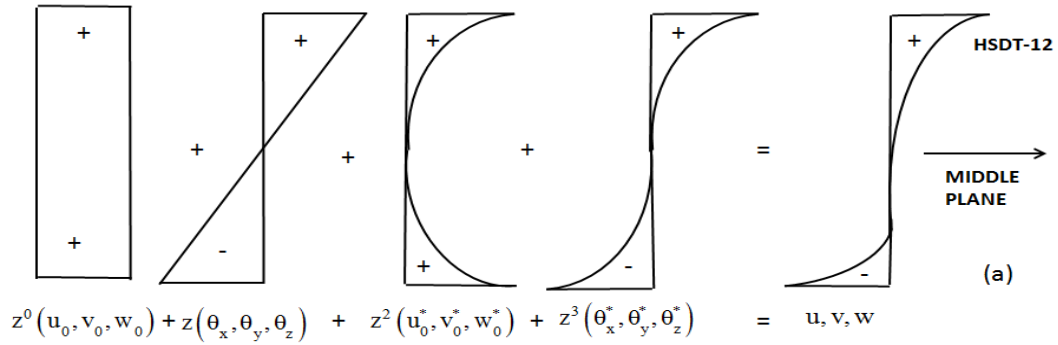


Fig. 3.2: Variation of the generalized displacement components across the thickness of an FGM plate using (a) HSDT-12, (b) HSDT-9, (c) HSDT-5 and (d) FSDT displacement models.

CHAPTER 4

ANALYTICAL SOLUTION METHOD

4.1 PRELIMINARY REMARKS

In order to solve the boundary value problem for stress analysis of FGM plates more accurately an exact three dimensional elasticity solution is needed. But the mathematical complexity involved in solving three dimensional problems necessitates the simplification of three dimensional problems to two dimensional problems with suitable assumptions, so that various two dimensional solution methods can be used effectively without sacrificing much on the accuracy. The assumption that the stress resultant rather than stresses are more reliable in the statement of governing equations helps in reducing the 3-D problem to 2-D problem. Among the analytical methods available, the Navier's solution technique is very simple and easy to use for plates with rectangular geometry with simply supported edge conditions. This method of solution for various plate problems with rectangular geometry is well documented in various texts (Timoshenko and Woinowsky-Krieger 1959, Szilard 1974, Reddy 1996). The main objective of the present investigation is to evaluate analytically the accuracy of various two dimensional theories. Therefore, for all the problems, a simply supported FGM plate subjected to constant, linear and nonlinearly varying thermal loads are considered for comparison purpose and the Navier's solution technique using double Fourier series is used to get the results with desired level of accuracy. The geometry of the plate with a positive set of the coordinate axes and physical mid-plane displacement terms are shown in Figure 3.1 in chapter 3. The various steps involved in using the above technique for the thermo-elastic bending stress analysis of FGM plates are discussed in this chapter.

4.2 NAVIER SOLUTION TECHNIQUE

In the following sections, the Navier's solution technique using the double Fourier series for the thermal stress analysis of FGM plates is presented. Various steps

involved in using the above technique are discussed in detail for HSDT-12 displacement model. Same procedure is used to obtain the solutions using other displacement models.

4.2.1 In-Plane Stresses

The FGM plate structure considered in the present work is a simply supported square / rectangular plate. Such supports imply the following boundary conditions.

At edges $x = 0$ and $x = a$:

$$\begin{aligned}
 v_0 = 0; \quad w_0 = 0; \quad \theta_y = 0; \quad \theta_z = 0; \quad M_x = 0; \\
 v_0^* = 0; \quad w_0^* = 0; \quad \theta_y^* = 0; \quad \theta_z^* = 0; \quad M_x^* = 0; \\
 N_x = 0; \quad N_x^* = 0;
 \end{aligned}
 \tag{4.1}$$

At edges $y = 0$ and $y = b$:

$$\begin{aligned}
 u_0 = 0; \quad w_0 = 0; \quad \theta_x = 0; \quad \theta_z = 0; \quad M_y = 0; \\
 u_0^* = 0; \quad w_0^* = 0; \quad \theta_x^* = 0; \quad \theta_z^* = 0; \quad M_y^* = 0; \\
 N_y = 0; \quad N_y^* = 0;
 \end{aligned}
 \tag{4.2}$$

To satisfy the above boundary conditions the generalized displacement field is expanded in double Fourier series as:

$$\begin{aligned}
 u_0 &= \sum_{m=1}^{\infty} \sum_{n=1}^{\infty} u_{0_{mn}} \cos \alpha x \sin \beta y \\
 v_0 &= \sum_{m=1}^{\infty} \sum_{n=1}^{\infty} v_{0_{mn}} \sin \alpha x \cos \beta y
 \end{aligned}$$

$$w_0 = \sum_{m=1}^{\infty} \sum_{n=1}^{\infty} w_{0_{mn}} \sin \alpha x \sin \beta y$$

$$\theta_x = \sum_{m=1}^{\infty} \sum_{n=1}^{\infty} \theta_{x_{mn}} \cos \alpha x \sin \beta y$$

$$\theta_y = \sum_{m=1}^{\infty} \sum_{n=1}^{\infty} \theta_{y_{mn}} \sin \alpha x \cos \beta y$$

$$\theta_z = \sum_{m=1}^{\infty} \sum_{n=1}^{\infty} \theta_{z_{mn}} \sin \alpha x \sin \beta y$$

$$u_0^* = \sum_{m=1}^{\infty} \sum_{n=1}^{\infty} u_{0_{mn}}^* \cos \alpha x \sin \beta y$$

$$v_0^* = \sum_{m=1}^{\infty} \sum_{n=1}^{\infty} v_{0_{mn}}^* \sin \alpha x \cos \beta y$$

$$w_0^* = \sum_{m=1}^{\infty} \sum_{n=1}^{\infty} w_{0_{mn}}^* \sin \alpha x \sin \beta y$$

$$\theta_x^* = \sum_{m=1}^{\infty} \sum_{n=1}^{\infty} \theta_{x_{mn}}^* \cos \alpha x \sin \beta y$$

$$\theta_y^* = \sum_{m=1}^{\infty} \sum_{n=1}^{\infty} \theta_{y_{mn}}^* \sin \alpha x \cos \beta y$$

$$\theta_z^* = \sum_{m=1}^{\infty} \sum_{n=1}^{\infty} \theta_{z_{mn}}^* \sin \alpha x \sin \beta y$$

(4.3)

The transverse load and thermal loading term is expanded as,

$$p_z^+ = \sum_{m=1}^{\infty} \sum_{n=1}^{\infty} p_{z_{mn}}^+ \sin \alpha x \sin \beta y$$

$$T_1 = \sum_{m=1}^{\infty} \sum_{n=1}^{\infty} T_{1_{mn}} \sin \alpha x \sin \beta y$$

$$T_0 = \sum_{m=1}^{\infty} \sum_{n=1}^{\infty} T_{0_{mn}} \sin \alpha x \sin \beta y$$

(4.4)

where $\alpha = \frac{m\pi}{a}$ and $\beta = \frac{n\pi}{b}$ $m, n = 1, 3, 5, 7, \dots$ odd.

Now the expressions for the curvature and slopes (Equation 3.15a and 3.15b) are substituted in the stress resultant-mid plane strain relationship (Equation 3.22) and the relation between the stress resultant and the mid plane strain quantities can be written as,

$$\begin{Bmatrix} N_x \\ N_y \\ N_x^* \\ N_y^* \\ N_z \\ N_z^* \\ M_x \\ M_y \\ M_x^* \\ M_y^* \\ M_z \\ M_z^* \end{Bmatrix} = [A] \begin{Bmatrix} \frac{\partial u_0}{\partial x} \\ \frac{\partial v_0}{\partial y} \\ \frac{\partial u_0^*}{\partial x} \\ \frac{\partial v_0^*}{\partial y} \\ \theta_z \\ \theta_z^* \\ \frac{\partial \theta_x}{\partial x} \\ \frac{\partial \theta_x}{\partial y} \\ \frac{\partial \theta_y}{\partial x} \\ \frac{\partial \theta_y}{\partial y} \\ \frac{\partial \theta_x^*}{\partial x} \\ \frac{\partial \theta_x^*}{\partial y} \\ \frac{\partial \theta_y^*}{\partial x} \\ \frac{\partial \theta_y^*}{\partial y} \\ w_0^* \end{Bmatrix} + [A^-] \begin{Bmatrix} \frac{\partial u_0}{\partial y} \\ \frac{\partial v_0}{\partial x} \\ \frac{\partial u_0^*}{\partial y} \\ \frac{\partial v_0^*}{\partial x} \\ \frac{\partial \theta_x}{\partial x} \\ \frac{\partial \theta_x}{\partial y} \\ \frac{\partial \theta_y}{\partial x} \\ \frac{\partial \theta_y}{\partial y} \\ \frac{\partial \theta_x^*}{\partial x} \\ \frac{\partial \theta_x^*}{\partial y} \\ \frac{\partial \theta_y^*}{\partial x} \\ \frac{\partial \theta_y^*}{\partial y} \end{Bmatrix} - \alpha_z \Delta T [C_T];$$

$$\begin{Bmatrix} N_{xy} \\ N_{xy}^* \\ M_{xy} \\ M_{xy}^* \end{Bmatrix} = [B^-] \begin{Bmatrix} \frac{\partial u_0}{\partial x} \\ \frac{\partial v_0}{\partial y} \\ \frac{\partial u_0^*}{\partial x} \\ \frac{\partial v_0^*}{\partial y} \\ \theta_z \\ \theta_z^* \\ \frac{\partial \theta_x}{\partial x} \\ \frac{\partial \theta_x}{\partial y} \\ \frac{\partial \theta_y}{\partial x} \\ \frac{\partial \theta_y}{\partial y} \\ \frac{\partial \theta_x^*}{\partial x} \\ \frac{\partial \theta_x^*}{\partial y} \\ \frac{\partial \theta_y^*}{\partial x} \\ \frac{\partial \theta_y^*}{\partial y} \\ w_0^* \end{Bmatrix} + [B] \begin{Bmatrix} \frac{\partial u_0}{\partial y} \\ \frac{\partial v_0}{\partial x} \\ \frac{\partial u_0^*}{\partial y} \\ \frac{\partial v_0^*}{\partial x} \\ \frac{\partial \theta_x}{\partial x} \\ \frac{\partial \theta_x}{\partial y} \\ \frac{\partial \theta_y}{\partial x} \\ \frac{\partial \theta_y}{\partial y} \\ \frac{\partial \theta_x^*}{\partial x} \\ \frac{\partial \theta_x^*}{\partial y} \\ \frac{\partial \theta_y^*}{\partial x} \\ \frac{\partial \theta_y^*}{\partial y} \end{Bmatrix}$$

(4.5)

$$\begin{Bmatrix} Q_x \\ Q_x^* \\ S_x \\ S_x^* \end{Bmatrix} = [D] \begin{Bmatrix} \theta_x \\ \frac{\partial w_0}{\partial x} \\ \theta_x^* \\ \frac{\partial w_0^*}{\partial x} \\ u_0^* \\ \frac{\partial \theta_z}{\partial x} \\ \frac{\partial \theta_z^*}{\partial x} \end{Bmatrix} + [D^-] \begin{Bmatrix} \theta_y \\ \frac{\partial w_0}{\partial y} \\ \theta_y^* \\ \frac{\partial w_0^*}{\partial y} \\ v_0^* \\ \frac{\partial \theta_z}{\partial y} \\ \frac{\partial \theta_z^*}{\partial y} \end{Bmatrix} \quad \begin{Bmatrix} Q_y \\ Q_y^* \\ S_y \\ S_y^* \end{Bmatrix} = [E^-] \begin{Bmatrix} \theta_x \\ \frac{\partial w_0}{\partial x} \\ \theta_x^* \\ \frac{\partial w_0^*}{\partial x} \\ u_0^* \\ \frac{\partial \theta_z}{\partial x} \\ \frac{\partial \theta_z^*}{\partial x} \end{Bmatrix} + [E] \begin{Bmatrix} \theta_y \\ \frac{\partial w_0}{\partial y} \\ \theta_y^* \\ \frac{\partial w_0^*}{\partial y} \\ v_0^* \\ \frac{\partial \theta_z}{\partial y} \\ \frac{\partial \theta_z^*}{\partial y} \end{Bmatrix} \quad (4.6)$$

where,

$$\begin{bmatrix} \frac{\partial u_0}{\partial x} & \frac{\partial v_0}{\partial y} & \frac{\partial u_0^*}{\partial x} & \frac{\partial v_0^*}{\partial y} & \theta_z & \theta_z^* \end{bmatrix}^t = \sum_{m=1}^{\infty} \sum_{n=1}^{\infty} \left\{ -\alpha u_{0mn} \quad -\beta v_{0mn} \quad -\alpha u_{0mn}^* \quad -\beta v_{0mn}^* \quad \theta_{zmn} \quad \theta_{zmn}^* \right\} \sin \alpha x \sin \beta y$$

$$\begin{bmatrix} \frac{\partial \theta_x}{\partial x} & \frac{\partial \theta_y}{\partial y} & \frac{\partial \theta_x^*}{\partial x} & \frac{\partial \theta_y^*}{\partial y} & w_0 & w_0^* \end{bmatrix}^t = \sum_{m=1}^{\infty} \sum_{n=1}^{\infty} \left\{ -\alpha \theta_{xmn} \quad -\beta \theta_{ymn} \quad -\alpha \theta_{xmn}^* \quad -\beta \theta_{ymn}^* \quad w_{0mn} \quad w_{0mn}^* \right\} \sin \alpha x \sin \beta y$$

$$\begin{bmatrix} \frac{\partial u_0}{\partial y} & \frac{\partial v_0}{\partial x} & \frac{\partial u_0^*}{\partial y} & \frac{\partial v_0^*}{\partial x} \end{bmatrix}^t = \sum_{m=1}^{\infty} \sum_{n=1}^{\infty} \left\{ \beta u_{0mn} \quad \alpha v_{0mn} \quad \beta u_{0mn}^* \quad \alpha v_{0mn}^* \right\} \cos \alpha x \cos \beta y$$

$$\begin{bmatrix} \frac{\partial \theta_x}{\partial y} & \frac{\partial \theta_y}{\partial x} & \frac{\partial \theta_x^*}{\partial y} & \frac{\partial \theta_y^*}{\partial x} \end{bmatrix}^t = \sum_{m=1}^{\infty} \sum_{n=1}^{\infty} \left\{ \beta \theta_{xmn} \quad \alpha \theta_{ymn} \quad \beta \theta_{xmn}^* \quad \alpha \theta_{ymn}^* \right\} \cos \alpha x \cos \beta y$$

$$\left[\begin{array}{cc} \theta_x & \frac{\partial w_0}{\partial x} \\ \theta_x^* & \frac{\partial w_0^*}{\partial x} \end{array} \right]^t = \sum_{m=1}^{\infty} \sum_{n=1}^{\infty} \left\{ \theta_{x_{mn}} \quad \alpha w_{0_{mn}} \quad \theta_{x_{mn}}^* \quad \alpha w_{0_{mn}}^* \right\} \cos \alpha x \sin \beta y$$

$$\left[\begin{array}{cc} u_0 & \frac{\partial \theta_z}{\partial x} \\ u_0^* & \frac{\partial \theta_z^*}{\partial x} \end{array} \right]^t = \sum_{m=1}^{\infty} \sum_{n=1}^{\infty} \left\{ u_{0_{mn}} \quad \alpha \theta_{z_{mn}} \quad u_{0_{mn}}^* \quad \alpha \theta_{z_{mn}}^* \right\} \cos \alpha x \sin \beta y$$

$$\left[\begin{array}{cc} \theta_y & \frac{\partial w_0}{\partial y} \\ \theta_y^* & \frac{\partial w_0^*}{\partial y} \end{array} \right]^t = \sum_{m=1}^{\infty} \sum_{n=1}^{\infty} \left\{ \theta_{y_{mn}} \quad \beta w_{0_{mn}} \quad \theta_{y_{mn}}^* \quad \beta w_{0_{mn}}^* \right\} \sin \alpha x \cos \beta y$$

$$\left[\begin{array}{cc} v_0 & \frac{\partial \theta_z}{\partial y} \\ v_0^* & \frac{\partial \theta_z^*}{\partial y} \end{array} \right]^t = \sum_{m=1}^{\infty} \sum_{n=1}^{\infty} \left\{ v_{0_{mn}} \quad \beta \theta_{z_{mn}} \quad v_{0_{mn}}^* \quad \beta \theta_{z_{mn}}^* \right\} \sin \alpha x \cos \beta y$$

(4.7)

The matrices $[A]$, $[A']$, $[C_T]$, $[B]$, $[B']$, $[D]$, $[D']$, $[E]$, $[E']$ are the matrices of plate stiffness whose elements are defined in Appendix-II. The same procedure is followed in obtaining the plate stiffness matrices of other models and they are also defined under the same appendix.

To solve the equilibrium equations represented by Equations 3.37 following steps are taken:

- (i) Substitute the Equations 4.5, 4.6 and 4.7 in to the equilibrium Equations 3.37.
- (ii) To solve for the unknowns u_0 , v_0 , w_0 , θ_x , θ_y , θ_z , u_0^* , v_0^* , w_0^* , θ_x^* , θ_y^* , θ_z^* for some fixed values $m = \bar{m}$ and $n = \bar{n}$, multiply the twelve equilibrium equations by

$$\begin{aligned}
& \cos \frac{\bar{m}\pi x}{a} \sin \frac{\bar{n}\pi y}{b}, \quad \sin \frac{\bar{m}\pi x}{a} \cos \frac{\bar{n}\pi y}{b}, \quad \sin \frac{\bar{m}\pi x}{a} \sin \frac{\bar{n}\pi y}{b}, \quad \cos \frac{\bar{m}\pi x}{a} \cos \frac{\bar{n}\pi y}{b}, \\
& \sin \frac{\bar{m}\pi x}{a} \cos \frac{\bar{n}\pi y}{b}, \quad \sin \frac{\bar{m}\pi x}{a} \sin \frac{\bar{n}\pi y}{b}, \quad \cos \frac{\bar{m}\pi x}{a} \sin \frac{\bar{n}\pi y}{b}, \quad \sin \frac{\bar{m}\pi x}{a} \cos \frac{\bar{n}\pi y}{b}, \\
& \sin \frac{\bar{m}\pi x}{a} \sin \frac{\bar{n}\pi y}{b}, \quad \cos \frac{\bar{m}\pi x}{a} \sin \frac{\bar{n}\pi y}{b}, \quad \sin \frac{\bar{m}\pi x}{a} \cos \frac{\bar{n}\pi y}{b}, \quad \sin \frac{\bar{m}\pi x}{a} \sin \frac{\bar{n}\pi y}{b}
\end{aligned}$$

respectively and let them be doubly integrated between the limits $(0 \leq x \leq a)$ and $(0 \leq y \leq b)$

(iii) Apply following orthogonally conditions.

$$\begin{aligned}
\int_0^a \sin \frac{m\pi x}{a} \sin \frac{\bar{m}\pi x}{a} dx &= 0 && \text{if } m \neq \bar{m} \\
&= a/2 && \text{if } m = \bar{m}
\end{aligned}$$

$$\begin{aligned}
\int_0^b \sin \frac{n\pi y}{b} \sin \frac{\bar{n}\pi y}{b} dy &= 0 && \text{if } n \neq \bar{n} \\
&= b/2 && \text{if } n = \bar{n}
\end{aligned}$$

$$\begin{aligned}
\int_0^a \cos \frac{m\pi x}{a} \cos \frac{\bar{m}\pi x}{a} dx &= 0 && \text{if } m \neq \bar{m} \\
&= a/2 && \text{if } m = \bar{m}
\end{aligned}$$

$$\begin{aligned}
\int_0^b \cos \frac{n\pi y}{b} \cos \frac{\bar{n}\pi y}{b} dy &= 0 && \text{if } n \neq \bar{n} \\
&= b/2 && \text{if } n = \bar{n}
\end{aligned}$$

and

$$\int_0^a \sin \frac{m\pi x}{a} \cos \frac{\bar{m}\pi x}{a} dx = 0;$$

$$\int_0^b \cos \frac{n\pi y}{b} \sin \frac{\bar{n}\pi y}{b} dy = 0;$$

$$\int_0^a \cos \frac{m\pi x}{a} \sin \frac{\bar{m}\pi x}{a} dx = 0;$$

$$\int_0^b \sin \frac{n\pi y}{b} \cos \frac{\bar{n}\pi y}{b} dy = 0;$$

irrespective of the values m and n.

After following the steps (i) to (iii) and collecting the coefficients, the solution for the Fourier amplitudes is obtained in the following form ;

$$[X]_{12 \times 12} \times \begin{Bmatrix} u_0 \\ v_0 \\ w_0 \\ \theta_x \\ \theta_y \\ \theta_z \\ u_0^* \\ v_0^* \\ w_0^* \\ \theta_x^* \\ \theta_y^* \\ \theta_z^* \end{Bmatrix}_{12 \times 1} = \begin{Bmatrix} 0 \\ 0 \\ p_z^+ \\ 0 \\ 0 \\ \frac{h}{2} p_z^+ \\ 0 \\ 0 \\ \frac{h^2}{4} p_z^+ \\ 0 \\ 0 \\ \frac{h^3}{8} p_z^+ \end{Bmatrix} + \{F_T\}_{12 \times 1}$$

(4.8)

For any fixed values of m and n. The elements of the coefficient matrix [X] are given in Appendix III and the coefficients of thermal force matrix {F_T} are given in Appendix IV. Similarly the elements of [X] and {F_T} matrices of other models are also given under the same appendix.

The Fourier amplitudes can be obtained by solving Equation 4.8. These amplitudes are used to evaluate the generalized displacement components and their derivatives to obtain the stress resultants by substituting in Equations 4.5 and 4.6. Further, these values (generalized displacement components and their derivatives) are back substituted into the strain-displacement relations i.e. in Equation 3.16a and 3.16b to obtain the values of strains. The complete three dimensional Hooke's law can be used

to compute the in-plane stress, and the transverse stresses can then be calculated using equilibrium equations.

4.2.1.1 Transverse Stress (τ_{xz} , τ_{yz} , σ_z)

The transverse stresses can be evaluated from the constitutive stress-strain relations, but they will not satisfy the stress boundary conditions at top and bottom surfaces of the plate. Whereas in-plane stress components are independent of boundary conditions and are evaluated from the constitutive relations and hence these are used for the computation of transverse stress components by integrating three dimensional elasticity equilibrium equations. The three dimensional equations of equilibrium without body forces are given by,

$$\begin{aligned}\frac{\partial \sigma_x}{\partial x} + \frac{\partial \tau_{xy}}{\partial y} + \frac{\partial \tau_{xz}}{\partial z} &= 0 \\ \frac{\partial \tau_{xy}}{\partial x} + \frac{\partial \sigma_y}{\partial y} + \frac{\partial \tau_{yz}}{\partial z} &= 0 \\ \frac{\partial \tau_{xz}}{\partial x} + \frac{\partial \tau_{yz}}{\partial y} + \frac{\partial \sigma_z}{\partial z} &= 0\end{aligned}\tag{4.9}$$

The transverse stresses are derived by integrating the above 3-D equilibrium equations across the thickness coordinate 'z' and are given by,

$$\begin{aligned}\tau_{xz} &= - \int_{-h/2}^z \left(\frac{\partial \sigma_x}{\partial x} + \frac{\partial \tau_{xy}}{\partial y} \right) dz \\ \tau_{yz} &= - \int_{-h/2}^z \left(\frac{\partial \sigma_y}{\partial y} + \frac{\partial \tau_{xy}}{\partial x} \right) dz \\ \sigma_z &= - \int_{-h/2}^z \left(\frac{\partial \tau_{xz}}{\partial x} + \frac{\partial \tau_{yz}}{\partial y} \right) dz\end{aligned}\tag{4.10}$$

The above equilibrium equations are valid throughout the plate thickness from bottom to top surface of the plate over the range of $-h/2$ to $h/2$.

The in-plane stresses σ_x , σ_y and τ_{xy} in Equation 4.10 are expressed in terms of expanded strain components from Equation 3.15a and 3.9a and thus the transverse stresses takes the form,

$$\begin{aligned}
\tau_{xz} = & - \int_{-h/2}^z \left[\frac{\partial}{\partial X} \left\{ Q_{11} \left(\varepsilon_{x_0} + z\kappa_x + z^2\varepsilon_{x_0}^* + z^3\kappa_x^* \right) + Q_{12} \left(\varepsilon_{y_0} + z\kappa_y + z^2\varepsilon_{y_0}^* + z^3\kappa_y^* \right) \right. \right. \\
& + Q_{13} \left(\varepsilon_{z_0} + z\kappa_z + z^2\varepsilon_{z_0}^* \right) - \left(Q_{11} + Q_{12} + Q_{13} \right) \alpha_z \Delta T \left. \left. \right\} \right. \\
& \left. + \frac{\partial}{\partial Y} \left\{ Q_{44} \left(\varepsilon_{xy_0} + z\kappa_{xy} + z^2\varepsilon_{xy_0}^* + z^3\kappa_{xy}^* \right) \right\} \right] dz \\
\tau_{yz} = & - \int_{-h/2}^z \left[\frac{\partial}{\partial Y} \left\{ Q_{12} \left(\varepsilon_{x_0} + z\kappa_x + z^2\varepsilon_{x_0}^* + z^3\kappa_x^* \right) + Q_{22} \left(\varepsilon_{y_0} + z\kappa_y + z^2\varepsilon_{y_0}^* + z^3\kappa_y^* \right) \right. \right. \\
& + Q_{23} \left(\varepsilon_{z_0} + z\kappa_z + z^2\varepsilon_{z_0}^* \right) - \left(Q_{12} + Q_{22} + Q_{23} \right) \alpha_z \Delta T \left. \left. \right\} \right. \\
& \left. + \frac{\partial}{\partial X} \left\{ Q_{44} \left(\varepsilon_{xy_0} + z\kappa_{xy} + z^2\varepsilon_{xy_0}^* + z^3\kappa_{xy}^* \right) \right\} \right] dz \\
\sigma_z = & - \int_{-h/2}^z \left[\frac{\partial}{\partial X} \left\{ Q_{66} \left(\phi_x + z\kappa_{xz} + z^2\phi_x^* + z^3\kappa_{xz}^* \right) \right\} \right. \\
& \left. + \frac{\partial}{\partial Y} \left\{ Q_{55} \left(\phi_y + z\kappa_{yz} + z^2\phi_y^* + z^3\kappa_{yz}^* \right) \right\} \right] dz
\end{aligned} \tag{4.11}$$

The general expression for transverse stresses in terms of expanded displacement components are expressed as,

$$\begin{aligned}
\tau_{xz} = & - \int_{-h/2}^z \left(Q_{11} \frac{\partial^2 u_0}{\partial x \partial y} + Q_{11} z \frac{\partial^2 \theta_x}{\partial x \partial y} + Q_{11} z^2 \frac{\partial^2 u_0^*}{\partial x \partial y} + Q_{11} z^3 \frac{\partial^2 \theta_x^*}{\partial x \partial y} + Q_{12} \frac{\partial^2 v_0}{\partial y^2} \right. \\
& + Q_{12} z \frac{\partial^2 \theta_y}{\partial y^2} + Q_{12} z^2 \frac{\partial^2 v_0^*}{\partial y^2} + Q_{12} z^3 \frac{\partial^2 \theta_y^*}{\partial y^2} + Q_{13} \frac{\partial \theta_z}{\partial y} \\
& + 2Q_{13} z \frac{\partial w_0^*}{\partial y} + 3Q_{13} z^2 \frac{\partial \theta_z^*}{\partial y} - Q_{11} \alpha_z \Delta T - Q_{12} \alpha_z \Delta T - Q_{13} \alpha_z \Delta T \\
& + Q_{44} \frac{\partial^2 u_0}{\partial x \partial y} + Q_{44} z \frac{\partial^2 \theta_x}{\partial x \partial y} + Q_{44} z^2 \frac{\partial^2 u_0^*}{\partial x \partial y} + Q_{44} z^3 \frac{\partial^2 \theta_x^*}{\partial x \partial y} + Q_{44} \frac{\partial^2 v_0}{\partial x^2} \\
& \left. + Q_{44} z \frac{\partial^2 \theta_y}{\partial x^2} + Q_{44} z^2 \frac{\partial^2 v_0^*}{\partial x^2} + Q_{44} z^3 \frac{\partial^2 \theta_y^*}{\partial x^2} \right) dz \\
\tau_{yz} = & - \int_{-h/2}^z \left(Q_{12} \frac{\partial^2 u_0}{\partial x \partial y} + Q_{12} z \frac{\partial^2 \theta_x}{\partial x \partial y} + Q_{12} z^2 \frac{\partial^2 u_0^*}{\partial x \partial y} + Q_{12} z^3 \frac{\partial^2 \theta_x^*}{\partial x \partial y} + Q_{22} \frac{\partial^2 v_0}{\partial y^2} \right. \\
& + Q_{22} z \frac{\partial^2 \theta_y}{\partial y^2} + Q_{22} z^2 \frac{\partial^2 v_0^*}{\partial y^2} + Q_{22} z^3 \frac{\partial^2 \theta_y^*}{\partial y^2} + Q_{23} \frac{\partial \theta_z}{\partial y} + 2Q_{23} z \frac{\partial w_0^*}{\partial y} \\
& + 3Q_{23} z^2 \frac{\partial \theta_z^*}{\partial y} - Q_{12} \alpha_z \Delta T - Q_{22} \alpha_z \Delta T - Q_{23} \alpha_z \Delta T + Q_{44} \frac{\partial^2 u_0}{\partial x \partial y} \\
& + Q_{44} z \frac{\partial^2 \theta_x}{\partial x \partial y} + Q_{44} z^2 \frac{\partial^2 u_0^*}{\partial x \partial y} + Q_{44} z^3 \frac{\partial^2 \theta_x^*}{\partial x \partial y} + Q_{44} \frac{\partial^2 v_0}{\partial x^2} \\
& \left. + Q_{44} z \frac{\partial^2 \theta_y}{\partial x^2} + Q_{44} z^2 \frac{\partial^2 v_0^*}{\partial x^2} + Q_{44} z^3 \frac{\partial^2 \theta_y^*}{\partial x^2} \right) dz \\
\sigma_z = & - \int_{-h/2}^z \left(Q_{66} \frac{\partial \theta_x}{\partial x} + 2Q_{66} z \frac{\partial u_0^*}{\partial x} + 3Q_{66} z^2 \frac{\partial \theta_x^*}{\partial x} + Q_{66} \frac{\partial^2 w_0}{\partial x^2} + Q_{66} z \frac{\partial^2 \theta_z}{\partial x^2} \right. \\
& + Q_{66} z^2 \frac{\partial^2 w_0^*}{\partial x^2} + Q_{66} z^3 \frac{\partial^2 \theta_z^*}{\partial x^2} + Q_{55} \frac{\partial \theta_y}{\partial y} + 2Q_{55} z \frac{\partial v_0^*}{\partial y} \\
& + 3Q_{55} z^2 \frac{\partial \theta_y^*}{\partial y} + Q_{55} \frac{\partial^2 w_0}{\partial y^2} + Q_{55} z \frac{\partial^2 \theta_z}{\partial y^2} + Q_{55} z^2 \frac{\partial^2 w_0^*}{\partial y^2} \\
& \left. + Q_{55} z^3 \frac{\partial^2 \theta_z^*}{\partial y^2} \right) dz
\end{aligned}$$

(4.12)

4.3 CLOSURE

The various steps involved in obtaining analytical solutions for the thermal stress analysis of FGM plates using Navier's solution technique is presented in this chapter. For brevity sake, Higher Order displacement model with twelve degrees of freedom HSDT-12 is discussed in detail. The elements of plate stiffness matrices, the coefficient matrix $[X]$ and thermal force matrix $\{F_T\}$ obtained using various displacement models are given in Appendices. The numerical results obtained considering the various displacement models and the discussion of results for various plate problems using the above technique are presented in the following chapter.

CHAPTER 5

NUMERICAL RESULTS AND DISCUSSIONS

5.1 PRELIMINARY REMARKS

In this chapter, various numerical examples solved are described and discussed for establishing the accuracy of various theories related to thermo-elastic analysis of FGM plates. For all the example problems, simply supported boundary condition is considered for the analysis. The plates are subjected to nonlinear, linear and constant variation of temperatures across the plate thickness, while in-plane is sinusoidal. The equations of equilibrium are derived using the Principle of Minimum Potential Energy (PMPE) and closed form solutions are obtained using Navier's solution technique. Firstly, the accuracy of the solutions obtained using the various displacement models considered in the present study is established by comparing the displacements and stresses with that of 3-D elasticity solutions wherever available in the literature. After establishing the accuracy of each model, comparative studies have been carried out and benchmark results using all the models are presented for FGM plates with different material properties, length to breadth ratio, length to thickness ratio and power law parameter.

For the solution of boundary value problem obtained using the various displacement models and their theoretical formulation given in Chapter 3 and the solution method given in Chapter 4, a set of computer codes using MATLAB-15 software were developed for numerical computation. In this investigation twelve separate computer programmes were developed for the thermo-elastic analysis of FGM plates. Out of twelve programmes, four each corresponds to nonlinear, linear and constant variation of temperature. All the numerical results shown in tables and figures using various displacement models are generated independently using various computer programmes developed during the present investigation. The numerical results of all the models compared are the in-plane/transverse displacements and stresses. A shear correction factor of $5/6$ is used for obtaining the results using

Whitney-Pagano's theory (Pagano and Hatfield, 1972). The various numerical examples are solved, and the results obtained using various theories, material properties and temperature profiles are discussed in detail in the following section.

5.2 THERMAL STRESS ANALYSIS

The following material set data are used in obtaining numerical results.

Material set - 1 (M1) [Alibeigloo (2010)]

Monel-Zirconia FGM plate (70Ni-30Cu- ZrO₂)

$E_m = 227.24$ GPa	$\alpha_m = 15 \times 10^{-6}$ /K	$k_m = 25$ W/mK	$\nu = 0.3$
$E_c = 125.83$ GPa	$\alpha_c = 10 \times 10^{-6}$ /K	$k_c = 2.09$ W/mK	$\nu = 0.3$.
$E_c / E_m = 0.5537$	$\alpha_c / \alpha_m = 0.6667$,	$k_c / k_m = 0.0836$	

Material set - 2 (M2) [Praveen and Reddy. (1998)]

Aluminium-Alumina FGM plate (Al- Al₂O₃)

$E_m = 70$ GPa	$\alpha_m = 23 \times 10^{-6}$ /K,	$k_m = 204$ W/mK,	$\nu = 0.3$
$E_c = 380$ GPa,	$\alpha_c = 7.4 \times 10^{-6}$ /K,	$k_c = 10.4$ W/mK,	$\nu = 0.3$.
$E_c / E_m = 5.429$,	$\alpha_c / \alpha_m = 0.3217$,	$k_c / k_m = 0.0510$	

Material-3 (M3) [Jabbari et. al. (2014)]

Titanium Alloy - Zirconia FGM plate (Ti-6Al-4V - ZrO₂)

$E_m = 66.2$ GPa,	$\alpha_m = 10.3 \times 10^{-6}$ /K,	$k_m = 18.1$ W/mK,	$\nu = 0.322$
$E_c = 117$ GPa,	$\alpha_c = 7.11 \times 10^{-6}$ /K,	$k_c = 2.036$ W/mK,	$\nu = 0.322$.
$E_c / E_m = 1.7673$,	$\alpha_c / \alpha_m = 0.690$,	$k_c / k_m = 0.1125$	

Results that are reported in tables and plots are obtained using the following nondimensionalized forms:

$$(\bar{u}, \bar{v}, \bar{w}) = \frac{(u, v, w)E^*}{Pa}$$

$$(\bar{\sigma}_x, \bar{\sigma}_y, \bar{\sigma}_z, \bar{\tau}_{xy}, \bar{\tau}_{xz}, \bar{\tau}_{yz}) = \frac{(\sigma_x, \sigma_y, \sigma_z, \tau_{xy}, \tau_{xz}, \tau_{yz})}{PE^*}$$

$$\bar{T} = \frac{\alpha^* T_z}{P}$$

Where, $P = p_0/E^*$ for applied transverse mechanical load p_0 and $P = \alpha^*/T_1$ for applied temperature T_1 at the top surface of the FGM plate. The scale factors corresponding to coefficient of thermal expansion and young's modulus of elasticity are $\alpha^* = 10^{-6} / K$ and $E^* = 1 \text{ Gpa}$ respectively.

Unless otherwise specified within the table(s) or plot(s) the location (i.e. x- and y-coordinates) for the maximum values of displacements and stresses for the present evaluations are as follows:

In-plane displacement (\bar{u}) : (0, b/2)

In-plane displacement (\bar{v}) : (a/2, 0)

Transverse displacement (\bar{w}) : (a/2, b/2)

In-plane normal stress ($\bar{\sigma}_x$) : (a/2, b/2)

In-plane normal stress ($\bar{\sigma}_y$) : (a/2, b/2)

Transverse normal stress ($\bar{\sigma}_z$) : (a/2, b/2)

In-plane shear stress ($\bar{\tau}_{xy}$) : (0, 0)

Transverse shear stress ($\bar{\tau}_{xz}$) : (0, b/2)

Transverse shear stress ($\bar{\tau}_{yz}$) : (a/2, 0)

5.2.1 Description of Examples and Discussions

In this section, various examples related to thermo-elastic analysis of FGM plates are described and discussed. Initially, through the thickness variation of thermo-physical

properties of various materials are presented and then the accuracy of the displacement models is established by comparing with the 3-D elasticity solutions available in the literature. Then the parametric studies are performed and results are presented for Monel-Zirconia, Aluminium-Alumina and Titanium Alloy-Zirconia FGM plates subjected to steady state thermal loads. Also the effect of temperature distribution (viz., nonlinear, linear and constant) on displacements and stresses are discussed.

Example 1: In this example, through the thickness variation of material properties and temperature field distribution for various FGMs considered in the study are presented. The effective material properties are evaluated using micromechanical scheme based on power law function. The volume fraction (V_f) distribution of the ceramic-metal constituent phases in an FGM plate is governed by power law parameter p . Fig. 5.1 shows through the thickness variation of volume fraction distribution V_f and temperature profile with increase in power law parameter p .

Three materials namely Monel-Zirconia (M1), Aluminium-Alumina (M2) and Titanium Alloy-Zirconia (M3) are considered in the analysis. Through the thickness variation of effective material properties like young's modulus of elasticity, thermal coefficient of expansion, thermal conductivity of M1, M2 and M3 using various power law parameters are presented. Similarly the nonlinear temperature variation obtained by solving steady state heat conduction equation is also presented. Through the thickness variation the material properties for various power law parameters are shown in Fig. 5.2, Fig. 5.3 and Fig. 5.4 for Monel-Zirconia (M1), Aluminium-Alumina (M2) and Titanium Alloy-Zirconia (M3) FGMs respectively. It is observed that, the volume fraction of metal constituent phase in an FGM plate increases with increase in p value and is purely ceramic for p equal to zero. Similar variations are observed in young's modulus of elasticity, thermal coefficient of expansion and thermal conductivity of FGMs. Also, the ceramic surface is exposed to temperature and is gradually reduced to reach zero / room temperature at the metal surface. Through the thickness variation of temperature is nonlinear for p value greater than or equal to one and is linear for p equal to zero.

Example 2: In order to establish the accuracy of various displacement models, a simply supported Monel-Zirconia (M1) FGM plate subjected to transverse sinusoidal load of intensity p_0 at the top surface of the plate is considered. The numerical results of displacements and stresses are compared with the three dimensional elasticity solutions reported by Reddy and Cheng, (2001a). The nondimensionalized in-plane displacement \bar{u} , transverse displacement \bar{w} and in-plane normal stress $\bar{\sigma}_x$ at various locations across the thickness of the FGM plate are given in Table 5.1, Table 5.2 and Table 5.3 respectively along with the percentage error with respect to 3-D elasticity solutions. The results clearly shows that the values obtained using HSDT-12 are in close agreement with the 3-D elasticity solutions for all a/h ratios. For a/h ratio equal to 4, HSDT-9 overpredicts the in-plane displacement \bar{u} by 11.42% and transverse displacement \bar{w} by 5.64% at the top surface of the plate as compared with the exact solutions. Whereas the in-plane normal stress $\bar{\sigma}_x$ at the top surface of the plate, are underpredicted by HSDT-9, HSDT-5 and FSDT by 3.76%, 3.76% and 9.16% respectively. Also, the maximum value of transverse shear stress $\bar{\tau}_{xz}$ and transverse normal stress $\bar{\sigma}_z$ at the middle surface of the plate are given in Table 5.4 along with the percentage of error with respect to 3-D elasticity solutions. It can be seen that, for all a/h ratios HSDT-12 gives better accuracy as compared to other displacement models. For a/h ratio equal to 10, HSDT-12 overpredicts the transverse shear stress $\bar{\tau}_{xz}$ by 0.14%, whereas transverse normal stress $\bar{\sigma}_z$ were predicted as accurate as exact solutions. The accuracy of the models in predicting the displacements and stresses increases with increase in slenderness ratio (a/h ratio). In all the parameters considered, the percentage error in the results obtained from HSDT-12 is less than 2.5% and is found to be in excellent agreement with the 3-D elasticity solutions.

Example 3: In this example, accuracy of the displacement models in predicting the thermal responses is established by comparing with the 3-D elasticity solutions reported by Alibeigloo (2010). A simply supported Monel-Zirconia (M1) FGM plate subjected to thermal load is considered. The temperature variation is assumed to be nonlinear and obeys steady state heat conduction equation. Through the thickness variation of nondimensionalized transverse displacement \bar{w} , transverse shear stress $\bar{\tau}_{xz}$ and transverse normal stress $\bar{\sigma}_z$ are compared with the 3-D elasticity solutions

reported for a square FGM plate with side-to-thickness ratio (a/h ratio) 5, 10 and 20. The graphical representations for the variation of transverse displacement \bar{w} using various a/h ratios are given in Fig. 5.5. The results clearly indicate that, only HSDT-12 predicts the nonlinear variation of transverse displacement most accurately and it is very much closer to the exact solutions whereas all other models predict the variation as linear. The variation of nondimensionalized transverse shear stress $\bar{\tau}_{xz}$ and transverse normal stress $\bar{\sigma}_z$ across the plate thickness direction are depicted in Fig. 5.6 and Fig. 5.7 respectively. It shows that HSDT-12 predicts transverse stresses as accurately as exact solutions, while all other models either underpredicts or overpredicts the transverse stresses. The effect of nonlinear transverse shear and normal stress / strain in HSDT-12 model has a significant effect in predicting the displacement and stresses in FGM plates. Thus it can be clearly seen from the graphs that for all values of a/h ratios considered, the transverse displacement and stresses computed using HSDT-12 model is very much closer to exact solutions as compared to other models considered for comparison. Therefore among various two dimensional theories considered, the results obtained using HSDT-12 are in good agreement with exact solutions and hence the same is used as reference for establishing the accuracy of other models in the subsequent examples.

Example 4: In order to study the effect of variations in geometric and power law parameters on displacements and stresses, a simply supported square / rectangular Monel-Zirconia (M1) FGM plate subjected to nonlinear thermal loads (T_{NL}) is considered. The nondimensionalized values of displacements \bar{u} , \bar{v} , \bar{w} and stresses $\bar{\sigma}_x$, $\bar{\sigma}_y$, $\bar{\tau}_{xy}$, $\bar{\tau}_{xz}$, $\bar{\tau}_{yz}$ in a thick (a/h equal to 4 and power law parameter equal to 3) FGM plate with various values of length-to-breadth ratios (a/b ratios) are given in Table 5.5 and Table 5.6 respectively. The difference in the values predicted using HSDT-12 and those obtained using other models increases with the increase in the value of length-to-breadth ratio and the minimum difference is observed in a square plate (a/b ratio equal to 1). For a/b ratio equal to 2, the values of in-plane displacements \bar{u} and \bar{v} predicted by HSDT-9, HSDT-5 and FSDT are 13.42%, 14.85%, 13.70% lower as compared to the values predicted by HSDT-12 and the values of transverse displacement \bar{w} predicted by HSDT-9, HSDT-5 and FSDT are

52.34%, 59.78%, 52.45% lower as compared to the values predicted by HSDT-12. For a square plate with a/b ratio equal to 1, the values of in-plane normal stresses $\bar{\sigma}_x$ and $\bar{\sigma}_y$ predicted by HSDT-9, HSDT-5 and FSDT are 9.77%, 9.86%, 9.87% lower as compared to the values predicted by HSDT-12, the values of in-plane shear stress $\bar{\tau}_{xy}$ predicted by HSDT-9, HSDT-5 and FSDT are 4.67%, 4.73%, 4.74% higher as compared to the values predicted by HSDT-12 and the values of transverse shear stresses $\bar{\tau}_{xz}$ and $\bar{\tau}_{yz}$ predicted by HSDT-9, HSDT-5 and FSDT are 33.02%, 78.81% and 37.16% higher as compared to the values predicted by HSDT-12.

The nondimensionalized values of the in-plane displacement \bar{u} and in-plane normal stress $\bar{\sigma}_x$ at bottom, middle and top surface of a rectangular (a/b ratio equal to 1.5) FGM plate are given in Table 5.7 and Table 5.8 respectively. The results clearly show that, the value of displacements and stress increase from bottom to top surface of the plate. Whereas the percentage difference in the values predicted by HSDT-12 and other models is found to be maximum at the bottom surface of the plate and minimum at the middle surface of the plate for all a/h ratios and power law parameters considered. For a/h ratio equal to 10 and power law parameter p equal to 2, the value of in-plane displacement \bar{u} predicted by HSDT-9, HSDT-5 and FSDT are 1.68%, 1.95%, 1.82% lower as compared to the values predicted by HSDT-12 at the top surface of the plate. For a/h ratio equal to 10 and power law parameter p equal to 5, the value of in-plane normal stress $\bar{\sigma}_x$ predicted by HSDT-9, HSDT-5 and FSDT are 48.21%, 60.42%, 51.04% higher as compared to the values predicted by HSDT-12 at the bottom surface of the plate. For all cases considered, HSDT-9 is found to predict closer results to HSDT-12 and with least percentage difference as compared to other models.

In order to study the effect of displacements and stresses with increase in a/h ratio and power law parameter p, a simply supported square FGM plate is considered. The nondimensionalized values of in-plane displacement \bar{u} and transverse displacement \bar{w} are given in Table 5.9 and Table 5.10 respectively. For a/h ratio equal to 4 and power law parameter p equal to 5, the value of in-plane displacement \bar{u} predicted by HSDT-9, HSDT-5 and FSDT are 6.38%, 6.65%, 6.13% lower as compared to the

values predicted by HSDT-12 and the value of transverse displacement \bar{w} predicted by HSDT-9, HSDT-5 and FSDT are 31.16%, 35.52%, 31.14% lower as compared to the values predicted by HSDT-12. The nondimensionalized values of in-plane normal stress $\bar{\sigma}_x$, in-plane shear stress $\bar{\tau}_{xy}$ and transverse shear stress $\bar{\tau}_{xz}$ are given in Table 5.11, Table 5.12 and Table 5.13 respectively. For a/h ratio equal to 4 and power law parameter p equal to 2, the value of in-plane normal stress $\bar{\sigma}_x$ predicted by HSDT-9, HSDT-5 and FSDT models are 7.09%, 5.86% and 6.50% lower as compared to the values predicted by HSDT-12, the value of in-plane shear stress $\bar{\tau}_{xy}$ predicted by HSDT-9, HSDT-5 and FSDT models are 5.98%, 6.98% and 6.46% lower as compared to the values predicted by HSDT-12 and the value of transverse stress $\bar{\tau}_{xz}$ predicted by HSDT-9, HSDT-5 and FSDT models are 11.48%, 34.21% and 14.02% higher as compared to the values predicted by HSDT-12. The percentage difference in the values predicted by HSDT-12 and other displacement models decreases with increase in a/h ratio and increases with increase in power law parameter. For plates with a/h ratio 20 and above, the differences in the displacements and stresses is found to be minimum. Among various models considered, the values predicted by HSDT-9 are found to be with least percentage difference as compared to HSDT-12 model.

Through the thickness variation of nondimensionalized in-plane displacements \bar{u} and \bar{v} , transverse displacement \bar{w} , in-plane shear stress $\bar{\tau}_{xy}$, in-plane normal stresses $\bar{\sigma}_x$ and $\bar{\sigma}_y$ and transverse shear stresses $\bar{\tau}_{xz}$ and $\bar{\tau}_{yz}$ for a rectangular plate with a/b ratio equal to 3, a/h ratio equal to 4 and power law parameter p equal to 4 are shown in Figs. 5.8 to 5.15 respectively. From the figures, it can be seen that considerable difference in the values is observed between HSDT-12 and rest of the models. The values predicted by HSDT-9, HSDT-5 and FSDT models are closer to each other and are much different from HSDT-12. This clearly indicates that the effect of transverse shear and normal strain / stress has a significant effect in predicting the overall thermo-elastic responses in an FGM plates.

Example 5: A simply supported square / rectangular Aluminium-Alumina (M2) FGM plate subjected to nonlinear thermal loads (T_{NL}) is considered. The behaviour of

displacements and stresses at various locations of the plate is studied by varying geometric parameters like a/b ratio and a/h ratio and power law parameter p. The nondimensionalized values of in-plane/transverse displacements and stresses in a rectangular (a/b ratio equal to 2 and p equal to 2) FGM plate for various values of side-to thickness ratios (a/h ratios) are given in Table 5.14 and Table 5.15 respectively. For a/h ratio equal to 4, the values of in-plane displacements \bar{u} and \bar{v} predicted by HSDT-9, HSDT-5 and FSDT are 10.52%, 13.01%, 9.47% lower as compared to the values predicted by HSDT-12, the values of transverse displacement \bar{w} predicted by HSDT-9, HSDT-5 and FSDT are 55.24%, 81.18%, 54.31% lower as compared to the values predicted by HSDT-12, the values of in-plane normal stresses $\bar{\sigma}_x$ predicted by HSDT-9, HSDT-5 and FSDT are 7.28%, 6.26%, 6.38% lower as compared to the values predicted by HSDT-12, the values of in-plane normal stress $\bar{\sigma}_y$ predicted by HSDT-9, HSDT-5 and FSDT are 28.15%, 23.74%, 24.26% lower as compared to the values predicted by HSDT-12, the values of in-plane shear stresses $\bar{\tau}_{xy}$ predicted by HSDT-9, HSDT-5 and FSDT are 9.95%, 8.17%, 8.38% higher as compared to the values predicted by HSDT-12, the values of transverse shear stress $\bar{\tau}_{xz}$ and $\bar{\tau}_{yz}$ predicted by HSDT-9, HSDT-5 and FSDT are 18.51%, 56.37%, 10.00% lower as compared to the values predicted by HSDT-12. It is observed that for all parameters considered, the in-plane displacements and stresses predicted by HSDT-9, HSDT-5 and FSDT are much closer to each other and deviate much from the values predicted by HSDT-12. For plates with a/h ratio 20 and above, the values predicted by all the models are almost same.

The nondimensionalized values of the in-plane displacement \bar{v} and in-plane shear stress $\bar{\tau}_{xy}$ at the bottom, middle and top surface of an FGM plate for a/h ratio 20 are given in Table 5.16 and Table 5.17 respectively. The results clearly shows that, the values of in-plane / transverse displacements and stresses predicted by all the models are very close to each other throughout the plate thickness direction in both square and rectangular plates and for various power law parameters. Hence, the percentage differences in the results predicted by various models and HSDT-12 is very less. For a/b ratio equal to 2 and power law parameter p equal to 3, the value of in-plane displacement \bar{v} and in-plane shear stress $\bar{\tau}_{xy}$ predicted by HSDT-9, HSDT-5 and

FSDT are 4.07%, 2.57%, 3.30% lower as compared to the values predicted by HSDT-12 at the bottom surface of the plate.

In order to study the effect of displacements and stresses with increase in a/b ratio and power law parameter p, a simply supported FGM plate with a/h ratio 10 is considered. The nondimensionalized values of in-plane displacement \bar{u} and transverse displacement \bar{w} are given in Table 5.18 and Table 5.19 respectively. For a/b ratio equal to 1.5 and power law parameter p equal to 2, the value of in-plane displacement \bar{u} predicted by HSDT-9, HSDT-5 and FSDT are 1.32%, 1.58%, 1.19% lower as compared to the values predicted by HSDT-12 and the value of transverse displacement \bar{w} predicted by HSDT-9, HSDT-5 and FSDT are 11.52%, 16.59%, 11.31% lower as compared to the values predicted by HSDT-12. The nondimensionalized values of in-plane normal stress $\bar{\sigma}_x$, in-plane shear stress $\bar{\tau}_{xy}$ and transverse shear stress $\bar{\tau}_{xz}$ are given in Table 5.20, Table 5.21 and Table 5.22 respectively. For a/b ratio equal to 2.5 and power law parameter p equal to 2, the value of in-plane normal stress $\bar{\sigma}_x$ predicted by HSDT-9, HSDT-5 and FSDT models are 2.52%, 2.98% and 2.28% higher as compared to the values predicted by HSDT-12, the value of in-plane shear stress $\bar{\tau}_{xy}$ predicted by HSDT-9, HSDT-5 and FSDT models are 2.87%, 3.45% and 2.58% lower as compared to the values predicted by HSDT-12 and the value of transverse stress $\bar{\tau}_{xz}$ predicted by HSDT-9, HSDT-5 and FSDT models are 37.15%, 24.20% and 40.53% higher as compared to the values predicted by HSDT-12. The percentage difference in the values predicted by HSDT-12 and other displacement models is found to be minimum in square plates and increases with increase in a/b ratio and power law parameter p. Also, least difference is observed in the results predicted by HSDT-9 as compared to other two models.

Figs. 5.16 to 5.20 shows through the thickness variation of nondimensionalized in-plane displacement \bar{u} , transverse displacement \bar{w} , in-plane normal stresses $\bar{\sigma}_x$, in-plane shear stress $\bar{\tau}_{xy}$ and transverse shear stresses $\bar{\tau}_{xz}$ in a square FGM plate with a/h ratio equal to 10 and power law parameter equal to 3. From the figures it can be seen that the differences in the values predicted by HSDT-12 and all other models is found to be more in transverse displacement and stresses than that of in-plane displacements

and stresses. This indicates the need for higher order polynomials in the displacement fields for accurate estimation of thermal displacements / stresses in an FGM plate.

Example 6: A simply supported square / rectangular Titanium Alloy-Zirconia (M3) FGM plate subjected to nonlinear thermal loads (T_{NL}) is considered. The thermo-elastic responses at various locations of the plate are studied by varying geometric and power law parameters. The variation of nondimensionalized displacements and stresses using various power law parameters are given in Table 5.23 and Table 5.24 respectively for a/b ratio equal to 2 and a/h ratio equal to 10. For power law parameter p equal to 3, the values of in-plane displacement \bar{u} and \bar{v} predicted by HSDT-9, HDT-5 and FSDT models are 2.09%, 2.57% and 2.14% lower as compared to the values obtained using HSDT-12, the values of transverse displacement \bar{w} predicted by HSDT-9, HDT-5 and FSDT models are 14.26%, 18.85%, 14.32% lower as compared to the values obtained using HSDT-12, the values of in-plane normal stress $\bar{\sigma}_x$ predicted by HSDT-9, HDT-5 and FSDT models are 4.37%, 4.40%, 4.40% lesser as compared to the values obtained using HSDT-12, the values of in-plane normal stress $\bar{\sigma}_y$ predicted by HSDT-9, HDT-5 and FSDT models are 19.96%, 20.17%, 20.17% lower as compared to the values obtained using HSDT-12, the values of in-plane shear stress $\bar{\tau}_{xy}$ predicted by HSDT-9, HDT-5 and FSDT models are 2.11%, 2.15%, 2.15% higher as compared to the values obtained using HSDT-12, the values of transverse shear stress $\bar{\tau}_{xz}$ and $\bar{\tau}_{yz}$ predicted by HSDT-9, HDT-5 and FSDT models are 41.85%, 71.24%, 43.95% higher as compared to the values obtained using HSDT-12. For all parameters considered the results predicted by HSDT-9 model are closer to HSDT-12 and with least percentage difference compared to HSDT-5 and FSDT models. It can also be noted that with increase in the value of power law parameter, the difference in the values obtained using HSDT-12 and all other models increases.

The variation of nondimensionalized transverse displacement \bar{w} and in-plane normal stress $\bar{\sigma}_y$ at various locations across the plate thickness direction are given in Table 5.25 and Table 5.26 respectively. The effect of increase in a/b ratio and a/h ratio in a plate with power law parameter p equal to 1 is studied. For a/b ratio equal to 2 and a/h ratio equal to 4, the values of transverse displacement \bar{w} predicted by HSDT-9, HDT-

5 and FSDT models are 47.59%, 63.12%, 48.05% lower as compared to the values obtained using HSDT-12 at the top surface of the plate. For a/b ratio equal to 1 and a/h ratio equal to 4, the values of in-plane normal stress $\bar{\sigma}_y$ predicted by HSDT-9, HSDT-5 and FSDT models are 15.84%, 17.55%, 17.55% lower as compared to the values obtained using HSDT-12 at the middle surface of the plate. For all parameters studied across the thickness direction, the percentage difference in the results decreases as the plate becomes thin and increases with increase in edge ratio (a/b ratio). Though the values of transverse displacement \bar{w} predicted by HSDT-12 and all other models are almost same in thin plates, the values of in-plane stress $\bar{\sigma}_y$ deviate much from HSDT-12. This clearly shows the need for including transverse shear and normal deformation effects during the analysis.

Example 7: A simply supported rectangular plate subjected to nonlinear thermal load (T_{NL}) is considered for the analysis. Material sets like Monel-Zirconia (M1), Aluminium-Alumina (M2) and Titanium Alloy-Zirconia (M3) are used. The plate responses with increase in the ratio of young's modulus of elasticity of ceramic-to-metal, E_c / E_m ratio is studied for various a/h ratios and power law parameters. The numerical results of in-plane / transverse displacements and stresses for a/b ratio equal to 2 and power law parameter equal to 2 are given in Table 5.27 and Table 5.28. For all E_c / E_m ratio studied, the percentage difference between HSDT-12 and other models are more in thin plates with a/h ratio equal to 10 and is considerably less in thick plates with a/h ratio equal to 50. The plate responses are dependent on overall thermal and physical properties of the material, and hence remarkable variations with increase in E_c / E_m ratio is not observed. In Titanium Alloy-Zirconia (M3, E_c / E_m ratio equal to 1.7673) FGM plate with a/h ratio equal to 10, the in-plane displacement \bar{u} and \bar{v} predicted by HSDT-9, HSDT-5 and FSDT are 2.01%, 2.59%, 2.18% lower than HSDT-12, the transverse displacement \bar{w} predicted by HSDT-9, HSDT-5 and FSDT are 13.67%, 18.12%, 13.78% lower than HSDT-12, in-plane normal stress $\bar{\sigma}_x$ predicted by HSDT-9, HSDT-5 and FSDT are 5.48%, 5.61%, 5.61% lower than HSDT-12, in-plane normal stress $\bar{\sigma}_y$ predicted by HSDT-9, HSDT-5 and FSDT are 28.92%, 29.93%, 29.96% lower than HSDT-12, transverse shear stress $\bar{\tau}_{xy}$ predicted by HSDT-9, HSDT-5 and FSDT are 2.04%, 2.19%, 2.19% higher than HSDT-12 and

transverse shear stress $\bar{\tau}_{xz}$ and $\bar{\tau}_{yz}$ predicted by HSDT-9, HSDT-5 and FSDT are 31.97%, 45.58%, 33.78% higher than HSDT-12. Table 5.29 and Table 5.30 shows the variation of in-plane displacement \bar{u} and in-plane normal stress $\bar{\sigma}_x$ predicted by different models for various power law parameters. For all E_c/E_m ratios considered, the percentage differences in the results predicted by HSDT-12 and other models is found to increase with increase in power law parameter.

Example 8: A simply supported rectangular plate subjected to nonlinear thermal load (T_{NL}) is considered for the analysis. Material sets like Monel-Zirconia (M1), Aluminium-Alumina (M2) and Titanium Alloy-Zirconia (M3) are used. The plate responses are studied for various parameters based on increase in the ratio of thermal conductivity of ceramic- to-metal viz., k_c/k_m ratio. The numerical results of in-plane / transverse displacements and stresses for a/h ratio equal to 10 and power law parameter equal to 2 are given in Table 5.31 and Table 5.32. For all k_c/k_m ratio studied, the percentage difference between HSDT-12 and other models are less in square plate with a/b ratio equal to 1 and more in rectangular plate with a/b ratio equal to 3. The plate responses are dependent on overall thermal and physical properties of the material, and thus significant variation with increase in k_c/k_m ratio is not observed. In Aluminium-Alumina (M2, k_c/k_m ratio equal to 0.0510) FGM plate with a/b ratio equal to 3, the in-plane displacement \bar{u} and \bar{v} predicted by HSDT-9, HSDT-5 and FSDT are 3.89%, 4.66%, 3.49% lower than HSDT-12, the transverse displacement \bar{w} predicted by HSDT-9, HSDT-5 and FSDT are 28.55%, 41.19%, 28.04% lower than HSDT-12, in-plane normal stress $\bar{\sigma}_x$ predicted by HSDT-9, HSDT-5 and FSDT are 1.80%, 1.52%, 1.55% lower than HSDT-12, in-plane normal stress $\bar{\sigma}_y$ predicted by HSDT-9, HSDT-5 and FSDT are 16.37%, 13.71%, 13.99% lower than HSDT-12, transverse shear stress $\bar{\tau}_{xy}$ predicted by HSDT-9, HSDT-5 and FSDT are 3.57%, 2.98%, 3.04% higher than HSDT-12 and transverse shear stress $\bar{\tau}_{xz}$ and $\bar{\tau}_{yz}$ predicted by HSDT-9, HSDT-5 and FSDT are 27.22%, 10.48%, 31.54% higher than HSDT-12. Table 5.33 and Table 5.34 shows the variation of transverse displacement \bar{w} and in-plane normal stress $\bar{\sigma}_y$ predicted by different models for various power law parameters. For all k_c/k_m ratios studied, the percentage difference

in the values predicted by HSDT-12 and other displacement models increases with increase in power law parameter.

Example 9: In order to study the effect of different types of temperature profiles in predicting the plate responses, a simply supported rectangular plate subjected to non-linear (T_{NL}), linear (T_L) and constant (T_C) temperature distribution across the plate thickness is considered. Material sets like Monel-Zirconia (M1), Aluminium-Alumina (M2) and Titanium Alloy-Zirconia (M3) are used. The behaviour of displacements and stresses with increase in E_c/E_m ratio and a/b ratio is studied for a plate with a/h ratio equal to 4 and power law parameter p equal to 2. The nondimensionalized in-plane displacement \bar{u} and transverse displacement \bar{w} at the top surface of the plate are given in Table 5.35. For a Monel-Zirconia (M1, E_c/E_m ratio equal to 0.5537) FGM plate with a/b ratio equal to 1.5, the values of in-plane displacement \bar{u} predicted by HSDT-12, HSDT-9, HSDT-5 and FSDT models using linear temperature distribution (T_L) are found to be 36.83%, 34.88%, 37.85%, 37.63% higher and by using constant temperature distribution (T_C) are found to be 40.02%, 26.93%, 31.87%, 29.00% higher as compared to the values obtained using nonlinear temperature profile (T_{NL}) and the values of transverse displacement \bar{w} predicted by HSDT-12, HSDT-9, HSDT-5 and FSDT models using linear temperature distribution (T_L) are found to be 30.31%, 23.74%, 25.08%, 23.93% higher and by using constant temperature distribution (T_C) are found to be 1.5 times lower as compared to the values obtained using nonlinear temperature profile (T_{NL}). The nondimensionalized in-plane normal stress $\bar{\sigma}_x$ and $\bar{\sigma}_y$ at the middle surface of the plate are given in Table 5.36. For a Titanium Alloy-Zirconia (M3, E_c/E_m ratio equal to 1.7673) FGM plate with a/b ratio equal to 1.5, the values of in-plane normal stress $\bar{\sigma}_x$ predicted by HSDT-12, HSDT-9, HSDT-5 and FSDT models using linear temperature distribution (T_L) are found to be 80.47%, 89.93%, 92.88%, 92.89% higher and by using constant temperature distribution (T_C) are found to be approximately 2.5 times higher as compared to the values obtained using nonlinear temperature profile (T_{NL}) and the values of in-plane normal stress $\bar{\sigma}_y$ predicted by all the models using linear temperature distribution (T_L) are found to be approximately 1.5 times higher and by using constant temperature distribution (T_C) are found to be approximately 3.5 times higher as compared to the

values obtained using nonlinear temperature profile (T_{NL}). The nondimensionalized values of in-plane shear stress $\bar{\tau}_{xy}$ at the top surface of the plate are given in Table 5.37. For a Aluminium-Alumina (M2, E_c/E_m ratio equal to 5.429) FGM plate with a/b ratio equal to 2.5, the values of in-plane shear stress $\bar{\tau}_{xy}$ predicted by HSDT-12, HSDT-9, HSDT-5 and FSDT models using linear temperature distribution (T_L) are found to be 33.02%, 28.48%, 33.03%, 32.71% higher and by using constant temperature distribution (T_C) are found to be 32.82%, 10.90%, 15.29%, 12.75% higher as compared to the values obtained using nonlinear temperature profile (T_{NL}). The nondimensionalized transverse shear stresses $\bar{\tau}_{xz}$ and $\bar{\tau}_{yz}$ at the middle surface of the plate are given in Table 5.38. For all the parameters studied, the values of transverse shear stresses $\bar{\tau}_{xz}$ and $\bar{\tau}_{yz}$ predicted by various displacement models using linear temperature distribution (T_L) and constant temperature distribution (T_C) are found to be approximately 2-3 times higher as compared to the values obtained using nonlinear temperature profile (T_{NL}). It was observed that, with increase in a/b ratio the percentage difference in the values obtained using linear(T_L) and constant (T_C) temperature increases whereas no remarkable differences are observed with increase in E_c/E_m ratio.

The variation of nondimensionalized in-plane / transverse displacements and stresses \bar{u} , \bar{v} , \bar{w} , $\bar{\sigma}_x$, $\bar{\sigma}_y$, $\bar{\tau}_{xy}$, $\bar{\tau}_{xz}$ and $\bar{\tau}_{yz}$ across the thickness of a simply supported rectangular Titanium Alloy-Zirconia (M3) FGM plate subjected to nonlinear (T_{NL}), linear (T_L) and constant (T_C) thermal loads are given in Figs. 5.21 to 5.28 respectively for a/b ratio equal to 2, a/h ratio equal to 10 and power law parameter p equal to 2. It can be noted that, displacements and stresses predicted using linear (T_L) and constant (T_C) temperature profiles deviate much from the results obtained using nonlinear (T_{NL}) temperature profiles in all the models considered. Remarkable differences are observed in the distribution pattern of displacements and stresses. The maximum deviation is observed in the values obtained using constant temperature (T_C) variation and FSDT model.

Example 10: A simply supported rectangular plate subjected to non-linear (T_{NL}), linear (T_L) and constant (T_C) temperature distribution across the plate thickness is

considered. Material sets like Monel-Zirconia (M1), Aluminium-Alumina (M2) and Titanium Alloy-Zirconia (M3) are used. The behaviour of displacements and stresses with increase in k_c/k_m ratio and a/h ratio is studied for a plate with a/b ratio equal to 2 and power law parameter p equal to 2. The nondimensionalized values of in-plane displacement \bar{u} and transverse displacement \bar{w} at the top surface of the plate are given in Table 5.39. For a Titanium Alloy-Zirconia (M3, k_c/k_m ratio equal to 0.1125) FGM plate with a/h ratio equal to 4, the values of in-plane displacement \bar{u} predicted by HSDT-12, HSDT-9, HSDT-5 and FSDT models using linear temperature distribution (T_L) are found to be 27.39%, 24.93%, 27.95%, 27.70% higher and by using constant temperature distribution (T_C) are found to be 32.78%, 19.38%, 24.21%, 21.47% higher as compared to the values obtained using nonlinear temperature profile (T_{NL}) and the values of transverse displacement \bar{w} predicted by HSDT-12, HSDT-9, HSDT-5 and FSDT models using linear temperature distribution (T_L) are found to be 21.81%, 9.92%, 8.35%, 11.61% higher and by using constant temperature distribution (T_C) are found to be approximately 1.5 times lower as compared to the values obtained using nonlinear temperature profile (T_{NL}). The nondimensionalized values of in-plane normal stress $\bar{\sigma}_x$ and $\bar{\sigma}_y$ at the middle surface of the plate are given in Table 5.40. For a Monel-Zirconia (M1, k_c/k_m ratio equal to 0.0836) FGM plate with a/h ratio equal to 4, the values of in-plane normal stress $\bar{\sigma}_x$ predicted by HSDT-12, HSDT-9, HSDT-5 and FSDT models using linear temperature distribution (T_L) are found to be 86.08%, 89.38%, 92.17%, 92.17% higher and by using constant temperature distribution (T_C) are found to be approximately 2.5 times higher as compared to the values obtained using nonlinear temperature profile (T_{NL}) and the values of in-plane normal stress $\bar{\sigma}_y$ predicted by HSDT-12, HSDT-9, HSDT-5 and FSDT models using linear temperature distribution (T_L) are found to be approximately 2 times higher and by using constant temperature distribution (T_C) are found to be 4 times higher as compared to the values obtained using nonlinear temperature profile (T_{NL}). The nondimensionalized values of in-plane shear stress $\bar{\tau}_{xy}$ at the top surface of the plate are given in Table 5.41. For a Titanium Alloy-Zirconia (M3, k_c/k_m ratio equal to 0.1125) FGM plate with a/h ratio equal to 20, the values of in-plane shear stress $\bar{\tau}_{xy}$ predicted by HSDT-12, HSDT-9, HSDT-5 and FSDT

models using linear temperature distribution (T_L) are found to be 27.70%, 27.57%, 27.71%, 27.70% higher and by using constant temperature distribution (T_C) are found to be 22.05%, 21.37%, 21.57%, 21.47% higher as compared to the values obtained using nonlinear temperature profile (T_{NL}). The nondimensionalized values of transverse shear stresses $\bar{\tau}_{xz}$ and $\bar{\tau}_{yz}$ at the middle surface of the plate are given in Table 5.42. For a Aluminium-Alumina (M2, k_c/k_m ratio equal to 0.0510) FGM plate with a/h ratio equal to 4, the values of transverse shear stresses $\bar{\tau}_{xz}$ and $\bar{\tau}_{yz}$ predicted by HSDT-12, HSDT-9, HSDT-5 and FSDT models using linear temperature distribution (T_L) are found to be 2.5 times higher and by using constant temperature distribution (T_C) are found to be very much higher as compared to the values obtained using nonlinear temperature profile (T_{NL}). For all values of a/h ratio and k_c/k_m ratio, the values obtained using nonlinear (T_{NL}) temperature and those predicted using linear (T_L) and constant (T_C) temperature distributions are very much different from each other and the percentage differences are too high. Maximum percentage differences are found to be more in FSDT models with constant (T_C) temperature distributions.

5.3 CLOSURE

The stress analysis results of FGM plates subjected to thermal loads are presented in this chapter. A simply supported Monel-Zirconia / Aluminium-Alumina / Titanium Alloy-Zirconia FGM plate with rectangular / square geometry is considered throughout as a test problem. The distribution of temperature is considered to be nonlinear / linear / constantly varying across the plate thickness direction, while in-plane is sinusoidal. Discussion mainly focused on evaluating the accuracy of solutions obtained using various displacement models and temperature profiles in predicting the thermo-elastic plate responses. Based on various examples solved and the numerical results obtained the general conclusions, and the suggestion for future work are presented in the next chapter.

Table 5.1. Nondimensionalized in-plane displacement (\bar{u}) at the bottom ($z= -h/2$), middle ($z=0$) and top ($z= h/2$) surface of a simply supported square FGM (Monel-Zirconia, M1) plate subjected to transverse sinusoidal mechanical load ($m=n=1$ and $p=2$)

		\bar{u}		
a/h	THEORY	(0, b/2, -h/2)	(0, b/2, 0)	(0, b/2, h/2)
4	3D-Exact [§]	-0.004069	-0.00008998	0.004021
	HSDT-12	-0.004067 [-0.05] [†]	-0.000091 [1.13]	0.00402 [-0.02]
	HSDT-9	-0.004172 [2.53]	-0.00015 [66.70]	0.00448 [11.42]
	HSDT-5	-0.003999 [-1.72]	-0.000194 [115.60]	0.004113 [2.29]
	FSDT	-0.003929 [-3.44]	-0.000149 [65.59]	0.004228 [5.15]
10	3D-Exact [§]	-0.02472	0.0007108	0.02617
	HSDT-12	-0.024723 [0.01]	0.000711 [0.03]	0.026172 [0.01]
	HSDT-9	-0.024806 [0.35]	0.00093 [30.84]	0.02668 [1.95]
	HSDT-5	-0.02463 [-0.36]	0.000981 [38.01]	0.026305 [0.52]
	FSDT	-0.024557 [-0.66]	0.000934 [31.04]	0.026425 [0.97]
50	3D-Exact [§]	-0.6141	0.0231	0.6603
	HSDT-12	-0.6140 [0.01]	0.0231 [0.04]	0.6603 [0.00]
	HSDT-9	-0.6142 [0.01]	0.0234 [0.99]	0.6609 [0.09]
	HSDT-5	-0.6140 [-0.02]	0.0234 [1.20]	0.6605 [0.03]
	FSDT	-0.6139 [-0.03]	0.0234 [1.00]	0.6606 [0.05]

[†] Numbers in parentheses are the percentage error with respect to 3-D elasticity values

[§] Reddy, J. N. and Cheng, Z. Q. (2001a).

Table 5.2. Nondimensionalized transverse displacement (\bar{w}) at the bottom ($z= -h/2$), middle ($z=0$) and top ($z= h/2$) surface of a simply supported square FGM (Monel-Zirconia, M1) plate subjected to transverse sinusoidal mechanical load ($m=n=1$ and $p=2$)

		\bar{w}		
a/h	THEORY	(a/2, b/2, -h/2)	(a/2, b/2, 0)	(a/2, b/2, h/2)
4	3D-Exact [§]	-0.0127	-0.0137	-0.0135
	HSDT-12	-0.0127 [-0.02] [†]	-0.0137 [0.04]	-0.0135 [-0.01]
	HSDT-9	-0.0142 [11.70]	-0.0142 [3.79]	-0.0142 [5.64]
	HSDT-5	-0.0104 [-17.95]	-0.0104 [-23.76]	-0.0104 [-22.40]
	FSDT	-0.0142 [11.90]	-0.0142 [3.98]	-0.0142 [5.83]
10	3D-Exact [§]	-0.1685	-0.1707	-0.1689
	HSDT-12	-0.1685 [0.00]	-0.1707 [-0.01]	-0.1689 [-0.01]
	HSDT-9	-0.1719 [2.02]	-0.1719 [0.70]	-0.1719 [1.78]
	HSDT-5	-0.1624 [-3.60]	-0.1624 [-4.84]	-0.1624 [-3.83]
	FSDT	-0.1719 [2.04]	-0.1719 [0.72]	-0.1719 [1.79]
50	3D-Exact [§]	-20.3200	-20.3300	-20.3200
	HSDT-12	-20.3139 [-0.03]	-20.3246 [-0.03]	-20.3145 [-0.03]
	HSDT-9	-20.3333 [0.07]	-20.3333 [0.02]	-20.3333 [0.07]
	HSDT-5	-20.2859 [-0.17]	-20.2859 [-0.22]	-20.2859 [-0.17]
	FSDT	-20.3334 [0.07]	-20.3334 [0.02]	-20.3334 [0.07]

[†] Numbers in parentheses are the percentage error with respect to 3-D elasticity values

[§] Reddy, J. N. and Cheng, Z. Q. (2001a).

Table 5.3. Nondimensionalized in-plane normal stress ($\bar{\sigma}_x$) at the bottom ($z= -h/2$), middle ($z=0$) and top ($z= h/2$) surface of a simply supported square FGM (Monel-Zirconia, M1) plate subjected to transverse sinusoidal mechanical load ($m=n=1$ and $p=2$)

		$\bar{\sigma}_x$		
a/h	THEORY	(a/2, b/2, -h/2)	(a/2, b/2, 0)	(a/2, b/2, h/2)
4	3D-Exact [§]	3.6310	-0.2037	-3.1540
	HSDT-12	3.7336 [2.83] [†]	-0.1976 [-2.98]	-3.2077 [1.70]
	HSDT-9	3.7232 [2.54]	-0.1230 [-39.62]	-3.0355 [-3.76]
	HSDT-5	3.7232 [2.54]	-0.1230 [-39.62]	-3.0355 [-3.76]
	FSDT	3.5062 [-3.44]	-0.1246 [-38.81]	-2.8652 [-9.16]
10	3D-Exact [§]	22.0600	-0.8722	-18.1700
	HSDT-12	21.8173 [-1.10]	-0.8836 [1.31]	-18.0287 [-0.78]
	HSDT-9	22.1360 [0.34]	-0.7774 [-10.87]	-18.0816 [-0.49]
	HSDT-5	21.9789 [-0.37]	-0.8182 [-6.19]	-17.8264 [-1.89]
	FSDT	21.9139 [-0.66]	-0.7790 [-10.69]	-17.9078 [-1.44]
50	3D-Exact [§]	548.0000	-19.5600	-447.9000
	HSDT-12	537.7070 [-1.88]	-20.0571 [2.54]	-442.2532 [-1.26]
	HSDT-9	548.0710 [0.01]	-19.4729 [-0.45]	-447.8683 [-0.01]
	HSDT-5	547.9140 [-0.02]	-19.5141 [-0.23]	-447.6117 [-0.06]
	FSDT	547.8481 [-0.03]	-19.4745 [-0.44]	-447.6940 [-0.05]

[†]Numbers in parentheses are the percentage error with respect to 3-D elasticity values

[§]Reddy, J. N. and Cheng, Z. Q. (2001a).

Table 5.4. Nondimensionalized transverse shear stress ($\bar{\tau}_{xz}$) and transverse normal stress ($\bar{\sigma}_z$) at the middle ($z=0$) surface of a simply supported square FGM (Monel-Zirconia, M1) plate subjected to transverse sinusoidal mechanical load ($m=n=1$ and $p=2$)

a/h	THEORY	$\bar{\tau}_{xz}$	$\bar{\sigma}_z$
4	3-D Exact [§]	-0.9500	-0.5130
	HSDT12	-0.9458 [-0.44] [†]	-0.5136 [0.12]
	HSDT-9	-0.9452 [-0.51]	-0.5137 [0.14]
	HSDT-5	-0.9452 [-0.51]	-0.5137 [0.14]
	FSDT	-0.9597 [1.03]	-0.5150 [0.39]
10	3-D Exact [§]	-2.3960	-0.5142
	HSDT12	-2.3994 [0.14]	-0.5142 [0.00]
	HSDT-9	-2.3934 [-0.11]	-0.5135 [-0.14]
	HSDT-5	-2.3996 [0.15]	-0.5137 [-0.10]
	FSDT-	-2.3994 [0.14]	-0.5150 [0.19]
50	3-D Exact [§]	-12.0000	-0.5141
	HSDT12	-12.0290 [0.24]	-0.5140 [-0.02]
	HSDT-9	-11.9955 [-0.04]	-0.5135 [-0.12]
	HSDT-5	-11.9968 [-0.03]	-0.5136 [-0.10]
	FSDT	-11.9967 [-0.03]	-0.5150 [0.18]

[†] Numbers in parentheses are the percentage error with respect to 3-D elasticity values

[§] Reddy, J. N. and Cheng, Z. Q. (2001a).

Table 5.5. Nondimensionalized in-plane displacements (\bar{u} , \bar{v}) and transverse displacement (\bar{w}) at the top ($z = h/2$) surface of a rectangular FGM (Monel-Zirconia, M1) plate subjected to nonlinear (T_{NL}) thermal load ($a/h=4$ and $p=3$)

a/b	THEORY	\bar{u}	\bar{v}	\bar{w}
1	HSDT-12	-1.9962	-1.9962	3.4373
	HSDT-9	-1.8718	-1.8718	2.3811
	HSDT-5	-1.8591	-1.8591	2.2312
	FSDT	-1.8692	-1.8692	2.3788
1.5	HSDT-12	-1.2738	-1.9107	2.5193
	HSDT-9	-1.1528	-1.7292	1.4661
	HSDT-5	-1.1403	-1.7104	1.3166
	FSDT	-1.1502	-1.7254	1.4639
2	HSDT-12	-0.8664	-1.7327	2.0010
	HSDT-9	-0.7501	-1.5003	0.9537
	HSDT-5	-0.7377	-1.4754	0.8048
	FSDT	-0.7477	-1.4953	0.9515
2.5	HSDT-12	-0.6282	-1.5705	1.6959
	HSDT-9	-0.5180	-1.2950	0.6584
	HSDT-5	-0.5057	-1.2643	0.5101
	FSDT	-0.5156	-1.2891	0.6562
3	HSDT-12	-0.4792	-1.4377	1.5007
	HSDT-9	-0.3761	-1.1283	0.4778
	HSDT-5	-0.3640	-1.0919	0.3304
	FSDT	-0.3738	-1.1215	0.4758
3.5	HSDT-12	-0.3795	-1.3283	1.3638
	HSDT-9	-0.2843	-0.9949	0.3611
	HSDT-5	-0.2723	-0.9532	0.2146
	FSDT	-0.2821	-0.9875	0.3591
4	HSDT-12	-0.3088	-1.2351	1.2590
	HSDT-9	-0.2219	-0.8877	0.2818
	HSDT-5	-0.2102	-0.8407	0.1364
	FSDT	-0.2199	-0.8796	0.2799

Table 5.6. Nondimensionalized in-plane normal stresses ($\bar{\sigma}_x, \bar{\sigma}_y$), in-plane shear stress ($\bar{\tau}_{xy}$) and transverse shear stresses ($\bar{\tau}_{xz}, \bar{\tau}_{yz}$) at the middle ($z=0$) surface of a rectangular FGM (Monel-Zirconia, M1) plate subjected to nonlinear (T_{NL}) thermal load ($a/h=4$ and $p=3$)

a/b	THEORY	$\bar{\sigma}_x$	$\bar{\sigma}_y$	$\bar{\tau}_{xy}$	$\bar{\tau}_{xz}$	$\bar{\tau}_{yz}$
1	HSDT-12	-539.65	-539.65	-462.89	1.5674	1.5674
	HSDT-9	-486.95	-486.95	-484.51	2.0850	2.0850
	HSDT-5	-486.45	-486.45	-484.78	2.8027	2.8027
	FSDT	-486.39	-486.39	-484.81	2.1498	2.1498
1.5	HSDT-12	-738.06	-391.31	-416.10	1.3407	2.0112
	HSDT-9	-673.55	-300.99	-447.08	2.0459	3.0688
	HSDT-5	-672.93	-300.04	-447.47	3.2083	4.8124
	FSDT	-672.86	-299.93	-447.52	2.1498	3.2247
2	HSDT-12	-859.30	-336.38	-348.61	1.0372	2.0745
	HSDT-9	-778.15	-197.21	-387.29	1.9928	3.9856
	HSDT-5	-777.38	-195.70	-387.79	3.7727	7.5454
	FSDT	-777.28	-195.51	-387.85	2.1498	4.2996
2.5	HSDT-12	-941.03	-333.31	-289.39	0.6656	1.6639
	HSDT-9	-838.54	-137.78	-333.69	1.9275	4.8187
	HSDT-5	-837.59	-135.61	-334.27	4.4928	11.2320
	FSDT	-837.46	-135.32	-334.35	2.1498	5.3745
3	HSDT-12	-1003.62	-356.86	-242.53	0.2319	0.6955
	HSDT-9	-875.55	-101.82	-290.15	1.8517	5.5550
	HSDT-5	-874.40	-98.95	-290.79	5.3645	16.0935
	FSDT	-874.24	-98.54	-290.89	2.1498	6.4494
3.5	HSDT-12	-1056.67	-392.08	-206.76	-0.2604	-0.9112
	HSDT-9	-899.56	-78.89	-255.32	1.7675	6.1861
	HSDT-5	-898.23	-75.31	-256.02	6.3829	22.3402
	FSDT	-898.02	-74.76	-256.13	2.1498	7.5243
4	HSDT-12	-1104.39	-429.50	-179.97	-0.8088	-3.3249
	HSDT-9	-915.93	-63.59	-227.29	1.6769	6.7076
	HSDT-5	-914.42	-59.32	-228.02	7.5425	30.1700
	FSDT	-914.17	-58.62	-228.15	2.1498	8.5993

Table 5.7. Nondimensionalized in-plane displacement (\bar{u}) at the bottom ($z= -h/2$), middle ($z=0$) and top ($z= h/2$) surface of a FGM (Monel-Zirconia, M1) plate subjected to nonlinear (T_{NL}) thermal load ($a/b=1.5$)

a/h	p	z	HSDT-12	HSDT-9	HSDT-5	FSDT
10	2	-h/2	0.0191	0.0281	0.0272	0.0287
		0	-0.5193	-0.5258	-0.5262	-0.5262
		h/2	-1.1011	-1.0826	-1.0796	-1.0811
	5	-h/2	-0.0402	-0.0271	-0.0293	-0.0276
		0	-0.6456	-0.6536	-0.6532	-0.6532
		h/2	-1.3013	-1.2780	-1.2771	-1.2789
	10	-h/2	-0.0542	-0.0381	-0.0410	-0.0388
		0	-0.7512	-0.7606	-0.7600	-0.7600
		h/2	-1.5060	-1.4793	-1.4790	-1.4812
20	2	-h/2	0.0263	0.0285	0.0283	0.0287
		0	-0.5245	-0.5261	-0.5262	-0.5262
		h/2	-1.0862	-1.0815	-1.0807	-1.0811
	5	-h/2	-0.0308	-0.0275	-0.0280	-0.0276
		0	-0.6513	-0.6533	-0.6532	-0.6532
		h/2	-1.2845	-1.2786	-1.2784	-1.2789
	10	-h/2	-0.0427	-0.0387	-0.0394	-0.0388
		0	-0.7578	-0.7602	-0.7600	-0.7600
		h/2	-1.4875	-1.4807	-1.4807	-1.4812
50	2	-h/2	0.0283	0.0287	0.0286	0.0287
		0	-0.5259	-0.5262	-0.5262	-0.5262
		h/2	-1.0819	-1.0812	-1.0811	-1.0811
	5	-h/2	-0.0281	-0.0276	-0.0277	-0.0276
		0	-0.6529	-0.6532	-0.6532	-0.6532
		h/2	-1.2798	-1.2788	-1.2788	-1.2789
	10	-h/2	-0.0395	-0.0388	-0.0389	-0.0388
		0	-0.7597	-0.7601	-0.7600	-0.7600
		h/2	-1.4822	-1.4811	-1.4811	-1.4812

Table 5.8. Nondimensionalized in-plane normal stress ($\bar{\sigma}_x$) at the bottom ($z= -h/2$), middle ($z=0$) and top ($z= h/2$) surface of a FGM (Monel-Zirconia, M1) plate subjected to nonlinear (T_{NL}) thermal load ($a/b=1.5$)

a/h	p	z	HSDT-12	HSDT-9	HSDT-5	FSDT
10	2	-h/2	24.00	-36.97	-35.73	-37.69
		0	-545.52	-527.46	-526.91	-526.91
		h/2	-1124.69	-1009.83	-1012.01	-1010.92
	5	-h/2	24.00	35.57	38.50	36.25
		0	-862.68	-850.06	-850.50	-850.48
		h/2	-897.16	-867.70	-868.31	-867.04
	10	-h/2	-2.72	50.11	53.89	51.05
		0	-995.68	-1004.98	-1005.80	-1005.75
		h/2	-574.58	-721.17	-721.43	-719.80
20	2	-h/2	16.14	-37.51	-37.20	-37.69
		0	-539.64	-527.05	-526.91	-526.91
		h/2	-1136.65	-1010.65	-1011.19	-1010.92
	5	-h/2	12.74	36.08	36.81	36.25
		0	-854.82	-850.37	-850.49	-850.48
		h/2	-910.24	-867.20	-867.35	-867.04
	10	-h/2	-16.90	50.81	51.76	51.05
		0	-986.29	-1005.56	-1005.76	-1005.75
		h/2	-588.80	-720.15	-720.21	-719.80
50	2	-h/2	13.91	-37.66	-37.61	-37.69
		0	-537.98	-526.93	-526.91	-526.91
		h/2	-1140.04	-1010.88	-1010.97	-1010.92
	5	-h/2	9.55	36.23	36.34	36.25
		0	-852.61	-850.46	-850.48	-850.48
		h/2	-913.95	-867.06	-867.09	-867.04
	10	-h/2	-20.91	51.01	51.16	51.05
		0	-983.65	-1005.72	-1005.76	-1005.75
		h/2	-592.83	-719.86	-719.87	-719.80

Table 5.9. Nondimensionalized in-plane displacement (\bar{u}) at the top ($z = h/2$) surface of a square FGM (Monel-Zirconia, M1) plate subjected to nonlinear (T_{NL}) thermal load

a/h	p	HSDT-12	HSDT-9	HSDT-5	FSDT
4	0	-2.1916	-2.0690	-2.0532	-2.0690
	1	-1.8058	-1.7066	-1.6803	-1.6908
	2	-1.8782	-1.7658	-1.7471	-1.7568
	5	-2.2140	-2.0727	-2.0668	-2.0782
	8	-2.4473	-2.2918	-2.2888	-2.3021
	10	-2.5567	-2.3956	-2.3925	-2.4070
10	0	-2.0893	-2.0690	-2.0666	-2.0690
	1	-1.7098	-1.6934	-1.6891	-1.6908
	2	-1.7769	-1.7583	-1.7553	-1.7568
	5	-2.1007	-2.0772	-2.0764	-2.0782
	8	-2.3263	-2.3004	-2.3001	-2.3021
	10	-2.4319	-2.4051	-2.4047	-2.4070
20	0	-2.0741	-2.0690	-2.0684	-2.0690
	1	-1.6955	-1.6914	-1.6904	-1.6908
	2	-1.7619	-1.7572	-1.7564	-1.7568
	5	-2.0838	-2.0779	-2.0777	-2.0782
	8	-2.3082	-2.3017	-2.3016	-2.3021
	10	-2.4132	-2.4065	-2.4064	-2.4070
50	0	-2.0698	-2.0690	-2.0689	-2.0690
	1	-1.6915	-1.6909	-1.6907	-1.6908
	2	-1.7576	-1.7569	-1.7568	-1.7568
	5	-2.0791	-2.0781	-2.0781	-2.0782
	8	-2.3031	-2.3021	-2.3021	-2.3021
	10	-2.4080	-2.4069	-2.4069	-2.4070
100	0	-2.0692	-2.0690	-2.0690	-2.0690
	1	-1.6910	-1.6908	-1.6907	-1.6908
	2	-1.7570	-1.7568	-1.7568	-1.7568
	5	-2.0784	-2.0782	-2.0781	-2.0782
	8	-2.3024	-2.3021	-2.3021	-2.3021
	10	-2.4072	-2.4070	-2.4070	-2.4070

Table 5.10. Nondimensionalized transverse displacement (\bar{w}) at the top ($z = h/2$) surface of a square FGM (Monel-Zirconia, M1) plate subjected to nonlinear (T_{NL}) thermal load

a/h	p	HSDT-12	HSDT-9	HSDT-5	FSDT
4	0	3.7688	2.6344	2.3923	2.6344
	1	3.2505	2.3122	2.1509	2.3107
	2	3.2891	2.2991	2.1510	2.2962
	5	3.7594	2.5880	2.4239	2.5889
	8	4.1389	2.8475	2.6591	2.8522
	10	4.3251	2.9781	2.7751	2.9843
10	0	7.0408	6.5859	6.4924	6.5859
	1	6.1522	5.7773	5.7151	5.7767
	2	6.1380	5.7417	5.6845	5.7405
	5	6.9423	6.4719	6.4086	6.4723
	8	7.6476	7.1286	7.0559	7.1306
	10	7.9995	7.4582	7.3798	7.4607
20	0	13.3992	13.1718	13.1252	13.1718
	1	11.7411	11.5538	11.5228	11.5535
	2	11.6797	11.4815	11.4531	11.4810
	5	13.1797	12.9444	12.9129	12.9446
	8	14.5198	14.2602	14.2240	14.2611
	10	15.1909	14.9201	14.8812	14.9214
50	0	33.0204	32.9294	32.9108	32.9294
	1	28.9588	28.8839	28.8715	28.8837
	2	28.7819	28.7026	28.6913	28.7024
	5	32.4555	32.3613	32.3487	32.3614
	8	35.7563	35.6524	35.6380	35.6528
	10	37.4113	37.3030	37.2874	37.3035
100	0	65.9043	65.8588	65.8495	65.8588
	1	57.8050	57.7675	57.7614	57.7675
	2	57.4445	57.4049	57.3992	57.4048
	5	64.7698	64.7228	64.7165	64.7228
	8	71.3574	71.3055	71.2983	71.3057
	10	74.6609	74.6067	74.5989	74.6069

Table 5.11. Nondimensionalized in-plane normal stress ($\bar{\sigma}_x$) at the top ($z = h/2$) surface of a square FGM (Monel-Zirconia, M1) plate subjected to nonlinear (T_{NL}) thermal load

a/h	p	HSDT-12	HSDT-9	HSDT-5	FSDT
4	0	-555.90	-629.15	-638.09	-629.15
	1	-871.09	-833.84	-848.66	-842.76
	2	-861.43	-800.36	-810.94	-805.45
	5	-590.71	-627.09	-630.38	-623.99
	8	-348.30	-503.34	-505.03	-497.50
	10	-223.87	-444.71	-446.44	-438.30
10	0	-617.03	-629.15	-630.53	-629.15
	1	-929.72	-841.27	-843.67	-842.76
	2	-922.98	-804.60	-806.30	-805.45
	5	-658.15	-624.50	-624.97	-623.99
	8	-419.76	-498.48	-498.67	-497.50
	10	-297.43	-439.36	-439.56	-438.30
20	0	-626.11	-629.15	-629.49	-629.15
	1	-938.41	-842.38	-842.99	-842.76
	2	-932.14	-805.24	-805.67	-805.45
	5	-668.22	-624.12	-624.23	-623.99
	8	-430.43	-497.75	-497.79	-497.50
	10	-308.41	-438.56	-438.61	-438.30
50	0	-628.66	-629.15	-629.20	-629.15
	1	-940.86	-842.70	-842.79	-842.76
	2	-934.72	-805.42	-805.49	-805.45
	5	-671.06	-624.01	-624.02	-623.99
	8	-433.44	-497.54	-497.55	-497.50
	10	-311.50	-438.34	-438.35	-438.30
100	0	-629.03	-629.15	-629.16	-629.15
	1	-941.21	-842.74	-842.77	-842.76
	2	-935.09	-805.45	-805.46	-805.45
	5	-671.47	-623.99	-623.99	-623.99
	8	-433.87	-497.51	-497.51	-497.50
	10	-311.95	-438.31	-438.31	-438.30

Table 5.12. Nondimensionalized in-plane shear stress ($\bar{\tau}_{xy}$) at the top ($z = h/2$) surface of a square FGM (Monel-Zirconia, M1) plate subjected to nonlinear (T_{NL}) thermal load

a/h	p	HSDT-12	HSDT-9	HSDT-5	FSDT
4	0	-666.44	-629.15	-624.33	-629.15
	1	-549.12	-518.93	-510.95	-514.13
	2	-571.14	-536.96	-531.26	-534.22
	5	-673.24	-630.26	-628.49	-631.93
	8	-744.18	-696.90	-695.98	-700.04
	10	-777.45	-728.47	-727.53	-731.92
10	0	-635.32	-629.15	-628.41	-629.15
	1	-519.90	-514.93	-513.64	-514.13
	2	-540.33	-534.67	-533.76	-534.22
	5	-638.80	-631.65	-631.40	-631.93
	8	-707.38	-699.51	-699.41	-700.04
	10	-739.49	-731.34	-731.24	-731.92
20	0	-630.70	-629.15	-628.96	-629.15
	1	-515.58	-514.33	-514.01	-514.13
	2	-535.75	-534.33	-534.10	-534.22
	5	-633.66	-631.86	-631.80	-631.93
	8	-701.88	-699.91	-699.88	-700.04
	10	-733.82	-731.77	-731.75	-731.92
50	0	-629.40	-629.15	-629.12	-629.15
	1	-514.36	-514.16	-514.11	-514.13
	2	-534.46	-534.24	-534.20	-534.22
	5	-632.21	-631.92	-631.91	-631.93
	8	-700.33	-700.02	-700.01	-700.04
	10	-732.22	-731.89	-731.89	-731.92
100	0	-629.21	-629.15	-629.14	-629.15
	1	-514.19	-514.14	-514.13	-514.13
	2	-534.28	-534.22	-534.21	-534.22
	5	-632.00	-631.93	-631.93	-631.93
	8	-700.11	-700.03	-700.03	-700.04
	10	-731.99	-731.91	-731.91	-731.92

Table 5.13. Nondimensionalized transverse shear stress ($\bar{\tau}_{xz}$) at the middle ($z = 0$) surface of a square FGM (Monel-Zirconia, M1) plate subjected to nonlinear (T_{NL}) thermal load

a/h	p	HSDT-12	HSDT-9	HSDT-5	FSDT
4	0	-0.5389	0.0000	0.6755	0.0000
	1	2.8597	2.7923	3.4518	2.8261
	2	3.0614	3.4130	4.1086	3.4906
	5	-2.0179	-1.5943	-0.8574	-1.6120
	8	-5.2314	-5.0354	-4.2561	-5.1570
	10	-6.1622	-6.0309	-5.2102	-6.1925
10	0	-0.0354	0.0000	0.0418	0.0000
	1	1.2742	1.1283	1.1691	1.1304
	2	1.3548	1.3912	1.4344	1.3962
	5	-0.6802	-0.6437	-0.5982	-0.6448
	8	-1.9559	-2.0549	-2.0071	-2.0628
	10	-2.3167	-2.4665	-2.4162	-2.4770
20	0	-0.0045	0.0000	0.0052	0.0000
	1	0.6468	0.5650	0.5700	0.5652
	2	0.6870	0.6975	0.7029	0.6981
	5	-0.3307	-0.3223	-0.3166	-0.3224
	8	-0.9678	-1.0304	-1.0245	-1.0314
	10	-1.1474	-1.2372	-1.2309	-1.2385
50	0	-0.0003	0.0000	0.0003	0.0000
	1	0.2598	0.2261	0.2264	0.2261
	2	0.2759	0.2792	0.2795	0.2792
	5	-0.1312	-0.1290	-0.1286	-0.1290
	8	-0.3860	-0.4125	-0.4121	-0.4126
	10	-0.4577	-0.4953	-0.4949	-0.4954
100	0	-0.0001	0.0000	0.0000	0.0000
	1	0.1300	0.1130	0.1131	0.1130
	2	0.1380	0.1396	0.1397	0.1396
	5	-0.0655	-0.0645	-0.0644	-0.0645
	8	-0.1929	-0.2063	-0.2062	-0.2063
	10	-0.2288	-0.2477	-0.2476	-0.2477

Table 5.14. Nondimensionalized in-plane displacements (\bar{u} , \bar{v}) and transverse displacement (\bar{w}) at the top ($z = h/2$) surface of a rectangular FGM (Aluminium-Alumina, M2) plate subjected to nonlinear (T_{NL}) thermal load ($a/b=2$ and $p=2$)

a/h	THEORY	\bar{u}	\bar{v}	\bar{w}
2	HSDT-12	-0.8692	-1.7385	1.8592
	HSDT-9	-0.6518	-1.3036	0.3396
	HSDT-5	-0.5591	-1.1182	-0.5677
	FSDT	-0.6748	-1.3497	0.3618
4	HSDT-12	-0.7454	-1.4908	1.5837
	HSDT-9	-0.6670	-1.3339	0.7089
	HSDT-5	-0.6484	-1.2967	0.2980
	FSDT	-0.6748	-1.3497	0.7236
10	HSDT-12	-0.6873	-1.3746	2.1633
	HSDT-9	-0.6734	-1.3469	1.8025
	HSDT-5	-0.6707	-1.3414	1.6434
	FSDT	-0.6748	-1.3497	1.8091
20	HSDT-12	-0.6780	-1.3560	3.7959
	HSDT-9	-0.6745	-1.3490	3.6148
	HSDT-5	-0.6738	-1.3476	3.5356
	FSDT	-0.6748	-1.3497	3.6181
50	HSDT-12	-0.6754	-1.3507	9.1164
	HSDT-9	-0.6748	-1.3496	9.0439
	HSDT-5	-0.6747	-1.3494	9.0123
	FSDT	-0.6748	-1.3497	9.0453
80	HSDT-12	-0.6750	-1.3501	14.5169
	HSDT-9	-0.6748	-1.3497	14.4716
	HSDT-5	-0.6748	-1.3496	14.4518
	FSDT	-0.6748	-1.3497	14.4724
100	HSDT-12	-0.6750	-1.3499	18.1261
	HSDT-9	-0.6748	-1.3497	18.0898
	HSDT-5	-0.6748	-1.3496	18.0740
	FSDT	-0.6748	-1.3497	18.0905

Table 5.15. Nondimensionalized in-plane normal stresses ($\bar{\sigma}_x, \bar{\sigma}_y$), in-plane shear stress ($\bar{\tau}_{xy}$) and transverse shear stresses ($\bar{\tau}_{xz}, \bar{\tau}_{yz}$) at the middle ($z=0$) surface of a rectangular FGM (Aluminium-Alumina, M2) plate subjected to nonlinear (T_{NL}) thermal load ($a/b=2$ and $p=2$)

a/h	THEORY	$\bar{\sigma}_x$	$\bar{\sigma}_y$	$\bar{\tau}_{xy}$	$\bar{\tau}_{xz}$	$\bar{\tau}_{yz}$
2	HSDT-12	-805.03	-436.57	-245.63	-34.6069	-69.2138
	HSDT-9	-641.02	-206.25	-289.85	-11.4758	-22.9517
	HSDT-5	-662.53	-248.30	-276.16	20.0078	40.0155
	FSDT	-658.83	-241.05	-278.52	-16.0020	-32.0041
4	HSDT-12	-703.75	-318.27	-256.98	-8.8901	-17.7802
	HSDT-9	-652.49	-228.67	-282.55	-7.2446	-14.4892
	HSDT-5	-659.67	-242.71	-277.98	-3.8791	-7.7582
	FSDT	-658.83	-241.05	-278.52	-8.0010	-16.0020
10	HSDT-12	-664.54	-253.18	-274.24	-2.1480	-4.2962
	HSDT-9	-657.68	-238.80	-279.25	-3.1467	-6.2935
	HSDT-5	-658.96	-241.31	-278.43	-2.9437	-5.8874
	FSDT	-658.83	-241.05	-278.52	-3.2004	-6.4008
20	HSDT-12	-658.61	-242.49	-277.42	-0.9646	-1.9292
	HSDT-9	-658.53	-240.48	-278.70	-1.5934	-3.1868
	HSDT-5	-658.86	-241.11	-278.50	-1.5682	-3.1365
	FSDT	-658.83	-241.05	-278.52	-1.6002	-3.2004
50	HSDT-12	-656.94	-239.43	-278.34	-0.3734	-0.7469
	HSDT-9	-658.78	-240.96	-278.55	-0.6396	-1.2793
	HSDT-5	-658.83	-241.06	-278.51	-0.6380	-1.2761
	FSDT	-658.83	-241.05	-278.52	-0.6401	-1.2802
80	HSDT-12	-656.75	-239.08	-278.45	-0.2325	-0.4650
	HSDT-9	-658.81	-241.01	-278.53	-0.3999	-0.7999
	HSDT-5	-658.83	-241.05	-278.52	-0.3996	-0.7991
	FSDT	-658.83	-241.05	-278.52	-0.4001	-0.8001
100	HSDT-12	-656.70	-239.00	-278.47	-0.1859	-0.3717
	HSDT-9	-658.81	-241.03	-278.52	-0.3200	-0.6400
	HSDT-5	-658.83	-241.05	-278.52	-0.3198	-0.6396
	FSDT	-658.83	-241.05	-278.52	-0.3200	-0.6401

Table 5.16. Nondimensionalized in-plane displacement (\bar{v}) at the bottom ($z= -h/2$), middle ($z=0$) and top ($z= h/2$) surface of a FGM (Aluminium-Alumina, M2) plate subjected to nonlinear (T_{NL}) thermal load ($a/h=20$)

a/b	p	z	HSDT-12	HSDT-9	HSDT-5	FSDT
1	1	-h/2	-0.0493	-0.0454	-0.0462	-0.0455
		0	-0.7742	-0.7755	-0.7755	-0.7755
		h/2	-1.5085	-1.5055	-1.5048	-1.5055
	3	-h/2	-0.4008	-0.3941	-0.3966	-0.3954
		0	-1.1360	-1.1385	-1.1379	-1.1380
		h/2	-1.8840	-1.8799	-1.8793	-1.8806
	8	-h/2	-0.5293	-0.5200	-0.5235	-0.5215
		0	-1.5493	-1.5537	-1.5529	-1.5528
		h/2	-2.5884	-2.5829	-2.5823	-2.5841
2	1	-h/2	-0.0439	-0.0362	-0.0379	-0.0364
		0	-0.6178	-0.6204	-0.6204	-0.6204
		h/2	-1.2104	-1.2044	-1.2029	-1.2044
	3	-h/2	-0.3271	-0.3138	-0.3187	-0.3163
		0	-0.9065	-0.9113	-0.9103	-0.9104
		h/2	-1.5112	-1.5032	-1.5019	-1.5045
	8	-h/2	-0.4327	-0.4142	-0.4212	-0.4172
		0	-1.2354	-1.2440	-1.2424	-1.2422
		h/2	-2.0759	-2.0649	-2.0636	-2.0673
3	1	-h/2	-0.0385	-0.0270	-0.0295	-0.0273
		0	-0.4614	-0.4654	-0.4653	-0.4653
		h/2	-0.9123	-0.9033	-0.9011	-0.9033
	3	-h/2	-0.2534	-0.2335	-0.2408	-0.2372
		0	-0.6771	-0.6842	-0.6827	-0.6828
		h/2	-1.1385	-1.1264	-1.1245	-1.1284
	8	-h/2	-0.3360	-0.3084	-0.3188	-0.3129
		0	-0.9215	-0.9343	-0.9319	-0.9317
		h/2	-1.5633	-1.5470	-1.5450	-1.5505

Table 5.17. Nondimensionalized in-plane shear stress ($\bar{\tau}_{xy}$) at the bottom ($z= -h/2$), middle ($z=0$) and top ($z= h/2$) surface of a FGM (Aluminium-Alumina, M2) plate subjected to nonlinear (T_{NL}) thermal load ($a/h=20$)

a/b	p	z	HSDT-12	HSDT-9	HSDT-5	FSDT
1	1	-h/2	-8.33	-7.68	-7.82	-7.70
		0	-420.96	-421.69	-421.68	-421.68
		h/2	-1385.30	-1382.55	-1381.86	-1382.54
	3	-h/2	-67.80	-66.67	-67.08	-66.88
		0	-298.56	-299.20	-299.06	-299.07
		h/2	-1730.10	-1726.38	-1725.81	-1726.99
	8	-h/2	-89.53	-87.96	-88.55	-88.22
		0	-266.62	-267.37	-267.23	-267.22
		h/2	-2376.96	-2371.92	-2371.33	-2373.00
2	1	-h/2	-7.42	-6.13	-6.41	-6.16
		0	-335.91	-337.36	-337.34	-337.34
		h/2	-1111.53	-1106.04	-1104.67	-1106.03
	3	-h/2	-55.34	-53.08	-53.91	-53.50
		0	-238.24	-239.51	-239.24	-239.26
		h/2	-1387.80	-1380.38	-1379.23	-1381.59
	8	-h/2	-73.20	-70.07	-71.24	-70.57
		0	-212.59	-214.08	-213.80	-213.77
		h/2	-1906.30	-1896.25	-1895.07	-1898.40
3	1	-h/2	-6.51	-4.57	-5.00	-4.62
		0	-250.87	-253.04	-253.01	-253.01
		h/2	-837.74	-829.53	-827.48	-829.53
	3	-h/2	-42.86	-39.49	-40.74	-40.13
		0	-177.93	-179.82	-179.41	-179.44
		h/2	-1045.46	-1034.38	-1032.65	-1036.19
	8	-h/2	-56.84	-52.18	-53.94	-52.93
		0	-158.57	-160.78	-160.37	-160.33
		h/2	-1435.60	-1420.59	-1418.80	-1423.80

Table 5.18. Nondimensionalized in-plane displacement (\bar{u}) at the top ($z = h/2$) surface of a FGM (Aluminium-Alumina, M2) plate subjected to nonlinear (T_{NL}) thermal load ($a/h=10$)

a/b	p	HSDT-12	HSDT-9	HSDT-5	FSDT
1	0	-1.5461	-1.5311	-1.5293	-1.5311
	1	-1.5175	-1.5055	-1.5025	-1.5055
	2	-1.6997	-1.6857	-1.6830	-1.6871
	5	-2.2308	-2.2116	-2.2090	-2.2156
	8	-2.6012	-2.5794	-2.5768	-2.5841
	10	-2.7871	-2.7640	-2.7615	-2.7689
1.5	0	-0.9572	-0.9422	-0.9404	-0.9422
	1	-0.9384	-0.9265	-0.9235	-0.9265
	2	-1.0507	-1.0368	-1.0341	-1.0382
	5	-1.3786	-1.3595	-1.3569	-1.3634
	8	-1.6073	-1.5856	-1.5829	-1.5902
	10	-1.7221	-1.6991	-1.6966	-1.7039
2	0	-0.6273	-0.6124	-0.6106	-0.6124
	1	-0.6141	-0.6022	-0.5992	-0.6022
	2	-0.6873	-0.6734	-0.6707	-0.6748
	5	-0.9013	-0.8823	-0.8797	-0.8862
	8	-1.0506	-1.0290	-1.0264	-1.0336
	10	-1.1256	-1.1028	-1.1002	-1.1076
2.5	0	-0.4371	-0.4224	-0.4206	-0.4224
	1	-0.4271	-0.4153	-0.4123	-0.4153
	2	-0.4778	-0.4640	-0.4613	-0.4654
	5	-0.6261	-0.6073	-0.6047	-0.6112
	8	-0.7297	-0.7083	-0.7056	-0.7129
	10	-0.7817	-0.7591	-0.7565	-0.7638
3	0	-0.3209	-0.3062	-0.3044	-0.3062
	1	-0.3128	-0.3011	-0.2981	-0.3011
	2	-0.3496	-0.3360	-0.3333	-0.3374
	5	-0.4579	-0.4393	-0.4366	-0.4431
	8	-0.5335	-0.5123	-0.5096	-0.5168
	10	-0.5715	-0.5491	-0.5464	-0.5538

Table 5.19. Nondimensionalized transverse displacement (\bar{w}) at the top ($z = h/2$) surface of a FGM (Aluminium-Alumina, M2) plate subjected to nonlinear (T_{NL}) thermal load ($a/h=10$)

a/b	p	HSDT-12	HSDT-9	HSDT-5	FSDT
1	0	5.2102	4.8735	4.8044	4.8735
	1	4.9567	4.6479	4.5331	4.6474
	2	4.8779	4.5160	4.3568	4.5226
	5	5.9596	5.4438	5.1802	5.4717
	8	7.1408	6.5327	6.2200	6.5655
	10	7.7930	7.1442	6.8183	7.1766
1.5	0	3.3357	2.9991	2.9300	2.9991
	1	3.1691	2.8604	2.7457	2.8599
	2	3.1380	2.7766	2.6174	2.7832
	5	3.8544	3.3394	3.0759	3.3672
	8	4.6150	4.0076	3.6951	4.0403
	10	5.0322	4.3841	4.0583	4.4164
2	0	2.2859	1.9494	1.8803	1.9494
	1	2.1678	1.8594	1.7448	1.8590
	2	2.1633	1.8025	1.6434	1.8091
	5	2.6749	2.1611	1.8976	2.1887
	8	3.1999	2.5937	2.2813	2.6262
	10	3.4856	2.8385	2.5129	2.8706
2.5	0	1.6807	1.3444	1.2754	1.3444
	1	1.5906	1.2825	1.1680	1.2820
	2	1.6011	1.2412	1.0821	1.2476
	5	1.9943	1.4820	1.2187	1.5094
	8	2.3836	1.7788	1.4666	1.8112
	10	2.5935	1.9477	1.6224	1.9797
3	0	1.3108	0.9747	0.9057	0.9747
	1	1.2375	0.9300	0.8155	0.9295
	2	1.2570	0.8981	0.7392	0.9045
	5	1.5775	1.0671	0.8040	1.0943
	8	1.8838	1.2810	0.9690	1.3131
	10	2.0474	1.4035	1.0785	1.4353

Table 5.20. Nondimensionalized in-plane normal stress ($\bar{\sigma}_x$) at the top ($z = h/2$) surface of a FGM (Aluminium-Alumina, M2) plate subjected to nonlinear (T_{NL}) thermal load ($a/h=10$)

a/b	p	HSDT-12	HSDT-9	HSDT-5	FSDT
1	0	-1378.91	-1406.00	-1409.09	-1406.00
	1	-1493.08	-1449.55	-1454.66	-1449.56
	2	-1118.08	-1142.31	-1146.91	-1139.87
	5	330.81	-245.36	-249.78	-238.59
	8	1551.05	381.90	377.41	389.86
	10	2205.75	696.77	692.48	705.05
1.5	0	-1911.51	-1946.77	-1950.75	-1946.77
	1	-2018.28	-1981.29	-1987.88	-1981.31
	2	-1707.09	-1738.88	-1744.83	-1735.76
	5	-443.72	-1029.81	-1035.54	-1021.13
	8	647.05	-533.04	-538.86	-522.84
	10	1236.80	-283.55	-289.10	-272.92
2	0	-2203.01	-2249.60	-2254.82	-2249.60
	1	-2306.96	-2279.06	-2287.71	-2279.09
	2	-2031.24	-2073.52	-2081.36	-2069.45
	5	-870.79	-1470.68	-1478.26	-1459.36
	8	148.03	-1047.27	-1054.97	-1033.94
	10	701.69	-834.46	-841.82	-820.58
2.5	0	-2363.16	-2424.14	-2430.96	-2424.14
	1	-2466.99	-2450.67	-2461.98	-2450.71
	2	-2211.41	-2267.05	-2277.32	-2261.78
	5	-1109.17	-1726.60	-1736.61	-1711.93
	8	-131.13	-1345.80	-1355.97	-1328.52
	10	402.03	-1154.23	-1163.95	-1136.23
3	0	-2452.54	-2530.80	-2539.57	-2530.80
	1	-2557.89	-2555.54	-2570.08	-2555.60
	2	-2314.29	-2386.01	-2399.29	-2379.31
	5	-1246.37	-1884.98	-1898.00	-1866.28
	8	-292.53	-1530.58	-1543.82	-1508.54
	10	228.45	-1352.08	-1364.75	-1329.13

Table 5.21. Nondimensionalized in-plane shear stress ($\bar{\tau}_{xy}$) at the top ($z = h/2$) surface of a FGM (Aluminium-Alumina, M2) plate subjected to nonlinear (T_{NL}) thermal load ($a/h=10$)

a/b	p	HSDT-12	HSDT-9	HSDT-5	FSDT
1	0	-1419.79	-1406.00	-1404.34	-1406.00
	1	-1393.51	-1382.55	-1379.80	-1382.54
	2	-1560.85	-1547.99	-1545.51	-1549.30
	5	-2048.55	-2030.96	-2028.58	-2034.60
	8	-2388.76	-2368.72	-2366.30	-2373.00
	10	-2559.45	-2538.26	-2535.95	-2542.72
1.5	0	-1318.45	-1297.85	-1295.35	-1297.85
	1	-1292.59	-1276.21	-1272.08	-1276.19
	2	-1447.36	-1428.16	-1424.44	-1430.12
	5	-1898.92	-1872.66	-1869.06	-1878.10
	8	-2214.00	-2184.06	-2180.42	-2190.46
	10	-2372.12	-2340.46	-2336.98	-2347.12
2	0	-1152.12	-1124.80	-1121.48	-1124.80
	1	-1127.78	-1106.05	-1100.55	-1106.03
	2	-1262.29	-1236.85	-1231.86	-1239.44
	5	-1655.28	-1620.48	-1615.65	-1627.68
	8	-1929.60	-1889.92	-1885.02	-1898.40
	10	-2067.31	-2025.35	-2020.66	-2034.17
2.5	0	-1003.56	-969.66	-965.50	-969.66
	1	-980.47	-953.50	-946.62	-953.48
	2	-1096.81	-1065.28	-1059.02	-1068.48
	5	-1437.39	-1394.24	-1388.15	-1403.18
	8	-1675.26	-1626.03	-1619.85	-1636.55
	10	-1794.71	-1742.65	-1736.73	-1753.60
3	0	-883.93	-843.60	-838.62	-843.60
	1	-861.65	-829.56	-821.31	-829.53
	2	-963.24	-925.78	-918.24	-929.58
	5	-1261.39	-1210.15	-1202.76	-1220.76
	8	-1469.80	-1411.29	-1403.78	-1423.80
	10	-1574.51	-1512.60	-1505.41	-1525.63

Table 5.22. Nondimensionalized transverse shear stress ($\bar{\tau}_{xz}$) at the middle ($z = 0$) surface of a FGM (Aluminium-Alumina, M2) plate subjected to nonlinear (T_{NL}) thermal load ($a/h=10$)

a/b	p	HSDT-12	HSDT-9	HSDT-5	FSDT
1	0	-0.0791	0.0000	0.0933	0.0000
	1	0.4227	0.5714	0.6646	0.5734
	2	-1.9733	-3.1787	-3.0976	-3.2004
	5	-5.7803	-8.2590	-8.1806	-8.3052
	8	-6.6672	-8.9704	-8.8872	-9.0147
	10	-6.7567	-8.9144	-8.8314	-8.9573
1.5	0	-0.1281	0.0000	0.1516	0.0000
	1	0.3441	0.5701	0.7216	0.5734
	2	-2.0465	-3.1653	-3.0334	-3.2004
	5	-5.8336	-8.2303	-8.1029	-8.3052
	8	-6.7086	-8.9429	-8.8077	-9.0147
	10	-6.7946	-8.8878	-8.7529	-8.9573
2	0	-0.1963	0.0000	0.2330	0.0000
	1	0.2347	0.5683	0.8013	0.5734
	2	-2.1481	-3.1467	-2.9437	-3.2004
	5	-5.9078	-8.1906	-7.9942	-8.3052
	8	-6.7663	-8.9047	-8.6965	-9.0147
	10	-6.8475	-8.8508	-8.6431	-8.9573
2.5	0	-0.2830	0.0000	0.3376	0.0000
	1	0.0953	0.5661	0.9036	0.5734
	2	-2.2773	-3.1233	-2.8285	-3.2004
	5	-6.0022	-8.1402	-7.8547	-8.3052
	8	-6.8400	-8.8561	-8.5537	-9.0147
	10	-6.9150	-8.8036	-8.5023	-8.9573
3	0	-0.3878	0.0000	0.4653	0.0000
	1	-0.0731	0.5633	1.0284	0.5734
	2	-2.4331	-3.0953	-2.6880	-3.2004
	5	-6.1161	-8.0795	-7.6847	-8.3052
	8	-6.9291	-8.7973	-8.3798	-9.0147
	10	-6.9969	-8.7466	-8.3306	-8.9573

Table 5.23. Nondimensionalized in-plane displacements (\bar{u} , \bar{v}) and transverse displacement (\bar{w}) at the top ($z = h/2$) surface of a rectangular FGM (Titanium Alloy-Zirconia, M3) plate subjected to nonlinear (T_{NL}) thermal load ($a/h=10$ and $a/b=2$)

p	THEORY	\bar{u}	\bar{v}	\bar{w}
1	HSDT-12	-0.5229	-1.0458	2.0461
	HSDT-9	-0.5129	-1.0258	1.7835
	HSDT-5	-0.5093	-1.0187	1.7006
	FSDT	-0.5114	-1.0229	1.7808
2	HSDT-12	-0.5366	-1.0731	2.0146
	HSDT-9	-0.5258	-1.0516	1.7393
	HSDT-5	-0.5227	-1.0454	1.6495
	FSDT	-0.5249	-1.0498	1.7369
3	HSDT-12	-0.5610	-1.1220	2.0511
	HSDT-9	-0.5493	-1.0986	1.7587
	HSDT-5	-0.5466	-1.0933	1.6644
	FSDT	-0.5490	-1.0980	1.7573
5	HSDT-12	-0.6080	-1.2160	2.1716
	HSDT-9	-0.5949	-1.1898	1.8494
	HSDT-5	-0.5928	-1.1856	1.7502
	FSDT	-0.5953	-1.1905	1.8500
7	HSDT-12	-0.6455	-1.2910	2.2889
	HSDT-9	-0.6313	-1.2626	1.9449
	HSDT-5	-0.6296	-1.2592	1.8433
	FSDT	-0.6321	-1.2642	1.9466
9	HSDT-12	-0.6747	-1.3495	2.3884
	HSDT-9	-0.6598	-1.3195	2.0281
	HSDT-5	-0.6582	-1.3164	1.9254
	FSDT	-0.6608	-1.3216	2.0304
10	HSDT-12	-0.6869	-1.3739	2.4317
	HSDT-9	-0.6717	-1.3433	2.0647
	HSDT-5	-0.6702	-1.3403	1.9616
	FSDT	-0.6727	-1.3455	2.0672

Table 5.24. Nondimensionalized in-plane normal stresses ($\bar{\sigma}_x, \bar{\sigma}_y$), in-plane shear stress ($\bar{\tau}_{xy}$) and transverse shear stresses ($\bar{\tau}_{xz}, \bar{\tau}_{yz}$) at the middle ($z=0$) surface of a rectangular FGM (Titanium Alloy-Zirconia, M3) plate subjected to nonlinear (T_{NL}) thermal load ($a/h=10$ and $a/b=2$)

p	THEORY	$\bar{\sigma}_x$	$\bar{\sigma}_y$	$\bar{\tau}_{xy}$	$\bar{\tau}_{xz}$	$\bar{\tau}_{yz}$
1	HSDT-12	-170.20	-22.22	-98.65	0.7389	1.4777
	HSDT-9	-161.34	-10.49	-100.57	0.9975	1.9950
	HSDT-5	-160.84	-9.53	-100.87	1.0771	2.1543
	FSDT	-160.84	-9.53	-100.87	1.0110	2.0220
2	HSDT-12	-183.26	-44.50	-92.50	0.5577	1.1154
	HSDT-9	-173.22	-31.63	-94.39	0.7360	1.4719
	HSDT-5	-172.97	-31.18	-94.53	0.8119	1.6239
	FSDT	-172.97	-31.17	-94.53	0.7461	1.4922
3	HSDT-12	-195.65	-57.46	-92.13	0.2437	0.4874
	HSDT-9	-187.10	-45.99	-94.07	0.3457	0.6913
	HSDT-5	-187.04	-45.87	-94.11	0.4173	0.8346
	FSDT	-187.04	-45.87	-94.11	0.3508	0.7015
5	HSDT-12	-212.51	-68.33	-96.12	-0.2593	-0.5185
	HSDT-9	-208.38	-61.03	-98.24	-0.2380	-0.4761
	HSDT-5	-208.49	-61.24	-98.17	-0.1722	-0.3445
	FSDT	-208.51	-61.26	-98.16	-0.2401	-0.4803
7	HSDT-12	-222.92	-71.17	-101.17	-0.5512	-1.1023
	HSDT-9	-222.64	-67.51	-103.42	-0.5604	-1.1209
	HSDT-5	-222.83	-67.87	-103.31	-0.4980	-0.9960
	FSDT	-222.85	-67.91	-103.30	-0.5666	-1.1333
9	HSDT-12	-229.89	-71.61	-105.52	-0.7044	-1.4086
	HSDT-9	-232.29	-70.48	-107.87	-0.7251	-1.4501
	HSDT-5	-232.51	-70.92	-107.73	-0.6647	-1.3294
	FSDT	-232.54	-70.97	-107.72	-0.7337	-1.4673
10	HSDT-12	-232.59	-71.57	-107.35	-0.7488	-1.4976
	HSDT-9	-235.94	-71.33	-109.74	-0.7718	-1.5435
	HSDT-5	-236.18	-71.78	-109.60	-0.7121	-1.4242
	FSDT	-236.21	-71.83	-109.59	-0.7812	-1.5623

Table 5.25. Nondimensionalized transverse displacement (\bar{w}) at the bottom ($z= -h/2$), middle ($z=0$) and top ($z= h/2$) surface of a FGM (Titanium Alloy-Zirconia, M3) plate subjected to nonlinear (T_{NL}) thermal load ($p=1$)

a/b	a/h	z	HSDT-12	HSDT-9	HSDT-5	FSDT
1	4	-h/2	1.5276	1.7874	1.5729	1.7808
		0	1.7193	1.7874	1.5729	1.7808
		h/2	2.4434	1.7874	1.5729	1.7808
	10	-h/2	4.3516	4.4547	4.3718	4.4520
		0	4.4285	4.4547	4.3718	4.4520
		h/2	4.7173	4.4547	4.3718	4.4520
	50	-h/2	22.2400	22.2606	22.2441	22.2601
		0	22.2554	22.2606	22.2441	22.2601
		h/2	22.3131	22.2606	22.2441	22.2601
2	4	-h/2	0.4584	0.7186	0.5057	0.7123
		0	0.6464	0.7186	0.5057	0.7123
		h/2	1.3711	0.7186	0.5057	0.7123
	10	-h/2	1.6801	1.7835	1.7006	1.7808
		0	1.7570	1.7835	1.7006	1.7808
		h/2	2.0461	1.7835	1.7006	1.7808
	50	-h/2	8.8840	8.9046	8.8881	8.9040
		0	8.8994	8.9046	8.8881	8.9040
		h/2	8.9571	8.9046	8.8881	8.9040
3	4	-h/2	0.1083	0.3619	0.1518	0.3562
		0	0.2844	0.3619	0.1518	0.3562
		h/2	1.0024	0.3619	0.1518	0.3562
	10	-h/2	0.7893	0.8931	0.8104	0.8904
		0	0.8661	0.8931	0.8104	0.8904
		h/2	1.1556	0.8931	0.8104	0.8904
	50	-h/2	4.4320	4.4526	4.4361	4.4520
		0	4.4473	4.4526	4.4361	4.4520
		h/2	4.5051	4.4526	4.4361	4.4520

Table 5.26. Nondimensionalized in-plane normal stress ($\bar{\sigma}_y$) at the bottom ($z= -h/2$), middle ($z=0$) and top ($z= h/2$) surface of a FGM (Titanium Alloy-Zirconia, M3) plate subjected to nonlinear (T_{NL}) thermal load ($p=1$)

a/b	a/h	z	HSDT-12	HSDT-9	HSDT-5	FSDT
1	4	-h/2	-2.58	-34.26	-32.66	-36.83
		0	-103.31	-86.95	-85.18	-85.18
		h/2	-552.48	-529.01	-541.17	-533.79
	10	-h/2	-13.39	-36.40	-36.19	-36.83
		0	-93.31	-85.48	-85.18	-85.18
		h/2	-587.19	-532.99	-534.93	-533.79
	50	-h/2	-15.45	-36.81	-36.80	-36.83
		0	-91.44	-85.19	-85.18	-85.18
		h/2	-593.74	-533.76	-533.84	-533.79
2	4	-h/2	14.43	-40.53	-34.60	-48.16
		0	-53.48	-14.84	-9.53	-9.53
		h/2	-254.48	-305.98	-344.46	-320.50
	10	-h/2	-19.55	-46.77	-46.06	-48.16
		0	-22.22	-10.49	-9.53	-9.53
		h/2	-359.00	-317.91	-324.22	-320.50
	50	-h/2	-26.58	-48.11	-48.08	-48.16
		0	-15.97	-9.57	-9.53	-9.53
		h/2	-379.84	-320.39	-320.64	-320.50
3	4	-h/2	47.41	-37.65	-23.00	-51.94
		0	-63.70	5.59	15.69	15.69
		h/2	-63.31	-221.38	-300.54	-249.40
	10	-h/2	-14.96	-49.01	-47.41	-51.94
		0	-4.43	13.67	15.69	15.69
		h/2	-263.61	-243.95	-257.41	-249.40
	50	-h/2	-30.00	-51.82	-51.76	-51.94
		0	8.93	15.61	15.69	15.69
		h/2	-307.74	-249.17	-249.72	-249.40

Table 5.27. Nondimensionalized in-plane displacements (\bar{u} , \bar{v}) and transverse displacement (\bar{w}) at the top ($z = h/2$) surface of a rectangular FGM plate subjected to nonlinear (T_{NL}) thermal load ($a/b=2$ and $p=2$)

E_c / E_m	a/h	THEORY	\bar{u}	\bar{v}	\bar{w}
Monel – Zirconia 0.5537	10	HSDT-12	-0.7226	-1.4453	2.6937
		HSDT-9	-0.7042	-1.4084	2.2974
		HSDT-5	-0.7012	-1.4025	2.2402
		FSDT	-0.7027	-1.4055	2.2962
	50	HSDT-12	-0.7035	-1.4071	11.5604
		HSDT-9	-0.7028	-1.4056	11.4812
		HSDT-5	-0.7027	-1.4053	11.4698
		FSDT	-0.7027	-1.4055	11.4810
Titanium Alloy – Zirconia 1.7673	10	HSDT-12	-0.5366	-1.0731	2.0146
		HSDT-9	-0.5258	-1.0516	1.7393
		HSDT-5	-0.5227	-1.0454	1.6495
		FSDT	-0.5249	-1.0498	1.7369
	50	HSDT-12	-0.5254	-1.0508	8.7400
		HSDT-9	-0.5250	-1.0499	8.6849
		HSDT-5	-0.5248	-1.0497	8.6671
		FSDT	-0.5249	-1.0498	8.6844
Aluminium – Alumina 5.429	10	HSDT-12	-0.6873	-1.3746	2.1633
		HSDT-9	-0.6734	-1.3469	1.8025
		HSDT-5	-0.6707	-1.3414	1.6434
		FSDT	-0.6748	-1.3497	1.8091
	50	HSDT-12	-0.6754	-1.3507	9.1164
		HSDT-9	-0.6748	-1.3496	9.0439
		HSDT-5	-0.6747	-1.3494	9.0123
		FSDT	-0.6748	-1.3497	9.0453

Table 5.28. Nondimensionalized in-plane normal stresses ($\bar{\sigma}_x, \bar{\sigma}_y$), in-plane shear stress ($\bar{\tau}_{xy}$) and transverse shear stresses ($\bar{\tau}_{xz}, \bar{\tau}_{yz}$) at the middle ($z=0$) surface of a rectangular FGM plate subjected to nonlinear (T_{NL}) thermal load ($a/b=2$ and $p=2$)

E_c / E_m	a/h	THEORY	$\bar{\sigma}_x$	$\bar{\sigma}_y$	$\bar{\tau}_{xy}$	$\bar{\tau}_{xz}$	$\bar{\tau}_{yz}$
Monel – Zirconia 0.5537	10	HSDT-12	-637.76	-147.22	-327.02	1.3167	2.6634
		HSDT-9	-617.48	-117.53	-333.30	1.3838	2.7675
		HSDT-5	-616.77	-116.14	-333.75	1.4915	2.9831
		FSDT	-616.77	-116.13	-333.75	1.3962	2.7925
	50	HSDT-12	-627.94	-127.72	-333.48	0.2756	0.5512
		HSDT-9	-616.79	-116.19	-333.73	0.2791	0.5583
		HSDT-5	-616.77	-116.14	-333.75	0.2800	0.5600
		FSDT	-616.77	-116.13	-333.75	0.2792	0.5585
Titanium Alloy – Zirconia 1.7673	10	HSDT-12	-183.26	-44.50	-92.50	0.5577	1.1154
		HSDT-9	-173.22	-31.63	-94.39	0.7360	1.4719
		HSDT-5	-172.97	-31.18	-94.53	0.8119	1.6239
		FSDT	-172.97	-31.17	-94.53	0.7461	1.4922
	50	HSDT-12	-180.24	-38.57	-94.45	0.1260	0.2519
		HSDT-9	-172.98	-31.19	-94.53	0.1491	0.2983
		HSDT-5	-172.97	-31.17	-94.53	0.1497	0.2995
		FSDT	-172.97	-31.17	-94.53	0.1492	0.2984
Aluminium – Alumina 5.429	10	HSDT-12	-664.54	-253.18	-274.24	-2.1481	-4.2961
		HSDT-9	-657.68	-238.80	-279.25	-3.1467	-6.2935
		HSDT-5	-658.96	-241.31	-278.43	-2.9437	-5.8874
		FSDT	-658.83	-241.05	-278.52	-3.2004	-6.4008
	50	HSDT-12	-656.94	-239.43	-278.34	-0.3734	-0.7469
		HSDT-9	-658.78	-240.96	-278.55	-0.6396	-1.2793
		HSDT-5	-658.83	-241.06	-278.51	-0.6380	-1.2761
		FSDT	-658.83	-241.05	-278.52	-0.6401	-1.2802

Table 5.29. Nondimensionalized in-plane displacement (\bar{u}) at the top ($z = h/2$) surface of a square FGM plate subjected to nonlinear (T_{NL}) thermal load ($a/b=1.5$ and $a/h=10$)

E_c / E_m	p	HSDT-12	HSDT-9	HSDT-5	FSDT
Monel – Zirconia 0.5537	0	-1.2935	-1.2732	-1.2708	-1.2732
	1	-1.0594	-1.0431	-1.0389	-1.0405
	2	-1.1011	-1.0826	-1.0796	-1.0811
	3	-1.1712	-1.1507	-1.1487	-1.1502
	5	-1.3013	-1.2780	-1.2771	-1.2789
	7	-1.4008	-1.3757	-1.3752	-1.3772
	9	-1.4755	-1.4493	-1.4489	-1.4511
	10	-1.5060	-1.4793	-1.4790	-1.4812
Titanium Alloy – Zirconia 1.7673	0	-0.9352	-0.9206	-0.9188	-0.9206
	1	-0.7983	-0.7883	-0.7847	-0.7868
	2	-0.8193	-0.8085	-0.8053	-0.8076
	3	-0.8566	-0.8449	-0.8422	-0.8446
	5	-0.9286	-0.9154	-0.9133	-0.9158
	7	-0.9859	-0.9717	-0.9699	-0.9725
	9	-1.0306	-1.0156	-1.0140	-1.0166
	10	-1.0493	-1.0339	-1.0324	-1.0350
Aluminium – Alumina 5.429	0	-0.9572	-0.9422	-0.9404	-0.9422
	1	-0.9384	-0.9265	-0.9235	-0.9265
	2	-1.0507	-1.0368	-1.0341	-1.0382
	3	-1.1707	-1.1547	-1.1521	-1.1573
	5	-1.3786	-1.3595	-1.3569	-1.3634
	7	-1.5400	-1.5190	-1.5163	-1.5235
	9	-1.6676	-1.6452	-1.6426	-1.6500
	10	-1.7221	-1.6991	-1.6966	-1.7039

Table 5.30. Nondimensionalized in-plane normal stress ($\bar{\sigma}_x$) at the top ($z = h/2$) surface of a FGM plate subjected to nonlinear (T_{NL}) thermal load ($a/b=1.5$ and $a/h=10$)

E_c / E_m	p	HSDT-12	HSDT-9	HSDT-5	FSDT
MoneI – Zirconia 0.5537	0	-855.35	-871.13	-872.91	-871.13
	1	-1123.87	-1038.59	-1041.68	-1040.50
	2	-1124.69	-1009.83	-1012.01	-1010.92
	3	-1060.23	-960.31	-961.75	-960.62
	5	-897.16	-867.70	-868.31	-867.04
	7	-748.99	-796.61	-796.92	-795.49
	9	-626.82	-743.05	-743.29	-741.72
	10	-574.58	-721.17	-721.43	-719.80
Titanium Alloy – Zirconia 1.7673	0	-564.63	-575.91	-577.20	-575.91
	1	-721.68	-669.48	-672.00	-670.52
	2	-727.43	-655.21	-657.43	-655.84
	3	-694.74	-629.42	-631.33	-629.66
	5	-605.10	-579.57	-581.05	-579.29
	7	-519.34	-539.78	-541.01	-539.21
	9	-445.93	-508.74	-509.84	-508.02
	10	-413.76	-495.77	-496.83	-495.00
Aluminium – Alumina 5.429	0	-1911.51	-1946.77	-1950.75	-1946.77
	1	-2018.28	-1981.29	-1987.88	-1981.31
	2	-1707.09	-1738.88	-1744.83	-1735.76
	3	-1293.15	-1479.86	-1485.45	-1474.11
	5	-443.72	-1029.81	-1035.54	-1021.13
	7	312.44	-679.32	-685.19	-669.45
	9	954.38	-401.91	-407.62	-391.47
	10	1236.80	-283.55	-289.10	-272.92

Table 5.31. Nondimensionalized in-plane displacements (\bar{u} , \bar{v}) and transverse displacement (\bar{w}) at the top ($z = h/2$) surface of a FGM plate subjected to nonlinear (T_{NL}) thermal load ($a/h=10$ and $p=2$)

k_c / k_m	a/b	THEORY	\bar{u}	\bar{v}	\bar{w}
Aluminium – Alumina 0.0510	1	HSDT-12	-1.6997	-1.6997	4.8779
		HSDT-9	-1.6857	-1.6857	4.5160
		HSDT-5	-1.6830	-1.6830	4.3568
		FSDT	-1.6871	-1.6871	4.5226
	3	HSDT-12	-0.3496	-1.0489	1.2570
		HSDT-9	-0.3360	-1.0081	0.8981
		HSDT-5	-0.3333	-0.9999	0.7392
		FSDT	-0.3374	-1.0123	0.9045
Monel – Zirconia 0.0836	1	HSDT-12	-1.7769	-1.7769	6.1380
		HSDT-9	-1.7583	-1.7583	5.7417
		HSDT-5	-1.7553	-1.7553	5.6845
		FSDT	-1.7568	-1.7568	5.7405
	3	HSDT-12	-0.3710	-1.1129	1.5454
		HSDT-9	-0.3528	-1.0585	1.1493
		HSDT-5	-0.3499	-1.0496	1.0922
		FSDT	-0.3514	-1.0541	1.1481
Titanium Alloy – Zirconia 0.1125	1	HSDT-12	-1.3240	-1.3240	4.6200
		HSDT-9	-1.3132	-1.3132	4.3447
		HSDT-5	-1.3101	-1.3101	4.2547
		FSDT	-1.3123	-1.3123	4.3422
	3	HSDT-12	-0.2739	-0.8218	1.1458
		HSDT-9	-0.2633	-0.7900	0.8708
		HSDT-5	-0.2602	-0.7807	0.7812
		FSDT	-0.2625	-0.7874	0.8684

Table 5.32. Nondimensionalized in-plane normal stresses ($\bar{\sigma}_x, \bar{\sigma}_y$), in-plane shear stress ($\bar{\tau}_{xy}$) and transverse shear stresses ($\bar{\tau}_{xz}, \bar{\tau}_{yz}$) at the middle ($z=0$) surface of a FGM plate subjected to nonlinear (T_{NL}) thermal load ($a/h=10$ and $p=2$)

k_c / k_m	a/b	THEORY	$\bar{\sigma}_x$	$\bar{\sigma}_y$	$\bar{\tau}_{xy}$	$\bar{\tau}_{xz}$	$\bar{\tau}_{yz}$
Aluminium – Alumina 0.0510	1	HSDT-12	-452.23	-452.23	-345.96	-1.9733	-1.9733
		HSDT-9	-449.25	-449.25	-348.52	-3.1787	-3.1787
		HSDT-5	-450.02	-450.02	-348.10	-3.0976	-3.0976
		FSDT	-449.94	-449.94	-348.15	-3.2004	-3.2004
	3	HSDT-12	-739.89	-199.31	-202.72	-2.4331	-7.2993
		HSDT-9	-726.57	-166.68	-209.96	-3.0953	-9.2858
		HSDT-5	-728.68	-171.98	-208.76	-2.6880	-8.0641
		FSDT	-728.45	-171.42	-208.89	-3.2004	-9.6012
Monel – Zirconia 0.0836	1	HSDT-12	-383.36	-383.36	-413.77	1.3953	1.3953
		HSDT-9	-366.88	-366.88	-416.96	1.3912	1.3912
		HSDT-5	-366.45	-366.45	-417.19	1.4344	1.4344
		FSDT	-366.45	-366.45	-417.19	1.3962	1.3962
	3	HSDT-12	-728.06	-86.76	-240.49	1.2549	3.7645
		HSDT-9	-701.37	-35.64	-249.65	1.3714	4.1141
		HSDT-5	-700.21	-32.72	-250.31	1.5865	4.7596
		FSDT	-700.20	-32.70	-250.32	1.3962	4.1887
Titanium Alloy – Zirconia 0.1125	1	HSDT-12	-111.09	-111.09	-117.14	0.6025	0.6025
		HSDT-9	-102.22	-102.22	-118.09	0.7420	0.7420
		HSDT-5	-102.07	-102.07	-118.17	0.7725	0.7725
		FSDT	-102.07	-102.07	-118.17	0.7461	0.7461
	3	HSDT-12	-209.05	-27.88	-67.94	0.4843	1.4530
		HSDT-9	-197.01	-8.51	-70.69	0.7261	2.1783
		HSDT-5	-196.61	-7.55	-70.90	0.8775	2.6326
		FSDT	-196.60	-7.54	-70.90	0.7461	2.2383

Table 5.33. Nondimensionalized transverse displacement (\bar{w}) at the top ($z = h/2$) surface of a square FGM plate subjected to nonlinear (T_{NL}) thermal load ($a/h=20$)

k_c / k_m	p	HSDT-12	HSDT-9	HSDT-5	FSDT
Aluminium – Alumina 0.0510	0	9.9154	9.7471	9.7127	9.7471
	1	9.4496	9.2950	9.2380	9.2948
	2	9.2231	9.0419	8.9627	9.0453
	3	9.6578	9.4475	9.3480	9.4554
	5	11.1878	10.9294	10.7983	10.9434
	7	12.7235	12.4318	12.2820	12.4480
	9	14.0639	13.7485	13.5891	13.7650
	10	14.6617	14.3369	14.1748	14.3532
Monel – Zirconia 0.0836	0	13.3992	13.1718	13.1252	13.1718
	1	11.7411	11.5538	11.5228	11.5535
	2	11.6797	11.4815	11.4531	11.4810
	3	12.1063	11.8945	11.8657	11.8940
	5	13.1797	12.9444	12.9129	12.9446
	7	14.1214	13.8686	13.8340	13.8694
	9	14.8746	14.6090	14.5714	14.6101
	10	15.1909	14.9201	14.8812	14.9214
Titanium Alloy – Zirconia 0.1125	0	9.6881	9.5236	9.4889	9.5236
	1	9.0367	8.9054	8.8641	8.9040
	2	8.8233	8.6857	8.6409	8.6844
	3	8.9336	8.7873	8.7403	8.7866
	5	9.4109	9.2496	9.2002	9.2499
	7	9.9042	9.7320	9.6815	9.7329
	9	10.3313	10.1510	10.0998	10.1522
	10	10.5185	10.3348	10.2835	10.3361

Table 5.34. Nondimensionalized in-plane normal stress ($\bar{\sigma}_y$) at the top ($z = h/2$) surface of a square FGM plate subjected to nonlinear (T_{NL}) thermal load ($a/h=20$)

k_c / k_m	p	HSDT-12	HSDT-9	HSDT-5	FSDT
Aluminium – Alumina 0.0510	0	-1399.20	-1406.00	-1406.77	-1406.00
	1	-1509.26	-1449.56	-1450.83	-1449.56
	2	-1135.08	-1140.48	-1141.62	-1139.87
	3	-654.38	-811.01	-812.08	-809.88
	5	310.63	240.29	241.38	238.59
	7	1156.62	203.02	201.91	204.95
	9	1869.58	553.49	552.41	555.53
	10	2182.26	702.97	701.92	705.05
Monel – Zirconia 0.0836	0	-626.11	-629.15	-629.49	-629.15
	1	-938.41	-842.38	-842.99	-842.76
	2	-932.14	-805.24	-805.67	-805.45
	3	-855.02	-741.96	-742.23	-742.02
	5	-668.22	-624.12	-624.23	-623.99
	7	-501.92	-533.97	-534.02	-533.75
	9	-366.17	-466.20	-466.25	-465.94
	10	-308.41	-438.56	-438.61	-438.30
Titanium Alloy – Zirconia 0.1125	0	-413.79	-415.94	-416.18	-415.94
	1	-592.30	-533.59	-534.07	-533.79
	2	-594.55	-515.38	-515.81	-515.50
	3	-555.61	-482.85	-483.22	-482.90
	5	-453.92	-420.21	-420.49	-420.15
	7	-358.62	-370.33	-370.57	-370.22
	9	-277.81	-331.51	-331.71	-331.37
	10	-242.56	-315.30	-315.50	-315.15

Table 5.35. Nondimensionalized in-plane displacement (\bar{u}) and transverse displacement (\bar{w}) at the top ($z = h/2$) surface of a FGM plate subjected to nonlinear (T_{NL}), linear (T_L) and constant (T_C) thermal loads ($a/h=4$ and $p=2$)

E_c / E_m	a/b	Theory	\bar{u}			\bar{w}		
			T_{NL}	T_L	T_C	T_{NL}	T_L	T_C
Monel - Zirconia 0.5537	1.5	HSDT-12	-1.1994	-1.6411	-1.6794	2.4042	3.1330	1.2947
		HSDT-9	-1.0899	-1.4701	-1.3834	1.4160	1.7521	-0.7766
		HSDT-5	-1.0714	-1.4769	-1.4129	1.2683	1.5864	-0.5057
		FSDT	-1.0811	-1.4879	-1.3946	1.4130	1.7512	-0.7792
	2.5	HSDT-12	-0.5929	-0.8049	-0.8806	1.6130	2.1379	1.6809
		HSDT-9	-0.4926	-0.6508	-0.6151	0.6363	0.7857	-0.3469
		HSDT-5	-0.4750	-0.6561	-0.6433	0.4898	0.6215	-0.0779
		FSDT	-0.4846	-0.6670	-0.6252	0.6334	0.7850	-0.3493
	3.5	HSDT-12	-0.3595	-0.4819	-0.5567	1.2971	1.7247	1.7402
		HSDT-9	-0.2723	-0.3508	-0.3333	0.3493	0.4300	-0.1890
		HSDT-5	-0.2557	-0.3542	-0.3600	0.2046	0.2680	0.0771
		FSDT	-0.2652	-0.3650	-0.3421	0.3466	0.4295	-0.1911
Titanium Alloy - Zirconia 1.7673	1.5	HSDT-12	-0.8772	-1.1189	-1.1359	1.7599	2.1098	0.8008
		HSDT-9	-0.8128	-1.0226	-0.9757	1.0747	1.1873	-0.5484
		HSDT-5	-0.7931	-1.0141	-0.9774	0.8429	0.9255	-0.6015
		FSDT	-0.8076	-1.0313	-0.9809	1.0689	1.1932	-0.5460
	2.5	HSDT-12	-0.4263	-0.5419	-0.5802	1.1601	1.4296	1.0694
		HSDT-9	-0.3668	-0.4544	-0.4350	0.4846	0.5294	-0.2469
		HSDT-5	-0.3476	-0.4453	-0.4362	0.2552	0.2696	-0.2997
		FSDT	-0.3620	-0.4623	-0.4397	0.4791	0.5349	-0.2448
	3.5	HSDT-12	-0.2547	-0.3212	-0.3601	0.9199	1.1451	1.1100
		HSDT-9	-0.2023	-0.2460	-0.2365	0.2672	0.2878	-0.1358
		HSDT-5	-0.1839	-0.2361	-0.2371	0.0412	0.0309	-0.1881
		FSDT	-0.1981	-0.2530	-0.2406	0.2622	0.2927	-0.1339
Aluminium - Alumina 5.429	1.5	HSDT-12	-1.1118	-1.4792	-1.3736	1.9847	2.2247	-0.8826
		HSDT-9	-1.0300	-1.3455	-1.1519	1.0979	0.9166	-2.8627
		HSDT-5	-1.0116	-1.3439	-1.1518	0.6859	0.4345	-3.1308
		FSDT	-1.0382	-1.3779	-1.1706	1.1133	0.9784	-2.8299
	2.5	HSDT-12	-0.5322	-0.7079	-0.7069	1.3435	1.6337	0.5999
		HSDT-9	-0.4579	-0.5883	-0.5079	0.4850	0.3820	-1.2984
		HSDT-5	-0.4391	-0.5841	-0.5062	0.0757	-0.1001	-1.5666
		FSDT	-0.4654	-0.6176	-0.5247	0.4990	0.4386	-1.2686
	3.5	HSDT-12	-0.3122	-0.4133	-0.4404	1.0727	1.3543	1.0402
		HSDT-9	-0.2481	-0.3122	-0.2724	0.2606	0.1896	-0.7203
		HSDT-5	-0.2287	-0.3049	-0.2688	-0.1442	-0.2911	-0.9879
		FSDT	-0.2547	-0.3380	-0.2871	0.2731	0.2400	-0.6941

Table 5.36. Nondimensionalized in-plane normal stresses ($\bar{\sigma}_x, \bar{\sigma}_y$), at the middle ($z = 0$) surface of a FGM plate subjected to nonlinear (T_{NL}), linear (T_L) and constant (T_C) thermal loads ($a/h=4$ and $p=2$)

E_c / E_m	a/b	Theory	$\bar{\sigma}_x$			$\bar{\sigma}_y$		
			T_{NL}	T_L	T_C	T_{NL}	T_L	T_C
Monel - Zirconia 0.5537	1.5	HSDT-12	-585.38	-1122.97	-2131.40	-288.65	-665.22	-1164.41
		HSDT-9	-530.07	-1040.88	-1975.14	-210.81	-548.82	-935.33
		HSDT-5	-526.93	-1048.62	-1980.28	-206.03	-560.61	-943.15
		FSDT	-526.91	-1048.60	-1980.32	-205.99	-560.57	-943.22
	2.5	HSDT-12	-759.95	-1391.94	-2698.52	-243.74	-579.56	-996.08
		HSDT-9	-673.46	-1252.05	-2430.06	-75.52	-317.94	-467.17
		HSDT-5	-668.60	-1264.05	-2438.08	-64.43	-345.27	-485.29
		FSDT	-668.55	-1264.00	-2438.08	-64.35	-345.16	-485.46
	3.5	HSDT-12	-859.74	-1546.57	-3023.54	-301.34	-640.27	-1146.28
		HSDT-9	-727.64	-1326.32	-2595.13	-30.93	-220.43	-286.50
		HSDT-5	-720.73	-1343.33	-2606.39	-12.40	-266.10	-316.72
		FSDT	-720.67	-1343.24	-2606.50	-12.23	-265.91	-317.04
Titanium Alloy - Zirconia 1.7673	1.5	HSDT-12	-169.42	-305.76	-583.21	-85.80	-182.79	-323.48
		HSDT-9	-148.60	-282.23	-534.25	-58.23	-149.28	-253.36
		HSDT-5	-147.54	-284.57	-535.76	-56.65	-152.70	-255.60
		FSDT	-147.52	-284.55	-535.76	-56.63	-152.67	-255.60
	2.5	HSDT-12	-220.27	-381.63	-743.25	-75.45	-164.36	-288.26
		HSDT-9	-189.33	-339.19	-657.05	-20.19	-86.66	-126.79
		HSDT-5	-187.67	-342.80	-659.42	-16.57	-94.54	-131.96
		FSDT	-187.64	-342.76	-659.41	-16.50	-94.46	-131.94
	3.5	HSDT-12	-250.93	-428.16	-840.93	-94.37	-185.61	-340.15
		HSDT-9	-204.81	-359.08	-701.53	-7.86	-60.08	-77.86
		HSDT-5	-202.45	-364.24	-704.92	-1.87	-73.20	-86.48
		FSDT	-202.40	-364.18	-704.91	-1.74	-73.04	-86.45
Aluminium - Alumina 5.429	1.5	HSDT-12	-617.07	-1199.70	-2220.79	-364.04	-775.99	-1264.98
		HSDT-9	-578.77	-1145.79	-2065.95	-308.31	-693.12	-1042.75
		HSDT-5	-584.49	-1165.71	-2078.83	-317.02	-723.45	-1062.36
		FSDT	-583.84	-1164.88	-2078.37	-316.04	-722.19	-1061.66
	2.5	HSDT-12	-761.82	-1443.80	-2774.16	-307.50	-670.28	-1070.90
		HSDT-9	-694.26	-1330.98	-2508.04	-180.09	-460.05	-569.43
		HSDT-5	-703.15	-1361.68	-2527.90	-200.35	-529.00	-614.68
		FSDT	-702.04	-1360.28	-2527.13	-197.83	-526.80	-612.91
	3.5	HSDT-12	-842.77	-1582.27	-3085.40	-325.84	-681.92	-1172.20
		HSDT-9	-734.61	-1391.10	-2665.43	-125.02	-344.66	-375.84
		HSDT-5	-747.30	-1434.42	-2693.48	-159.09	-460.95	-451.14
		FSDT	-745.53	-1432.17	-2692.23	-154.34	-454.91	-447.80

Table 5.37. Nondimensionalized in-plane shear stress ($\bar{\tau}_{xy}$) at the top ($z = h/2$) surface of a FGM plate subjected to nonlinear (T_{NL}), linear (T_L) and constant (T_C) thermal loads ($a/h=4$ and $p=2$)

E_c / E_m	a/b	Theory	$\bar{\tau}_{xy}$		
			T_{NL}	T_L	T_C
Monel - Zirconia 0.5537	1.5	HSDT-12	-547.07	-748.53	-765.99
		HSDT-9	-497.12	-670.53	-631.02
		HSDT-5	-488.71	-673.65	-644.45
		FSDT	-493.12	-678.68	-636.11
	2.5	HSDT-12	-450.74	-611.86	-669.41
		HSDT-9	-374.50	-494.77	-467.62
		HSDT-5	-361.12	-498.75	-489.05
		FSDT	-368.43	-507.06	-475.25
	3.5	HSDT-12	-382.59	-512.91	-592.52
		HSDT-9	-289.77	-373.38	-354.77
		HSDT-5	-272.12	-376.93	-383.15
		FSDT	-282.23	-388.43	-364.06
Titanium Alloy - Zirconia 1.7673	1.5	HSDT-12	-365.83	-466.64	-473.74
		HSDT-9	-338.97	-426.48	-406.93
		HSDT-5	-330.75	-422.93	-407.62
		FSDT	-336.80	-430.10	-409.10
	2.5	HSDT-12	-296.34	-376.68	-403.30
		HSDT-9	-254.95	-315.87	-302.39
		HSDT-5	-241.64	-309.50	-303.20
		FSDT	-251.63	-321.34	-305.65
	3.5	HSDT-12	-247.82	-312.55	-350.41
		HSDT-9	-196.89	-239.44	-230.16
		HSDT-5	-178.96	-229.80	-230.75
		FSDT	-192.76	-246.16	-234.14
Aluminium - Alumina 5.429	1.5	HSDT-12	-1531.41	-2037.56	-1892.10
		HSDT-9	-1418.76	-1853.37	-1586.64
		HSDT-5	-1393.47	-1851.21	-1586.60
		FSDT	-1430.12	-1897.85	-1612.40
	2.5	HSDT-12	-1221.87	-1625.30	-1622.87
		HSDT-9	-1051.33	-1350.70	-1165.93
		HSDT-5	-1007.99	-1340.94	-1162.07
		FSDT	-1068.48	-1417.93	-1204.67
	3.5	HSDT-12	-1003.43	-1328.42	-1415.37
		HSDT-9	-797.43	-1003.44	-875.47
		HSDT-5	-735.00	-979.93	-864.04
		FSDT	-818.50	-1086.19	-922.82

Table 5.38. Nondimensionalized transverse shear stresses ($\bar{\tau}_{xz}, \bar{\tau}_{yz}$) at a distance $0.1h$ from the bottom surface of a FGM plate subjected to nonlinear (T_{NL}), linear (T_L) and constant (T_C) thermal loads ($a/h=4$ and $p=2$)

E_c / E_m	a/b	Theory	$\bar{\tau}_{xz}$			$\bar{\tau}_{yz}$		
			T_{NL}	T_L	T_C	T_{NL}	T_L	T_C
Monel - Zirconia 0.5537	1.5	HSDT-12	2.9647	13.9793	24.2141	4.4471	20.9689	36.3211
		HSDT-9	4.2094	15.5802	12.4761	6.3142	23.3703	18.7142
		HSDT-5	3.7593	18.3006	11.8122	5.6390	27.4509	17.7183
		FSDT	4.7307	17.1951	13.6473	7.0961	25.7926	20.4710
	2.5	HSDT-12	7.2219	20.3670	42.0790	18.0547	50.9175	105.1980
		HSDT-9	3.7007	13.9550	11.2878	9.2518	34.8874	28.2194
		HSDT-5	2.5808	19.6418	9.5857	6.4520	49.1046	23.9643
		FSDT	4.7307	17.1951	13.6473	11.8268	42.9876	34.1184
	3.5	HSDT-12	11.8694	27.0794	62.0890	41.5428	94.7780	217.3120
		HSDT-9	3.1298	12.0521	9.8814	10.9543	42.1823	34.5849
		HSDT-5	0.8474	21.6146	6.3110	2.9659	75.6510	22.0886
		FSDT	4.7307	17.1951	13.6473	16.5575	60.1827	47.7657
Titanium Alloy - Zirconia 1.7673	1.5	HSDT-12	1.6290	7.3376	12.4362	2.4435	11.0064	18.6543
		HSDT-9	1.4174	3.9790	3.0228	2.1261	5.9685	4.5342
		HSDT-5	1.1814	4.9083	3.4302	1.7721	7.3624	5.1452
		FSDT	1.5946	4.4188	3.3288	2.3919	6.6282	4.9932
	2.5	HSDT-12	4.0358	10.8290	21.6676	10.0894	27.0725	54.1690
		HSDT-9	1.2447	3.5394	2.7147	3.1117	8.8485	6.7868
		HSDT-5	0.6812	5.5008	3.5529	1.7030	13.7521	8.8822
		FSDT	1.5946	4.4188	3.3288	3.9865	11.0470	8.3220
	3.5	HSDT-12	6.6014	14.3757	31.6935	23.1048	50.3149	110.9270
		HSDT-9	1.0510	3.0289	2.3537	3.6784	10.6013	8.2379
		HSDT-5	0.0525	6.3700	3.7328	0.1838	22.2949	13.0649
		FSDT	1.5946	4.4188	3.3288	5.5812	15.4657	11.6508
Aluminium - Alumina 5.429	1.5	HSDT-12	-12.8302	-35.7072	-45.9506	-19.2453	-53.5608	-68.9258
		HSDT-9	-7.5103	-27.9690	-20.2461	-11.2655	-41.9535	-30.3692
		HSDT-5	-9.1016	-32.2324	-22.9816	-13.6523	-48.3487	-34.4724
		FSDT	-8.4188	-31.3635	-22.5009	-12.6282	-47.0453	-33.7513
	2.5	HSDT-12	-17.6842	-42.9192	-68.6582	-44.2104	-107.2980	-171.6450
		HSDT-9	-6.6108	-24.6150	-18.0045	-16.5270	-61.5376	-45.0113
		HSDT-5	-9.9273	-33.2833	-23.5630	-24.8183	-83.2082	-58.9074
		FSDT	-8.4188	-31.3635	-22.5009	-21.0469	-78.4088	-56.2521
	3.5	HSDT-12	-22.2336	-49.1668	-91.9541	-77.8175	-172.0840	-321.8390
		HSDT-9	-5.5773	-20.7730	-15.4150	-19.5205	-72.7054	-53.9526
		HSDT-5	-11.1367	-34.8223	-24.4144	-38.9784	-121.8780	-85.4505
		FSDT	-8.4188	-31.3635	-22.5009	-29.4657	-109.7720	-78.7530

Table 5.39. Nondimensionalized in-plane displacement (\bar{u}) and transverse displacement (\bar{w}) at the top ($z = h/2$) surface of a FGM plate subjected to nonlinear (T_{NL}), linear (T_L) and constant (T_C) thermal loads ($a/b=2$ and $p=2$)

k_c / k_m	a/h	Theory	\bar{u}			\bar{w}		
			T_{NL}	T_L	T_C	T_{NL}	T_L	T_C
Aluminium - Alumina 0.0510	4	HSDT-12	-0.7454	-0.9920	-0.9547	1.5837	1.8604	0.0750
		HSDT-9	-0.6670	-0.8647	-0.7430	0.7089	0.5766	-1.8708
		HSDT-5	-0.6484	-0.8618	-0.7422	0.2980	0.0944	-2.1391
		FSDT	-0.6748	-0.8956	-0.7609	0.7236	0.6360	-1.8394
	10	HSDT-12	-0.6873	-0.9129	-0.7954	2.1633	2.0998	-3.8037
		HSDT-9	-0.6734	-0.8900	-0.7577	1.8025	1.5637	-4.6126
		HSDT-5	-0.6707	-0.8903	-0.7580	1.6434	1.3787	-4.7154
		FSDT	-0.6748	-0.8956	-0.7609	1.8091	1.5899	-4.5986
	20	HSDT-12	-0.6780	-0.9000	-0.7696	3.7959	3.4361	-8.7981
		HSDT-9	-0.6745	-0.8942	-0.7600	3.6148	3.1666	-9.2043
		HSDT-5	-0.6738	-0.8942	-0.7601	3.5356	3.0747	-9.2554
		FSDT	-0.6748	-0.8956	-0.7609	3.6181	3.1799	-9.1972
Monel – Zirconia 0.0836	4	HSDT-12	-0.8166	-1.1135	-1.1783	1.9055	2.5088	1.5512
		HSDT-9	-0.7111	-0.9501	-0.8959	0.9214	1.1391	-0.5040
		HSDT-5	-0.6931	-0.9562	-0.9247	0.7742	0.9741	-0.2339
		FSDT	-0.7027	-0.9672	-0.9065	0.9185	1.1383	-0.5065
	10	HSDT-12	-0.7226	-0.9932	-0.9550	2.6937	3.4031	-0.4313
		HSDT-9	-0.7042	-0.9641	-0.9046	2.2974	2.8461	-1.2651
		HSDT-5	-0.7012	-0.9655	-0.9093	2.2402	2.7820	-1.1603
		FSDT	-0.7027	-0.9672	-0.9065	2.2962	2.8457	-1.2662
	20	HSDT-12	-0.7078	-0.9738	-0.9188	4.7911	5.9705	-2.1146
		HSDT-9	-0.7031	-0.9664	-0.9060	4.5930	5.6916	-2.5318
		HSDT-5	-0.7024	-0.9667	-0.9072	4.5645	5.6597	-2.4797
		FSDT	-0.7027	-0.9672	-0.9065	4.5924	5.6914	-2.5324
Titanium Alloy – Zirconia 0.1125	4	HSDT-12	-0.5922	-0.7544	-0.7863	1.3821	1.6835	0.9795
		HSDT-9	-0.5299	-0.6620	-0.6326	0.7004	0.7699	-0.3572
		HSDT-5	-0.5105	-0.6532	-0.6341	0.4697	0.5089	-0.4101
		FSDT	-0.5249	-0.6703	-0.6376	0.6948	0.7755	-0.3549
	10	HSDT-12	-0.5366	-0.6851	-0.6638	2.0146	2.3093	-0.3440
		HSDT-9	-0.5258	-0.6688	-0.6367	1.7393	1.9364	-0.8883
		HSDT-5	-0.5227	-0.6677	-0.6371	1.6495	1.8352	-0.9088
		FSDT	-0.5249	-0.6703	-0.6376	1.7369	1.9389	-0.8873
	20	HSDT-12	-0.5279	-0.6741	-0.6442	3.6127	4.0633	-1.5026
		HSDT-9	-0.5251	-0.6699	-0.6374	3.4750	3.8765	-1.7751
		HSDT-5	-0.5244	-0.6697	-0.6375	3.4303	3.8261	-1.7853
		FSDT	-0.5249	-0.6703	-0.6376	3.4738	3.8777	-1.7746

Table 5.40. Nondimensionalized in-plane normal stresses ($\bar{\sigma}_x, \bar{\sigma}_y$) at the middle ($z = 0$) surface of a FGM plate subjected to nonlinear (T_{NL}), linear (T_L) and constant (T_C) thermal loads ($a/b=2$ and $p=2$)

k_c / k_m	a/h	Theory	$\bar{\sigma}_x$			$\bar{\sigma}_y$		
			T_{NL}	T_L	T_C	T_{NL}	T_L	T_C
Aluminium - Alumina 0.0510	4	HSDT-12	-703.75	-1345.28	-2551.67	-318.27	-695.07	-1100.16
		HSDT-9	-652.49	-1264.99	-2347.53	-228.67	-551.63	-746.65
		HSDT-5	-659.67	-1289.92	-2363.65	-242.71	-600.35	-778.15
		FSDT	-658.83	-1288.84	-2363.05	-241.05	-598.24	-776.98
	10	HSDT-12	-664.54	-1278.03	-2394.78	-253.18	-595.95	-834.85
		HSDT-9	-657.68	-1284.51	-2360.24	-238.80	-589.78	-771.49
		HSDT-5	-658.96	-1289.01	-2363.14	-241.31	-598.57	-777.17
		FSDT	-658.83	-1288.84	-2363.05	-241.05	-598.24	-776.98
	20	HSDT-12	-658.61	-1267.72	-2371.03	-242.49	-579.33	-791.67
		HSDT-9	-658.53	-1287.73	-2362.33	-240.48	-596.08	-775.58
		HSDT-5	-658.86	-1288.88	-2363.07	-241.11	-598.32	-777.03
		FSDT	-658.83	-1288.84	-2363.05	-241.05	-598.24	-776.98
Monel - Zirconia 0.0836	4	HSDT-12	-689.63	-1283.23	-2469.75	-243.58	-589.23	-1008.77
		HSDT-9	-620.74	-1175.57	-2264.21	-123.90	-405.01	-640.12
		HSDT-5	-616.80	-1185.28	-2270.66	-116.19	-423.99	-652.72
		FSDT	-616.77	-1185.25	-2270.72	-116.13	-423.92	-652.83
	10	HSDT-12	-637.76	-1204.09	-2303.66	-147.22	-455.63	-715.34
		HSDT-9	-617.48	-1183.51	-2269.55	-117.53	-420.53	-650.55
		HSDT-5	-616.77	-1185.25	-2270.71	-116.14	-423.93	-652.81
		FSDT	-616.77	-1185.25	-2270.72	-116.13	-423.92	-652.83
	20	HSDT-12	-630.09	-1192.24	-2278.98	-132.03	-434.21	-668.65
		HSDT-9	-616.95	-1184.80	-2270.42	-116.49	-423.06	-652.25
		HSDT-5	-616.77	-1185.25	-2270.71	-116.14	-423.92	-652.82
		FSDT	-616.77	-1185.25	-2270.72	-116.13	-423.92	-652.83
Titanium Alloy - Zirconia 0.1125	4	HSDT-12	-199.53	-350.44	-677.58	-74.11	-164.45	-286.17
		HSDT-9	-174.33	-318.60	-612.30	-33.74	-110.31	-173.56
		HSDT-5	-173.00	-321.51	-614.21	-31.22	-115.79	-177.17
		FSDT	-172.97	-321.48	-614.20	-31.17	-115.74	-177.15
	10	HSDT-12	-183.26	-325.32	-624.60	-44.50	-123.38	-196.19
		HSDT-9	-173.22	-320.96	-613.86	-31.63	-114.76	-176.51
		HSDT-5	-172.97	-321.48	-614.20	-31.18	-115.75	-177.16
		FSDT	-172.97	-321.48	-614.20	-31.17	-115.74	-177.15
	20	HSDT-12	-180.90	-321.61	-616.81	-39.88	-116.84	-181.97
		HSDT-9	-173.03	-321.35	-614.11	-31.29	-115.49	-176.99
		HSDT-5	-172.97	-321.48	-614.20	-31.17	-115.74	-177.15
		FSDT	-172.97	-321.48	-614.20	-31.17	-115.74	-177.15

Table 5.41. Nondimensionalized in-plane shear stress ($\bar{\tau}_{xy}$) at the top ($z = h/2$) surface of a FGM plate subjected to nonlinear (T_{NL}), linear (T_L) and constant (T_C) thermal loads ($a/b=2$ and $p=2$)

k_c / k_m	a/h	Theory	$\bar{\tau}_{xy}$		
			T_{NL}	T_L	T_C
Aluminium - Alumina 0.0510	4	HSDT-12	-1369.02	-1822.00	-1753.37
		HSDT-9	-1224.95	-1588.05	-1364.62
		HSDT-5	-1190.78	-1582.88	-1363.16
		FSDT	-1239.44	-1644.80	-1397.42
	10	HSDT-12	-1262.29	-1676.69	-1460.91
		HSDT-9	-1236.85	-1634.67	-1391.53
		HSDT-5	-1231.86	-1635.14	-1392.07
		FSDT	-1239.44	-1644.80	-1397.42
	20	HSDT-12	-1245.23	-1652.91	-1413.52
		HSDT-9	-1238.78	-1642.23	-1395.92
		HSDT-5	-1237.55	-1642.40	-1396.09
		FSDT	-1239.44	-1644.80	-1397.42
Monel - Zirconia 0.0836	4	HSDT-12	-496.62	-677.20	-716.58
		HSDT-9	-432.48	-577.80	-544.83
		HSDT-5	-421.50	-581.51	-562.38
		FSDT	-427.37	-588.19	-551.29
	10	HSDT-12	-439.48	-604.03	-580.78
		HSDT-9	-428.28	-586.33	-550.13
		HSDT-5	-426.46	-587.15	-553.02
		FSDT	-427.37	-588.19	-551.29
	20	HSDT-12	-430.44	-592.21	-558.77
		HSDT-9	-427.60	-587.72	-551.00
		HSDT-5	-427.15	-587.93	-551.72
		FSDT	-427.37	-588.19	-551.29
Titanium Alloy - Zirconia 0.1125	4	HSDT-12	-329.32	-419.52	-437.22
		HSDT-9	-294.68	-368.14	-351.80
		HSDT-5	-283.86	-363.23	-352.58
		FSDT	-291.90	-372.75	-354.56
	10	HSDT-12	-298.37	-380.98	-369.12
		HSDT-9	-292.39	-371.93	-354.06
		HSDT-5	-290.65	-371.27	-354.25
		FSDT	-291.90	-372.75	-354.56
	20	HSDT-12	-293.53	-374.83	-358.24
		HSDT-9	-292.02	-372.54	-354.43
		HSDT-5	-291.59	-372.38	-354.48
		FSDT	-291.90	-372.75	-354.56

Table 5.42. Nondimensionalized transverse shear stresses ($\bar{\tau}_{xz}, \bar{\tau}_{yz}$) at a distance 0.1h from the bottom surface of a FGM plate subjected to nonlinear (T_{NL}), linear (T_L) and constant (T_C) thermal loads (a/b=2 and p=2)

k_c / k_m	a/h	Theory	$\bar{\tau}_{xz}$			$\bar{\tau}_{yz}$		
			T_{NL}	T_L	T_C	T_{NL}	T_L	T_C
Aluminium - Alumina 0.0510	4	HSDT-12	-15.1556	-39.2069	-56.6782	-30.3112	-78.4138	-113.356
		HSDT-9	-7.09127	-26.4055	-19.2031	-14.1825	-52.8109	-38.4061
		HSDT-5	-9.4648	-32.6947	-23.2373	-18.9296	-65.3894	-46.4746
		FSDT	-8.4188	-31.3635	-22.5009	-16.8376	-62.7271	-45.0017
	10	HSDT-12	-3.6041	-11.9304	-11.4850	-7.20822	-23.8608	-22.9700
		HSDT-9	-3.2710	-12.1843	-8.7610	-6.5419	-24.3687	-17.522
		HSDT-5	-3.4327	-12.6285	-9.0463	-6.8653	-25.2569	-18.0925
		FSDT	-3.3676	-12.5454	-9.0004	-6.7350	-25.0908	-18.0007
	20	HSDT-12	-1.5942	-5.6404	-4.8162	-3.1883	-11.2808	-9.6325
		HSDT-9	-1.6715	-6.2267	-4.4697	-3.3429	-12.4533	-8.9394
		HSDT-5	-1.6919	-6.2831	-4.5059	-3.3838	-12.5661	-9.0118
		FSDT	-1.6838	-6.2727	-4.5002	-3.3675	-12.5454	-9.0004
Monel - Zirconia 0.0836	4	HSDT-12	4.9468	16.9764	32.5046	9.8935	33.9528	65.0095
		HSDT-9	3.9714	14.8264	11.9263	7.9427	29.6529	23.8526
		HSDT-5	3.2414	18.8900	10.8338	6.4828	37.7800	21.6675
		FSDT	4.7307	17.1951	13.6473	9.4614	34.3901	27.2947
	10	HSDT-12	0.0485	3.6964	4.5375	0.0971	7.3928	9.0750
		HSDT-9	1.8366	6.7074	5.3355	3.6733	13.4147	10.6710
		HSDT-5	1.7999	6.9833	5.2842	3.5998	13.9666	10.5683
		FSDT	1.8923	6.8780	5.4589	3.7846	13.7560	10.9179
	20	HSDT-12	0.1862	1.5969	1.5937	0.3724	3.1937	3.1872
		HSDT-9	0.9390	3.4173	2.7138	1.8781	6.8346	5.4275
		HSDT-5	0.9346	3.4521	2.7077	1.8693	6.9042	5.4154
		FSDT	0.9461	3.4390	2.7294	1.8923	6.8780	5.4589
Titanium Alloy - Zirconia 0.1125	4	HSDT-12	2.7529	8.9837	16.7417	5.5057	17.9674	33.4834
		HSDT-9	1.3365	3.7747	2.8799	2.6731	7.5494	5.7599
		HSDT-5	0.9615	5.1688	3.4841	1.9229	10.3377	6.9682
		FSDT	1.5946	4.4188	3.3288	3.1892	8.8376	6.6576
	10	HSDT-12	0.0500	1.8877	2.2813	0.1001	3.7753	4.5625
		HSDT-9	0.6189	1.7209	1.2992	1.2378	3.4419	2.5984
		HSDT-5	0.5985	1.8142	1.3412	1.1970	3.6284	2.6824
		FSDT	0.6378	1.7675	1.3315	1.2757	3.5350	2.6631
	20	HSDT-12	0.1170	0.8046	0.7861	0.2341	1.6091	1.5721
		HSDT-9	0.3165	0.8778	0.6617	0.6330	1.7557	1.3233
		HSDT-5	0.3140	0.8896	0.6670	0.6281	1.7791	1.3339
		FSDT	0.3189	0.8838	0.6658	0.6378	1.7675	1.3315

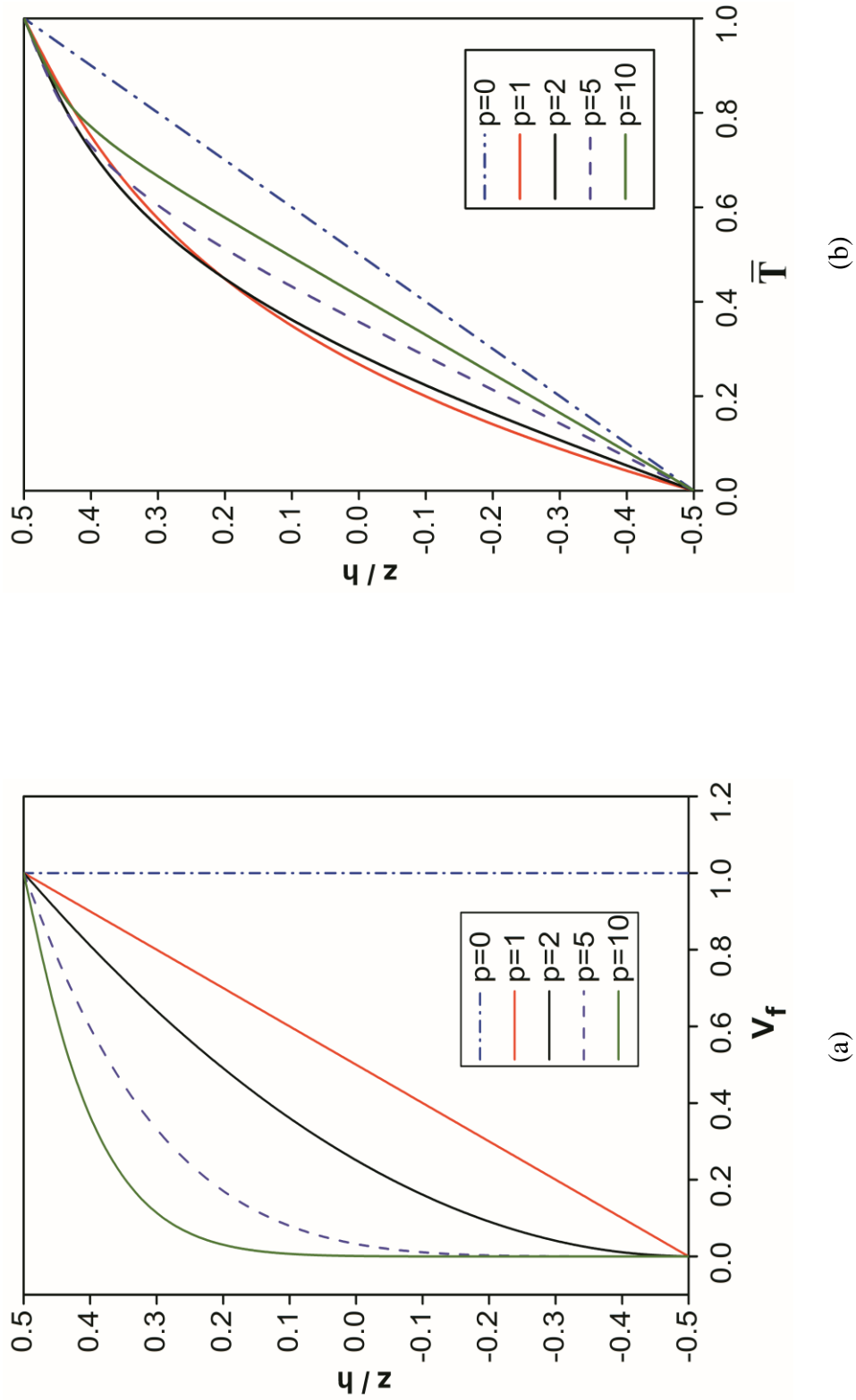


Fig. 5.1. Variation of (a) Volume fraction distribution (V_f) of ceramic-metal constituent phase and (b) Nondimensionalized Temperature field through the thickness (z/h) of an FGM plate for various power law parameters.

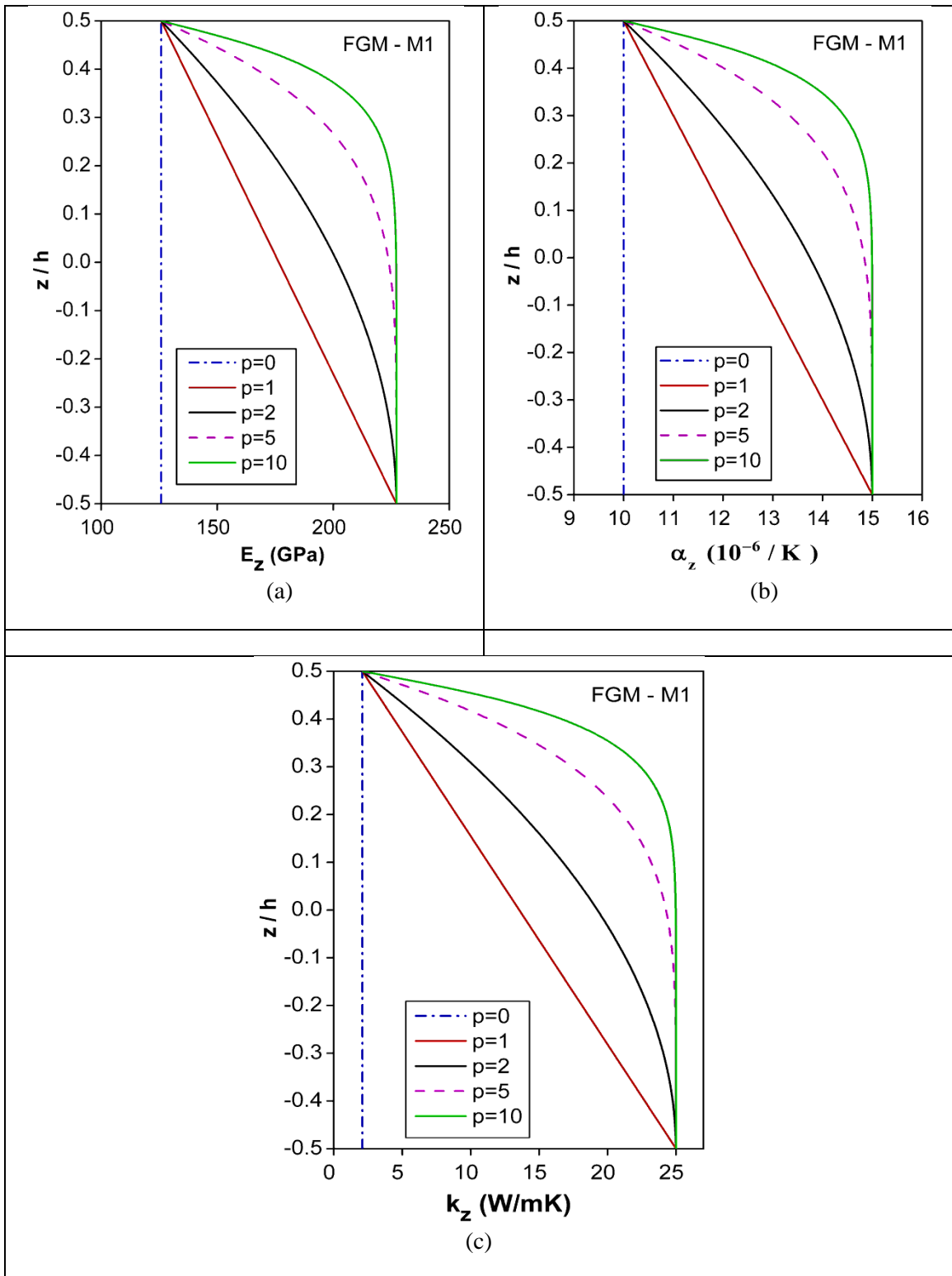


Fig. 5.2. Variation of effective material properties through the thickness (z/h) of Monel-Zirconia (M1) FGM plate (a) Young's modulus of elasticity, (b) Thermal coefficient of expansion and (c) Thermal conductivity.

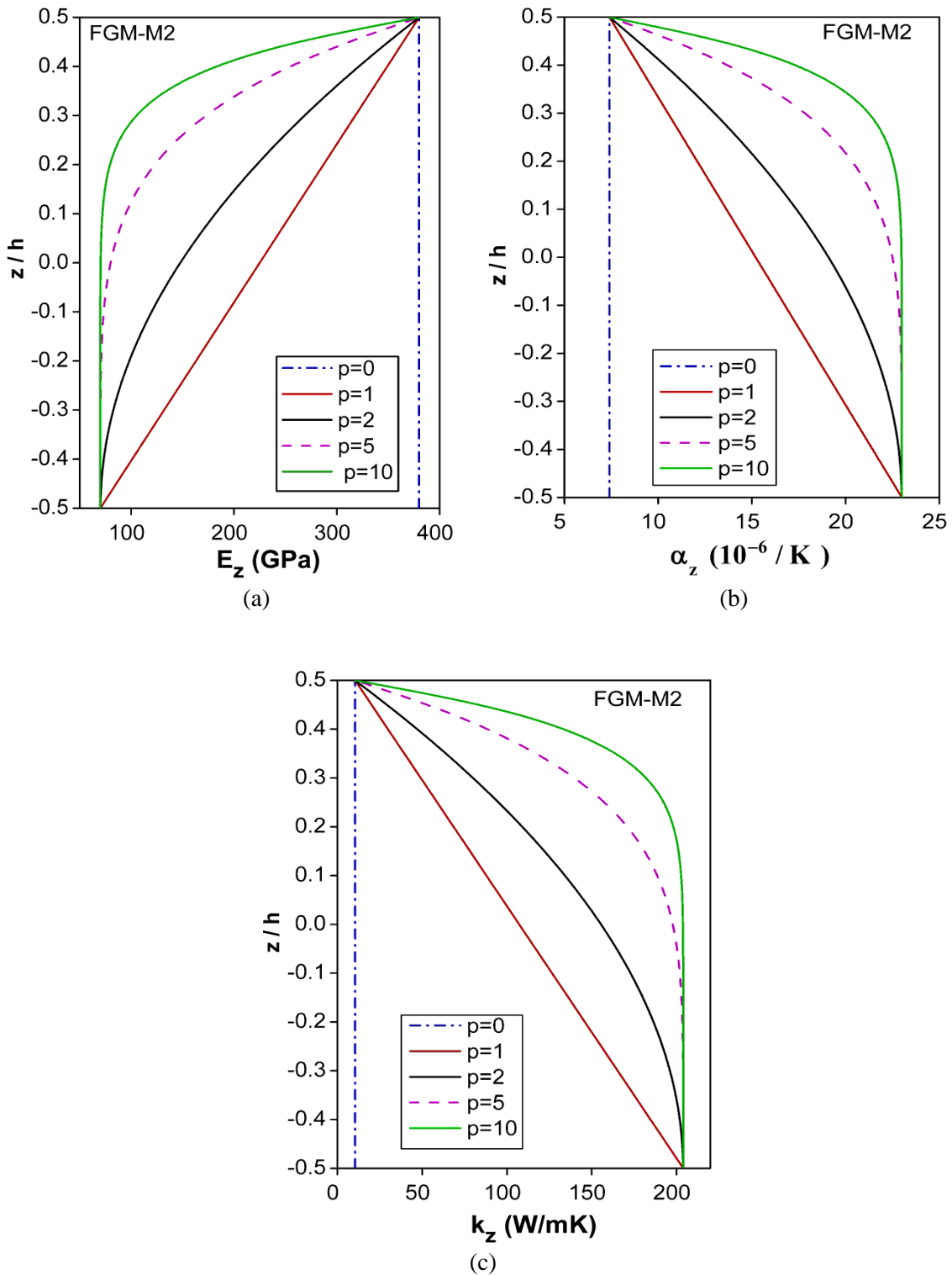


Fig. 5.3. Variation of effective material properties through the thickness (z/h) of Aluminium-Alumina (M2) FGM plate (a) Young's modulus of elasticity, (b) Thermal coefficient of expansion and (c) Thermal conductivity.

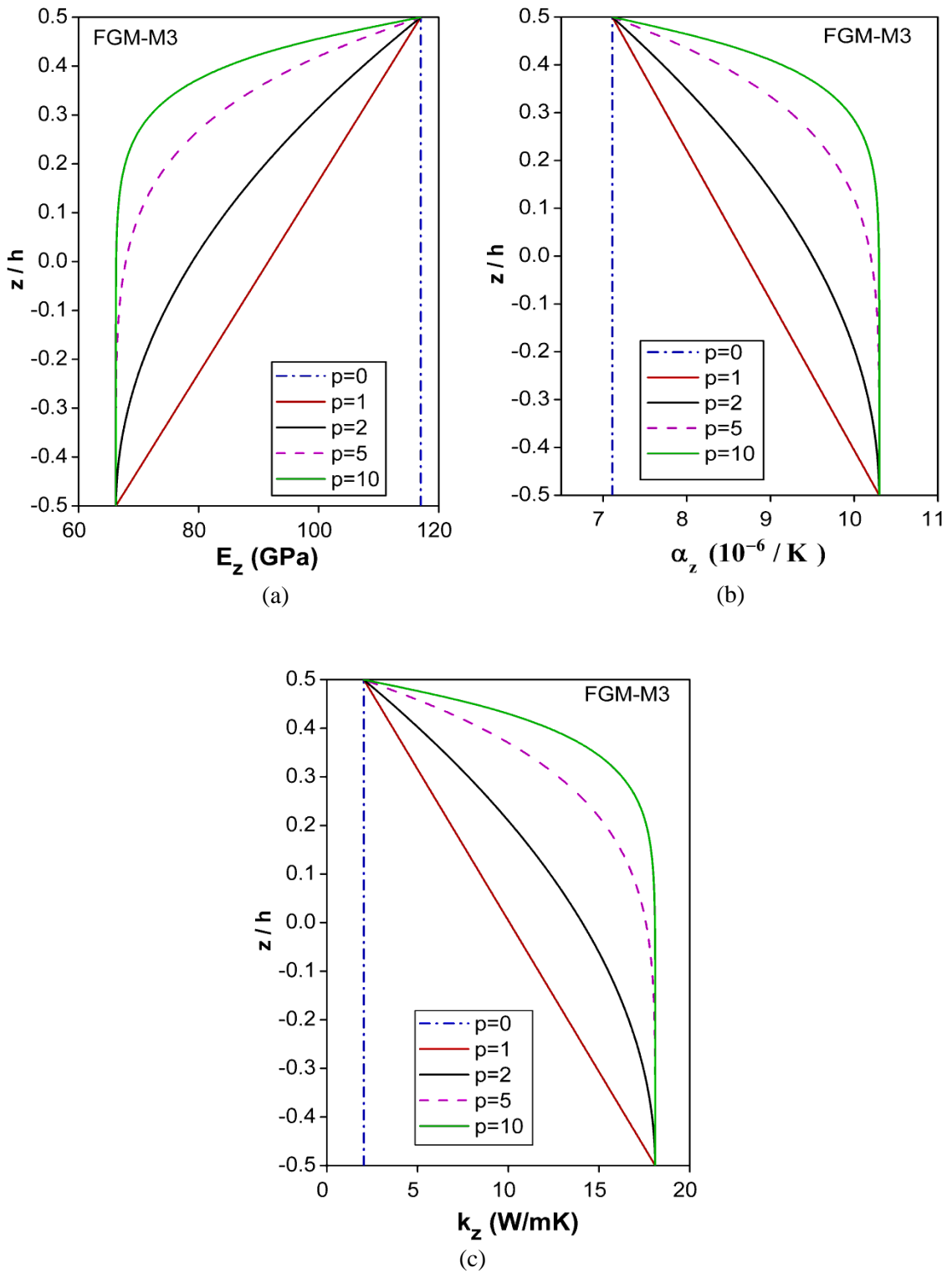


Fig.5.4. Variation of effective material properties through the thickness (z/h) of Titanium Alloy-Zirconia (M3) FGM plate (a) Young's modulus of elasticity, (b) Thermal coefficient of expansion and (c) Thermal conductivity.

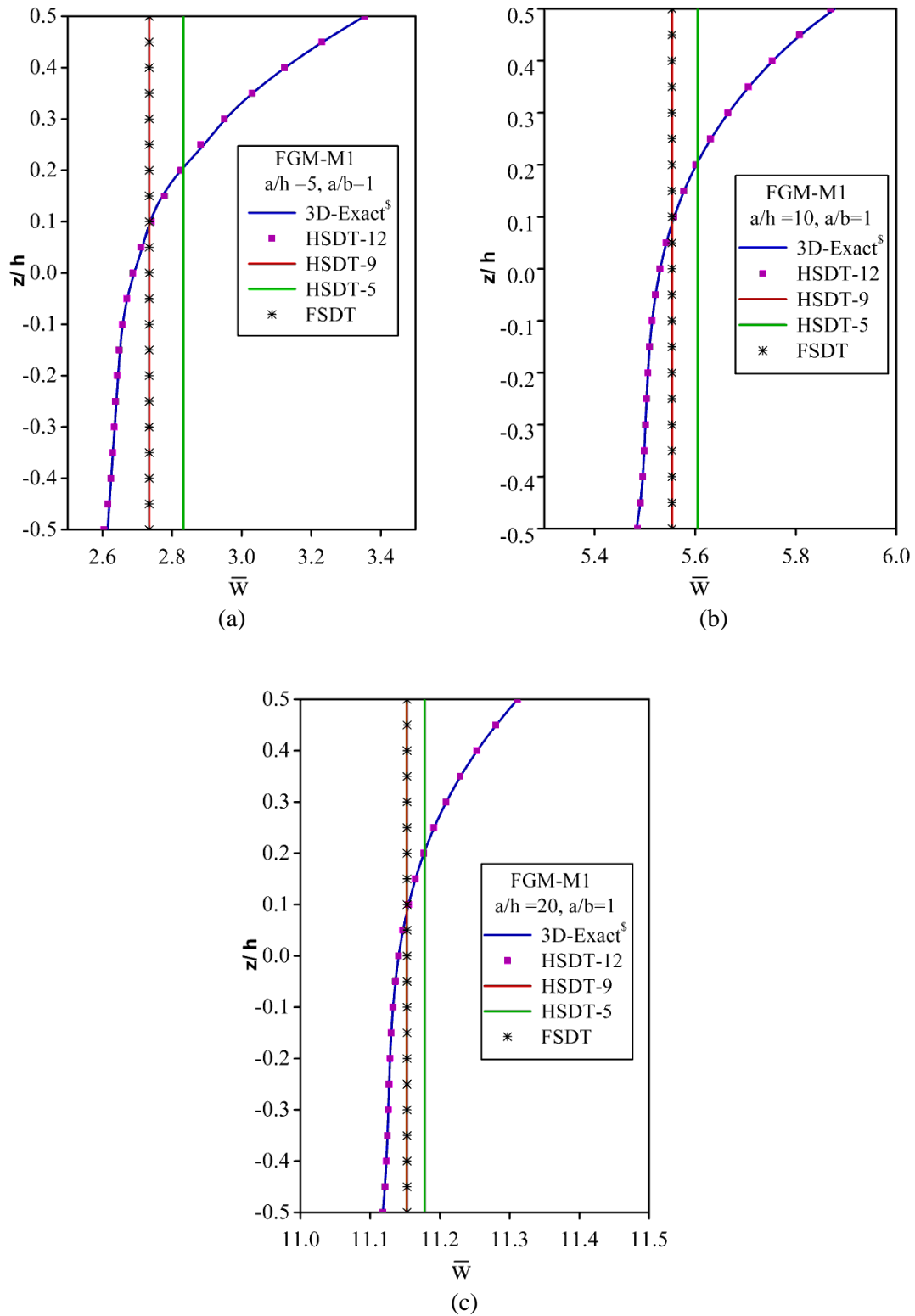


Fig. 5.5. Variation of nondimensionalized transverse displacement (\bar{w}) through the thickness (z/h) of a simply supported square Monel-Zirconia (M1) FGM plate subjected to nonlinear thermal load for (a) $a/h = 5$, (b) $a/h = 10$ and (c) $a/h = 20$. [^sAlibeigloo, A. (2010)]

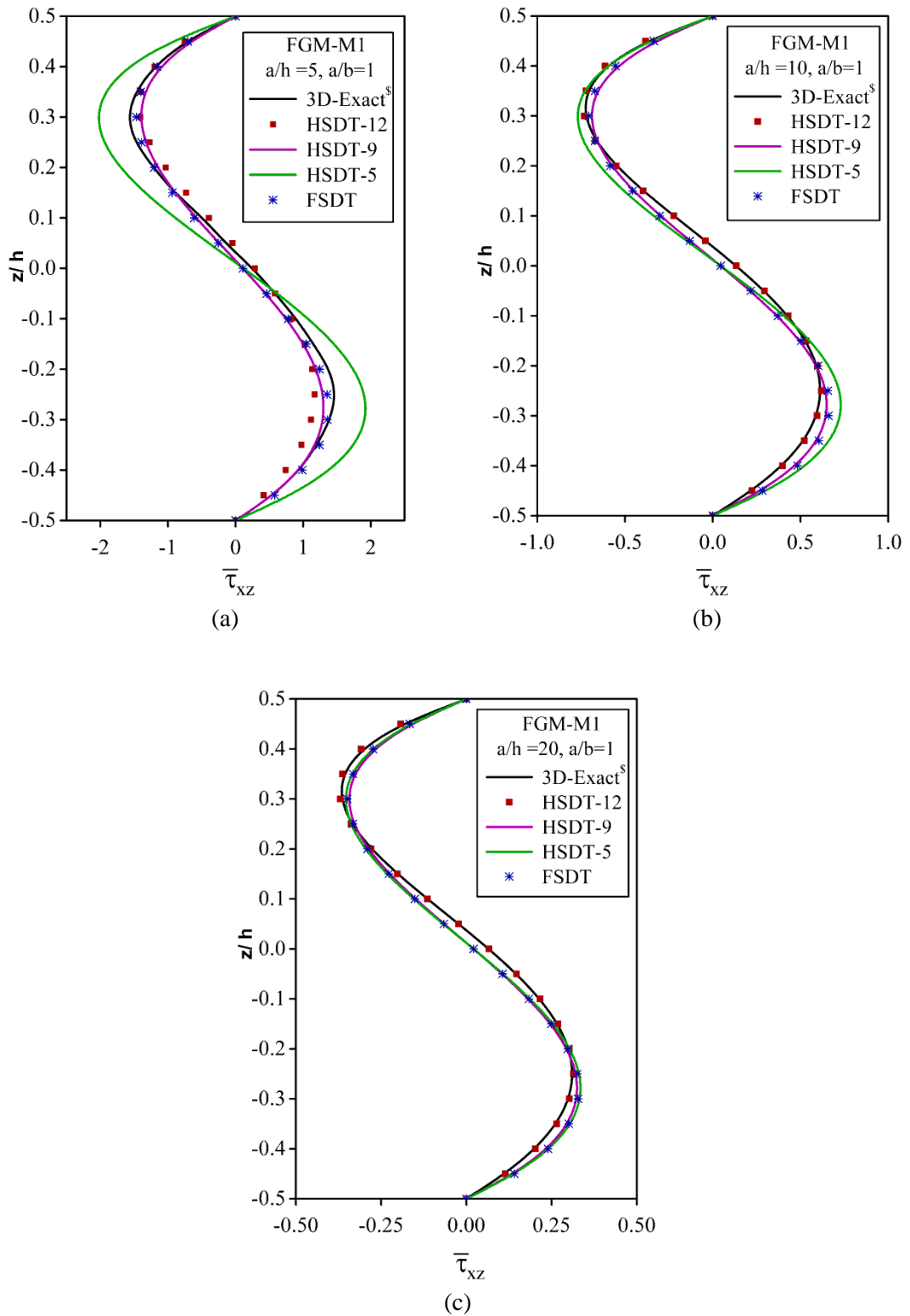


Fig. 5.6. Variation of nondimensionalized transverse shear stress ($\bar{\tau}_{xz}$) through the thickness (z/h) of a simply supported square Monel-Zirconia (M1) FGM plate subjected to nonlinear thermal load for (a) $a/h = 5$, (b) $a/h = 10$ and (c) $a/h = 20$. [^sAlibeigloo, A. (2010)]

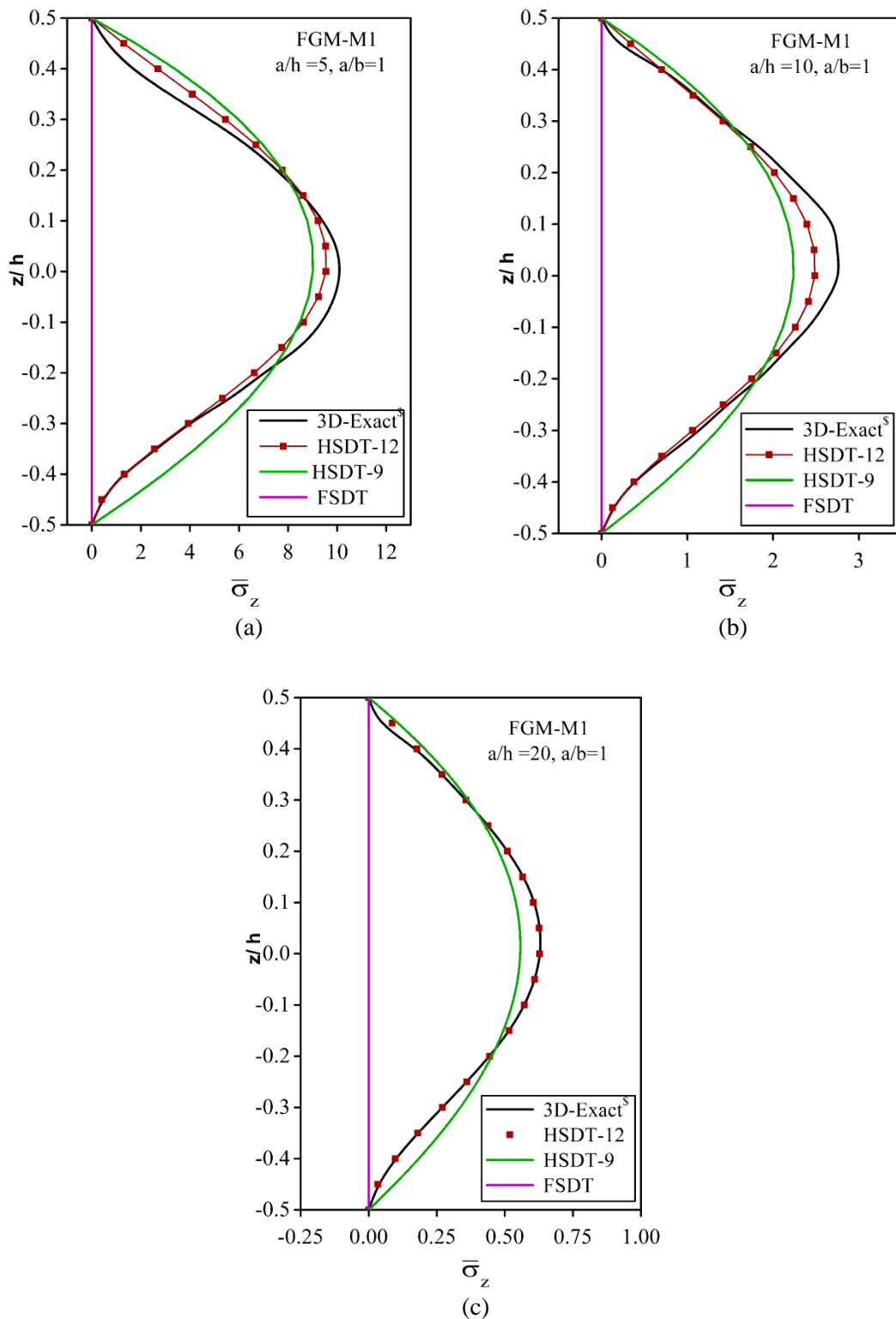


Fig. 5.7. Variation of nondimensionalized transverse normal stress ($\bar{\sigma}_z$) through the thickness (z/h) of a simply supported square Monel-Zirconia (M1) FGM plate subjected to nonlinear thermal load for (a) $a/h = 5$, (b) $a/h = 10$ and (c) $a/h = 20$. [^sAlibeigloo, A. (2010)]

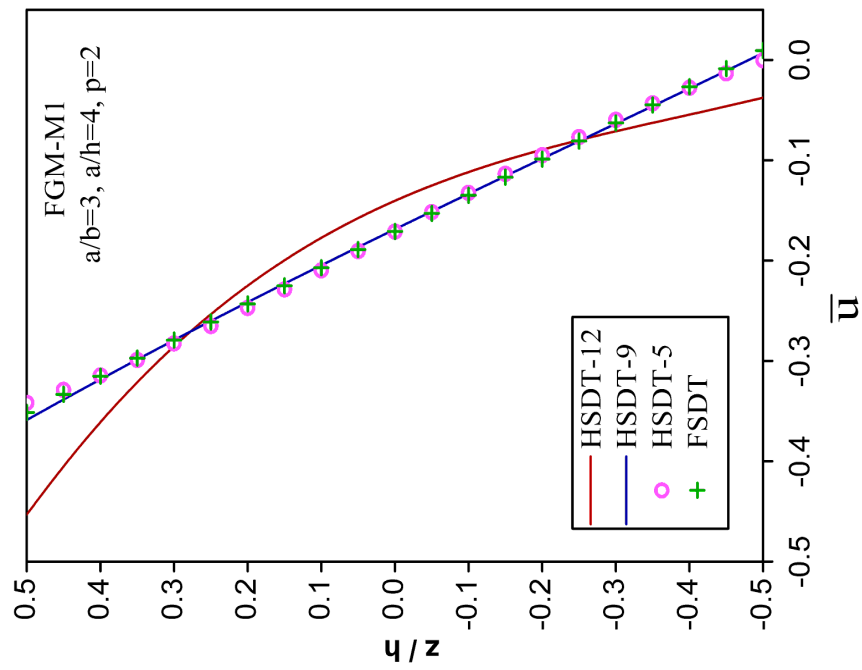


Fig. 5.8. Variation of nondimensionalized in-plane displacement (\bar{u}) through the thickness (z/h) of a simply supported rectangular Monel-Zirconia (M1) FGM plate subjected to nonlinear (T_{NL}) thermal load

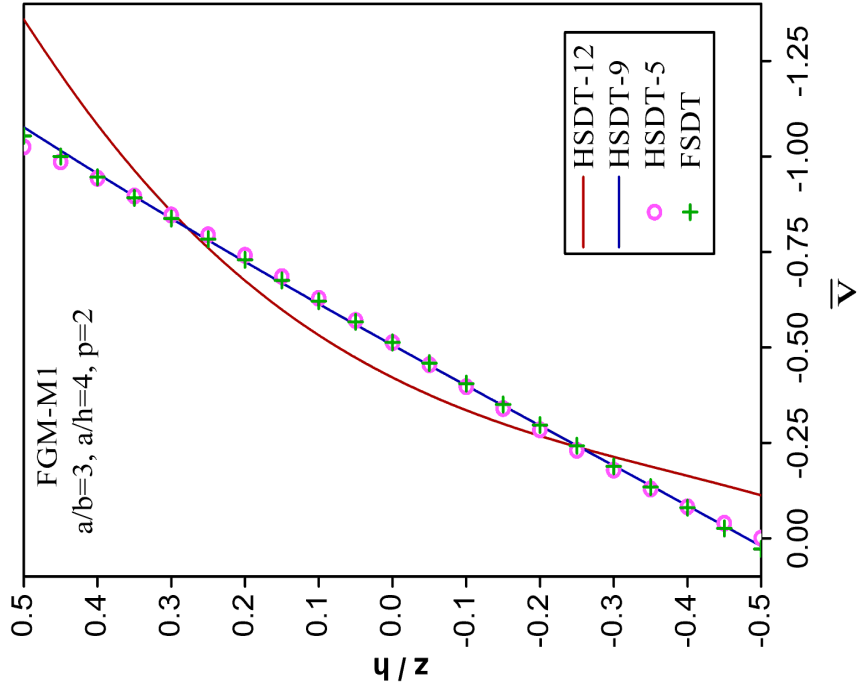


Fig. 5.9. Variation of nondimensionalized in-plane displacement (\bar{v}) through the thickness (z/h) of a simply supported rectangular Monel-Zirconia (M1) FGM plate subjected to nonlinear (T_{NL}) thermal load

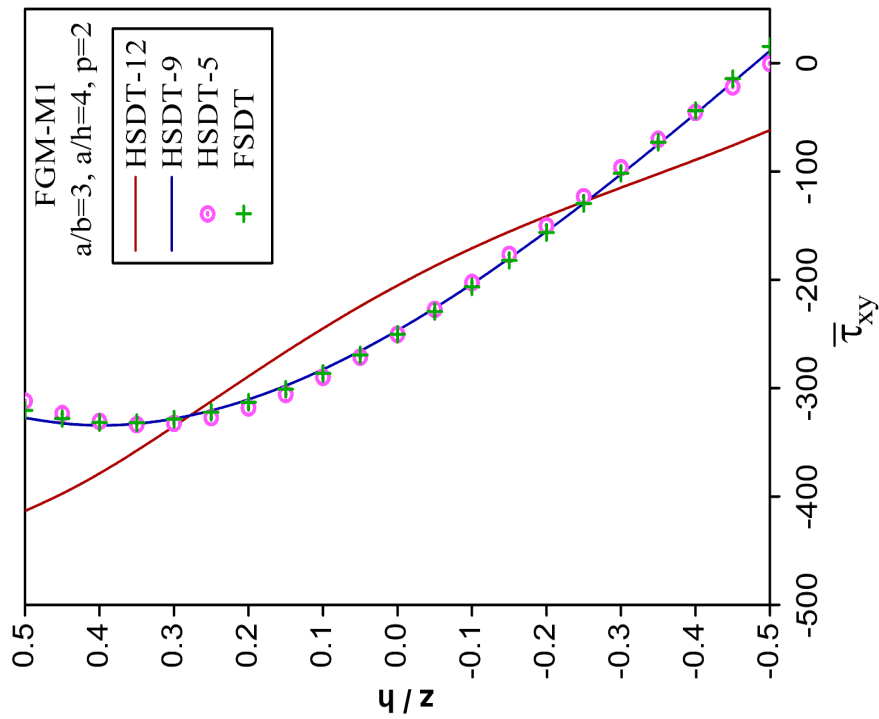


Fig. 5.10. Variation of nondimensionalized transverse displacement (\bar{w}) through the thickness (z/h) of a simply supported rectangular Monel-Zirconia (M1) FGM plate subjected to nonlinear (T_{NL}) thermal load

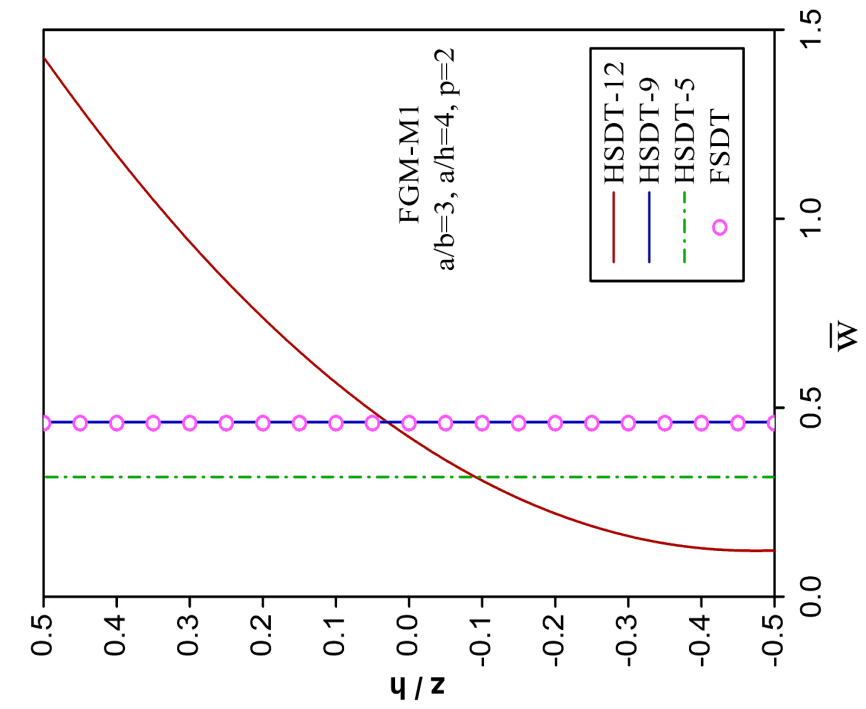


Fig. 5.11. Variation of nondimensionalized in-plane shear stress ($\bar{\tau}_{xy}$) through the thickness (z/h) of a simply supported rectangular Monel-Zirconia (M1) FGM plate subjected to nonlinear (T_{NL}) thermal load

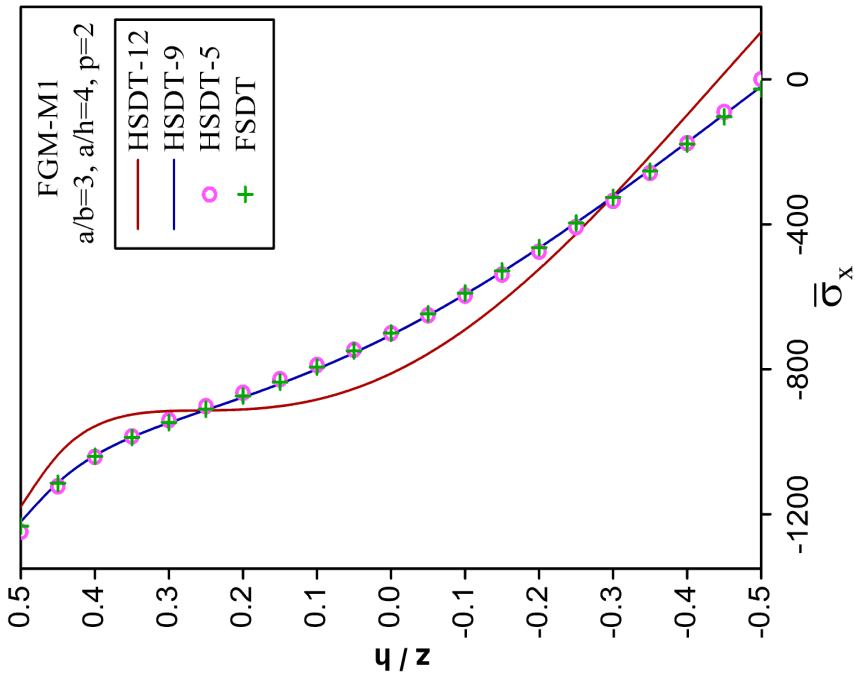


Fig. 5.12. Variation of nondimensionalized in-plane normal stress ($\bar{\sigma}_x$) through the thickness (z/h) of a simply supported rectangular Monel-Zirconia (M1) FGM plate subjected to nonlinear (T_{NL}) thermal load

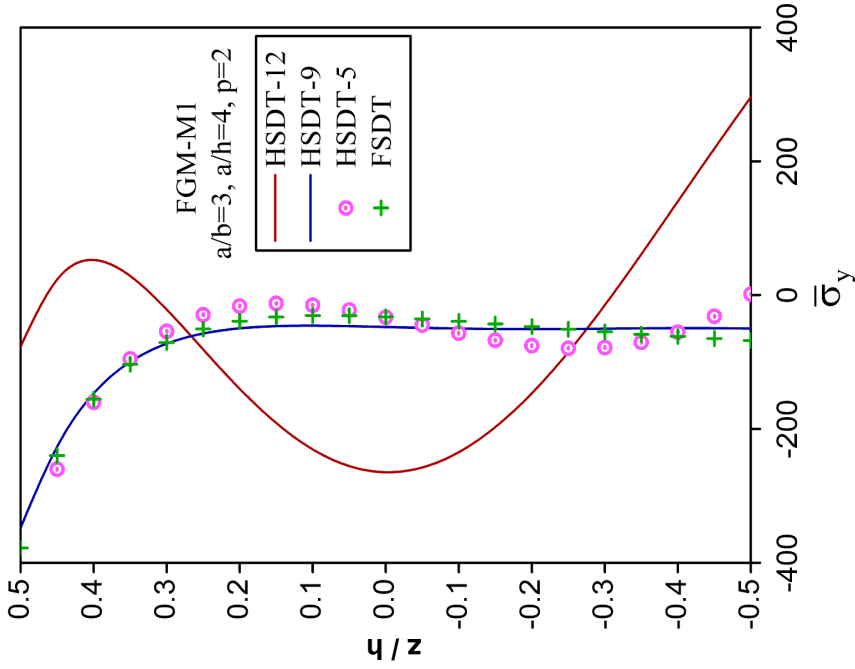


Fig. 5.13. Variation of nondimensionalized in-plane normal stress ($\bar{\sigma}_y$) through the thickness (z/h) of a simply supported rectangular Monel-Zirconia (M1) FGM plate subjected to nonlinear (T_{NL}) thermal load

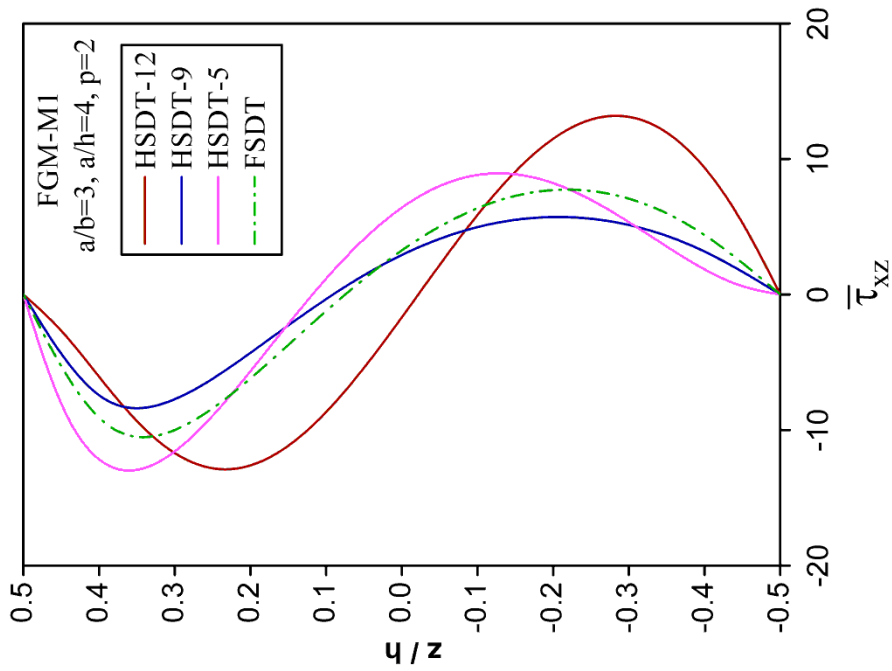


Fig. 5.14. Variation of nondimensionalized transverse shear stress ($\bar{\tau}_{xz}$) through the thickness (z/h) of a simply supported rectangular Monel-Zirconia (M1) FGM plate subjected to nonlinear (T_{NL}) thermal load

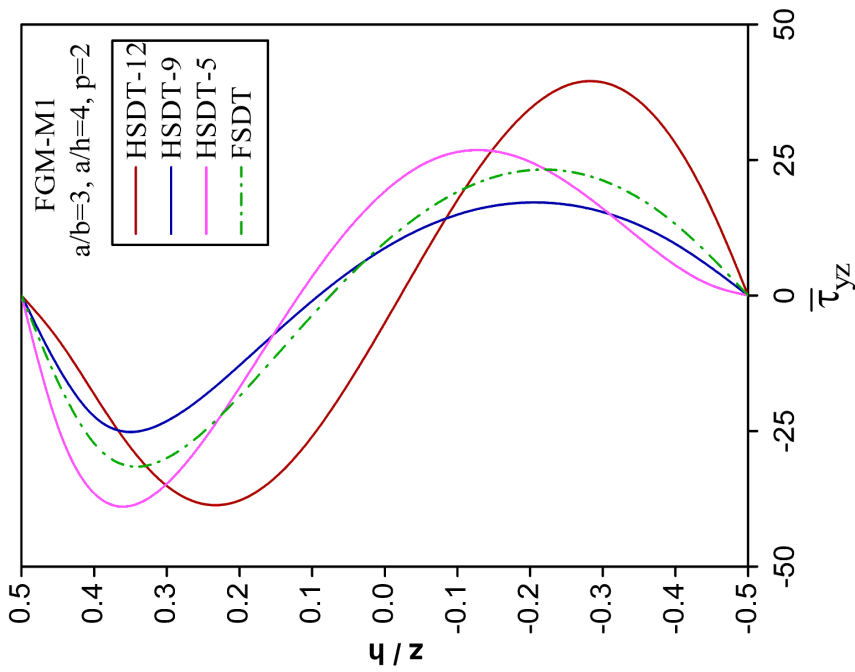


Fig. 5.15. Variation of nondimensionalized transverse shear stress ($\bar{\tau}_{yz}$) through the thickness (z/h) of a simply supported rectangular Monel-Zirconia (M1) FGM plate subjected to nonlinear (T_{NL}) thermal load

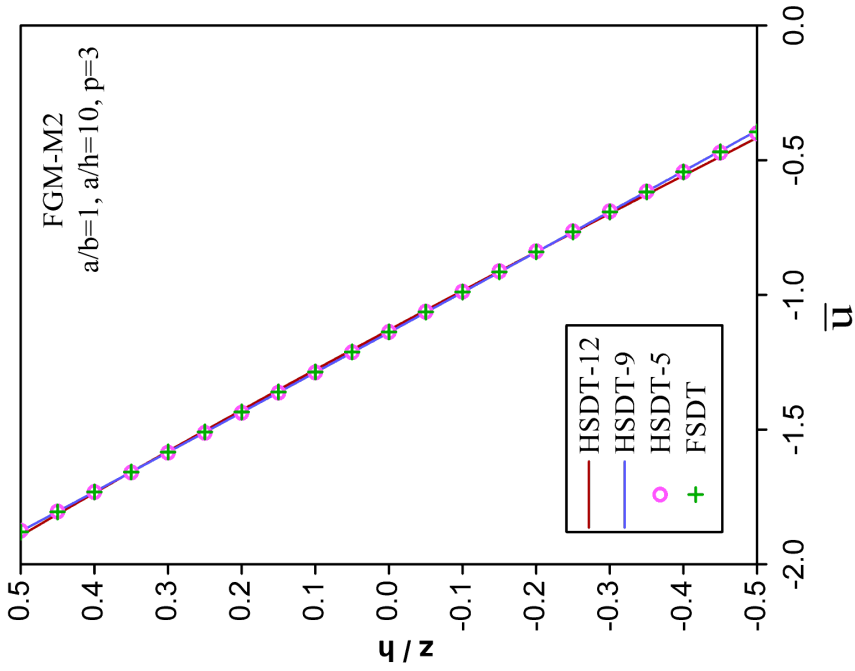


Fig. 5.16. Variation of nondimensionalized in-plane displacement (\bar{u}) through the thickness (z/h) of a simply supported square Aluminium-Alumina (M2) FGM plate subjected to nonlinear (T_{NL}) thermal load.

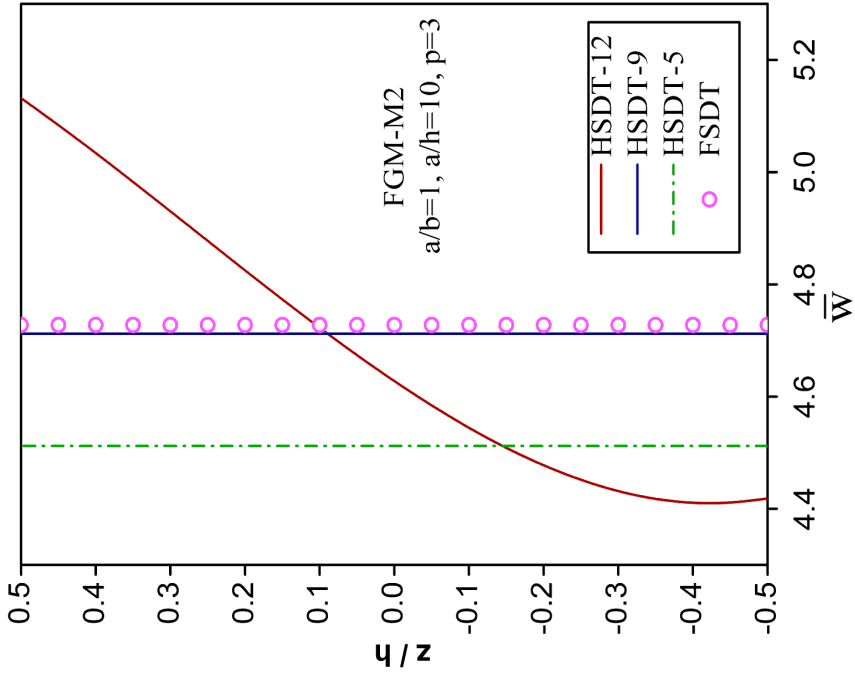


Fig. 5.17. Variation of nondimensionalized transverse displacement (\bar{w}) through the thickness (z/h) of a simply supported square Aluminium-Alumina (M2) FGM plate subjected to nonlinear (T_{NL}) thermal load.

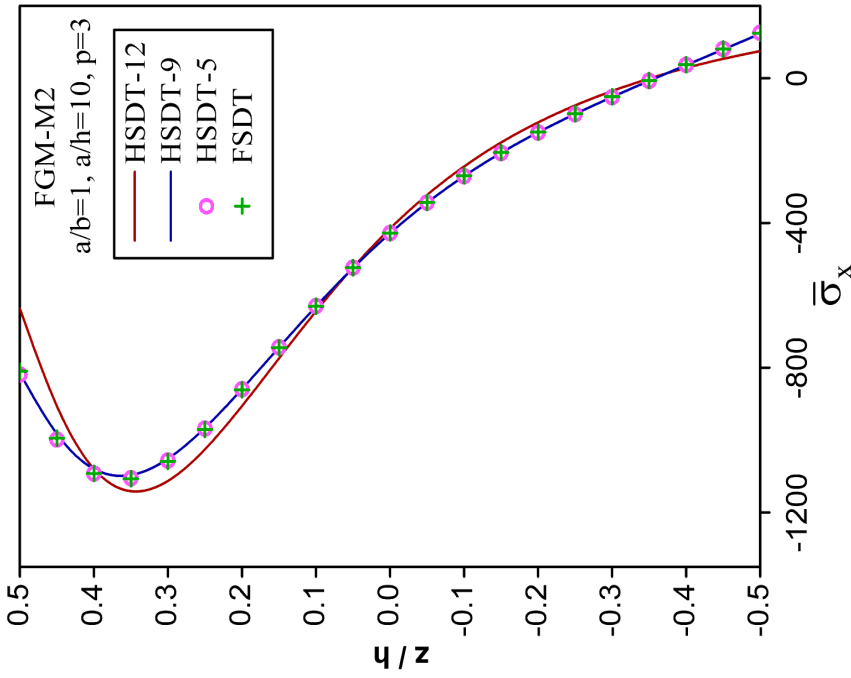


Fig. 5.18. Variation of nondimensionalized in-plane normal stress ($\bar{\sigma}_x$) through the thickness (z/h) of a simply supported square Aluminium-Alumina (M2) FGM plate subjected to nonlinear (T_{NL}) thermal load.

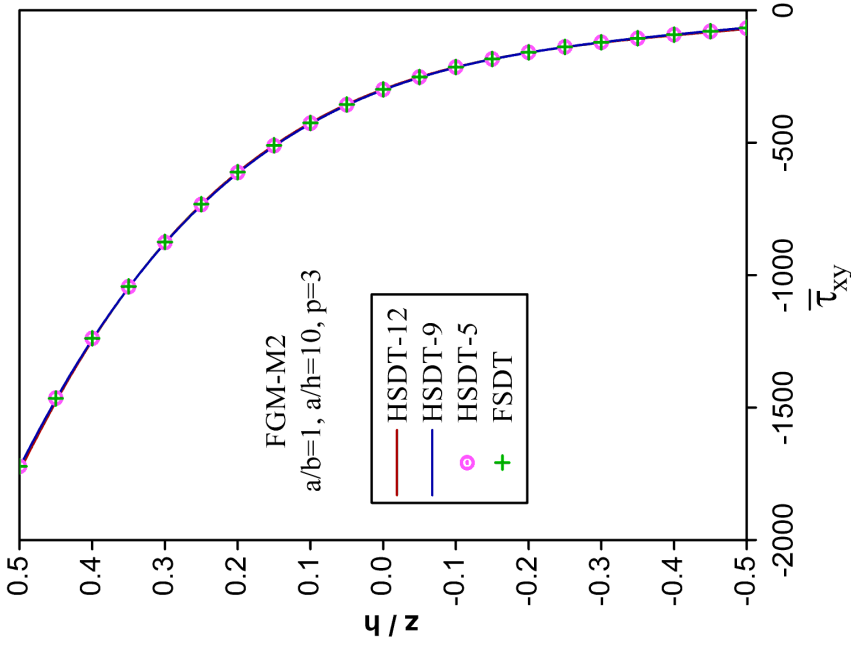


Fig. 5.19. Variation of nondimensionalized in-plane shear stress ($\bar{\tau}_{xy}$) through the thickness (z/h) of a simply supported square Aluminium-Alumina (M2) FGM plate subjected to nonlinear (T_{NL}) thermal load.

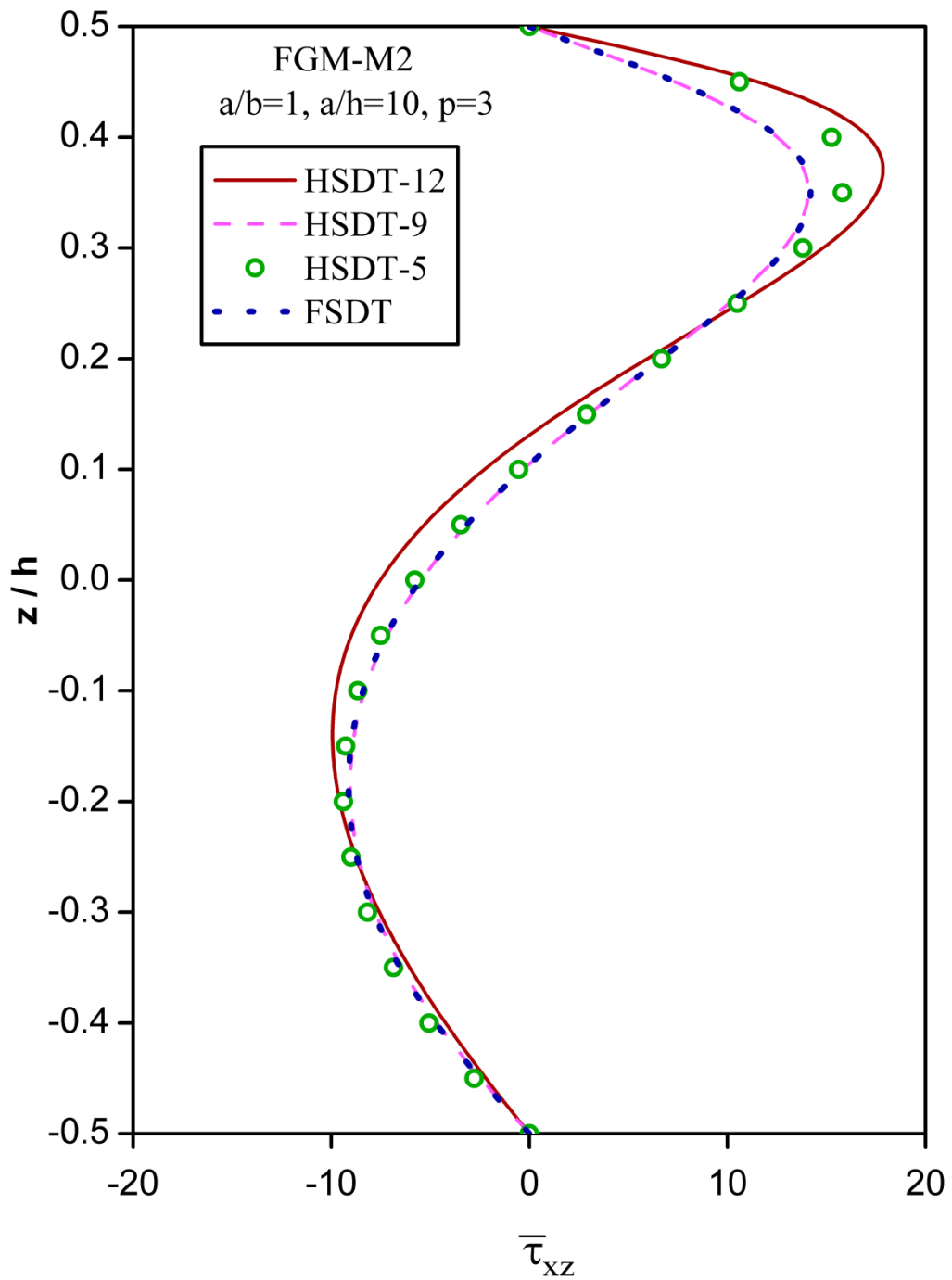


Fig. 5.20. Variation of nondimensionalized transverse shear stress ($\bar{\tau}_{xz}$) through the thickness (z/h) of a simply supported square Aluminium-Alumina (M2) FGM plate subjected to nonlinear (T_{NL}) thermal load.

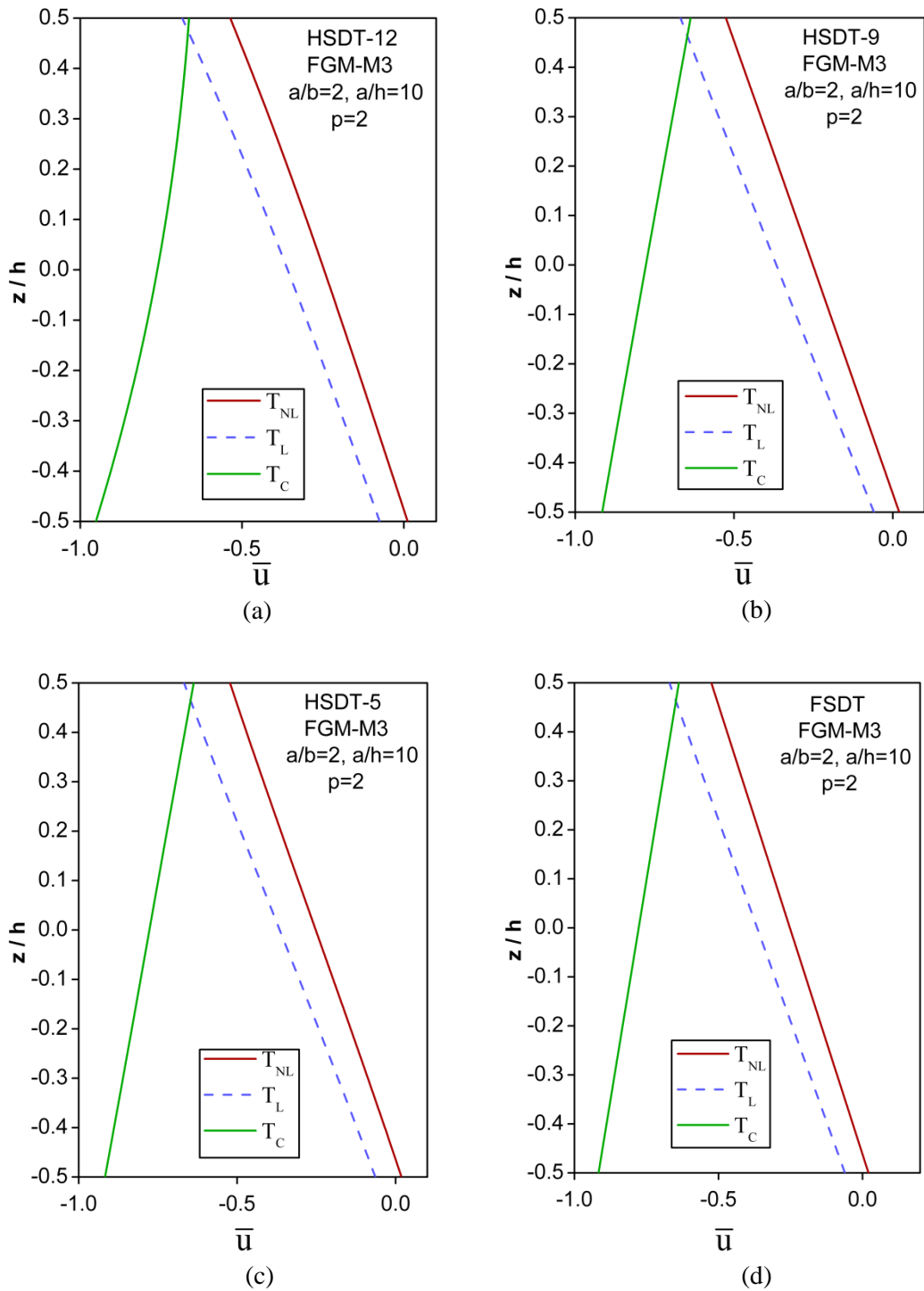


Fig. 5.21. Variation of nondimensionalized in-plane displacement (\bar{u}) through the thickness (z/h) of a simply supported rectangular Titanium Alloy-Zirconia (M3) FGM plate subjected to nonlinear (T_{NL}), linear (T_L) and constant (T_C) thermal loads based on (a) HSDT-12, (b) HSDT-9, (c) HSDT-5 and (d) FSDT displacement models.

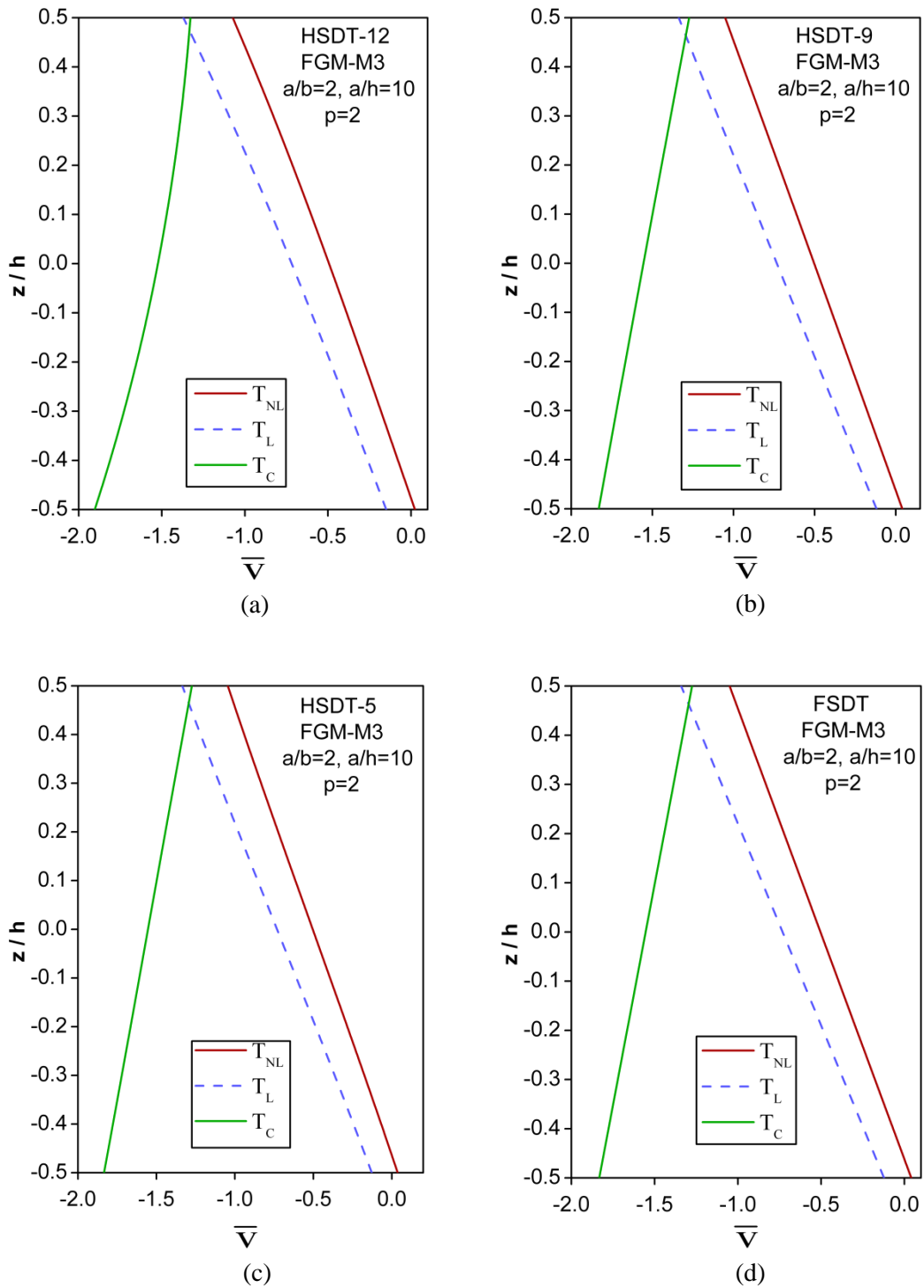


Fig. 5.22. Variation of nondimensionalized in-plane displacement (\bar{v}) through the thickness (z/h) of a simply supported rectangular Titanium Alloy-Zirconia (M3) FGM plate subjected to nonlinear (T_{NL}), linear (T_L) and constant (T_C) thermal loads based on (a) HSDT-12, (b) HSDT-9, (c) HSDT-5 and (d) FSDT displacement models.

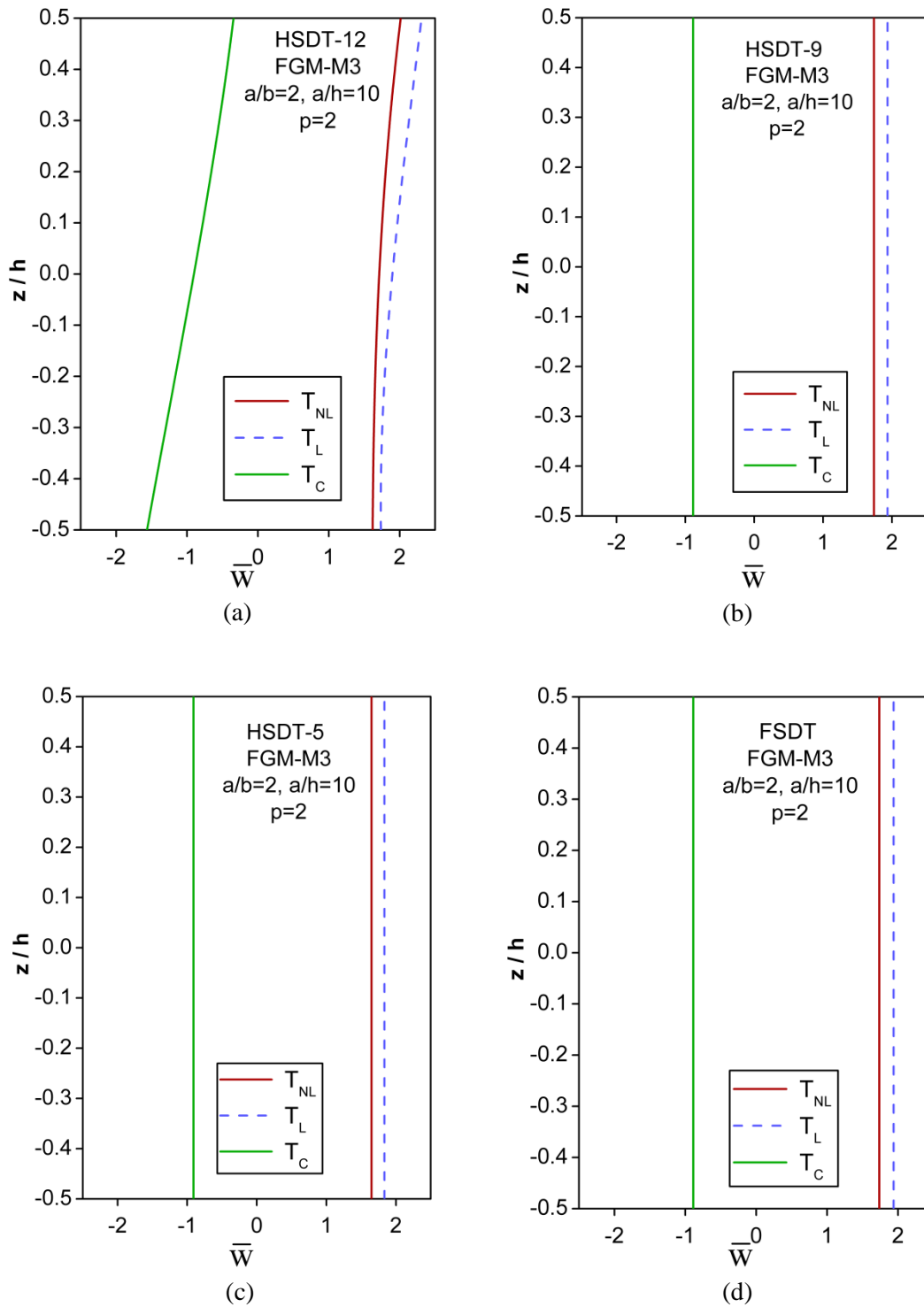


Fig. 5.23. Variation of nondimensionalized transverse displacement (\bar{w}) through the thickness (z/h) of a simply supported rectangular Titanium Alloy-Zirconia (M3) FGM plate subjected to nonlinear (T_{NL}), linear (T_L) and constant (T_C) thermal loads based on (a) HSDT-12, (b) HSDT-9, (c) HSDT-5 and (d) FSDT displacement models.

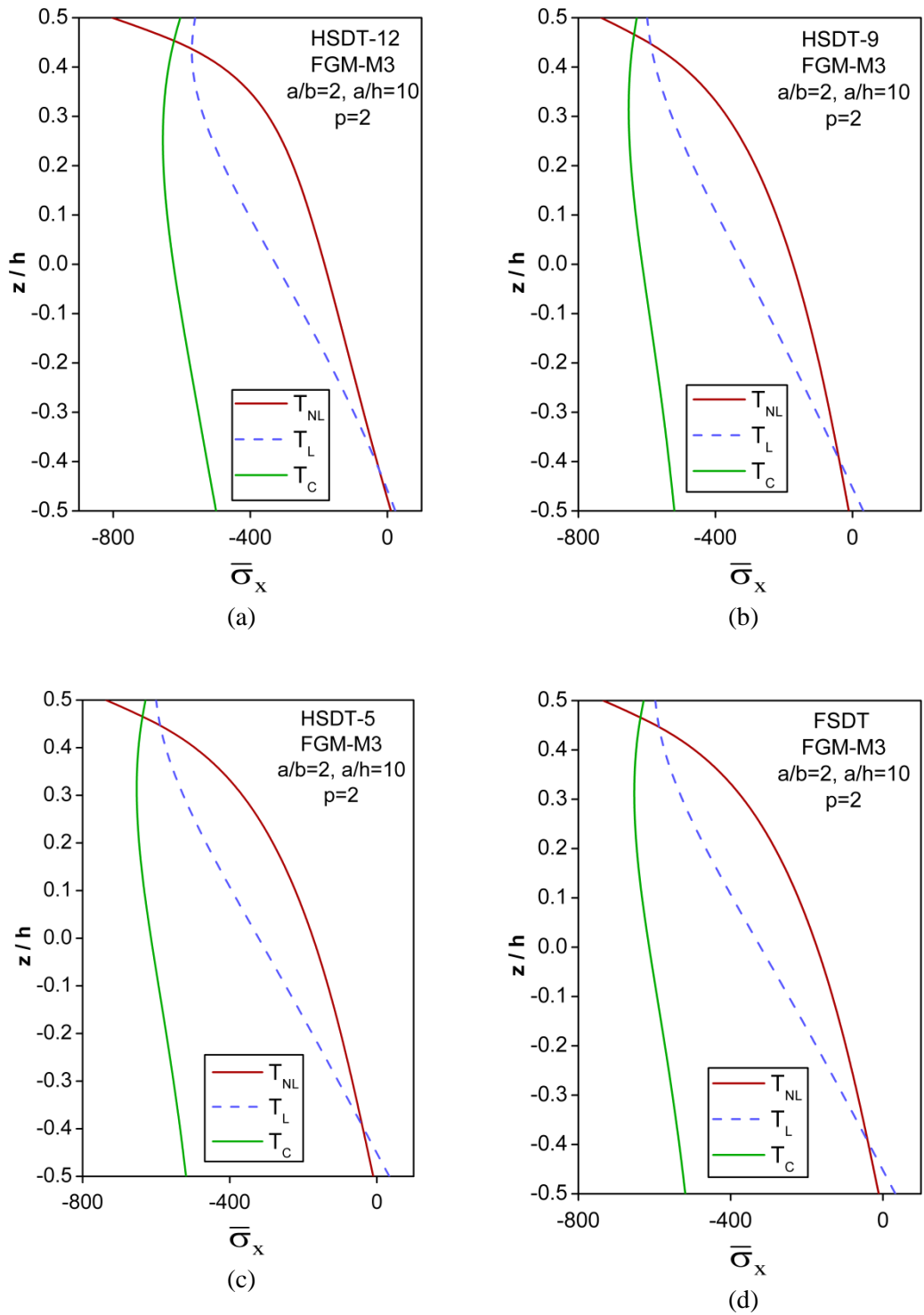


Fig. 5.24. Variation of nondimensionalized in-plane normal stress ($\bar{\sigma}_x$) through the thickness (z/h) of a simply supported rectangular Titanium Alloy-Zirconia (M3) FGM plate subjected to nonlinear (T_{NL}), linear (T_L) and constant (T_C) thermal loads based on (a) HSDT-12, (b) HSDT-9, (c) HSDT-5 and (d) FSDT displacement models.

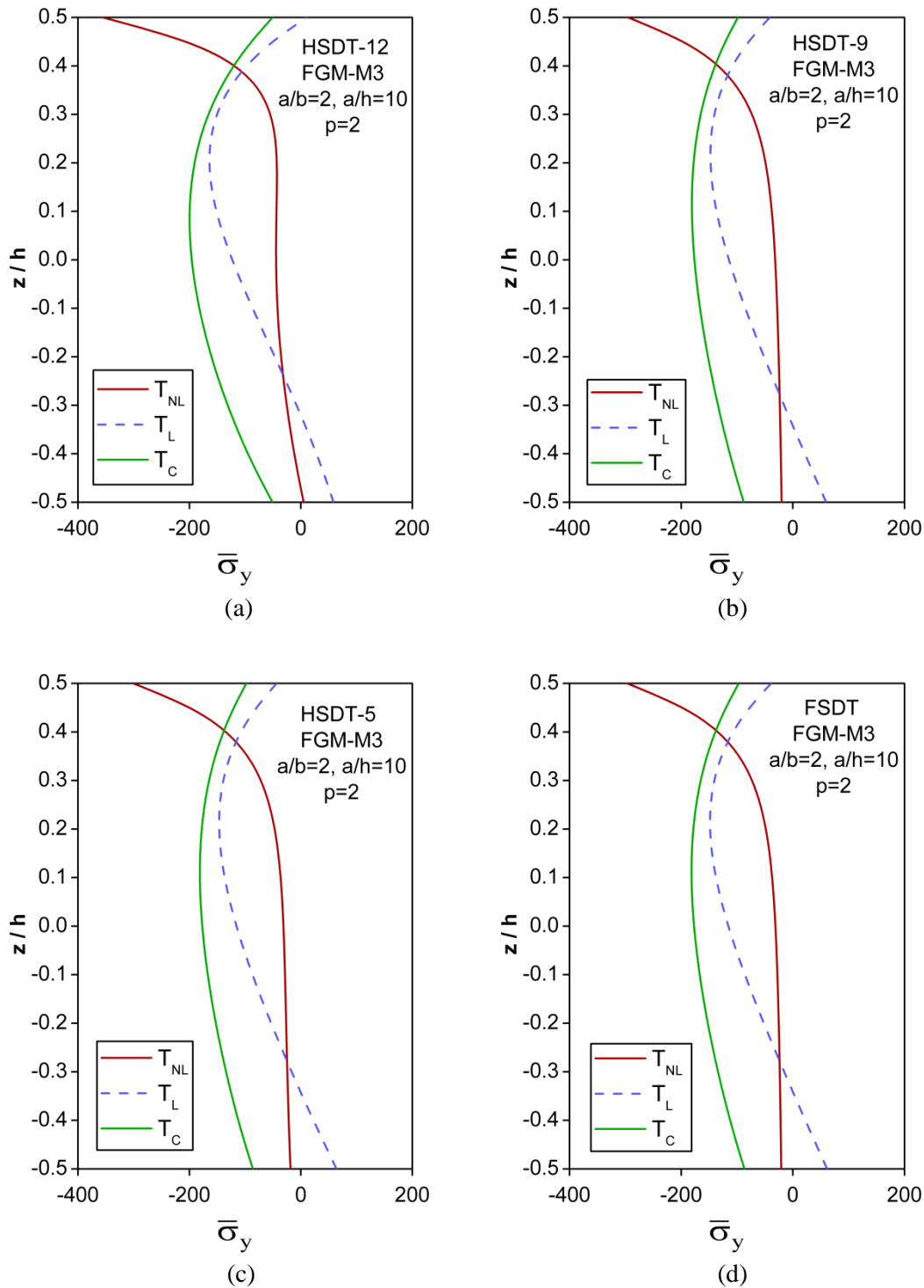


Fig. 5.25. Variation of nondimensionalized in-plane normal stress ($\bar{\sigma}_y$) through the thickness (z/h) of a simply supported rectangular Titanium Alloy-Zirconia (M3) FGM plate subjected to nonlinear (T_{NL}), linear (T_L) and constant (T_C) thermal loads based on (a) HSDT-12, (b) HSDT-9, (c) HSDT-5 and (d) FSDT displacement models.

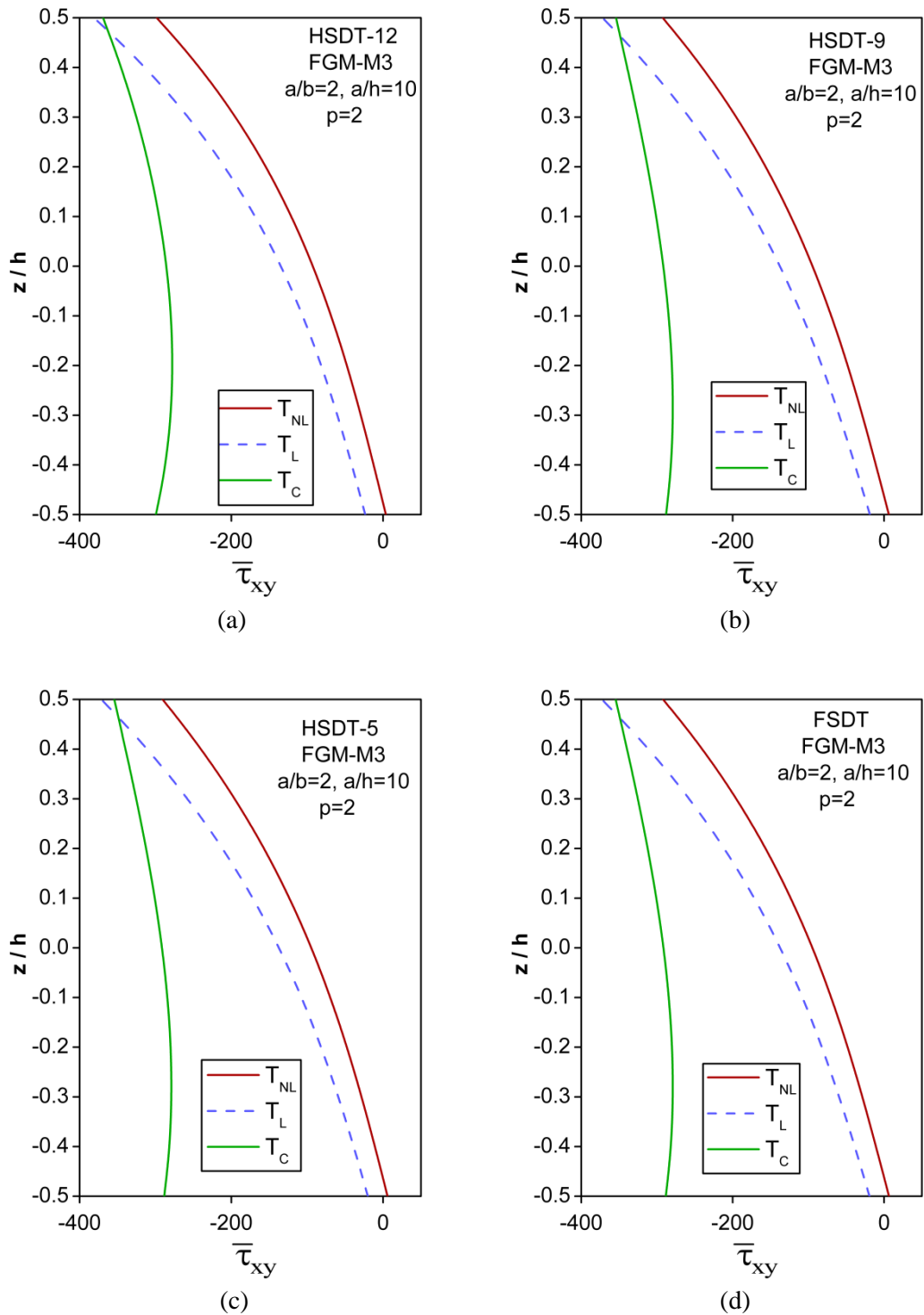


Fig. 5.26. Variation of nondimensionalized in-plane shear stress ($\bar{\tau}_{xy}$) through the thickness (z/h) of a simply supported rectangular Titanium Alloy-Zirconia (M3) FGM plate subjected to nonlinear (T_{NL}), linear (T_L) and constant (T_C) thermal loads based on (a) HSDT-12, (b) HSDT-9, (c) HSDT-5 and (d) FSDT displacement models.

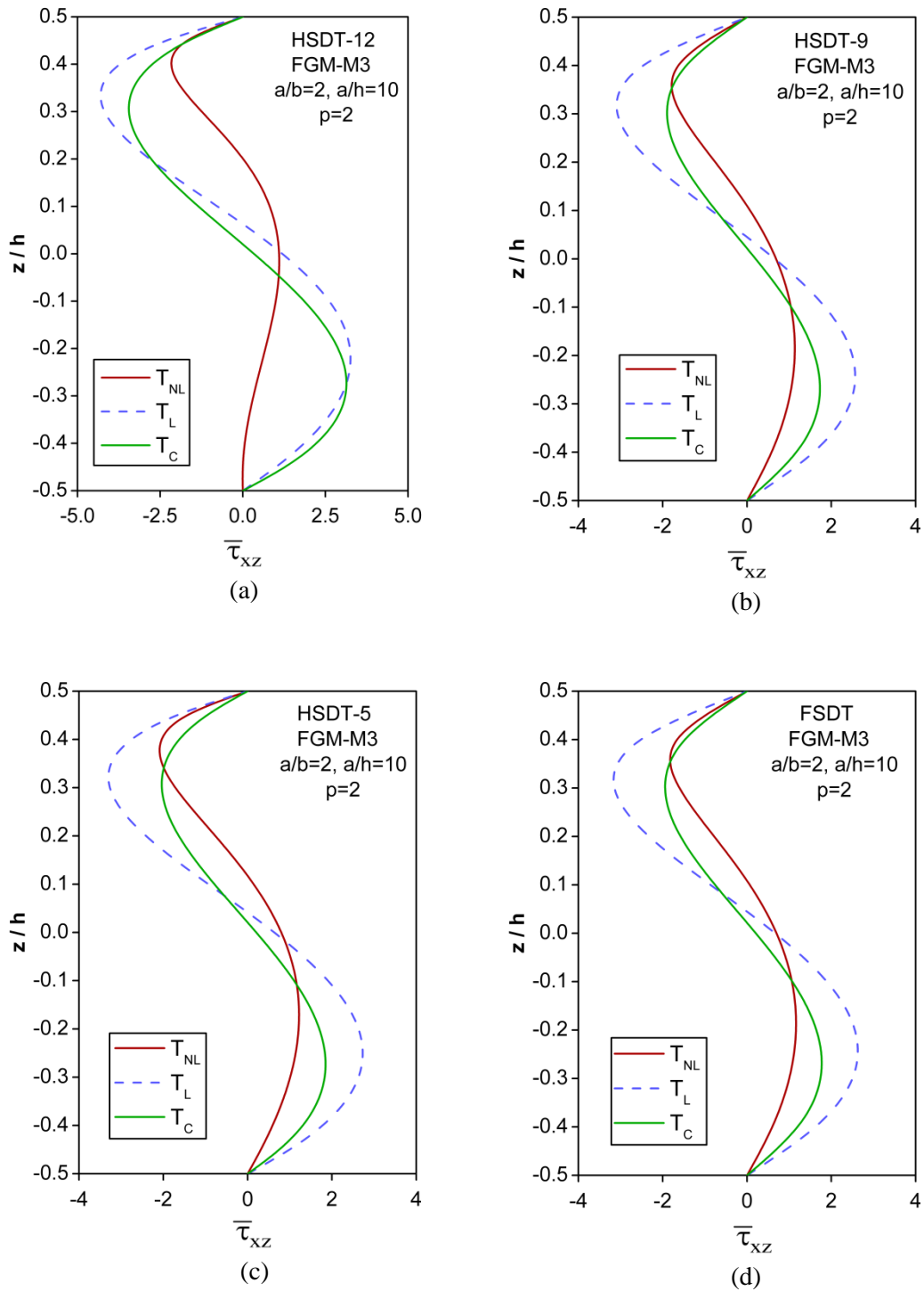


Fig. 5.27. Variation of nondimensionalized transverse shear stress ($\bar{\tau}_{xz}$) through the thickness (z/h) of a simply supported rectangular Titanium Alloy-Zirconia (M3) FGM plate subjected to nonlinear (T_{NL}), linear (T_L) and constant (T_C) thermal loads based on (a) HSDT-12, (b) HSDT-9, (c) HSDT-5 and (d) FSDT displacement models.

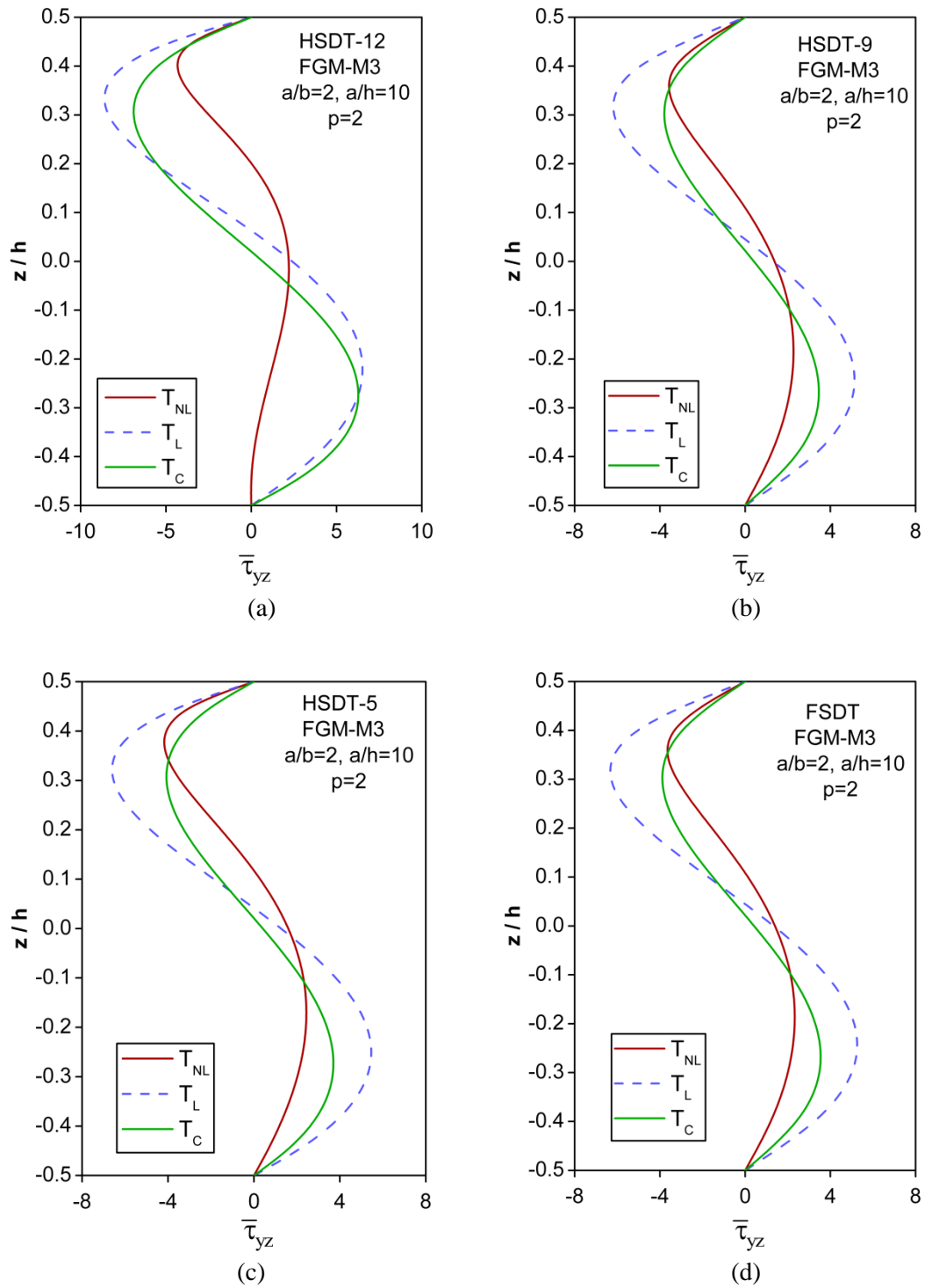


Fig. 5.28. Variation of nondimensionalized transverse shear stress ($\bar{\tau}_{yz}$) through the thickness (z/h) of a simply supported rectangular Titanium Alloy-Zirconia (M3) FGM plate subjected to nonlinear (T_{NL}), linear (T_L) and constant (T_C) thermal loads based on (a) HSDT-12, (b) HSDT-9, (c) HSDT-5 and (d) FSDT displacement models.

CHAPTER 6

CONCLUSION

6.1 GENERAL

Analytical formulations and solutions using a set of higher-order refined shear deformation theories have been developed for the stress analysis of FGM plates subjected to thermal loads. These theories consider the realistic parabolic distribution of transverse shear strain across the plate thickness direction. The displacement model with twelve degrees-of-freedom HSDT-12 considers the effects of both transverse shear and normal stress/strain, while the other models include only the effects of transverse shear deformation. The accuracy of the higher-order refined theories in predicting the displacements and stresses is established by comparing the results with the available 3D-Exact solutions in the literature. After establishing the accuracy, numerical results are also compared with the results obtained by independently developing the theoretical formulations and analytical solutions using the other higher order and first order theory available in the literature to show the improvement in the accuracy of higher-order refined theories in predicting the thermo-elastic responses in an FGM plate. The accuracy of solutions obtained using nonlinear temperature distribution with various displacement models, is evaluated by comparing with the results obtained using other temperature distributions viz., linear and constant profiles, to show the improvement in the accuracy of solutions using nonlinear temperature distribution with various theories.

On the basis of the analysis carried out and the numerical results obtained, the following conclusions are arrived

- For FGM plates subjected to mechanical load, the various static-flexural responses predicted by HSDT-12 model are found to be most accurate as compared to other displacement models used in this investigation and is less than 2.5% for all parameters considered. This reveals the significance of

considering both transverse shear and normal deformation effects in analysis of FGM plates.

- In cases of FGM plates subjected to thermal loads, the transverse stresses and transverse displacement predicted by HSDT-12 model are as accurate as three dimensional exact solutions while other models under predicts the transverse normal stress and over-predicts the transverse shear stresses. This clearly shows the need for using higher order polynomials in the in-plane and transverse displacement fields to achieve the desired accuracy in the thermo-elastic analysis of FGM plates.
- The accuracy of solutions is found to decrease with the decrease in the total number of functional degrees of freedom. Therefore there is a large deviation of the displacements and stress values predicted by HSDT-9, HSDT-5 and FSDT models compared to that HSDT-12. Comparatively least difference is observed in the values predicted by HSDT-9 displacement model.
- Considerable difference is observed in displacements and stresses predicted by HSDT-12 and all other models. The percentage difference in values predicted by the other models increases with the increase in power law parameter and edge ratio (a/b ratio), while decreases with the increase in a/h ratio as compared with HSDT-12 model.
- Maximum percentage difference is observed in rectangular plate and the least percentage difference in square plates. The percentage difference increases with increase in a/b ratio. Also, for FGM thin plates with a/h ratio 50 and above, the results predicted by all the models are almost same.
- Though the values of in-plane displacements \bar{u} and \bar{v} are different, their percentage differences remain same for all parameters. Similarly equal differences are observed in the values of transverse shear stresses $\bar{\tau}_{xz}$ and $\bar{\tau}_{yz}$.
- In all the displacement models considered for the analysis of FGM plates, as the thickness of the plate decreases the values of transverse deflection increases but the percentage difference between the values decreases. This

shows that the effect of transverse shear and normal strains in predicting the deflection and stresses reduces in thin plates.

- In most of the cases considered the maximum percentage difference in the displacements and stresses are observed in Monel-Zirconia FGM plate and the least percentage difference in Titanium Alloy-Zirconia FGM plates. This indicates that FGM plate responses are sensitive to thermo-physical properties.
- For any given displacement model and the material set, the thermal responses predicted using nonlinear, linear and constant forms of temperature distributions are found to be very much different from each other. This shows the need for adopting an appropriate temperature field that can predict most accurate thermal responses.
- In case of thin plates, the differences in the results predicted by various models are almost same, but significant differences are observed when different temperature distributions are adopted for the same model during the analysis. This shows that the type of thermal field adopted during the analysis has its effect in both thin and thick plates.
- The displacements and stresses predicted using nonlinear form of temperature distribution are as accurate as three dimensional elasticity solutions when used with HSDT-12 model. The accuracy of solutions reduces with other lower order displacement models. Further the percentage difference in results increases when the same plate is subjected to other form of temperature profile namely linear or constant type of variation across the thickness.
- The variation of in-plane / transverse displacements and stresses plotted across the plate thickness using all the temperature profiles clearly indicates that results obtained using linear and constant temperature profile are very much different from those of nonlinear temperature distribution for all the models considered. Remarkable differences are noticed in the distribution pattern also. Among various models considered, maximum deviation is observed in FSDT models.

6.2 SUGGESTIONS FOR FUTURE WORK

- In the present investigation only the stress analysis of FGM plates subjected to thermal loads has been carried out. Further studies can be extended for the development of formulations and solutions for thermal vibration and thermal buckling analyses of FGM plates using various displacement models.
- The analysis carried out here is for plates subjected to thermal loads only. Other combination of loads such as thermomechanical, hygro-thermal, thermo-peizo-electric, hygro-thermo-mechanical can also be incorporated to study static, free vibration and stability analyses of FGM plates using different theories.
- Static analysis is carried out in the present investigation. The work can be extended towards developing formulations for transient analysis of flat panels.
- The plate geometry considered here is a flat panel. However, further formulations can be developed for thermally loaded curved panels and comparative studies can be carried out.
- Only plates with simply supported boundary conditions are considered in the present investigation. Analytical formulations and solutions can be developed for thermally stressed FGM plates with different combinations of boundary conditions.
- The analytical model developed in the present investigation for HSDT-12 displacement model can be used for developing formulations and solutions using numerical methods like Finite Element Methods (FEM) and Meshless methods.

REFERENCE

- Aboudi, J., Arnold, S. M. and Pindera, M. J. (1994a). "Response of functionally graded composites to thermal gradients." *Composites Engineering*, 4(1), 1–18.
- Aboudi, J., Pindera, M. J. and Arnold, S. M. (1994b). "Elastic response of metal matrix composites with tailored microstructures to thermal gradients." *International Journal of Solids and Structures*, 31(10), 1393–1428.
- Aboudi, J., Pindera, M. J. and Arnold, S. M. (1995a). "A coupled higher-order theory for functionally graded composites with partial homogenization." *Composites Engineering*, 5(7), 771–92.
- Aboudi, J., Pindera, M. J. and Arnold, S. M. (1995b). "Thermo-inelastic response of functionally graded composites." *International Journal of Solids and Structures*, 32(12), 1675–1710.
- Aboudi, J., Pindera, M. J. and Arnold, S. M. (1996). "Thermoelastic theory for the response of materials functionally graded in two directions." *International Journal of Solids and Structures*, 33(7), 931–66.
- Alibeigloo, A. (2010). "Exact solution for thermo-elastic response of functionally graded rectangular plates." *Composite Structures*, 92(1), 113–21.
- Alibeigloo, A. (2012). "Three-dimensional semi-analytical thermo-elasticity solution for a functionally graded solid and an annular circular plate." *Journal of Thermal Stresses*, 35(8), 653–76.
- Alibeigloo, A. (2016). "Thermo elasticity solution of sandwich circular plate with functionally graded core using generalized differential quadrature method." *Composite Structures*, 136, 229–40.
- Apalak, M. K. and Gunes, R. (2005). "Thermal residual stress analysis of Ni-Al₂O₃, Ni-TiO₂, and Ti-SiC functionally graded composite plates subjected to various thermal fields." *Journal of Thermoplastic Composite Materials*, 18(2), 119–52.
- Behravan, R. A. (2015). "Thermo-elastic analysis of functionally graded circular plates resting on a gradient hybrid foundation." *Applied Mathematics and Computation*, 256, 276–98.
- Behravan, R. A. and Shariyat M. (2016). "Thermo-magneto-elasticity analysis of variable thickness annular FGM plates with asymmetric shear and normal loads and non-uniform elastic foundations" *Archives of Civil and Mechanical Engineering*, 16(3), 448–66.
- Bhandari, M. and Purohit, K. (2015). "Response of functionally graded material plate under thermomechanical load subjected to various boundary conditions." *International Journal of Metals*, 2015, 1–16.
- Bouchafa, A., Benzair, A., Tounsi, A., Draiche, Kada, D., Ismail M. and Bedia, E. A. A. (2010). "Analytical modelling of thermal residual stresses in exponential functionally graded material system." *Materials and Design*, 31(1), 560–63.

- Bouderba, B., Mohammed S. A. H. and Tounsi, A. (2013). “Thermomechanical bending response of FGM thick plates resting on winkler–pasternak elastic foundations.” *Steel and composite structures*, 14(1), 85–104.
- Brischetto, S., Leetsch, R., Carrera, E., Wallmersperger, T. and Kroplin, B. (2008). “Thermo-mechanical bending of functionally graded plates.” *Journal of Thermal Stresses*, 31(3), 286–308.
- Bui, T. Q., Do, T. V., Ton, L. H. T., Doan, D. H., Tanaka, S., Pham, D.T., Nguyen-Van T., Yu, T. and Hirose, S. (2016). “On the high temperature mechanical behaviors analysis of heated functionally graded plates using FEM and a new third-order shear deformation plate theory.” *Composites Part B: Engineering*, 92, 218–41.
- Burlayenko, V. N., Altenbach, H., Sadowski, T. and Dimitrova, S.D. (2016). “Computational simulations of thermal shock cracking by the virtual crack closure technique in a functionally graded plate.” *Computational Materials Science*, 116, 11–21.
- Burlayenko, V. N., Altenbach, H., Sadowski, T., Dimitrova, S. D. and Bhaskar, A. (2017). “Modelling functionally graded materials in heat transfer and thermal stress analysis by means of graded finite elements.” *Applied Mathematical Modelling*; 45, 422–38.
- Cheng, Z. Q. and Batra, R. C. (2000). “Three-dimensional thermoelastic deformations of a functionally graded elliptic plate.” *Composites Part B: Engineering*, 31(2), 97–106.
- Cho, J. R., and Oden, J. T. (2000). “Functionally graded material: A parametric study on thermal-stress characteristics using the crank–nicolson–galerkin scheme.” *Computer Methods in Applied Mechanics and Engineering*, 188(1-3), 17–38.
- Chung, Y. L. and Chang, H. X. (2008). “Mechanical behavior of rectangular plates with functionally graded coefficient of thermal expansion subjected to thermal loading.” *Journal of Thermal Stresses*, 31(4), 368–88.
- Dai, K. Y., Liu, G. R., Han, X. and Lim, K. M. (2005). “Thermomechanical analysis of functionally graded material (FGM) plates using element-free galerkin method.” *Computers & Structures*, 83(17-18), 1487–1502.
- Dym, C. L. and Shames, I. H. (1973). “Solid mechanics: A variational approach.” *McGraw-Hill*, New York.
- Dong, Y. H. and Li, Y. H. (2017). “A unified nonlinear analytical solution of bending, buckling and vibration for the temperature-dependent FG rectangular plates subjected to thermal load.” *Composite Structures*, 159, 689-701.
- Eshraghi, I., Dag, S. and Soltani, N. (2016). “Bending and free vibrations of functionally graded annular and circular micro-plates under thermal loading.” *Composite Structures*, 137, 196–207.
- Fahsi, B., Kaci A., Tounsi, A. and Bedia, E. A. A. (2012). “A four variable refined plate theory for nonlinear cylindrical bending analysis of functionally graded plates under thermomechanical loadings.” *Journal of Mechanical Science and Technology*, 26(12), 4073–79.

- Fallah, F. and Nosier, A. (2012). "Nonlinear behavior of functionally graded circular plates with various boundary supports under asymmetric thermo-mechanical loading." *Composite Structures*, 94(9), 2834–50.
- Fukui, Y., Yamanaka N. and Wakashima, K. (1993). "The stresses and strains in a thick-walled tube for functionally graded material under uniform thermal loading." *JSME International Journal. Series A, Mechanics and Material Engineering*, 36(2), 156–62.
- Golmakani, M. E. and Kadkhodayan, M. (2011). "Large deflection analysis of circular and annular FGM plates under thermo-mechanical loadings with temperature-dependent properties." *Composites Part B: Engineering*, 42(4), 614–25.
- Gulshan-Taj M. N. A., Anupam C. and Abdul H. S. (2013). "Analysis of functionally graded plates using higher order shear deformation theory." *Applied Mathematical Modelling*, 37(18-19), 8484–94.
- Hildebrand, F. B., Reissner, E. and Thomas, G. B. (1949). "Note on the foundations of the theory of small displacements of orthotropic shells." *NACA TN-1833*.
- Houari, M. S. A., Tounsi, A. and Beg O. A. (2013). "Thermoelastic bending analysis of functionally graded sandwich plates using a new higher order shear and normal deformation theory." *International Journal of Mechanical Sciences*, 76, 102–11.
- Jabbari, M., Shahryari, E., Haghghat, H. and Eslami, M.R. (2014). "An analytical solution for steady state three dimensional thermoelasticity of functionally graded circular plates due to axisymmetric loads." *European Journal of Mechanics A/Solids*, 47, 124–42.
- Jafarinezhad, M. R. and Eslami, M.R. (2017). "Coupled thermoelasticity of FGM annular plate under lateral thermal shock." *Composite Structures*, 168, 758-71.
- Jha, D. K., Kant, T. and Singh, R. K. (2013). "A critical review of recent research on functionally graded plates." *Composite Structures*, 96, 833–849.
- Jiang, H. J., Liang, L. H., Ma, L., Guo, J., Dai, H. L. and Wang, X. G. (2017). "An analytical solution of three-dimensional steady thermodynamic analysis for a piezoelectric laminated plate using refined plate theory." *Composite Structures*, 162:194–209.
- Jin, Z. H., and Batra, R. C. (1996). "Some basic fracture mechanics concepts in functionally graded materials." *Journal of the Mechanics and Physics of Solids*, 44(8), 1221–35.
- Jin, Z. H. and Noda, N. (1994). "Transient thermal stress intensity factors for a crack in a semi-infinite plate of a functionally gradient material." *International Journal of Solids and Structures*, 31(2), 203–18.
- Kant, T. (1982), "Numerical analysis of thick plates", *Computer Methods in Applied Mechanics and Engineering*, 31, 1-18.
- Kant, T. and Manjunatha, B. S. (1988). "An unsymmetric frc laminate C⁰ finite element model with 12 degrees of freedom per node." *Engineering Computation*, 5(3), 300-308.

- Kant, T. and Swaminathan, K. (2001). "Estimation of transverse/interlaminar stresses in laminated composites - a selective review and survey of current developments." *Composite Structures*, 49(1), 65-75.
- Kant, T. and Swaminathan, K. (2002). "Analytical solutions for static analysis of laminated composite and sandwich plates based on a higher-order refined theory." *Composite Structures*, 56(4), 329-344.
- Kiani, K. (2016). "Thermo-mechanical analysis of functionally graded plate-like nanorotors: a surface elasticity model." *International Journal of Mechanical Sciences*, 106, 39-49.
- Koizumi, M. (1997). "FGM activities in Japan." *Composites Part B Engineering*, 28(B), 1-4.
- Kulikov, G. M., and Plotnikova, S.V. (2015). "A sampling surfaces method and its implementation for 3d thermal stress analysis of functionally graded plates." *Composite Structures*, 120, 315-25.
- Kumar, J. S., Bathini, S. R., Eswara, R. C. and Kontakkagari, V. K. R. (2011). "Nonlinear thermal analysis of functionally graded plates using higher order theory." *Innovative Systems Design and Engineering*, 2(5), 1-13.
- Levinson, M. (1980). "An accurate simple theory of the statics and dynamics of elastic plates." *Mechanics Research Communications*, 7, p.343.
- Li, D., Deng, Z., Chen, G., Xiao, H. and Zhu, L. (2017). "Thermomechanical bending analysis of sandwich plates with both functionally graded face sheets and functionally graded core." *Composite Structures*, 169, 29-41.
- Liu, W. and Zhong, Z. (2011). "Three-dimensional thermoelastic analysis of functionally graded plate." *Acta Mechanica Solida Sinica*, 24(3), 241-49.
- Lo, K. H., Christensen, R. M. and Wu, E. M. (1977a). "A higher-order theory of plate deformation, part 1: homogeneous plates." *ASME Journal of Applied Mechanics*, 44(4), 663-668.
- Lo, K. H., Christensen, R. M. and Wu, E. M. (1977b). "A higher-order theory of plate deformation, part 2: laminated plates." *ASME Journal of Applied Mechanics*, 44(4), 669-676.
- Mantari, J. L., and Granados, E. V. (2015). "Thermoelastic behavior of advanced composite sandwich plates by using a new 6 unknown quasi-3d hybrid type HSDT". *Composite Structures*, 126, 132-44.
- Markworth, A. J., Ramesh, K. S. and Parks, W. P. (1995). "Modelling studies applied to functionally graded materials." *Journal of Materials Science*, 30(9), 2183-93.
- Matsunaga, H. (2009). "Stress analysis of functionally graded plates subjected to thermal and mechanical loadings." *Composite Structures*, 87(4), 344-57.
- Mian, M. A. and Spencer, A. J. M. (1998). "Exact solutions for functionally graded and laminated elastic materials." *Journal of the Mechanics and Physics of Solids*, 46(12), 2283-95.

- Mindlin, R. D. (1951). "Influence of rotary inertia and shear on flexural motions of isotropic elastic plates." *ASME Journal of Applied Mechanics*, 18, 31-38.
- Muliana, A. H. (2009). "A micromechanical model for predicting thermal properties and thermo-viscoelastic responses of functionally graded materials." *International Journal of Solids and Structures*, 46(9), 1911–24.
- Murthy, M. V. V. (1981). "An improved transverse shear deformation theory for laminated anisotropic plates." *NASA Technical Paper*, No. 1903.
- Natarajan, S, Ferreira, A. J. M., Bordas, S., Carrera, E., Cinefra, M. and Zenkour, A. M (2014). "Analysis of functionally graded material plates using triangular elements with cell-based smoothed discrete shear gap method." *Mathematical Problems in Engineering*, 2014, 1–13.
- Natarajan, S. and Ganapathi M. (2012). "Bending and vibration of functionally graded material sandwich plates using an accurate theory." *Finite Elements in Analysis and Design*, 52, 32–42.
- Noda, N. (1999). "Thermal stresses in functionally graded materials." *Journal of Thermal Stresses*, 22(4-5), 477–512.
- Noda, N. and Jin, Z. H. (1993). "Thermal stress intensity factors for a crack in a strip of a functionally gradient material." *International Journal of Solids and Structures*, 30(8), 1039–56.
- Nosier, A. and Fallah, F. (2008). "Reformulation of Mindlin-Reissner governing equations of functionally graded circular plates." *Acta Mechanica*, 198(3-4), 209–33.
- Ootao, Y. and Ishihara, M. (2013). "Three-dimensional solution for transient thermoelastic problem of a functionally graded rectangular plate with piecewise exponential law." *Composite Structures*, 106, 672–80.
- Ootao, Y. and Tanigawa, Y. (1999). "Three-dimensional transient thermal stresses of functionally graded rectangular plate due to partial heating." *Journal of Thermal Stresses*, 22(1), 35–55.
- Ootao, Y. and Tanigawa, Y. (2005). "Three-dimensional solution for transient thermal stresses of functionally graded rectangular plate due to nonuniform heat supply." *International Journal of Mechanical Sciences*, 47(11), 1769–88.
- Ootao, Y. and Tanigawa, Y. (2007). "Three-dimensional solution for transient thermal stresses of an orthotropic functionally graded rectangular plate." *Composite Structures*, 80(1), 10–20.
- Pagano, N. J., and Hatfield, H. J. (1972). "Elastic behavior of multilayered bidirectional composites." *AIAA Journal*, 10(7), 931-933.
- Pandey, S. and Pradyumna, S. (2017). "Stress analysis of functional graded sandwich beams subjected to thermal shock." *Procedia Engineering*, 173, 837-43.
- Pandya, B. N. and Kant, T. (1988a). "Higher-order shear deformable theories for flexure of sandwich plates – finite element evaluations." *International Journal of Solids and Structures*, 24(12), 1267-1286.

- Pandya, B. N. and Kant, T. (1988b). "Flexure analysis of laminated composites using refined higher-order C^0 plate bending elements." *Computer Methods in Applied Mechanics and Engineering*, 66, 173-198.
- Pandya, B. N. and Kant, T. (1988c). "A refined higher order generally orthotropic C^0 plate bending element." *Computers and Structures*, 28, 119-133.
- Pandya, B. N. and Kant, T. (1988d). "Finite element stress analysis of laminated composite plates using higher-order displacement model." *Composite Science and Technology*, 32, 137-155.
- Praveen, G. N., Chin, C. D. and Reddy, J. N. (1999). "Thermoelastic analysis of functionally graded ceramic-metal cylinder." *Journal of Engineering Mechanics*, 125(11), 1259–67.
- Praveen, G. N. and Reddy J. N. (1998). "Nonlinear transient thermoelastic analysis of functionally graded ceramic-metal plates." *International Journal of Solids and Structures*, 35(33), 4457–79.
- Ramos, I. A., Mantari, J. L., Pagani, A. and Carrera, E. (2016). "Refined theories based on non-polynomial kinematics for the thermoelastic analysis of functionally graded plates." *Journal of Thermal Stresses*, 39(7), 835–53.
- Ravichandran, K. S. (1995). "Thermal residual stresses in a functionally graded material system." *Materials Science and Engineering A*, 201(1-2), 269–76.
- Reddy, J. N. (1984a). "A simple higher-order theory for laminated composite plates." *ASME Journal of Applied Mechanics*, 51, 745-752.
- Reddy, J. N. (1984b). "Energy and Variational Methods in Applied Mechanics." *John Wiley and Sons*, New York, USA.
- Reddy J. N. (1996). "*Mechanics of laminated composite plates, theory and analysis.*" *CRC Press*, Inc. Boca Raton, Florida, USA.
- Reddy, J. N. (2000). "Analysis of functionally graded plates." *International Journal for Numerical Methods in Engineering*, 47(1-3), 663–84.
- Reddy, J. N. and Cheng, Z. Q. (2001a). "Three-dimensional thermomechanical deformations of functionally graded rectangular plates." *European Journal of Mechanics A/Solids*, 20(5), 841–55.
- Reddy, J. N. and Cheng, Z. Q. (2001b). "Three-dimensional solutions of smart functionally graded plates." *Journal of Applied Mechanics*, 68(2), 234–41.
- Reddy, J. N. and Chin, C. D. (1998). "Thermomechanical analysis of functionally graded cylinders and plates." *Journal of Thermal Stresses*, 21(6), 593–626.
- Reissner, E. (1945). "The effect of transverse shear deformation on the bending of elastic plates." *ASME Journal of Applied Mechanics*, 12 (2), 69-77.
- Reissner, E. (1975). "On transverse bending of plates including the effects of transverse shear deformation." *International Journal of Solids and Structures*, 11, 569-573.

- Reissner, E. and Stavsky, Y. (1961). "Bending and stretching of certain types of heterogeneous anisotropic elastic plates." *ASME Journal of Applied Mechanics*, 28, 402-408.
- Rohwer K., Rolfes R. and Sparr H. (2001). "High-order theories for thermal stresses in layered plates." *International Journal of Solids and Structures*, 38(21), 3673–87.
- Sadowski, T., Birsan, M. and Pietras, D. (2015). "Multilayered and FGM structural elements under mechanical and thermal loads. part I: Comparison of finite elements and analytical models." *Archives of Civil and Mechanical Engineering*, 15(4), 1180–92.
- Shen, H.S. (2002). "Nonlinear bending response of functionally graded plates subjected to transverse loads and in thermal environments." *International Journal of Mechanical Sciences*, 44(3), 561–84.
- Shen, H.S. (2007). "Nonlinear thermal bending response of FGM plates due to heat conduction." *Composites Part B: Engineering*, 38(2), 201–15.
- Sladek, J., Vladimir, S., Peter, S., Zhang, C, and Michael, W. (2013). "Analysis of the bending of circular piezoelectric plates with functionally graded material properties by a MLPG method." *Engineering Structures*, 47, 81–89.
- Swaminathan, K., Naveenkumar, D. T., Zenkour, A. M. and Carrera, E. (2014). "Stress, vibration and buckling analyses of FGM plates—A state-of-the-art review." *Composite Structures*, 120, 10–31.
- Swaminathan, K., Patil, S.S., Nataraja, M.S., and Mahabaleswara, K.S. (2006). "Bending of sandwich plates with anti-symmetric angle-ply face sheets – Analytical evaluation of higher order refined computational models." *Composite Structures*, 75(1-4) , 114–120.
- Swaminathan, K. and Patil, S.S. (2007). "Higher order refined computational model with 12 degrees of freedom for the stress analysis of antisymmetric angle-ply plates – analytical solutions." *Composite Structures*, 80(4) , 595–608.
- Swaminathan, K. and Ragounadin, D. (2004). "Analytical solutions using a higher-order refined theory for the static analysis of antisymmetric angle-ply composite and sandwich plates." *Composite Structures*, 64(3-4), 405–417.
- Szilar, R. (1974). "Theory and analysis of plates (classical and numerical methods)." *Prentice-Hall Inc*, Engle Wood Cliffs, New Jersey.
- Tahani, M., and Mirzababae, S. M. (2009). "Non-linear analysis of functionally graded plates in cylindrical bending under thermomechanical loadings based on a layerwise theory." *European Journal of Mechanics A/Solids*, 28(2), 248–56.
- Tanaka, K., Tanaka, Y., Enomoto, K., Poterasu, V. F. and Sugano, Y. (1993a). "Design of thermoelastic materials using direct sensitivity and optimization methods-Reduction of thermal stresses in functionally gradient materials." *Computer Methods in Applied Mechanics and Engineering*, 106(1-2), 271–84.
- Tanaka, K., Tanaka, Y., Watanabe, H., Poterasu, V. F. and Sugano, Y. (1993b). "An improved solution to thermoelastic material design in functionally gradient materials:

scheme to reduce thermal stresses.” *Computer Methods in Applied Mechanics and Engineering*, 109(3-4), 377–89.

Tanigawa, Y. (1993). “Theoretical approach of optimum design for a plate of functionally gradient materials under thermal loading.” *Thermal shock and thermal fatigue behavior of advanced ceramics*. Springer Netherlands, Dordrecht, 171–80.

Tanigawa, Y. (1995). “Some basic thermoelastic problems for nonhomogeneous structural materials.” *Applied Mechanics Reviews*, 48(6), 287–300.

Thai, C. H., Zenkour, A. M., Wahab M. A. and Nguyen, X. H. (2016). “A simple four-unknown shear and normal deformations theory for functionally graded isotropic and sandwich plates based on isogeometric analysis.” *Composite Structures*, 139, 77–95.

Thai, H. T. and Kim, S. E. (2015). “A review of theories for the modeling and analysis of functionally graded plates and shells.” *Composite Structures*, 128, 70–86.

Timoshenko, S. P. and Goodier, J. N. (1970). “Theory of Elasticity.” 3rd Edition, *McGraw-Hill*, New York.

Timoshenko, S. P. and Woinowsky-Krieger, S. (1959). “Theory of Plates and Shells.” *McGraw-Hill*, New York.

Tounsi, A., Mohammed S. A. H., Benyoucef, S. and Bedia, E. A. A. (2013). “A refined trigonometric shear deformation theory for thermoelastic bending of functionally graded sandwich plates.” *Aerospace Science and Technology*, 24(1), 209–20.

Trinh, L. C., Vo, T.P., Thai, H. T. and Mantari, J. L. (2017). “Size-dependent behaviour of functionally graded sandwich microplates under mechanical and thermal loads.” *Composites Part B: Engineering*, 124, 218-41.

Tsukamoto, H. (2003). “Analytical method of inelastic thermal stresses in a functionally graded material plate by a combination of micro- and macromechanical approaches.” *Composites Part B: Engineering*, 34(6), 561–68.

Valizadeh, N., Natarajan, S., Gonzalez-Estrada, O. A., Timon, R., Bui, T.Q. and Bordas, S. P. A. (2013). “NURBS-based finite element analysis of functionally graded plates: static bending, vibration, buckling and flutter.” *Composite Structures*, 99, 309-26.

Vel, S. S. and Batra, R. C. (2002). “Exact solution for thermoelastic deformations of functionally graded thick rectangular plates.” *AIAA Journal*, 40(7), 1421–33.

Vel, S. S. and Batra, R. C. (2003). “Three-dimensional analysis of transient thermal stresses in functionally graded plates.” *International Journal of Solids and Structures*, 40(25), 7181–96.

Wang, Y. Z., Liu, D., Wang, Q. and Zhou, J. Z. (2016). “Asymptotic analysis of thermoelastic response in functionally graded thin plate subjected to a transient thermal shock.” *Composite Structures*, 139, 233–42.

Whitney, J. M. and Pagano, N. J. (1970). “Shear deformation in heterogeneous anisotropic plates.” *ASME Journal of Applied Mechanics*, 37(4), 1031-1036.

- Woo, J. and Meguid, S. A. (2001). "Nonlinear analysis of functionally graded plates and shallow shells." *International Journal of Solids and Structures*, 38(42-43), 7409-21.
- Wu, C. P., Chiu, K. H. and Jiang, R. Y. (2012). "A meshless collocation method for the coupled analysis of functionally graded piezo-thermo-elastic shells and plates under thermal loads." *International Journal of Engineering Science*, 56, 29–48.
- Wu, C. P. and Liu, Y. C. (2016). "A review of semi-analytical numerical methods for laminated composite and multilayered functionally graded elastic/piezoelectric plates and shells." *Composite Structures*, 147, 1-15.
- Xu, Y., Zhou, D. and Liu, K. (2010). "Three-dimensional thermoelastic analysis of rectangular plates with variable thickness subjected to thermomechanical loads." *Journal of Thermal Stresses*, 33(12), 1136–55.
- Yang, B., Kitipornchai, S., Yang, Y. F. and Yang, J. (2017). "3D thermo-mechanical bending solution of functionally graded graphene reinforced circular and annular plates." *Applied Mathematical Modelling*, 49, 69-86.
- Yang, J. and Huang, X. L. (2007). "Nonlinear transient response of functionally graded plates with general imperfections in thermal environments." *Computer Methods in Applied Mechanics and Engineering*, 196(25-28), 2619–2630.
- Yang, J. and Shen, H. S. (2003). "Nonlinear bending analysis of shear deformable functionally graded plates subjected to thermo-mechanical loads under various boundary conditions." *Composites Part B: Engineering*, 34(2), 103–115.
- Ying, J., Lu, C. F. and Lim, C. W. (2009). "3D thermoelasticity solutions for functionally graded thick plates." *Journal of Zhejiang University Science A*, 10(3), 327–336.
- Zenkour, A. M. (2010). "Hygro-thermo-mechanical effects on FGM plates resting on elastic foundations." *Composite Structures*, 93(1), 234–38.
- Zenkour, A. M. (2012). "Hygrothermal analysis of exponentially graded rectangular plates." *Journal of Mechanics of Materials and Structures*, 7(7), 687–700.
- Zenkour, A. M. and Alghamdi, N. A. (2010). "Bending analysis of functionally graded sandwich plates under the effect of mechanical and thermal loads." *Mechanics of Advanced Materials and Structures*, 17(6), 419–32.
- Zhang, D. G. and Zhou, H. M. (2015). "Nonlinear bending analysis of FGM circular plates based on physical neutral surface and higher-order shear deformation theory." *Aerospace Science and Technology*, 41, 90–98.
- Zhao, J., Li, Y. and Ai, X. (2008). "Analysis of transient thermal stress in sandwich plate with functionally graded coatings." *Thin Solid Films*, 516(21), 7581–87.
- Zidi, M., Tounsi, A., Mohammed, S. A. H., Bedia, E. A. A, and Anwar, B. Q. (2014). "Bending analysis of FGM plates under hygro-thermo-mechanical loading using a four variable refined plate theory." *Aerospace Science and Technology*, 34, 24–34.

APPENDIX – I

Equilibrium equations obtained using various displacement models for stress analysis of FGM plates

- **Model – HSDT-9 (Pandya and Kant 1988)**

$$\delta u_0 : \frac{\partial N_x}{\partial x} + \frac{\partial N_{xy}}{\partial y} = 0$$

$$\delta v_0 : \frac{\partial N_y}{\partial y} + \frac{\partial N_{xy}}{\partial x} = 0$$

$$\delta w_0 : \frac{\partial Q_x}{\partial x} + \frac{\partial Q_y}{\partial y} + p_z^+ = 0$$

$$\delta \theta_x : \frac{\partial M_x}{\partial x} + \frac{\partial M_{xy}}{\partial y} - Q_x = 0$$

$$\delta \theta_y : \frac{\partial M_y}{\partial y} + \frac{\partial M_{xy}}{\partial x} - Q_y = 0$$

$$\delta u_0^* : \frac{\partial N_x^*}{\partial x} + \frac{\partial N_{xy}^*}{\partial y} - 2S_x = 0$$

$$\delta v_0^* : \frac{\partial N_y^*}{\partial y} + \frac{\partial N_{xy}^*}{\partial x} - 2S_y = 0$$

$$\delta \theta_x^* : \frac{\partial M_x^*}{\partial x} + \frac{\partial M_{xy}^*}{\partial y} - 3Q_x^* = 0$$

$$\delta \theta_y^* : \frac{\partial M_y^*}{\partial y} + \frac{\partial M_{xy}^*}{\partial x} - 3Q_y^* = 0$$

APPENDIX - I (contd.)

• **Model – HSDT-5 (Reddy 1984)**

$$\delta u_0 : \frac{\partial N_x}{\partial x} + \frac{\partial N_{xy}}{\partial y} = 0$$

$$\delta v_0 : \frac{\partial N_y}{\partial y} + \frac{\partial N_{xy}}{\partial x} = 0$$

$$\delta \theta_x : \frac{\partial M_x}{\partial x} + \frac{\partial M_{xy}}{\partial y} - Q_x + \left(\frac{4}{h^2}\right) Q_x^* - \left(\frac{4}{3h^2}\right) \left[\frac{\partial M_x^*}{\partial x} + \frac{\partial M_{xy}^*}{\partial y} \right] = 0$$

$$\delta \theta_y : \frac{\partial M_y}{\partial y} + \frac{\partial M_{xy}}{\partial x} - Q_y + \left(\frac{4}{h^2}\right) Q_y^* - \left(\frac{4}{3h^2}\right) \left[\frac{\partial M_y^*}{\partial y} + \frac{\partial M_{xy}^*}{\partial x} \right] = 0$$

$$\delta w_0 : \frac{\partial Q_x}{\partial x} + \frac{\partial Q_y}{\partial y} - \left(\frac{4}{h^2}\right) \left[\frac{\partial Q_x^*}{\partial x} + \frac{\partial Q_y^*}{\partial y} \right] + \left(\frac{4}{3h^2}\right) \left[\frac{\partial^2 M_x^*}{\partial x^2} + 2 \frac{\partial^2 M_{xy}^*}{\partial x \partial y} + \frac{\partial^2 M_y^*}{\partial y^2} \right] + p_z^+ = 0$$

• **Model – FSDT (Whitney and Pagano 1970)**

$$\delta u_0 : \frac{\partial N_x}{\partial x} + \frac{\partial N_{xy}}{\partial y} = 0$$

$$\delta v_0 : \frac{\partial N_y}{\partial y} + \frac{\partial N_{xy}}{\partial x} = 0$$

$$\delta \theta_x : \frac{\partial M_x}{\partial x} + \frac{\partial M_{xy}}{\partial y} - Q_x = 0$$

$$\delta \theta_y : \frac{\partial M_y}{\partial y} + \frac{\partial M_{xy}}{\partial x} - Q_y = 0$$

$$\delta w_0 : \frac{\partial Q_x}{\partial x} + \frac{\partial Q_y}{\partial y} + p_z^+ = 0$$

APPENDIX – II

Elements of plate stiffness matrices [A], [A'], [C_T], [B], [B'], [D], [D'], [E], [E'] for various displacement models used in the thermo-elastic analysis of FGM plates

- **Model – HSDT-12 (Kant and Manjunatha 1988)**

$$[A] = \int_{-h/2}^{h/2} \begin{bmatrix}
 Q_{11} & Q_{12} & Q_{11}Z^2 & Q_{12}Z^2 & Q_{13} & 3Q_{13}Z^2 & Q_{11}Z & Q_{12}Z & Q_{11}Z^3 & Q_{12}Z^3 & 2Q_{13}Z \\
 Q_{12} & Q_{22} & Q_{12}Z^2 & Q_{22}Z^2 & Q_{23} & 3Q_{23}Z^2 & Q_{12}Z & Q_{22}Z & Q_{12}Z^3 & Q_{22}Z^3 & 2Q_{23}Z \\
 Q_{11}Z^2 & Q_{12}Z^2 & Q_{11}Z^4 & Q_{12}Z^4 & Q_{13}Z^2 & 3Q_{13}Z^4 & Q_{11}Z^3 & Q_{12}Z^3 & Q_{11}Z^5 & Q_{12}Z^5 & 2Q_{13}Z^3 \\
 Q_{12}Z^2 & Q_{22}Z^2 & Q_{12}Z^4 & Q_{22}Z^4 & Q_{23}Z^2 & 3Q_{23}Z^4 & Q_{12}Z^3 & Q_{22}Z^3 & Q_{12}Z^5 & Q_{22}Z^5 & 2Q_{23}Z^3 \\
 Q_{13} & Q_{23} & Q_{13}Z^2 & Q_{23}Z^2 & Q_{33} & 3Q_{33}Z^2 & Q_{13}Z & Q_{23}Z & Q_{13}Z^3 & Q_{23}Z^3 & 2Q_{33}Z \\
 Q_{13}Z^2 & Q_{23}Z^2 & Q_{13}Z^4 & Q_{23}Z^4 & Q_{33}Z^2 & 3Q_{33}Z^4 & Q_{13}Z^3 & Q_{23}Z^3 & Q_{13}Z^5 & Q_{23}Z^5 & 2Q_{33}Z^3 \\
 Q_{11}Z & Q_{12}Z & Q_{11}Z^3 & Q_{12}Z^3 & Q_{13}Z & 3Q_{13}Z^3 & Q_{11}Z^2 & Q_{12}Z^2 & Q_{11}Z^4 & Q_{12}Z^4 & 2Q_{13}Z^2 \\
 Q_{12}Z & Q_{22}Z & Q_{12}Z^3 & Q_{22}Z^3 & Q_{23}Z & 3Q_{23}Z^3 & Q_{12}Z^2 & Q_{22}Z^2 & Q_{12}Z^4 & Q_{22}Z^4 & 2Q_{23}Z^2 \\
 Q_{11}Z^3 & Q_{12}Z^3 & Q_{11}Z^5 & Q_{12}Z^5 & Q_{13}Z^3 & 3Q_{13}Z^5 & Q_{11}Z^4 & Q_{12}Z^4 & Q_{11}Z^6 & Q_{12}Z^6 & 2Q_{13}Z^4 \\
 Q_{12}Z^3 & Q_{22}Z^3 & Q_{12}Z^5 & Q_{22}Z^5 & Q_{23}Z^3 & 3Q_{23}Z^5 & Q_{12}Z^4 & Q_{22}Z^4 & Q_{12}Z^6 & Q_{22}Z^6 & 2Q_{23}Z^4 \\
 Q_{13}Z & Q_{23}Z & Q_{13}Z^3 & Q_{23}Z^3 & Q_{33}Z & 3Q_{33}Z^3 & Q_{13}Z^2 & Q_{23}Z^2 & Q_{13}Z^4 & Q_{23}Z^4 & 2Q_{33}Z^2
 \end{bmatrix} dz \quad -+$$

APPENDIX - II (contd.)

$$[C_T] = \int_{-h/2}^{h/2} \begin{bmatrix} Q_{11} + Q_{12} + Q_{13} \\ Q_{21} + Q_{22} + Q_{23} \\ Q_{11}z^2 + Q_{12}z^2 + Q_{13}z^2 \\ Q_{21}z^2 + Q_{22}z^2 + Q_{23}z^2 \\ Q_{31} + Q_{32} + Q_{33} \\ Q_{31}z^2 + Q_{32}z^2 + Q_{33}z^2 \\ Q_{11}z + Q_{12}z + Q_{13}z \\ Q_{21}z + Q_{22}z + Q_{23}z \\ Q_{11}z^3 + Q_{12}z^3 + Q_{13}z^3 \\ Q_{21}z^3 + Q_{22}z^3 + Q_{23}z^3 \\ Q_{31}z + Q_{32}z + Q_{33}z \end{bmatrix} dz$$

APPENDIX - II (contd.)

$$[B] = \int_{-h/2}^{h/2} \begin{bmatrix} Q_{44} & Q_{44} & Q_{44}Z^2 & Q_{44}Z^2 & Q_{44}Z & Q_{44}Z & Q_{44}Z^3 & Q_{44}Z^3 \\ Q_{44}Z^2 & Q_{44}Z^2 & Q_{44}Z^4 & Q_{44}Z^4 & Q_{44}Z^3 & Q_{44}Z^3 & Q_{44}Z^5 & Q_{44}Z^5 \\ Q_{44}Z & Q_{44}Z & Q_{44}Z^3 & Q_{44}Z^3 & Q_{44}Z^2 & Q_{44}Z^2 & Q_{44}Z^4 & Q_{44}Z^4 \\ Q_{44}Z^3 & Q_{44}Z^3 & Q_{44}Z^5 & Q_{44}Z^5 & Q_{44}Z^4 & Q_{44}Z^4 & Q_{44}Z^6 & Q_{44}Z^6 \end{bmatrix} dz$$

$$[D] = \int_{-h/2}^{h/2} \begin{bmatrix} Q_{66} & Q_{66} & 3Q_{66}Z^2 & Q_{66}Z^2 & 2Q_{66}Z & Q_{66}Z & Q_{66}Z^3 \\ Q_{66}Z^2 & Q_{66}Z^2 & 3Q_{66}Z^4 & Q_{66}Z^4 & 2Q_{66}Z^3 & Q_{66}Z^3 & Q_{66}Z^5 \\ Q_{66}Z & Q_{66}Z & 3Q_{66}Z^3 & Q_{66}Z^3 & 2Q_{66}Z^2 & Q_{66}Z^2 & Q_{66}Z^4 \\ Q_{66}Z^3 & Q_{66}Z^3 & 3Q_{66}Z^5 & Q_{66}Z^5 & 2Q_{66}Z^4 & Q_{66}Z^4 & Q_{66}Z^6 \end{bmatrix} dz$$

$$[E] = \int_{-h/2}^{h/2} \begin{bmatrix} Q_{55} & Q_{55} & 3Q_{55}Z^2 & Q_{55}Z^2 & 2Q_{55}Z & Q_{55}Z & Q_{55}Z^3 \\ Q_{55}Z^2 & Q_{55}Z^2 & 3Q_{55}Z^4 & Q_{55}Z^4 & 2Q_{55}Z^3 & Q_{55}Z^3 & Q_{55}Z^5 \\ Q_{55}Z & Q_{55}Z & 3Q_{55}Z^3 & Q_{55}Z^3 & 2Q_{55}Z^2 & Q_{55}Z^2 & Q_{55}Z^4 \\ Q_{55}Z^3 & Q_{55}Z^3 & 3Q_{55}Z^5 & Q_{55}Z^5 & 2Q_{55}Z^4 & Q_{55}Z^4 & Q_{55}Z^6 \end{bmatrix} dz$$

APPENDIX - II (contd.)

$$[A'] = [B'] = [D'] = [E'] = 0$$

- **Model – HSDT-9 (Pandya and Kant 1988)**

$$[A] = \int_{-h/2}^{h/2} \begin{bmatrix} Q_{11} & Q_{12} & Q_{11}z^2 & Q_{12}z^2 & Q_{11}z & Q_{12}z & Q_{11}z^3 & Q_{12}z^3 \\ Q_{12} & Q_{22} & Q_{12}z^2 & Q_{22}z^2 & Q_{12}z & Q_{22}z & Q_{12}z^3 & Q_{22}z^3 \\ Q_{11}z^2 & Q_{12}z^2 & Q_{11}z^4 & Q_{12}z^4 & Q_{11}z^3 & Q_{12}z^3 & Q_{11}z^5 & Q_{12}z^5 \\ Q_{12}z^2 & Q_{22}z^2 & Q_{12}z^4 & Q_{22}z^4 & Q_{12}z^3 & Q_{22}z^3 & Q_{12}z^5 & Q_{22}z^5 \\ Q_{11}z & Q_{12}z & Q_{11}z^3 & Q_{12}z^3 & Q_{11}z^2 & Q_{12}z^2 & Q_{11}z^4 & Q_{12}z^4 \\ Q_{12}z & Q_{22}z & Q_{12}z^3 & Q_{22}z^3 & Q_{12}z^2 & Q_{22}z^2 & Q_{12}z^4 & Q_{22}z^4 \\ Q_{11}z^3 & Q_{12}z^3 & Q_{11}z^5 & Q_{12}z^5 & Q_{11}z^4 & Q_{12}z^4 & Q_{11}z^6 & Q_{12}z^6 \\ Q_{12}z^3 & Q_{22}z^3 & Q_{12}z^5 & Q_{22}z^5 & Q_{12}z^4 & Q_{22}z^4 & Q_{12}z^6 & Q_{22}z^6 \end{bmatrix} dz$$

APPENDIX - II (contd.)

$$[C_T] = \int_{-h/2}^{h/2} \begin{bmatrix} Q_{11} + Q_{12} \\ Q_{12} + Q_{22} \\ Q_{11}Z^2 + Q_{12}Z^2 \\ Q_{12}Z^2 + Q_{22}Z^2 \\ Q_{11}Z + Q_{12}Z \\ Q_{12}Z + Q_{22}Z \\ Q_{11}Z^3 + Q_{12}Z^3 \\ Q_{12}Z^3 + Q_{22}Z^3 \end{bmatrix} dz$$

$$[B] = \int_{-h/2}^{h/2} \begin{bmatrix} Q_{44} & Q_{44} & Q_{44}Z^2 & Q_{44}Z^2 & Q_{44}Z & Q_{44}Z & Q_{44}Z^3 & Q_{44}Z^3 \\ Q_{44}Z^2 & Q_{44}Z^2 & Q_{44}Z^4 & Q_{44}Z^4 & Q_{44}Z^3 & Q_{44}Z^3 & Q_{44}Z^5 & Q_{44}Z^5 \\ Q_{44}Z & Q_{44}Z & Q_{44}Z^3 & Q_{44}Z^3 & Q_{44}Z^2 & Q_{44}Z^2 & Q_{44}Z^4 & Q_{44}Z^4 \\ Q_{44}Z^3 & Q_{44}Z^3 & Q_{44}Z^5 & Q_{44}Z^5 & Q_{44}Z^4 & Q_{44}Z^4 & Q_{44}Z^6 & Q_{44}Z^6 \end{bmatrix} dz$$

APPENDIX - II (contd.)

$$[D] = \int_{-h/2}^{h/2} \begin{bmatrix} Q_{66} & Q_{66} & 3Q_{66}z^2 & 2Q_{66}z \\ Q_{66}z^2 & Q_{66}z^2 & 3Q_{66}z^4 & 2Q_{66}z^3 \\ Q_{66}z & Q_{66}z & 3Q_{66}z^3 & 2Q_{66}z^2 \end{bmatrix} dz$$

$$[E] = \int_{-h/2}^{h/2} \begin{bmatrix} Q_{55} & Q_{55} & 3Q_{55}z^2 & 2Q_{55}z \\ Q_{55}z^2 & Q_{55}z^2 & 3Q_{55}z^4 & 2Q_{55}z^3 \\ Q_{55}z & Q_{55}z & 3Q_{55}z^3 & 2Q_{55}z^2 \end{bmatrix} dz$$

$$[A'] = [B'] = [D'] = [E'] = 0$$

APPENDIX - II (contd.)

- **Model – HSDT-5 (Reddy 1984)**

$$[A] = \int_{-h/2}^{h/2} \begin{bmatrix} Q_{11} & Q_{12} & Q_{11} \left(z - \frac{4z^3}{3h^2} \right) & Q_{12} \left(z - \frac{4z^3}{3h^2} \right) & -Q_{11} \frac{4z^3}{3h^2} & -Q_{12} \frac{4z^3}{3h^2} \\ Q_{12} & Q_{22} & Q_{12} \left(z - \frac{4z^3}{3h^2} \right) & Q_{22} \left(z - \frac{4z^3}{3h^2} \right) & -Q_{12} \frac{4z^3}{3h^2} & -Q_{22} \frac{4z^3}{3h^2} \\ Q_{11}z & Q_{12}z & Q_{11} \left(z^2 - \frac{4z^4}{3h^2} \right) & Q_{12} \left(z^2 - \frac{4z^4}{3h^2} \right) & -Q_{11} \frac{4z^4}{3h^2} & -Q_{12} \frac{4z^4}{3h^2} \\ Q_{12}z & Q_{22}z & Q_{12} \left(z^2 - \frac{4z^4}{3h^2} \right) & Q_{22} \left(z^2 - \frac{4z^4}{3h^2} \right) & -Q_{12} \frac{4z^4}{3h^2} & -Q_{22} \frac{4z^4}{3h^2} \\ Q_{11}z^3 & Q_{12}z^3 & Q_{11} \left(z^4 - \frac{4z^6}{3h^2} \right) & Q_{12} \left(z^4 - \frac{4z^6}{3h^2} \right) & -Q_{11} \frac{4z^6}{3h^2} & -Q_{12} \frac{4z^6}{3h^2} \\ Q_{12}z^3 & Q_{22}z^3 & Q_{12} \left(z^4 - \frac{4z^6}{3h^2} \right) & Q_{22} \left(z^4 - \frac{4z^6}{3h^2} \right) & -Q_{12} \frac{4z^6}{3h^2} & -Q_{22} \frac{4z^6}{3h^2} \end{bmatrix} dz$$

APPENDIX - II (contd.)

$$[C_T] = \int_{-h/2}^{h/2} \begin{bmatrix} Q_{11} + Q_{12} \\ Q_{12} + Q_{22} \\ Q_{11}z + Q_{12}z \\ Q_{12}z + Q_{22}z \\ Q_{11}z^3 + Q_{12}z^3 \\ Q_{12}z^3 + Q_{22}z^3 \end{bmatrix} dz$$

$$[B] = \int_{-h/2}^{h/2} \begin{bmatrix} Q_{44} & Q_{44} & Q_{44} \left(z - \frac{4z^3}{3h^2} \right) & Q_{44} \left(z - \frac{4z^3}{3h^2} \right) & Q_{44} \frac{-8z^3}{3h^2} \\ Q_{44}z & Q_{44}z & Q_{44} \left(z^2 - \frac{4z^4}{3h^2} \right) & Q_{44} \left(z^2 - \frac{4z^4}{3h^2} \right) & Q_{44} \frac{-8z^4}{3h^2} \\ Q_{44}z^3 & Q_{44}z^3 & Q_{44} \left(z^4 - \frac{4z^6}{3h^2} \right) & Q_{44} \left(z^4 - \frac{4z^6}{3h^2} \right) & Q_{44} \frac{-8z^6}{3h^2} \end{bmatrix} dz$$

APPENDIX - II (contd.)

$$[E] = \sum_{L=1}^{NL} \int_{z_L}^{z_{L+1}} \begin{bmatrix} Q_{55} \left(1 - \frac{4z^2}{h^2} \right) & Q_{55} \left(1 - \frac{4z^2}{h^2} \right) \\ Q_{55} \left(z^2 - \frac{4z^4}{h^2} \right) & Q_{55} \left(z^2 - \frac{4z^4}{h^2} \right) \end{bmatrix} dz$$

$$[A'] = [B'] = [D'] = [E'] = 0$$

- **Model – FSDT (Whitney and Pagano 1970)**

$$[A] = \int_{-h/2}^{h/2} \begin{bmatrix} Q_{11} & Q_{12} & Q_{11}z & Q_{12}z \\ Q_{12} & Q_{22} & Q_{12}z & Q_{22}z \\ Q_{11}z & Q_{12}z & Q_{11}z^2 & Q_{12}z^2 \\ Q_{12}z & Q_{22}z & Q_{12}z^2 & Q_{22}z^2 \end{bmatrix} dz$$

APPENDIX - II (contd.)

$$[C_T] = \int_{-h/2}^{h/2} \begin{bmatrix} Q_{11} + Q_{12} \\ Q_{12} + Q_{22} \\ Q_{11}z + Q_{12}z \\ Q_{12}z + Q_{22}z \end{bmatrix} dz$$

$$[B] = \int_{-h/2}^{h/2} \begin{bmatrix} Q_{44} & Q_{44} & Q_{44}z & Q_{44}z \\ Q_{44}z & Q_{44}z & Q_{44}z^2 & Q_{44}z^2 \end{bmatrix} dz$$

$$[D] = \int_{-h/2}^{h/2} [Q_{66} \quad Q_{66}] dz$$

APPENDIX - II (contd.)

$$[E] = \int_{-h/2}^{h/2} [Q_{55} \quad Q_{55}] dz$$

$$[A'] = [B'] = [D'] = [E'] = 0$$

APPENDIX – III

Elements of the coefficient matrix [X] using various displacement models for thermo-elastic analysis of FGM plates

- **Model - HSDT-12 (Kant and Manjunatha 1988)**

$$X_{1,1} = A_{1,1} \alpha^2 + B_{1,1} \beta^2$$

$$X_{1,2} = A_{1,2} \alpha\beta + B_{1,2} \alpha\beta$$

$$X_{1,3} = 0$$

$$X_{1,4} = A_{1,7} \alpha^2 + B_{1,5} \beta^2$$

$$X_{1,5} = A_{1,8} \alpha\beta + B_{1,6} \alpha\beta$$

$$X_{1,6} = -A_{1,5} \alpha$$

$$X_{1,7} = A_{1,3} \alpha^2 + B_{1,3} \beta^2$$

$$X_{1,8} = A_{1,4} \alpha\beta + B_{1,4} \alpha\beta$$

$$X_{1,9} = -A_{1,11} \alpha$$

$$X_{1,10} = A_{1,9} \alpha^2 + B_{1,7} \beta^2$$

$$X_{1,11} = A_{1,10} \alpha\beta + B_{1,8} \alpha\beta$$

$$X_{1,12} = -A_{1,6} \alpha$$

$$X_{2,2} = A_{2,2} \beta^2 + B_{1,2} \alpha^2$$

$$X_{2,3} = 0$$

$$X_{2,4} = A_{2,7} \alpha\beta + B_{1,5} \alpha\beta$$

$$X_{2,5} = A_{2,8} \beta^2 + B_{1,6} \alpha^2$$

$$X_{2,6} = -A_{2,5} \beta$$

$$X_{2,7} = A_{2,3} \alpha\beta + B_{1,3} \alpha\beta$$

$$X_{2,8} = A_{2,4} \beta^2 + B_{1,4} \alpha^2$$

$$X_{2,9} = -A_{2,11} \beta$$

$$X_{2,10} = A_{2,9} \alpha\beta + B_{1,7} \alpha\beta$$

$$X_{2,11} = A_{1,10} \beta^2 + B_{1,8} \alpha^2$$

$$X_{2,12} = -A_{2,6} \beta$$

$$X_{3,3} = D_{1,2} \alpha^2 + E_{1,2} \beta^2$$

$$X_{3,4} = D_{1,1} \alpha$$

$$X_{3,5} = E_{1,1} \beta$$

$$X_{3,6} = D_{1,6} \alpha^2 + E_{1,6} \beta^2$$

$$X_{3,7} = D_{1,5} \alpha$$

APPENDIX - III (contd.)

$$X_{3,8} = E_{1,5} \beta$$

$$X_{3,9} = D_{1,4} \alpha^2 + E_{1,4} \beta^2$$

$$X_{3,10} = D_{1,3} \alpha$$

$$X_{3,11} = E_{1,3} \beta$$

$$X_{3,12} = D_{1,7} \alpha^2 + E_{1,7} \beta^2$$

$$X_{44} = A_{7,7} \alpha^2 + B_{3,5} \beta^2 + D_{1,1}$$

$$X_{4,5} = A_{7,8} \alpha\beta + B_{3,6} \alpha\beta$$

$$X_{46} = -A_{7,5} \alpha + D_{1,6} \alpha$$

$$X_{4,7} = A_{7,3} \alpha^2 + B_{3,3} \beta^2 + D_{1,5}$$

$$X_{4,8} = A_{7,4} \alpha\beta + B_{3,4} \alpha\beta$$

$$X_{4,9} = -A_{7,11} \alpha + D_{1,4} \alpha$$

$$X_{4,10} = A_{7,9} \alpha^2 + B_{3,7} \beta^2 + D_{1,3}$$

$$X_{4,11} = A_{7,10} \alpha\beta + B_{3,8} \alpha\beta$$

$$X_{4,12} = -A_{7,6} \alpha + D_{1,7} \alpha$$

$$X_{5,5} = A_{8,8} \beta^2 + B_{3,6} \alpha^2 + E_{1,1}$$

$$X_{5,6} = -A_{8,5} \beta + E_{1,6} \beta$$

$$X_{5,7} = A_{8,3} \alpha\beta + B_{3,3} \alpha\beta$$

$$X_{5,8} = A_{8,4} \beta^2 + B_{3,4} \alpha^2 + E_{1,5}$$

$$X_{5,9} = -A_{8,11} \beta + E_{1,4} \beta$$

$$X_{5,10} = A_{8,9} \alpha\beta + B_{3,7} \alpha\beta$$

$$X_{5,11} = A_{8,10} \beta^2 + B_{3,8} \alpha^2 + E_{1,3}$$

$$X_{5,12} = -A_{8,6} \beta + E_{1,7} \beta$$

$$X_{6,6} = A_{5,5} + D_{3,6} \alpha^2 + E_{3,6} \beta^2$$

$$X_{6,7} = -A_{5,3} \alpha + D_{3,5} \alpha$$

$$X_{6,8} = -A_{5,4} \beta + E_{3,5} \beta$$

$$X_{69} = A_{5,11} + D_{3,4} \alpha^2 + E_{3,4} \beta^2$$

$$X_{6,10} = -A_{5,9} \alpha + D_{3,3} \alpha$$

$$X_{6,11} = -A_{5,10} \beta + E_{3,3} \beta$$

$$X_{6,12} = A_{5,6} + D_{3,7} \alpha^2 + E_{3,7} \beta^2$$

$$X_{7,7} = -A_{3,5} \alpha + 2D_{3,6} \alpha$$

$$X_{7,8} = -A_{3,6} \alpha + 2D_{3,7} \alpha$$

$$X_{7,9} = -A_{3,11} \alpha + 2D_{3,4} \alpha$$

APPENDIX - III (contd.)

$$\begin{aligned}
 X_{7,10} &= A_{3,9} \alpha^2 + B_{2,7} \beta^2 + 2D_{3,3} & X_{7,11} &= A_{3,10} \alpha\beta + B_{2,8} \alpha\beta \\
 X_{7,12} &= -A_{3,6} \alpha + 2D_{3,7} \alpha & X_{8,8} &= A_{4,4} \beta^2 + B_{2,4} \alpha^2 + 2E_{3,5} \\
 X_{8,9} &= -A_{4,11} \beta + 2E_{3,4} \beta & X_{8,10} &= A_{4,9} \alpha\beta + B_{2,7} \alpha\beta \\
 X_{8,11} &= A_{4,10} \beta^2 + B_{2,8} \alpha^2 + 2E_{3,3} & X_{8,12} &= -A_{4,6} \beta + 2E_{3,7} \beta \\
 X_{9,9} &= 2A_{11,11} + D_{2,4} \alpha^2 + E_{2,4} \beta^2 & X_{9,10} &= -2A_{11,9} \alpha + D_{2,3} \alpha \\
 X_{9,11} &= -2A_{11,10} \beta + E_{2,3} \beta & X_{9,12} &= 2A_{11,6} + D_{2,7} \alpha^2 + E_{2,7} \beta^2 \\
 X_{10,10} &= A_{9,9} \alpha^2 + B_{4,7} \beta^2 + 3D_{2,3} & X_{10,11} &= A_{9,10} \alpha\beta + B_{4,8} \alpha\beta \\
 X_{10,12} &= -A_{9,6} \alpha + 3D_{2,7} \alpha & X_{11,11} &= A_{10,10} \beta^2 + B_{4,8} \alpha^2 + 3E_{2,3} \\
 X_{11,12} &= -A_{10,6} \beta + 3E_{2,7} \beta & X_{12,12} &= 3A_{6,6} + D_{4,7} \alpha^2 + E_{4,7} \beta^2
 \end{aligned}$$

and $X_{ij} = X_{ji}$ (i, j=1 to 12)

• **Model – HSDT-9 (Pandya and Kant 1988)**

$$\begin{aligned}
 X_{1,1} &= A_{1,1} \alpha^2 + B_{1,1} \beta^2 & X_{1,2} &= A_{1,2} \alpha\beta + B_{1,2} \alpha\beta \\
 X_{1,3} &= 0 & X_{1,4} &= A_{1,5} \alpha^2 + B_{1,5} \beta^2 \\
 X_{1,5} &= A_{1,6} \alpha\beta + B_{1,6} \alpha\beta & X_{1,6} &= A_{1,3} \alpha^2 + B_{1,3} \beta^2 \\
 X_{1,7} &= A_{1,4} \alpha\beta + B_{1,4} \alpha\beta & X_{1,8} &= A_{1,7} \alpha^2 + B_{1,7} \beta^2 \\
 X_{1,9} &= A_{1,8} \alpha\beta + B_{1,8} \alpha\beta & X_{2,2} &= A_{2,2} \beta^2 + B_{1,2} \alpha^2
 \end{aligned}$$

APPENDIX - III (contd.)

$$X_{2,3} = 0$$

$$X_{2,4} = A_{2,5} \alpha\beta + B_{1,5} \alpha\beta$$

$$X_{2,5} = A_{2,6} \beta^2 + B_{1,6} \alpha^2$$

$$X_{2,6} = A_{2,3} \alpha\beta + B_{1,3} \alpha\beta$$

$$X_{2,7} = A_{2,4} \beta^2 + B_{1,4} \alpha^2$$

$$X_{2,8} = A_{2,7} \alpha\beta + B_{1,7} \alpha\beta$$

$$X_{2,9} = A_{2,8} \beta^2 + B_{1,8} \alpha^2$$

$$X_{3,3} = D_{1,2} \alpha^2 + E_{1,2} \beta^2$$

$$X_{3,4} = D_{1,1} \alpha$$

$$X_{3,5} = E_{1,1} \beta$$

$$X_{3,6} = D_{1,4} \alpha$$

$$X_{3,7} = E_{1,4} \beta$$

$$X_{3,8} = D_{1,3} \alpha$$

$$X_{3,9} = E_{1,3} \beta$$

$$X_{4,4} = A_{5,5} \alpha^2 + B_{3,5} \beta^2 + D_{1,1}$$

$$X_{4,5} = A_{5,6} \alpha\beta + B_{3,6} \alpha\beta$$

$$X_{4,6} = A_{5,3} \alpha^2 + B_{3,3} \beta^2 + D_{1,4}$$

$$X_{4,7} = A_{5,4} \alpha\beta + B_{3,4} \alpha\beta$$

$$X_{4,8} = A_{5,7} \alpha^2 + B_{3,7} \beta^2 + D_{1,3}$$

$$X_{4,9} = A_{5,8} \alpha\beta + B_{3,8} \alpha\beta$$

$$X_{5,5} = A_{6,6} \beta^2 + B_{3,6} \alpha^2 + E_{1,1}$$

$$X_{5,6} = A_{6,3} \alpha\beta + B_{3,3} \alpha\beta$$

$$X_{5,7} = A_{6,4} \beta^2 + B_{3,4} \alpha^2 + E_{1,4}$$

$$X_{5,8} = A_{6,7} \alpha\beta + B_{3,7} \alpha\beta$$

$$X_{5,9} = A_{6,8} \beta^2 + B_{3,8} \alpha^2 + E_{1,3}$$

$$X_{6,6} = A_{3,3} \alpha^2 + B_{2,3} \beta^2 + 2D_{3,4}$$

$$X_{6,7} = A_{3,4} \alpha\beta + B_{2,4} \alpha\beta$$

$$X_{6,8} = A_{3,7} \alpha^2 + B_{2,7} \beta^2 + 2D_{3,3}$$

$$X_{6,9} = A_{3,8} \alpha\beta + B_{2,8} \alpha\beta$$

$$X_{7,7} = A_{4,4} \beta^2 + B_{2,4} \alpha^2 + 2E_{3,4}$$

$$X_{7,8} = A_{4,7} \alpha\beta + B_{2,7} \alpha\beta$$

$$X_{7,9} = A_{4,8} \beta^2 + B_{2,8} \alpha^2 + 2E_{3,3}$$

APPENDIX - III (contd.)

$$X_{8,8} = A_{7,7} \alpha^2 + B_{4,7} \beta^2 + 3D_{2,3} \quad X_{89} = A_{7,8} \alpha\beta + B_{4,8} \alpha\beta$$

$$X_{9,9} = A_{8,8} \beta^2 + B_{4,8} \alpha^2 + 3E_{2,3} \quad \text{and } X_{i,j} = X_{j,i} \quad (i, j=1 \text{ to } 9)$$

• **Model - HSDT-5 (Reddy 1984)**

$$X_{1,1} = A_{1,1} \alpha^2 + B_{1,1} \beta^2 \quad X_{1,2} = A_{1,2} \alpha\beta + B_{1,2} \alpha\beta$$

$$X_{1,3} = A_{1,3} \alpha^2 + B_{1,3} \beta^2 \quad X_{1,4} = A_{1,4} \alpha\beta + B_{1,4} \alpha\beta$$

$$X_{1,5} = A_{1,5} \alpha^3 + A_{1,6} \alpha^2\beta + B_{1,5} \alpha\beta^2 \quad X_{2,2} = A_{2,2} \beta^2 + B_{1,2} \alpha^2$$

$$X_{2,3} = A_{2,3} \alpha\beta + B_{1,3} \alpha\beta \quad X_{2,4} = A_{2,4} \beta^2 + B_{1,4} \alpha^2$$

$$X_{2,5} = A_{2,5} \alpha^2\beta + A_{2,6} \beta^3 + B_{1,5} \alpha^2\beta$$

$$X_{3,3} = A_{3,3} \alpha^2 + B_{2,3} \beta^2 + D_{1,1} - \frac{4}{3h^2} (A_{5,3} \alpha^2 + B_{3,3} \beta^2) - \frac{4}{h^2} D_{2,1}$$

$$X_{3,4} = A_{3,4} \alpha\beta + B_{2,4} \alpha\beta - \frac{4}{3h^2} (A_{5,4} \alpha\beta + B_{3,4} \alpha\beta)$$

$$X_{3,5} = A_{3,5} \alpha^3 + A_{3,6} \alpha\beta^2 + B_{2,5} \alpha\beta^2 + D_{1,2} \alpha - \frac{4}{h^2} D_{2,2} \alpha \\ - \frac{4}{3h^2} (A_{5,5} \alpha^3 + A_{5,6} \alpha\beta^2 + B_{3,5} \alpha\beta^2)$$

$$X_{4,4} = A_{4,4} \alpha\beta^2 + B_{2,4} \alpha^2 + E_{1,1} - \frac{4}{3h^2} (A_{6,4} \beta^2 + B_{3,4} \alpha^2) - \frac{4}{h^2} E_{2,1}$$

$$X_{4,5} = A_{4,5} \alpha^2\beta + A_{4,6} \beta^3 + B_{2,5} \alpha^2\beta + E_{1,2} \beta - \frac{4}{h^2} E_{2,2} \beta \\ - \frac{4}{3h^2} (A_{6,5} \alpha^2\beta + A_{6,6} \beta^3 + B_{3,5} \alpha^2\beta)$$

APPENDIX - III (contd.)

$$X_{5,5} = \frac{4}{3h^2} \left(A_{5,5} \alpha^4 + A_{5,6} \alpha^2 \beta^2 + A_{6,5} \alpha^2 \beta^2 + A_{6,6} \beta^4 + B_{3,5} \alpha^2 \beta^2 \right) - \left(D_{1,2} \alpha^2 + E_{1,2} \beta^2 \right) + \frac{4}{h^2} \left(D_{2,2} \alpha^2 + E_{2,2} \beta^2 \right)$$

and $X_{i,j} = X_{j,i}$ (i, j=1 to 5)

• **Model - FSDT (Whitney and Pagano 1970)**

$$X_{1,1} = A_{1,1} \alpha^2 + B_{1,1} \beta^2 \qquad X_{1,2} = A_{1,2} \alpha \beta + B_{1,2} \alpha \beta$$

$$X_{1,3} = 0 \qquad X_{1,4} = A_{1,3} \alpha^2 + B_{1,3} \beta^2$$

$$X_{1,5} = A_{1,4} \alpha \beta + B_{1,4} \alpha \beta \qquad X_{2,2} = A_{2,2} \beta^2 + B_{1,2} \alpha^2$$

$$X_{2,3} = 0 \qquad X_{2,4} = A_{2,3} \alpha \beta + B_{1,3} \alpha \beta$$

$$X_{2,5} = A_{2,4} \beta^2 + B_{1,4} \alpha^2 \qquad X_{3,3} = D_{1,2} \alpha^2 + E_{1,2} \beta^2$$

$$X_{3,4} = D_{1,1} \alpha \qquad X_{3,5} = E_{1,1} \beta$$

$$X_{4,4} = A_{3,3} \alpha^2 + B_{2,3} \beta^2 + D_{1,1} \qquad X_{4,5} = A_{3,4} \alpha \beta + B_{2,4} \alpha \beta$$

$$X_{5,5} = A_{4,4} \beta^2 + B_{2,4} \alpha^2 + E_{1,1} \qquad \text{and } X_{i,j} = X_{j,i} \text{ (i, j=1 to 5)}$$

APPENDIX – IV

Elements of Thermal Force Matrix { F_T } for various displacement models used in the thermo-elastic analysis of FGM plates

- **Model – HSDT-12 (Kant and Manjunatha 1988)**

$$\{F_T\}^t = \left\{ -\alpha N_{x_T} \quad -\beta N_{y_T} \quad 0 \quad -\alpha M_{x_T} \quad -\beta M_{y_T} \quad N_{z_T} \quad -\alpha N_{x_T}^* \quad -\beta N_{y_T}^* \quad 2M_{z_T}^* \quad -\alpha M_{x_T}^* \quad -\beta M_{y_T}^* \quad 3N_{z_T}^* \right\}$$

- **Model – HSDT-9 (Pandya and Kant 1988)**

$$\{F_T\}^t = \left\{ -\alpha N_{x_T} \quad -\beta N_{y_T} \quad 0 \quad -\alpha M_{x_T} \quad -\beta M_{y_T} \quad -\alpha N_{x_T}^* \quad -\beta N_{y_T}^* \quad -\alpha M_{x_T}^* \quad -\beta M_{y_T}^* \right\}$$

- **Model – HSDT-5 (Reddy 1984)**

$$\{F_T\}^t = \left\{ -\alpha N_{x_T} \quad -\beta N_{y_T} \quad -\alpha (M_{x_T} + M_{x_T}^*) \quad -\beta (M_{y_T} + M_{y_T}^*) \quad (\alpha^2 M_{x_T}^* + \beta^2 M_{y_T}^*) \right\}$$

- **Model – FSDT (Whitney and Pagano 1970)**

$$\{F_T\}^t = \left\{ -\alpha N_{x_T} \quad -\beta N_{y_T} \quad 0 \quad -\alpha M_{x_T} \quad -\beta M_{y_T} \right\}$$

LIST OF PUBLICATIONS BASED ON PRESENT RESEARCH WORK

International Journals:

1. Swaminathan K. and Sangeetha D. M., (2017). “Thermal Analysis of FGM Plates – A Critical Review of Various Modelling Techniques and Solution Methods.” *Composite Structures*, 160, 43-60.
2. Swaminathan K. and Sangeetha D. M. “FGM Plates subjected to Thermal Loads – Analytical Evaluation of Higher Order Refined Computational Models.” *Structural Engineering and Mechanics* (To be communicated)
3. Swaminathan K. and Sangeetha D. M., (2015). “Thermo-Elastic Analysis of FGM Plates based on Higher Order Refined Computational Model.” *International Journal of Research in Engineering and Technology*, 4(13), 1-6.
4. Swaminathan K. and Sangeetha D. M., (2015). “Temperature Dependent and Independent Material Properties of FGM Plates.” *IOSR Journal of Mechanical and Civil Engineering*, 2, 84-88.

International Conferences:

1. Swaminathan K. and Sangeetha D. M. (2016), “Higher Order Computational Models for the Thermo-Elastic Analysis of FGM Plate – An Assessment.” *Proc. of The 2nd International Conference on Advanced Composite Materials, ACM - 2016*, July 25-27, 2016, Suzhou, China.
2. Swaminathan K. and Sangeetha D. M. (2016), “Higher Order Refined Computational Models for the Thermo-Elastic Analysis of FGM Plates.” *Proc. of The Sixth International Conference on Structural Engineering, Mechanics and Computation, SEMC - 2016*, September 5-7, 2016, Cape Town, South Africa.

BIO-DATA

SANGEETHA D. M.

“Sanvi shree”,
IH-61, 7th cross, 2nd main,
Landlinks Township,
Derebail, Konchady Post,
Mangalore-575008.
Karnataka, INDIA

Phone : +91-7795787676 (M)

E-mail : ursang2008@gmail.com

QUALIFICATIONS:

M.Tech. in Structures -2009 (First Class with Distinction)
B.V.B. College of Engineering and Technology, Hubli.
Visweswaraiiah Technological, University, Belgaum

B.E. in Civil Engineering -2007 (First Class with Distinction)
Jawaharlal Nehru National College of Engineering, Shimoga.
Visweswaraiiah Technological, University, Belgaum

School :

Primary Education : Vasavi Vidyalaya, Shimoga.

Date of Joining Ph.D : 9th Dec 2010

PERSONAL PROFILE:

Date of Birth : 31st May 1985

Gender : Female

Nationality : Indian

Spouse Name : Dr. Vinay Kumar V.